Shear Wave Velocity Profiling and Liquefaction Assessment of Sites Shaken by the 1999 Kocaeli, Turkey Earthquake

by

Dr. James A. Bay
Assistant Professor

Brady R. Cox
Graduate Research Assistant

Department of Civil and Environmental Engineering
Utah State University
Logan, Utah 84322-4110

March 26, 2001

for

PEER project SA3017-18336

TABLE OF CONTENTS

CHAPTER 1

INTRODUCTION

On August 17, 1999, at 3:02 in the morning, a powerful earthquake ripped through northern Turkey. In the aftermath of the earthquake, the Turkish government reported 17,439 people dead, 43,953 injured, and more than 500,000 left homeless (EERI, 2000). This earthquake was later termed the Kocaeli earthquake (after the name of the providence where the epicenter was located) and was estimated as having a moment magnitude (M_W) of 7.4. The actual epicenter was located on the North Anatolian fault, just southeast of the city of Izmit (about 80 km southeast of Istanbul). From this location, the fault ruptured approximately 90 km to the east and 30 km to the west. The rupture was predominantly right-lateral strike-slip, with ground displacements ranging from 1 - 5.5 meters (EERI, 2000).

The Kocaeli earthquake generated intense interest within the engineering community due to reports of massive ground failures and structural collapse. A reconnaissance team from the Earthquake Engineering Research Institute (EERI) arrived in Turkey just days after the earthquake. This group assisted in organizing the efforts of other reconnaissance teams and private researchers so as to optimize the effort to investigate earthquake damage and plan further research. One of these important groups was the U.S.-Turkey NSF Geotechnical Earthquake Engineering reconnaissance team. This team performed aerial and land surveys directed at investigating ground failures that developed during the earthquake. From these reconnaissance efforts, a number of "representative" case histories were selected for further detailed study. These researchers found particular interest in liquefaction-related ground failures that occurred throughout the city of Adapazari, and lateral spreading that occurred along the shores of Lake Sapanca and Izmit Bay. A full account of their reconnaissance efforts can by found in EERI (2000).

Post-earthquake research at these ground failure sites was spearheaded by a joint group of researchers from the University of California at Berkeley, Brigham Young University, the University of California at Los Angeles, ZETAS Earth Technology Corporation, Middle East Technical University, and Sakarya University. Their investigations included large-scale SPT and CPT testing, in addition to detailed site mapping (www.eerc.berkeley.edu/turkey/adapazari).

In August of 2000, a joint investigation team comprised of researchers from Utah State University (USU) and The University of Texas at Austin (UT) traveled to Turkey in order to perform spectral-analysis-of-surface-waves (SASW) testing at many of these same sites. The National Science Foundation (NSF) and the Pacific Earthquake Engineering Research Center (PEER) sponsored this research due to the desire for combining accurate shear wave velocity profiles with standard penetration test (SPT) and cone penetration test (CPT) data from the same sites. These three testing methods comprise the current realm of simplified procedures for evaluating earthquake-induced soil liquefaction.

Fifteen different liquefaction sites were tested using the SASW method. Chapter 2 of this report presents the SASW results and shear wave velocity profiles that were developed for each of these sites. Chapter 2 also contains detailed site information and maps showing the locations of SASW centerlines, SPT boreholes, and CPT soundings.

Chapter 3 provides a detailed liquefaction analysis of each site aimed at determining the soil layer/layers most likely to have initiated these ground failures. This was accomplished by delineating a potentially liquefiable region at each site using the simplified shear wave velocity procedure (Andrus et al., 2001). Locating this region at each site allowed for the separation of soils that were too stiff to liquefy from soils that were soft enough to liquefy. Once these soft regions had been identified, they were evaluated to separate granular soils expected to liquefy, from fine-grained soils expected not to liquefy. At sites where actual soil samples were available, this was accomplished by using the Chinese Criteria (Seed and Idriss, 1982) and the Andrews and Martin Criteria (Andrews and Martin, 2000). At sites where only CPT data were available, this

was accomplished by developing profiles of soil behavior type index (I_C) (Robertson and Wride, 1998).

Granular soil layers were located within the liquefiable region at 11 of the liquefaction test sites. It is assumed that these layers were involved in the observed ground failures. The depth and thickness of each of these layers have been identified. However, at four of the liquefaction sites, only soils predicted as not susceptible to liquefaction were encountered. In these cases, the layer coming closest to fulfilling the Chinese Criteria and the Andrews and Martin Criteria is identified. At each of these four sites, this layer appeared to be primarily made up of non-plastic silts having 2 μm clay contents ranging from 15 - 25 %.

These findings suggest that soils, having a high percentage of clay size particles, should not be classified as nonliquefiable based upon clay fraction alone.

CHAPTER 2

FIELD TESTING AND SASW RESULTS

2.1 INTRODUCTION

In August of 2000, a joint investigation team comprised of researchers from Utah State University (USU) and The University of Texas at Austin (UT) traveled to Turkey in order to perform spectral-analysis-of-surface-waves (SASW) testing at key geotechnical sites from the 1999 Kocaeli and Duzce earthquakes. The National Science Foundation (NSF) and the Pacific Earthquake Engineering Research Center (PEER) sponsored this research due to the need for accurate shear wave velocity profiles at both strong motion stations and liquefaction sites. Members of the USU testing team were Professor James A. Bay, Brady R. Cox, and Aaron Budge. Members of the UT testing team were Professor Kenneth H. Stokoe, II, Professor Ellen Rathje, Brent Rosenblad, and Mehmet Darendeli. As a division of labor, the team from UT typically tested at strong motion stations, while the team from USU tested at liquefaction sites. Only the liquefaction testing is addressed in this report. Nineteen SASW case histories have been developed from 15 different liquefaction sites.

In-depth descriptions and explanations of the SASW method can be found in Nazarian and Stokoe (1984), Stokoe et al. (1988), Stokoe et al. (1994), and Brown et al. (2000). A detailed description of the general procedures that were employed while testing at the liquefaction sites in Turkey can be found in Cox (2001). Cross power spectrum phase-plots, experimental dispersion curves, and theoretical dispersion curves for each site can also be found in Cox (2001). The remainder of this chapter will present detailed site descriptions and shear wave velocity profiles for 15 sites shaken by the 1999 Kocaeli, Turkey earthquake.

Shear wave velocity profiles were generated to a depth of at least 10 m at each of the sites. This was accomplished using hammers and a 90-kg drop weight as wave

sources. The drop weight was raised with about 1.5 m with a portable tripod and winch and released with a quick-release hook. 1-Hz and 4.5-Hz geophones were used to measure the generated waveforms. Details on field procedures employed can be found in Cox (2001).

2.2 Liquefaction Sites

A reconnaissance team from the Earthquake Engineering Research Institute (EERI) arrived in Turkey just days after the Kocaeli earthquake. This group assisted in organizing the efforts of other reconnaissance teams and private researchers so as to optimize the effort to investigate earthquake damage and plan further research. One of these important groups was the U.S.-Turkey NSF Geotechnical Earthquake Engineering reconnaissance team. This team performed aerial and land surveys directed at investigating ground failures that developed during the earthquake. From these reconnaissance efforts, a number of "representative" case histories were selected for further detailed study. These researchers found particular interest in liquefaction ground failures that occurred throughout the city of Adapazari, and lateral spreading that occurred along the shores of Lake Sapanca and Izmit Bay. A full account of reconnaissance efforts and participants can by found in EERI (2000).

Additional post-earthquake research at these ground failure sites was spearheaded by a joint group of researchers from the University of California at Berkeley, Brigham Young University, the University of California at Los Angeles, ZETAS Earth Technology Corporation, Middle East Technical University, and Sakarya University. Their investigations have included large-scale SPT and CPT testing in addition to detailed site mapping. It was desired that SASW testing should be performed at many of the same sites where these investigators were focusing their efforts. Professor Ellen Rathje from UT was able to coordinate efforts with these other researchers to determine at which liquefaction sites shear wave velocity profiles would be most helpful. Therefore, the majority of site maps and pictures for the SASW case histories presented below have been obtained from the above-mentioned researchers at a website detailing all of their efforts (www.peer.berkeley.edu) Professor John D. Bray and Rodolfo B. Sancio

of the University of California at Berkeley, and Professor T. L. Youd of Brigham Young University have since provided particular help and cooperation with liquefaction site details.

Nineteen SASW centerlines were tested at 15 different liquefaction sites. The locations of these sites are shown on a large-scale map in Figure 2.1. Since the majority of sites are located in the city of Adapazari, a separate map detailing the test locations in this city is shown in Figure 2.2. Full descriptions of each site can be found in EERI (2000). Additional work provided by other researchers at these same sites can also be found at the website listed above. The SASW results from each test are given below.

2.2.1 Adapazari

The city of Adapazari, located approximately 7 km north of the fault rupture, suffered the highest degree of property damage and life loss of any city affected by the Kocaeli earthquake. Turkish federal government data indicates that 27% of the buildings in Adapazari were either severely damaged or destroyed. Literally thousands of people lost their lives. The city also experienced one of the most spectacular and extensive occurrences of soil liquefaction as hundreds of buildings settled, tilted, or translated excessively (EERI, 2000).

The city of Adapazari is founded primarily on Holocene alluvial deposits. The Turkish word Adapazari actually means "island market," which reflects the fact that the city occupies a landmass between two meandering rivers. Due to the depositional environment, the subsurface conditions at Adapazari are such that large variations in the soil are expected in both the horizontal and vertical directions. Depth to groundwater in the basin is most typically around 1 meter, and buildings are primarily constructed on shallow, reinforced concrete mat and grade beam foundations (EERI, 2000). A detailed description of each site is given below.

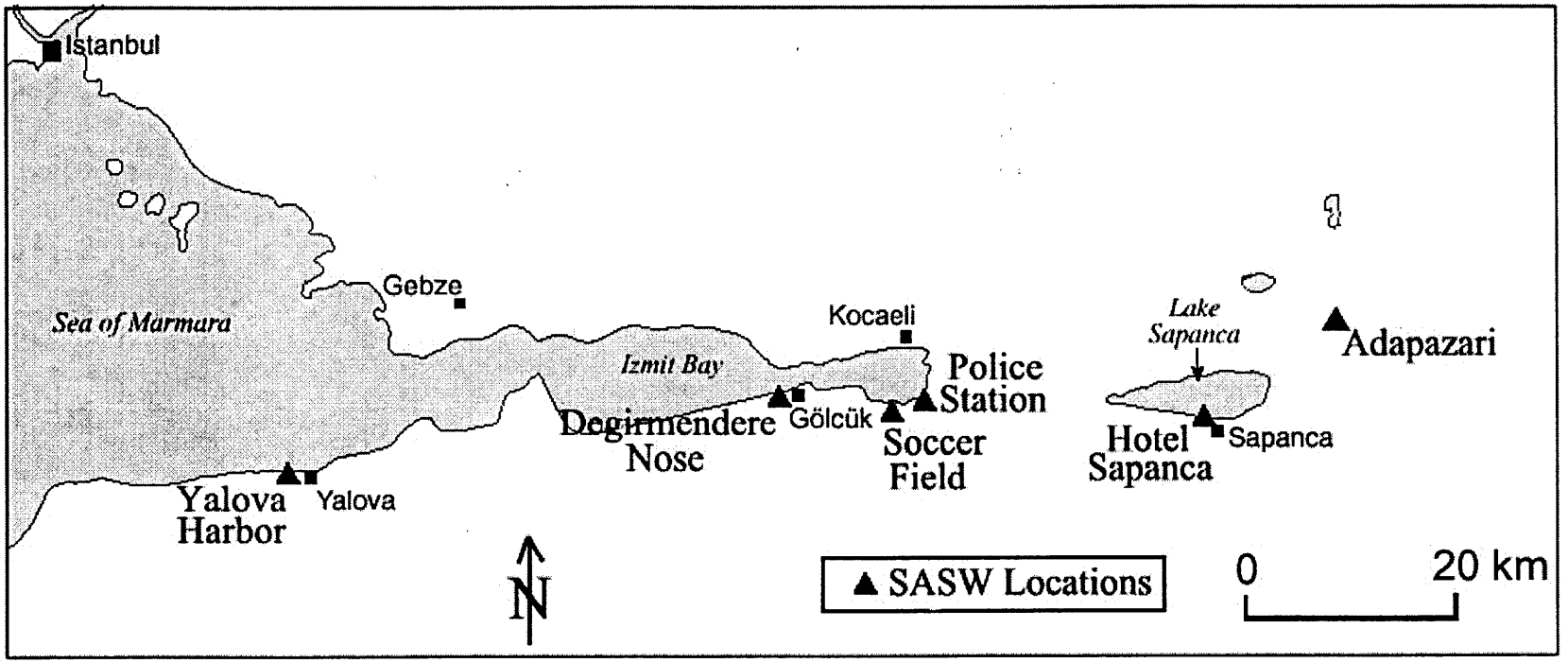

Figure 2.1 Map showing the location of the liquefaction sites that were tested using SASW in August of 2000 (modified from http://peer.berkeley.edu/turkey/adapazari).

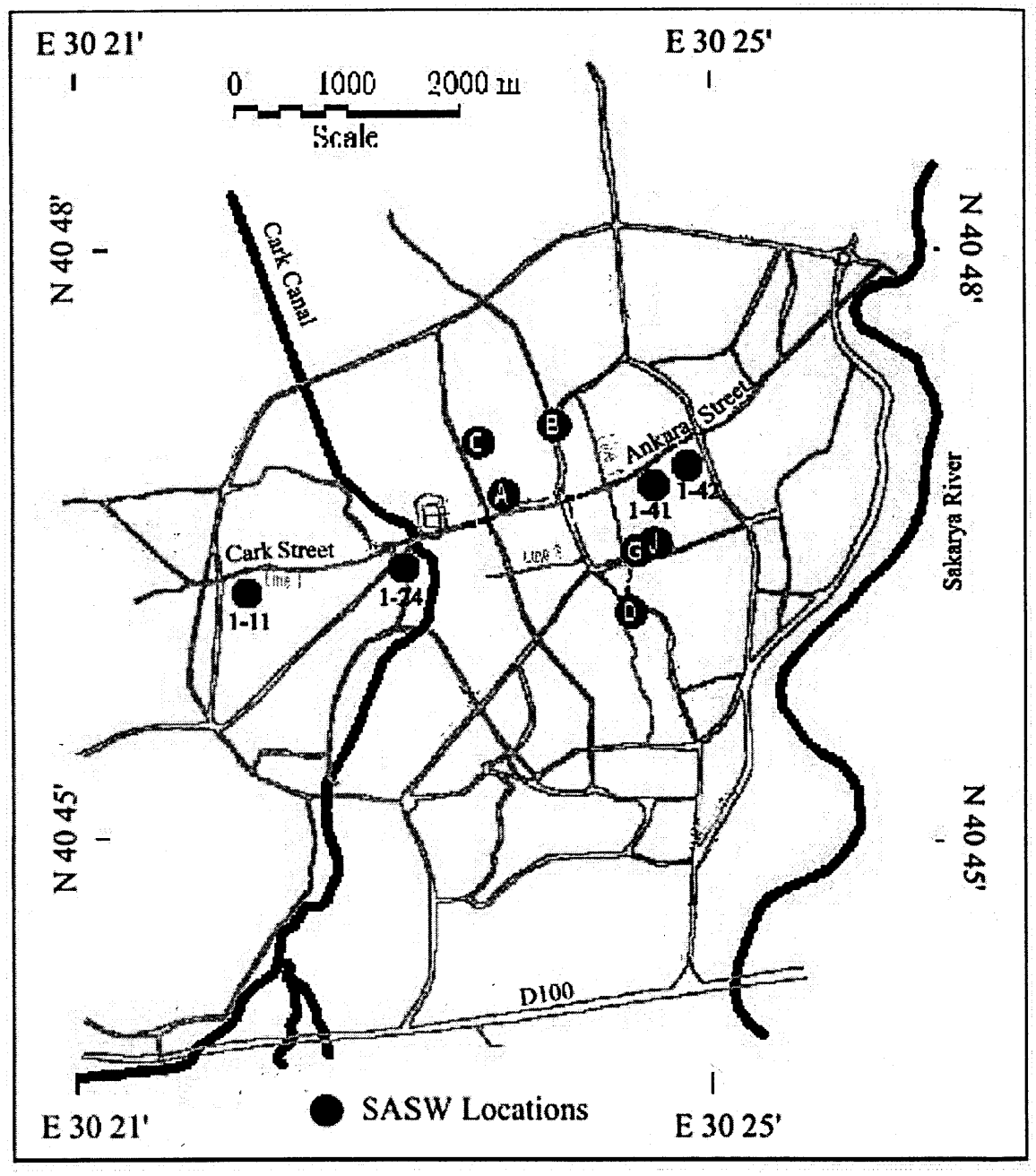

Figure 2.2 Map showing the location of 10 liquefaction sites in the city of Adapazari that were tested using SASW in August of 2000 (modified from http://peer.berkeley.edu/turkey/adapazari).

2.2.1.1 Site A Site A is located at the intersection of Tul and Yakin Streets in the Cumhuriyet District of Adapazari. Its latitude and longitude coordinates are 40.77922° north and 30.39487° east, respectively. A plan view of Site A is shown in Figure 2.3. This map also shows the SASW centerline location with respect to the SPT and CPT test locations. Here, a five-story apartment building, designated A1 in Figure 2.3, tilted excessively when its northwest corner settled approximately 1.5 meters. A photograph of this building is shown in Figure 2.4. At this same location, another five-story building, designated A2 in Figure 2.3, settled approximately 60 cm. Figure 2.5 shows the shear wave velocity profile at the site determined from forward modeling, and Table 2.1 presents the tabulated values of layer properties that were used to generate the theoretical dispersion curve and shear wave velocity profile.

The water table at Site A is located at a depth of approximately 0.75 meters. Sufficient wavelengths were generated at this site to extend the shear wave velocity profile to a depth of 25 meters. Two extremely soft layers were identified here between the depths of 0.75 – 6 meters.

2.2.1.2 Site B Site B is located at the intersection of Kuyudibi Avenue and Yaprak Street in the Karaosman District of Adapazari. Its latitude and longitude coordinates are 40.78513° north and 30.40024° east, respectively. A plan view of Site B is shown in Figure 2.6. This map also shows the SASW centerline location with respect to the SPT and CPT test locations. Here, liquefaction of foundation soil induced a bearing capacity failure that caused a five-story building, designated B1 in Figure 2.6, to tip over. A photograph of building B1 is shown in Figure 2.7. Figure 2.8 shows the shear wave velocity profile at the site determined from forward modeling, and Table 2.2 presents the tabulated values of layer properties that were used to generate the theoretical dispersion curve and shear wave velocity profile.

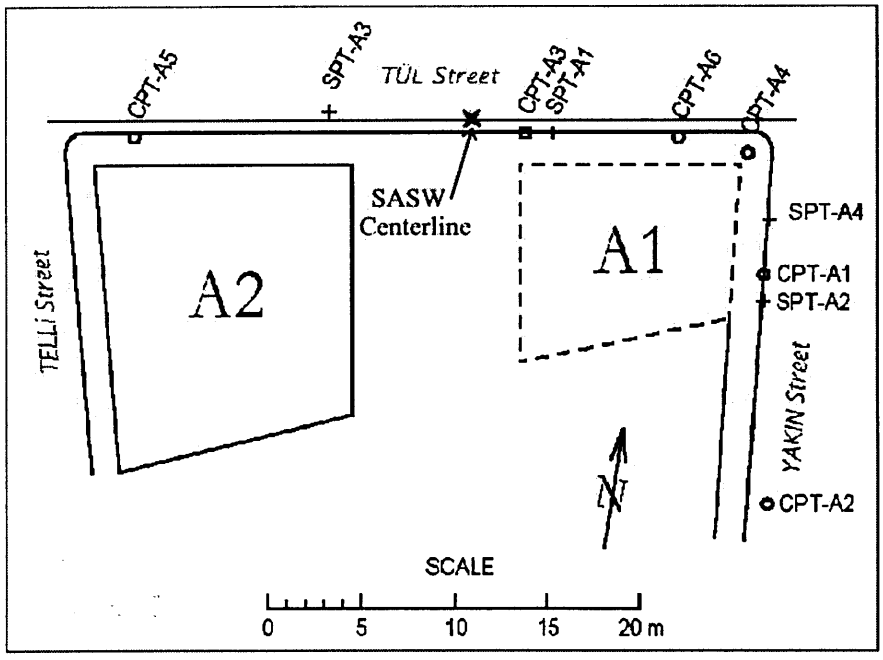

Figure 2.3 Plan view of Site A showing the location of one SASW centerline (modified from www.eerc.berkeley.edu/turkey/adapazari).

Figure 2.4 Photograph of building A1 showing the severe tilting that occurred when its northwest corner settled approximately 1.5 meters (from http://peer.berkeley.edu/turkey/adapazari).

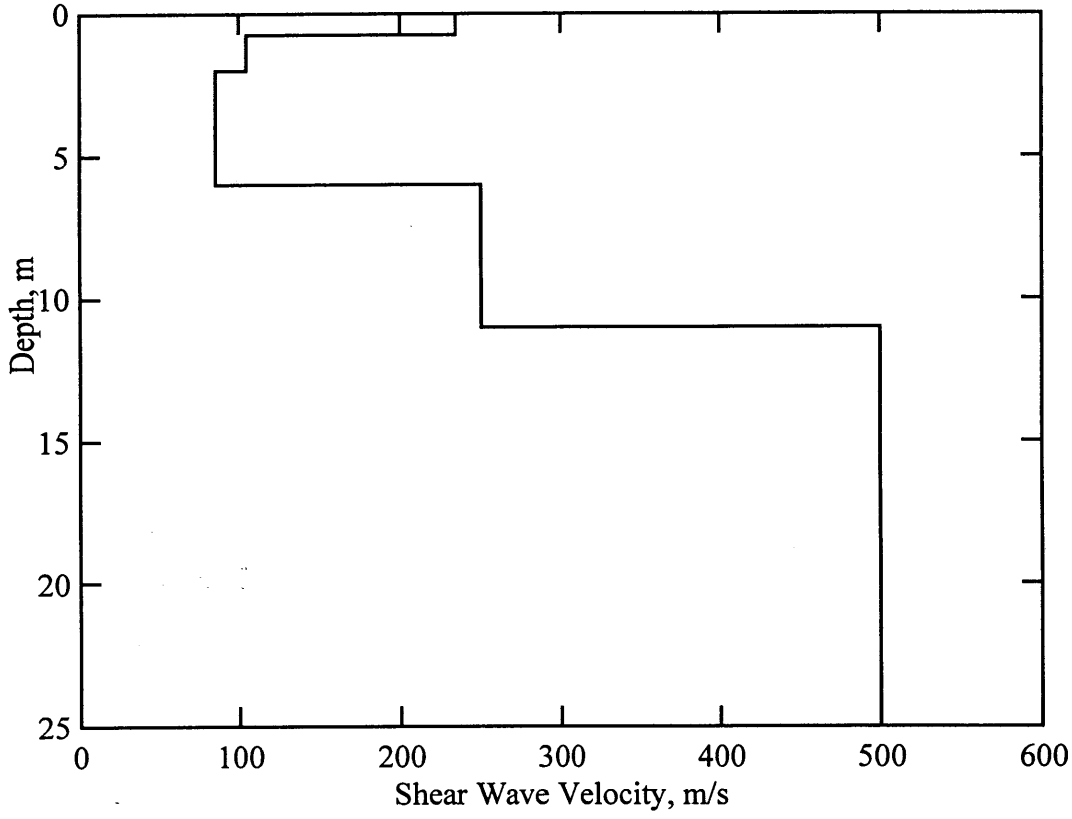

Figure 2.5 Shear wave velocity profile determined from forward modeling of Site A.

Table 2.1 Tabulated values of layer properties determined from forward modeling of Site A

			Assumed Values		
Depth to Top of Layer, m	Layer Thickness, m	Shear Wave Velocity, m/s	P-Wave Velocity, m/s	Poisson's Ratio	Mass Density, g/cc
0	0.75	235	439.6	0.3	1.92
0.75	1.25	105	615.2	0.485	2.0
2.0	4.0	85	1500	0.4984	2.0
6.0	5.0	250	1500	0.4857	2.0
11.0	14.0	500	1500	0.4375	2.0

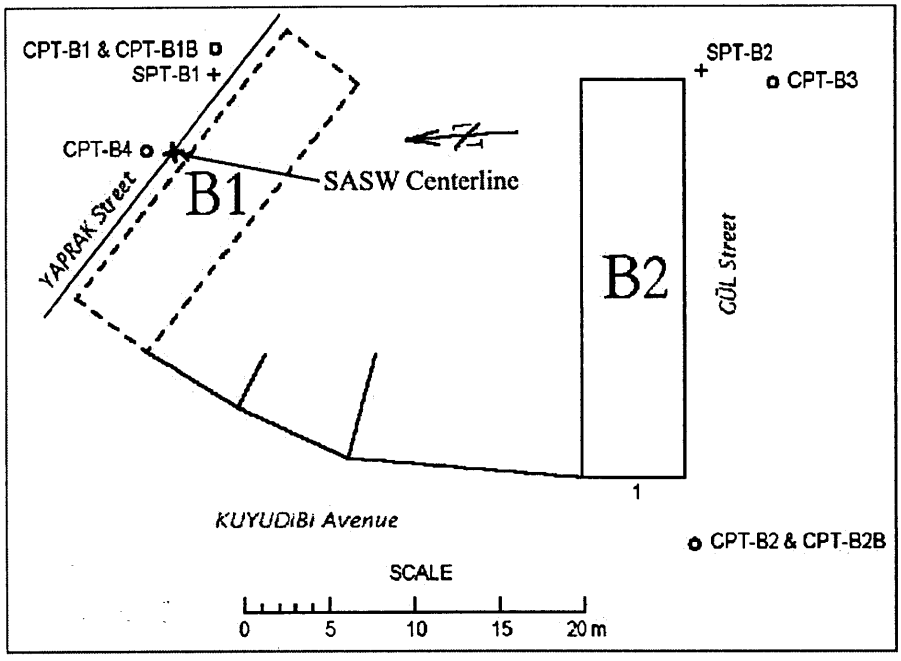

Figure 2.6 Plan view of Site B showing the location of one SASW centerline (modified from http://peer.berkeley.edu/turkey/adapazari).

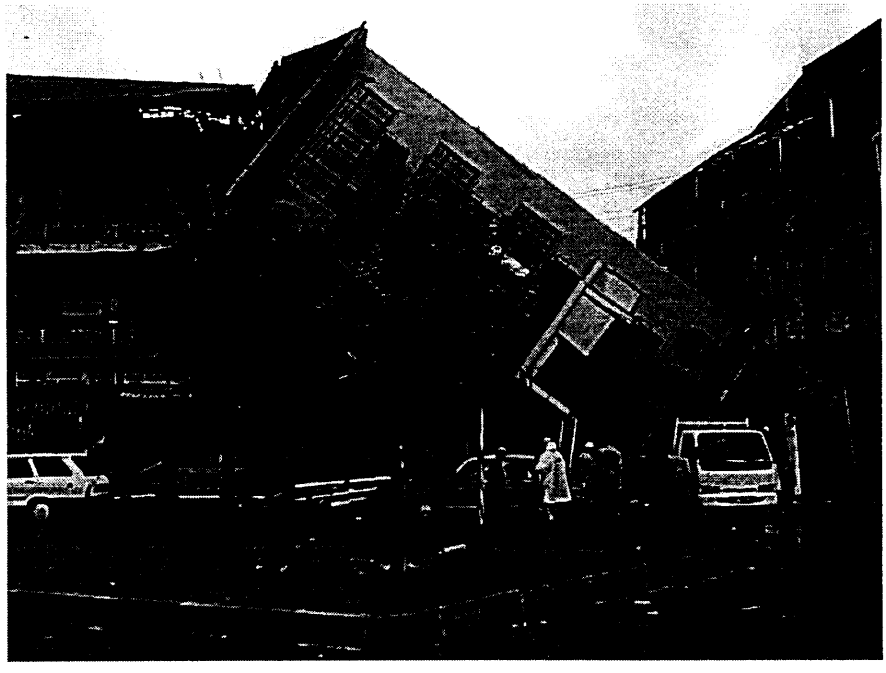

Figure 2.7 Photograph showing building B1 after it tipped over due to liquefaction of its foundation soil (from http://peer.berkeley.edu/turkey/adapazari).

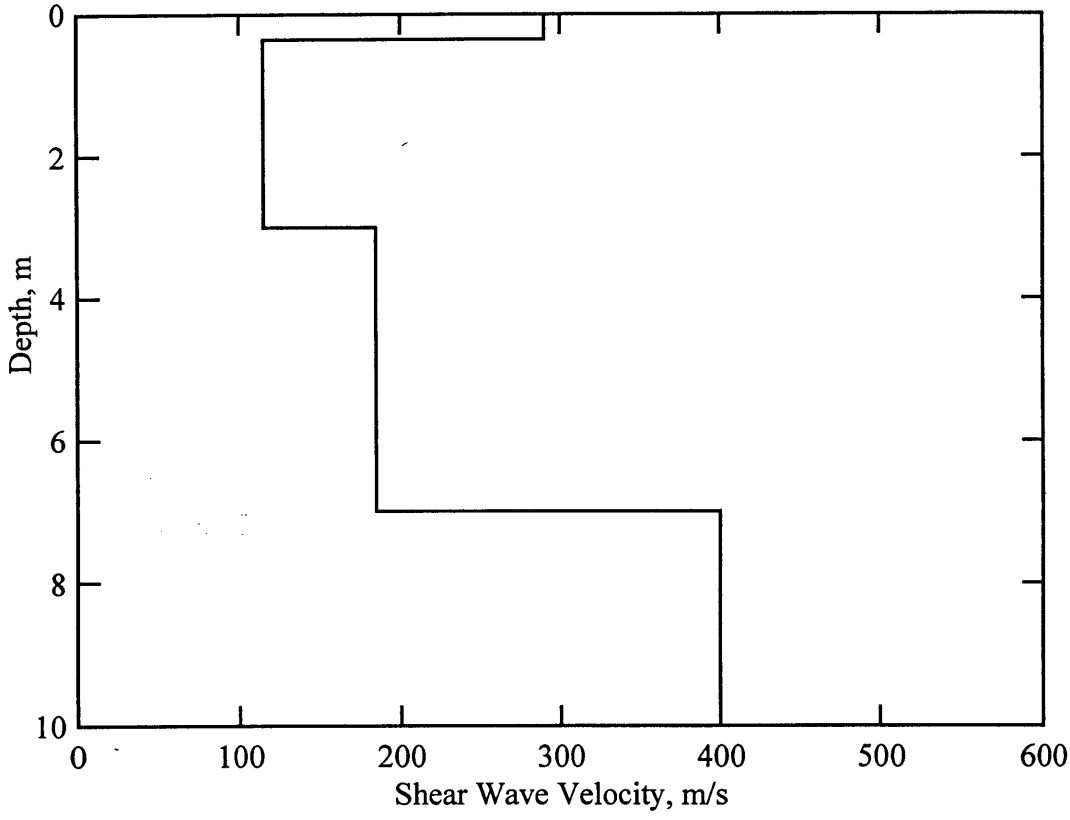

Figure 2.8 Shear wave velocity profile determined from forward modeling of Site B.

Table 2.2 Tabulated values of layer properties determined from forward modeling of Site B

			Assumed Values		
Depth to Top of Layer, m	Layer Thickness, m	Shear Wave Velocity, m/s	P-Wave Velocity, m/s	Poisson's Ratio	Mass Density, g/cc
0	0.35	290	542.5	0.3	1.92
0.35	1.65	115	215.2	0.3	1.92
2.0	1.0	115	1500	0.497	2.0
3.0	4.0	185	1500	0.4923	2.0
7.0	3.0	400	1500	0.4617	2.0

The water table at Site B is located at a depth of approximately 2 meters. Sufficient wavelengths were generated at this site to extend the shear wave velocity profile to a depth of 10 meters. The soil profile is extremely soft here between the depths of 0.35 - 7 meters.

2.2.1.3 Site C Site C is located on Boluk Street in the Istikal District of Adapazari. Its latitude and longitude coordinates are 40.78370° north and 30.39221° east, respectively. Here, three identical buildings experienced widely varying degrees of liquefaction-induced deformation. A plan view of Site C is shown in Figure 2.9. This map also shows the location of two SASW centerlines with respect to the SPT and CPT test locations. Buildings C1 and C2 settled approximately 30 - 40 cm, additionally C2 translated west toward the street 57 cm (see Figure 2.10). Building C3 experienced no visible distress. Also, the alley between buildings C1 and C2 was crumpled by the building deformations but the alley between C2 and C3 was not damaged.

Two SASW tests were performed at Site C to investigate the lateral variability that caused the two northernmost buildings to experience large deformations, while the identical southernmost building experienced no deformation. However, on the day of testing, a bazaar located on the road in front of the buildings necessitated testing in a small area behind the buildings. Due to a lack of space, the southern centerline was positioned much closer to the northern centerline than desired.

Figure 2.11 shows the shear wave velocity profile determined from forward modeling at Site C North Centerline, and Table 2.3 presents the tabulated values of layer properties that were used to generate the theoretical dispersion curve and shear wave velocity profile for the north centerline.

Figure 2.12 shows the shear wave velocity profile determined from forward modeling at Site C South Centerline, and Table 2.4 presents the tabulated values of layer properties that were used to generate the theoretical dispersion curve and shear wave velocity profile for the south centerline.

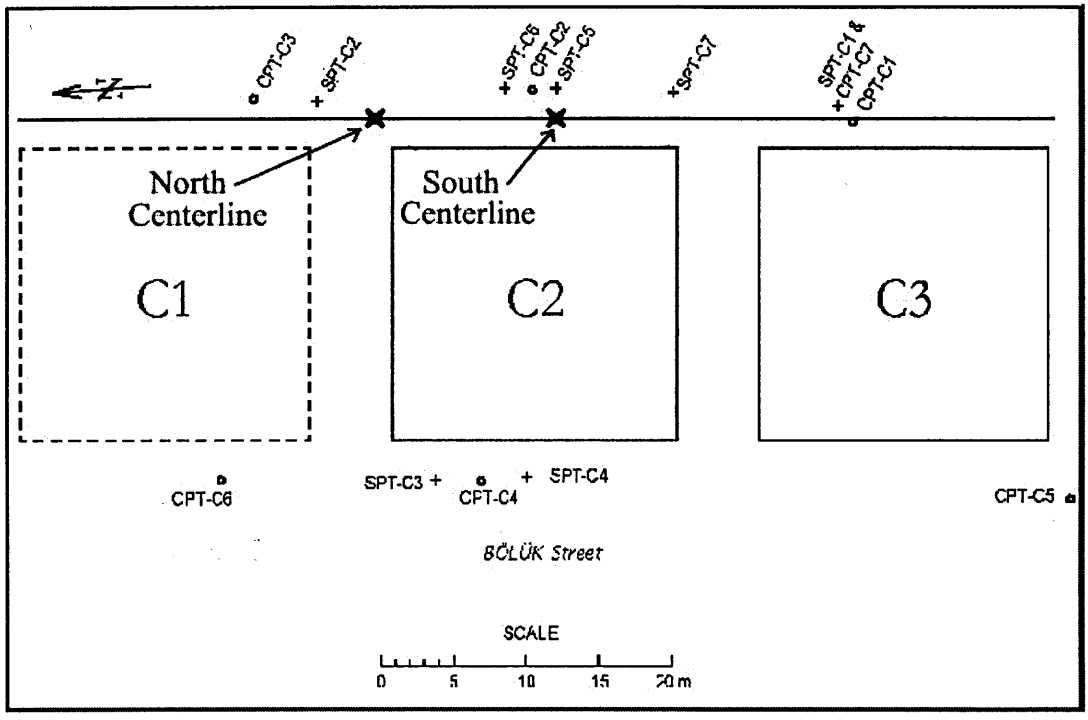

Figure 2.9 Plan view of Site C showing the location of two SASW centerlines (modified from http://peer.berkeley.edu/turkey/adapazari).

Figure 2.10 Photograph of building C2, which translated 57 cm towards the street (right). Notice the gap between the building and the sidewalk.

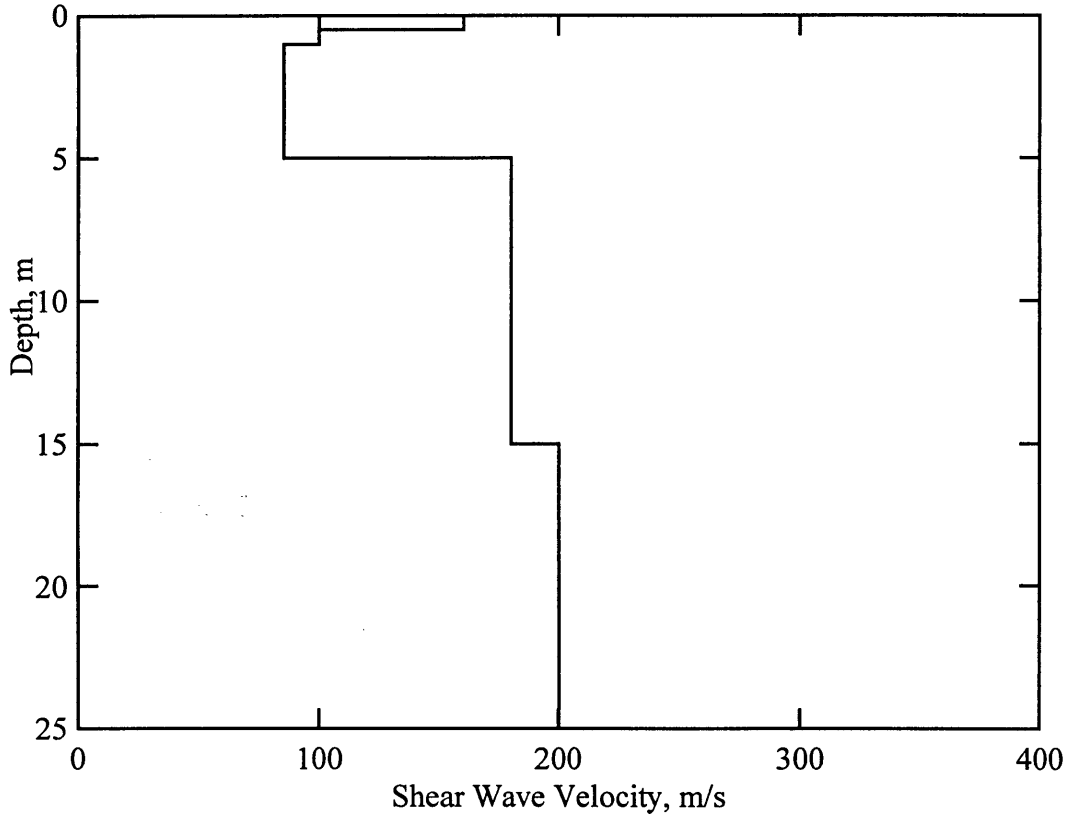

Fig. 2.11 Shear wave velocity profile determined from forward modeling of Site C North Centerline.

Table 2.3 Tabulated values of layer properties determined from forward modeling of Site C North Centerline

			Assumed Values		
Depth to Top of Layer, m	Layer Thickness, m	Shear Wave Velocity, m/s	P-Wave Velocity, m/s	Poisson's Ratio	Mass Density, g/cc
0	0.5	160	299.3	0.3	1.92
0.5	0.5	100	187.1	0.3	1.92
1.0	4.0	85	1500	0.4984	2.0
5.0	10.0	180	1500	0.4927	2.0
15.0	10.0	200	1500	0.491	2.0

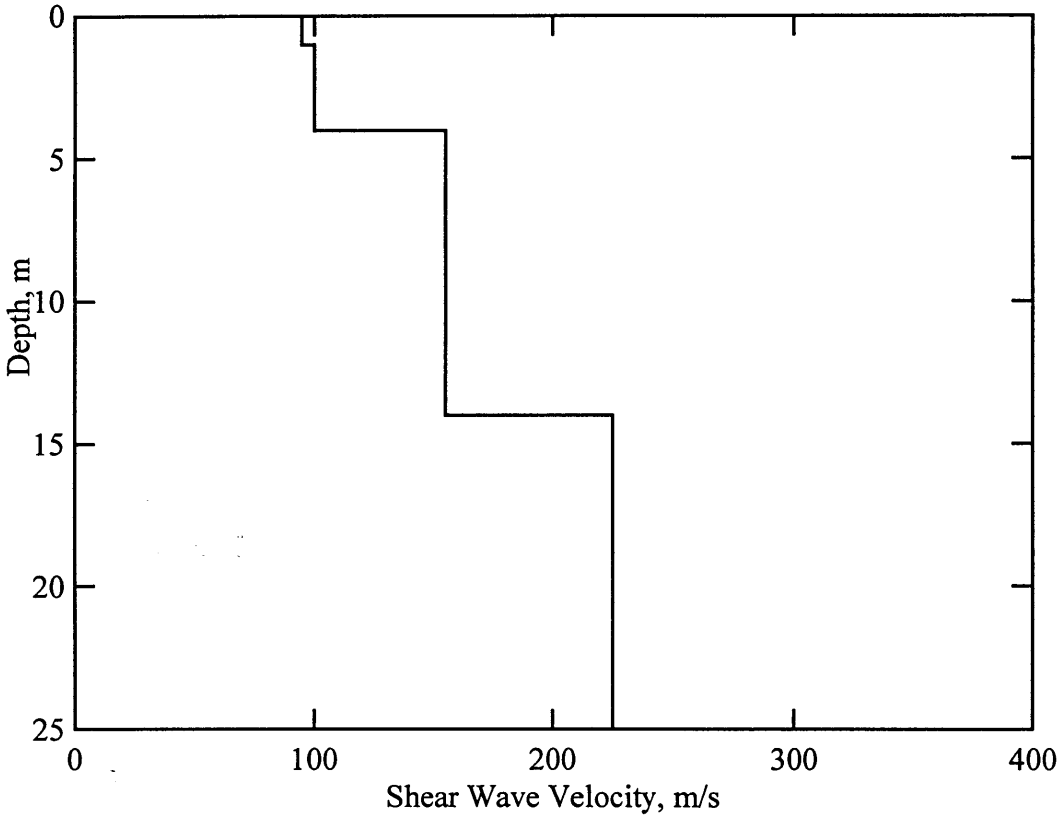

Figure 2.12 Shear wave velocity profile determined from forward modeling of Site C South Centerline.

Table 2.4 Tabulated values of layer properties determined from forward modeling of Site C South Centerline

			Assumed Values		
Depth to Top of Layer, m	Layer Thickness, m	Shear Wave Velocity, m/s	P-Wave Velocity, m/s	Poisson's Ratio	Mass Density, g/cc
0	1.0	95	177.7	0.3	1.92
1.0	3.0	100	1500	0.4978	2.0
4.0	10.0	155	1500	0.4946	2.0
14.0	11.0	225	1500	0.4885	2.0

The water table at Site C is located at a depth of approximately 1 meter. Sufficient wavelengths were generated at this site to extend the shear wave velocity profiles to a depth of 25 meters. Both shear wave velocity profiles show extremely soft soils from the ground surface to a depth of approximately 5 meters.

2.2.1.4 Site D Site D is located on Meydan Street in the Cukurahmediye District of Adapazari. Its latitude and longitude coordinates are 40.76929° north and 30.40828° east, respectively. A plan view of Site D is shown in Figure 2.13. This map also shows the SASW centerline location with respect to the SPT and CPT test locations. Here, liquefaction of foundation soil caused a five-story building, designated D1in Figure 2.13, to settle approximately 44 cm, and translate approximately 55 cm to the west and 100 cm to the south. A picture of building D1 is shown in Figure 2.14. Figure 2.15 shows the shear wave velocity profile at the site determined from forward modeling, and Table 2.5 presents the tabulated values of layer properties that were used to generate the theoretical dispersion curve and shear wave velocity profile.

The water table at Site D is located at a depth of approximately 1.5 meters. Sufficient wavelengths were generated at this site to extend the shear wave velocity profile to a depth of 15 meters. The entire soil profile consists of soft soils having shear wave velocities of less than 200 m/s.

2.2.1.5 Site G Site G is located on Hasircilar Avenue in the Yeniqun District of Adapazari. Its latitude and longitude coordinates are 40.77450° north and 30.40896° east, respectively. A plan view of Site G is shown in Figure 2.16. This map also shows the SASW centerline location with respect to the SPT and CPT test locations. Here, liquefaction of foundation soil caused a four-story and a five-story building, designated G2 and G3, respectively, in Figure 2.16, to tip over in a "V". A picture of this failure is shown in Figure 2.17. Figure 2.18 shows the shear wave velocity profile at the site determined from forward modeling, and Table 2.6 presents the tabulated values of layer properties that were used to generate the theoretical dispersion curve and shear wave velocity profile.

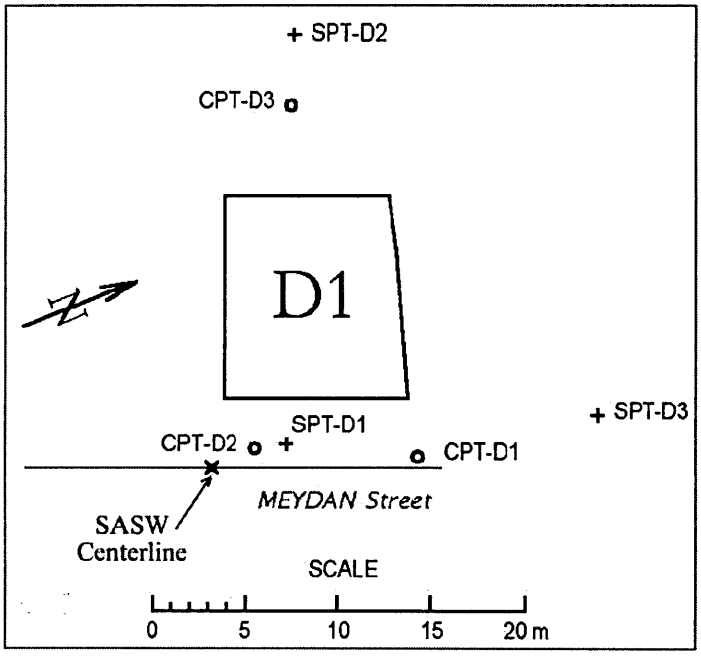

Figure 2.13 Plan view of Site D showing the location of one SASW centerline (modified from http://peer.berkeley.edu/turkey/adapazari).

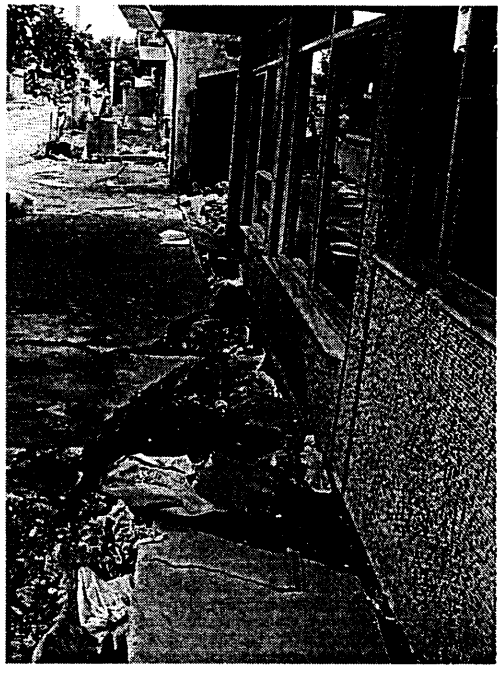

Figure 2.14 Photograph of building D1, which settled and translated during the earthquake. Notice the liquefaction ejecta next to the building (from http://peer.berkeley.edu/turkey/adapazari).

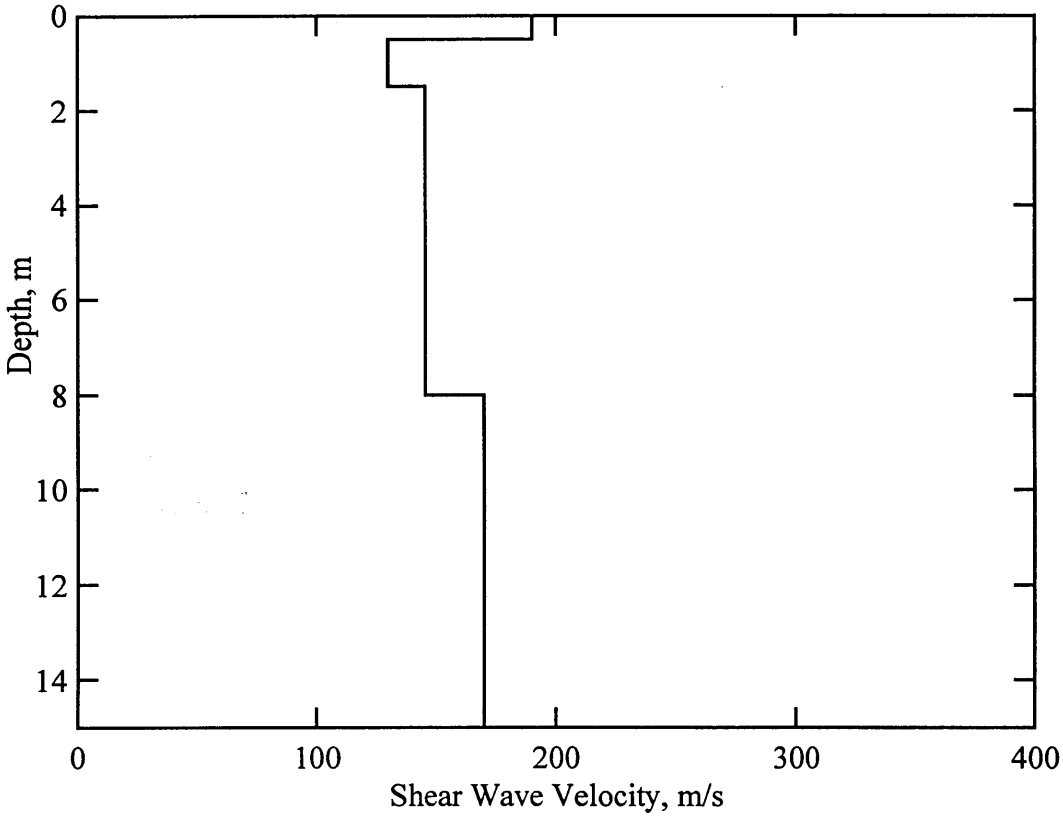

Figure 2.15 Shear wave velocity profile determined from forward modeling of Site D.

Table 2.5 Tabulated values of layer properties determined from forward modeling of Site D

			Assumed Values		
Depth to Top of Layer, m	Layer Thickness, m	Shear Wave Velocity, m/s	P-Wave Velocity, m/s	Poisson's Ratio	Mass Density, g/cc
0	0.5	190	355.5	0.3	1.92
0.5	1.0	130	243.2	0.3	1.92
1.5	6.5	145	1500	0.4953	2.0
8.0	7.0	170	1500	0.4935	2.0

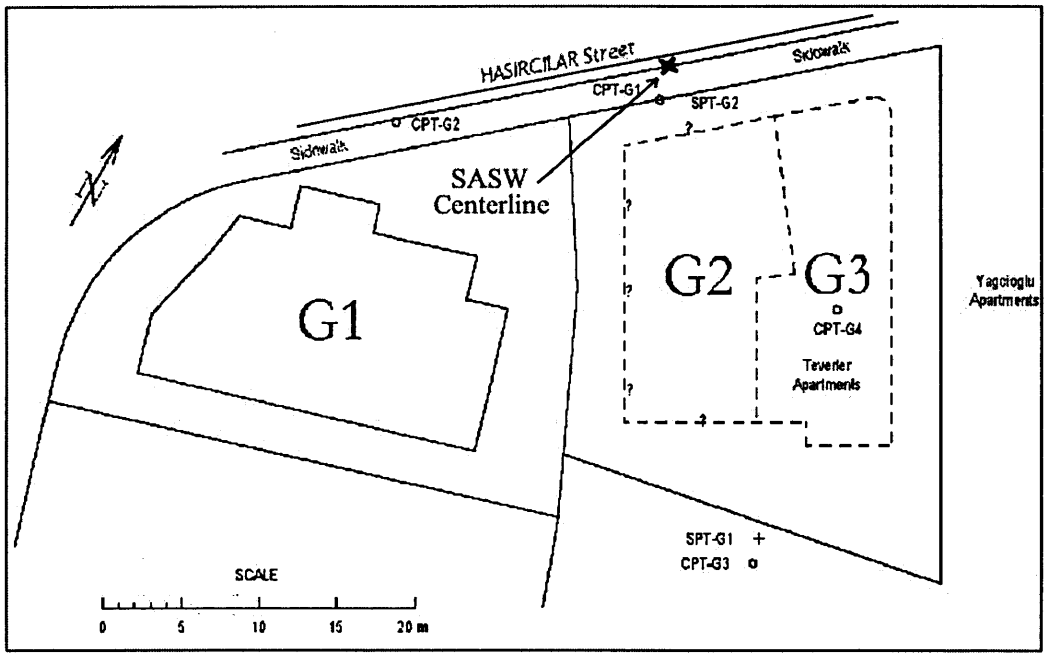

Figure 2.16 Plan view of Site G showing the location of one SASW centerline (modified from http://peer.berkeley.edu/turkey/adapazari).

Figure 2.17 Photograph of Site G, where liquefaction of foundation soil caused buildings G2 (right) and G3 (left) to tip apart in a "V" (from http://peer.berkeley.edu/turkey/adapazari).

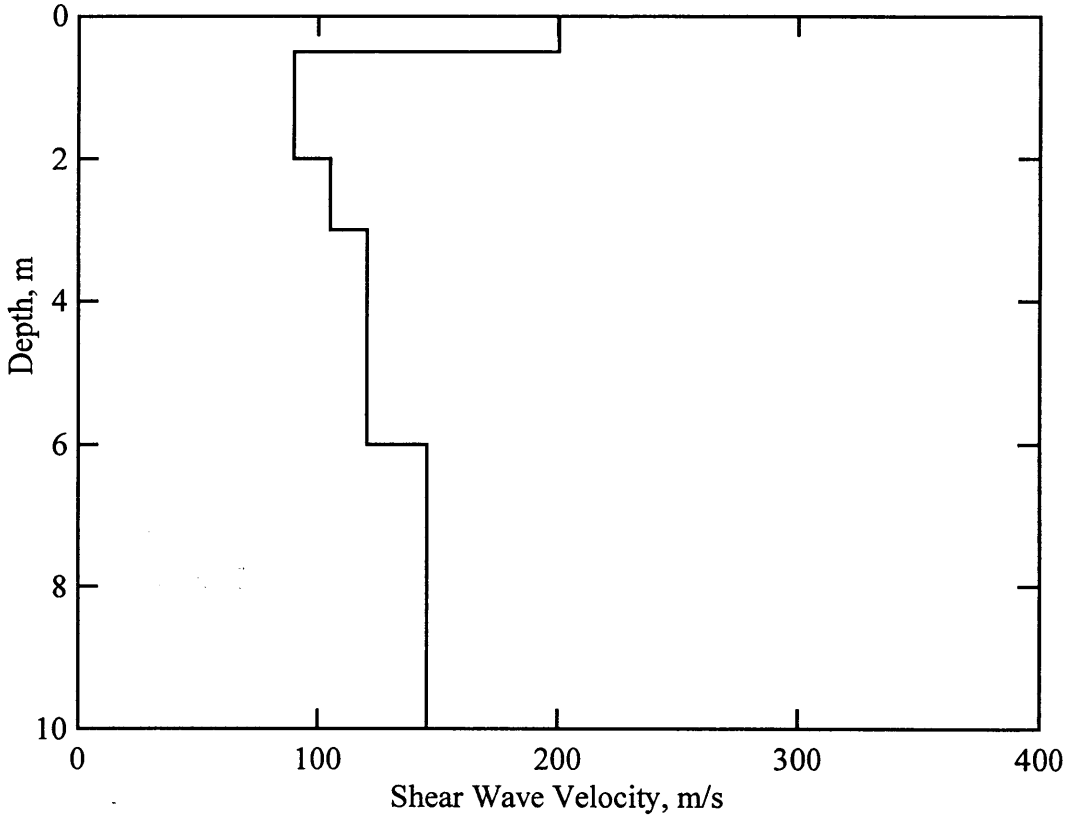

Figure 2.18 Shear wave velocity profile determined from forward modeling of Site G.

Table 2.6 Tabulated values of layer properties determined from forward modeling of Site G

			Assumed Values		
Depth to Top of Layer, m	Layer Thickness, m	Shear Wave Velocity, m/s	P-Wave Velocity, m/s	Poisson's Ratio	Mass Density, g/cc
0	0.5	200	374.2	0.3	1.92
0.5	1.5	90	527.4	0.485	2.0
2.0	1.0	105	1500	0.4975	2.0
3.0	3.0	120	1500	0.4968	2.0
6.0	4.0	145	1500	0.4953	2.0

The water table at Site G is located at a depth of approximately 0.5 meters. Sufficient wavelengths were generated at this site to extend the shear wave velocity profile to a depth of 10 meters. The entire soil profile is extremely soft, having shear wave velocities of less than 200 m/s. The softest soil in the profile is located between the depths of 0.5 – 6 meters.

2.2.1.6 Site J Site J is located on Cirak Street in the Yeniqun District of Adapazari. Its latitude and longitude coordinates are 40.77518° north and 30.41077° east, respectively. A plan view of Site J is shown in Figure 2.19. This map also shows the SASW centerline location with respect to the SPT and CPT test locations. Here, liquefaction of foundation soil caused two five-story apartment buildings, designated J1 and J2, respectively, in Figure 2.19 to settle approximately 25 cm. A picture of this failure is shown in Figure 2.20. Figure 2.21 shows the shear wave velocity profile at the site determined from forward modeling, and Table 2.7 presents the tabulated values of layer properties that were used to generate the theoretical dispersion curve and shear wave velocity profile.

The water table at Site J is located at a depth of approximately 0.7 meters. Sufficient wavelengths were generated at this site to extend the shear wave velocity profile to a depth of 50 meters. The soil profile is extremely soft down to a depth of 36 meters. The softest soil in the profile is located between the depths of 0.7 – 11 meters.

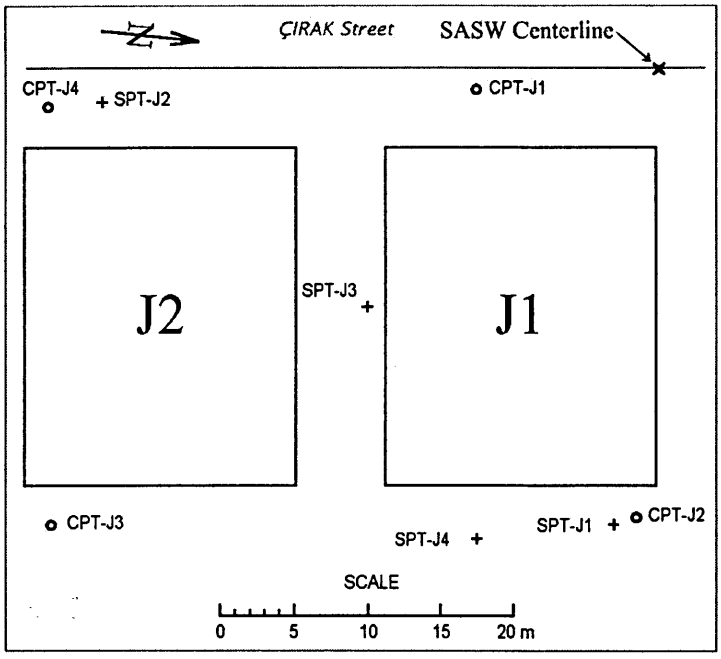

Figure 2.19 Plan view of Site J showing the location of one SASW centerline (modified from http://peer.berkeley.edu/turkey/adapazari).

Figure 2.20 Photograph showing the liquefaction-induced settlement at Site J. Notice the liquefaction ejecta (from http://peer.berkeley.edu/turkey/adapazari).

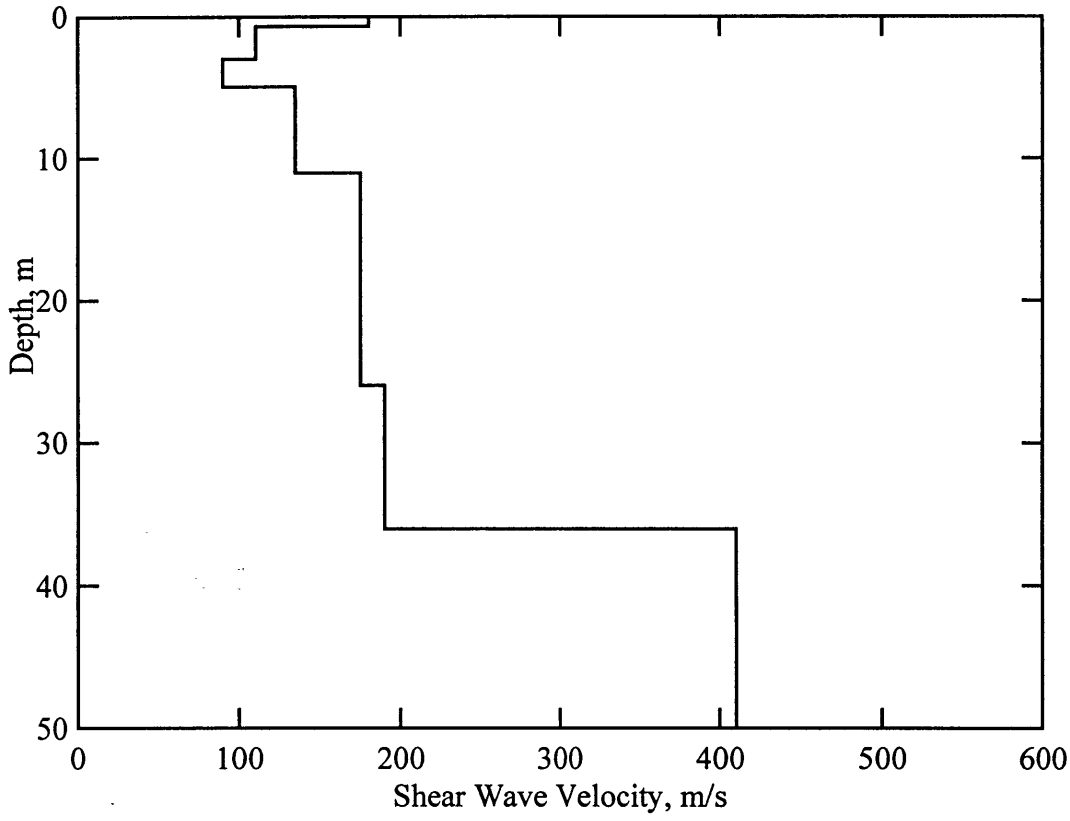

Figure 2.21 Shear wave velocity profile determined from forward modeling of Site J.

Table 2.7 Tabulated values of layer properties determined from forward modeling of Site J

			Assumed Values		
Depth to Top of Layer, m	Layer Thickness, m	Shear Wave Velocity, m/s	P-Wave Velocity, m/s	Poisson's Ratio	Mass Density, g/cc
0	0.7	180	336.8	0.3	1.92
0.7	2.3	110	1500	0.4973	2.0
3.0	2.0	90	1500	0.4982	2.0
5.0	6.0	135	1500	0.4959	2.0
11.0	15.0	175	1500	0.4931	2.0
26.0	10.0	190	1500	0.4918	2.0
36.0	14.0	410	1500	0.4596	2.0

2.2.1.7 Site 1-11 Site 1-11 is located on Cark Street in the Arabacialani District of Adapazari. Its latitude and longitude coordinates are 40.77380° north and 30.37207° east, respectively. A plan view of Site 1-11 is shown in Figure 2.22. This map also shows the SASW centerline location with respect to the CPT test locations. Here, liquefaction of foundation soil caused a five-story building, designated N-1 in Figure 2.22, to settle approximately 30 cm. A picture of this failure is shown in Figure 2.23. Figure 2.24 shows the shear wave velocity profile at the site determined from forward modeling, and Table 2.8 presents the tabulated values of layer properties that were used to generate the theoretical dispersion curve and shear wave velocity profile.

The water table at Site 1-11 is located at a depth of approximately 0.5 meters. Sufficient wavelengths were generated at this site to extend the shear wave velocity profile to a depth of 10 meters. The soil profile is extremely soft from the water table throughout the entire depth of the shear wave velocity profile.

2.2.1.8 Site 1-24 Site 1-24 is located on Cark Street in the Mithatpasa District of Adapazari. Its latitude and longitude coordinates are 40.77629° north and 30.38307° east, respectively. A plan view of Site 1-24 is shown in Figure 2.25. This map also shows the SASW centerline location with respect to the CPT test locations. This site is of interest because conditions seemed ideal for lateral spreading, however, no lateral movements were observed here along the bank of the Cark Canal. A photograph of this site is shown in Figure 2.26. Figure 2.27 shows the shear wave velocity profile at the site determined from forward modeling, and Table 2.9 presents the tabulated values of layer properties that were used to generate the theoretical dispersion curve and shear wave velocity profile.

The water table at Site 1-24 is located at a depth of approximately 2.5 meters. Sufficient wavelengths were generated at this site to extend the shear wave velocity profile to a depth of 15 meters. The soil profile is extremely soft from a depth of 1 meter throughout the entire depth of the shear wave velocity profile.

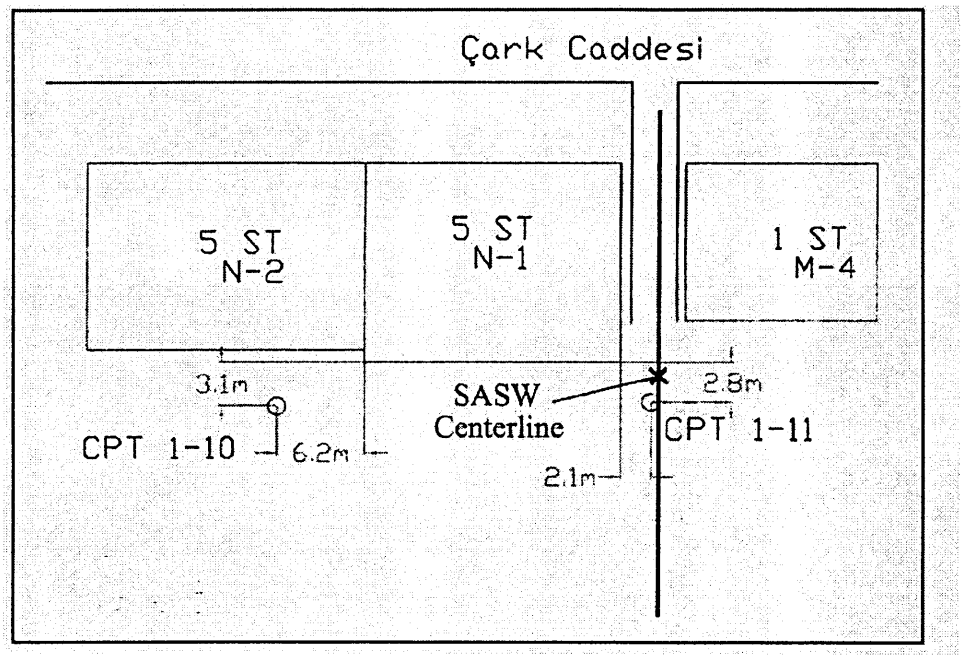

Figure 2.22 Plan view of Site 1-11 showing the location of one SASW centerline (modified from http://peer.berkeley.edu/turkey/adapazari).

Figure 2.23 Photograph showing approximately 30 cm of settlement between the stairs and the doorway of building N-1 at Site 1-11.

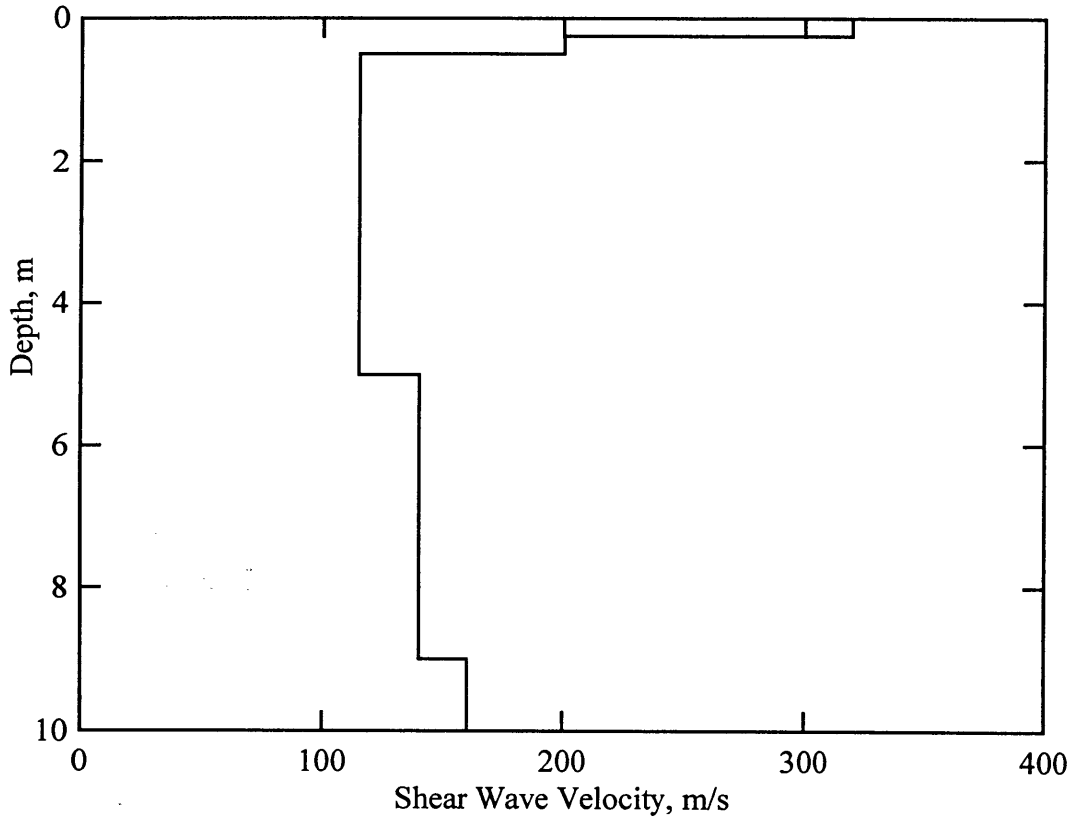

Figure 2.24 Shear wave velocity profile determined from forward modeling of Site 1-11.

Table 2.8 Tabulated values of layer properties determined from forward modeling of Site 1-11

			Assumed Values		
Depth to Top of Layer, m	Layer Thickness, m	Shear Wave Velocity, m/s	P-Wave Velocity, m/s	Poisson's Ratio	Mass Density, g/cc
0	0.25	320	598.7	0.3	1.92
0.25	0.25	200	489.9	0.4	1.92
0.5	4.5	115	1500	0.497	2.0
5.0	4.0	140	1500	0.4956	2.0
9.0	1.0	160	1500	0.4942	2.0

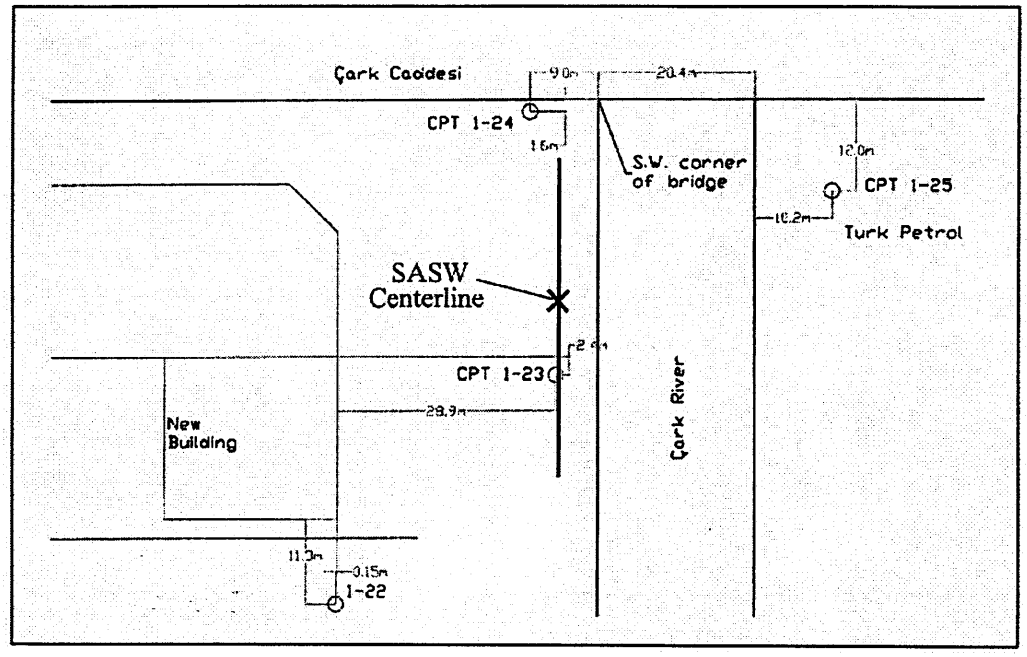

Figure 2.25 Plan view of Site 1-24 showing the location of one SASW centerline (modified from http://peer.berkeley.edu/turkey/adapazari).

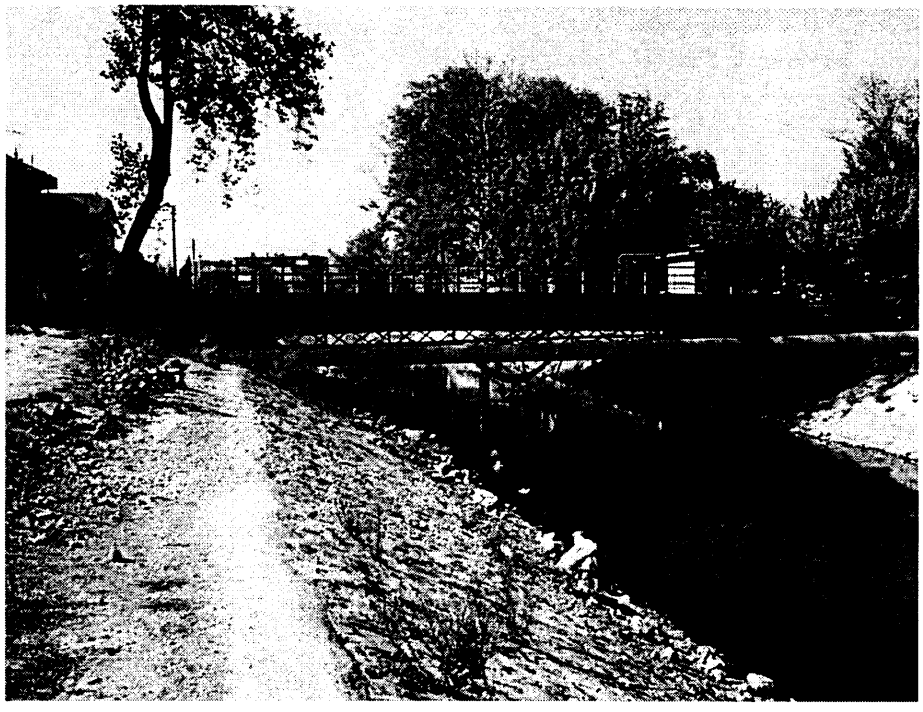

Figure 2.26 Photograph of Site 1-24. No lateral movements were noticed here along the banks of the Cark Canal.

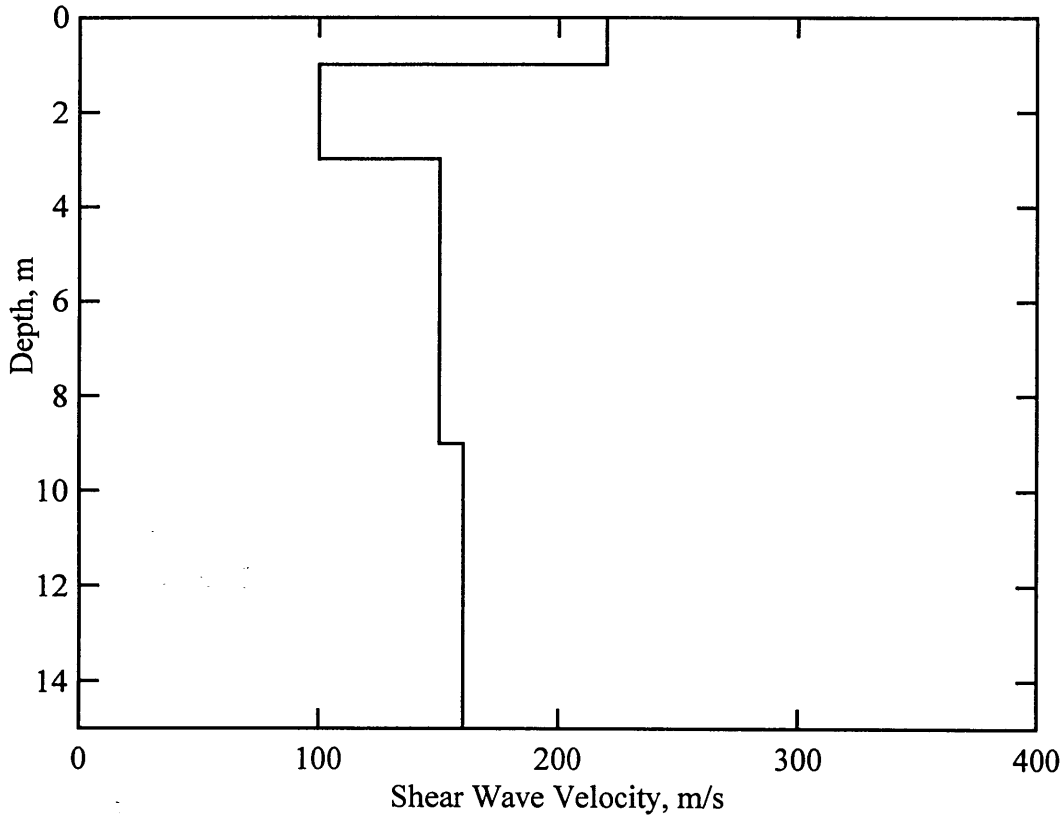

Figure 2.27 Shear wave velocity profile determined from forward modeling of SASW results at Site 1-24.

Table 2.9 Tabulated values of layer properties determined from forward modeling of Site 1-24

			Assumed Values		
Depth to Top of Layer, m	Layer Thickness, m	Shear Wave Velocity, m/s	P-Wave Velocity, m/s	Poisson's Ratio	Mass Density, g/cc
0	1.0	220	411.6	0.3	1.92
1.0	1.5	100	187.1	0.3	1.92
2.5	0.5	100	1500	0.4978	2.0
3.0	6.0	150	1500	0.4949	2.0
9.0	6.0	160	1500	0.4942	2.0

2.2.1.9 Site 1-41 Site 1-41 is located on Ipci Sokak one block south of Ankara Street in the Orta District of Adapazari. Its latitude and longitude coordinates are 40.77906° north and 30.40523° east, respectively. A plan view of Site 1-41 is shown in Figure 2.28. This map also shows the SASW centerline location with respect to the CPT test locations. At this site several buildings settled between 10 and 20 cm. Figure 2.29 shows the shear wave velocity profile at the site determined from forward modeling, and Table 2.10 presents the tabulated values of layer properties that were used to generate the theoretical dispersion curve and shear wave velocity profile.

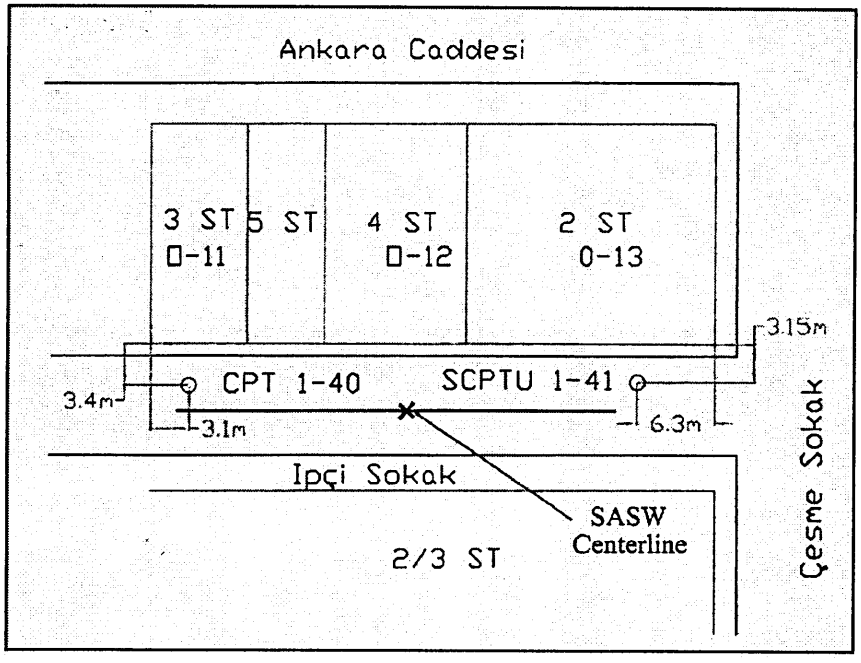

Figure 2.28 Plan view of Site 1-41 showing the location of one SASW centerline (modified from http://peer.berkeley.edu/turkey/adapazari).

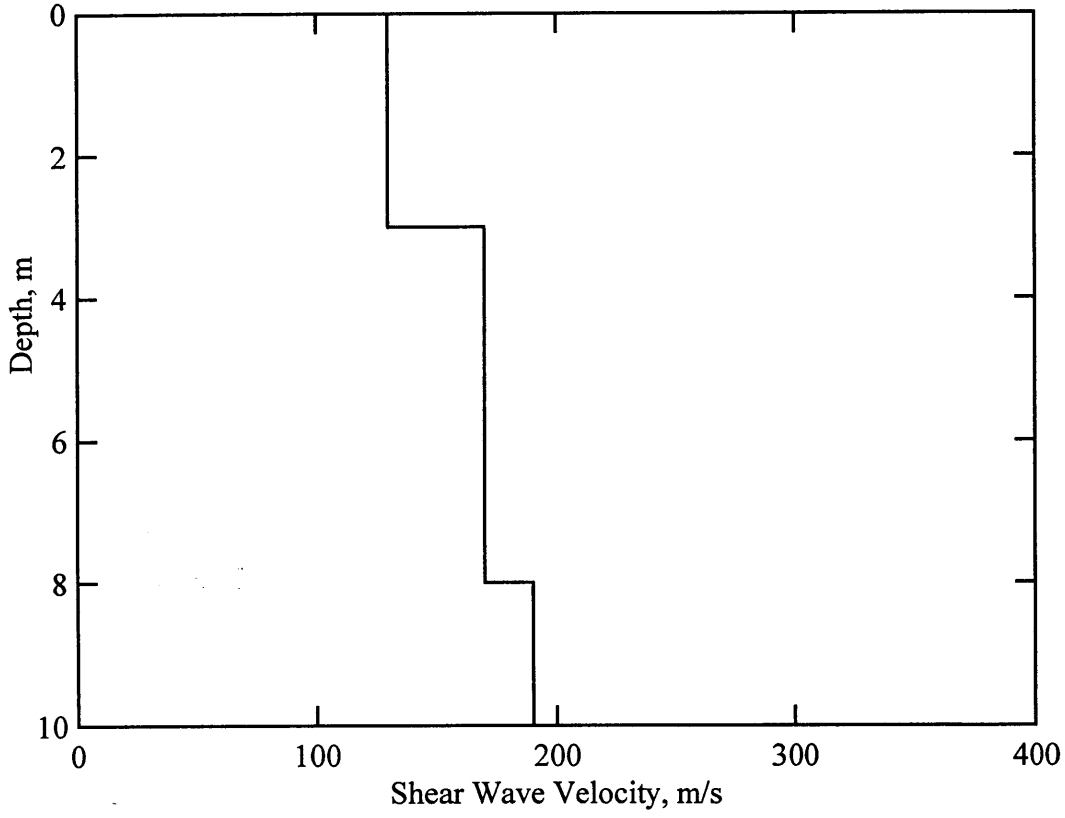

Figure 2.29 Shear wave velocity profile determined from forward modeling of SASW results at Site 1-41.

Table 2.10 Tabulated values of layer properties determined from forward modeling of Site 1-41

			Assumed Values		
Depth to Top of Layer, m	Layer Thickness, m	Shear Wave Velocity, m/s	P-Wave Velocity, m/s	Poisson's Ratio	Mass Density, g/cc
0	0.5	130	243.2	0.3	1.92
0.5	2.5	130	1500	0.4962	2.0
3.0	5.0	170	1500	0.4935	2.0
8.0	2.0	190	1500	0.4918	2.0

The water table at Site 1-41 is located at a depth of approximately 0.5 meters. Sufficient wavelengths were generated at this site to extend the shear wave velocity profile to a depth of 10 meters. The soil profile is extremely soft throughout the entire depth of the shear wave velocity profile.

2.2.1.10 Site 1-42 Site 1-42 is located on Ankara Street in the Yahyalar District of Adapazari. Its latitude and longitude coordinates are 40.77948° north and 30.40696° east, respectively. A plan view of Site 1-42 is shown in Figure 2.30. This map also shows the SASW centerline location with respect to the CPT test location. Two buildings at this site experienced minor settlements of approximately 4 cm. Figure 2.31 shows the shear wave velocity profile at the site determined from forward modeling, and Table 2.11 presents the tabulated values of layer properties that were used to generate the theoretical dispersion curve and shear wave velocity profile.

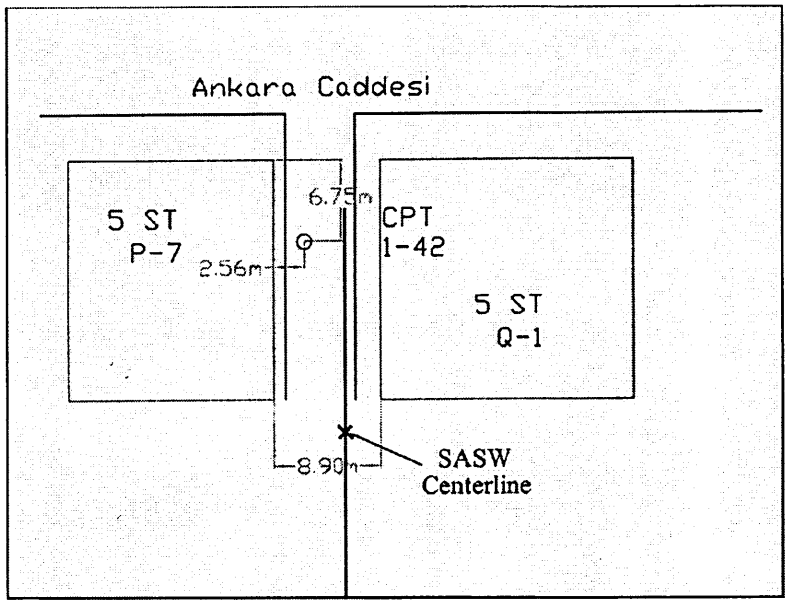

Figure 2.30 Plan view of Site 1-42 showing the location of one SASW centerline (modified from hthttp://peer.berkeley.edu/turkey/adapazari).

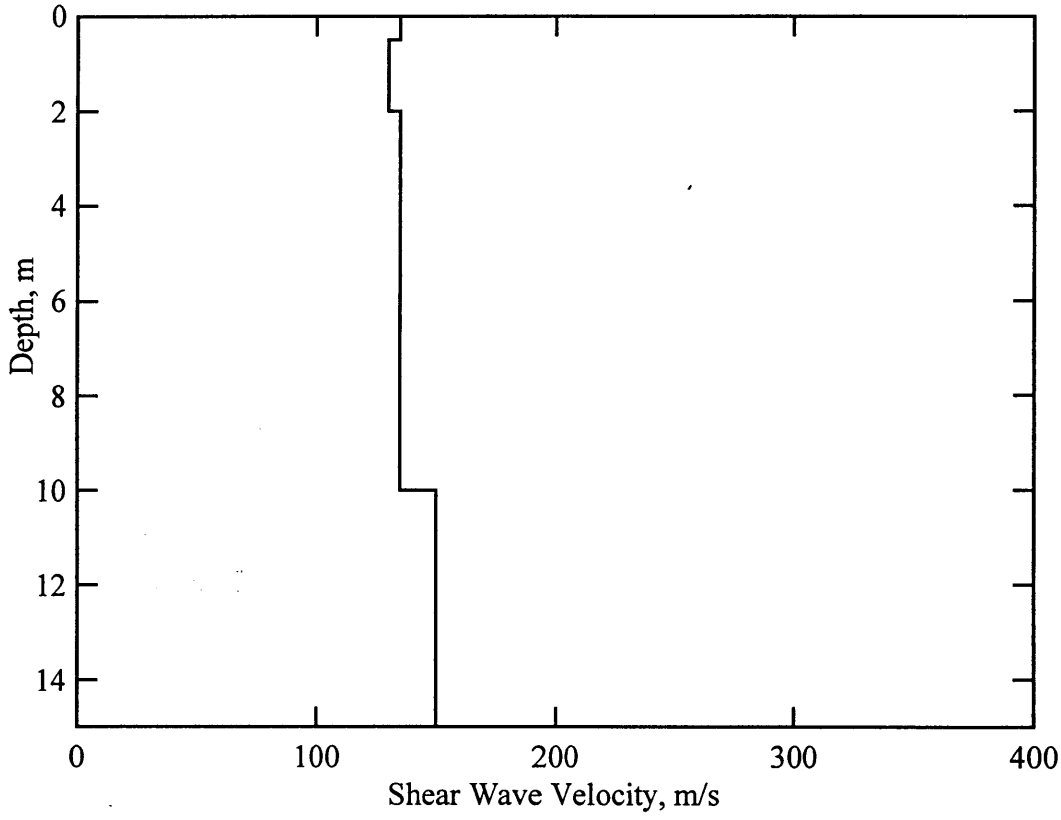

Figure 2.31 Shear wave velocity profile determined from forward modeling of SASW results at Site 1-42.

Table 2.11 Tabulated values of layer properties determined from forward modeling of Site 1-42

			Assumed Values		
Depth to Top of Layer, m	Layer Thickness, m	Shear Wave Velocity, m/s	P-Wave Velocity, m/s	Poisson's Ratio	Mass Density, g/cc
0	0.5	135	252.6	0.3	1.92
0.5	1.5	130	761.7	0.485	2.0
2.0	8.0	135	1500	0.4959	2.0
10.0	5.0	150	1500	0.4949	2.0

The water table at Site 1-42 is located at a depth of approximately 0.5 meters. Sufficient wavelengths were generated at this site to extend the shear wave velocity profile to a depth of 15 meters. The soil profile is extremely soft throughout the entire depth of the shear wave velocity profile.

2.2.2 Hotel Sapanca

Hotel Sapanca is located on the southern shore of Lake Sapanca. Its latitude and longitude coordinates are 40.6987° north and 30.2654° east, respectively. Tectonic subsidence, liquefaction-induced settlement, and lateral spreading were all observed on hotel grounds during the Kocaeli earthquake. As a result of these events, the four-story hotel was carried partially into the lake (see Figure 2.32). Lateral movements toward the lake were on the order of 2 meters and the hotel settled between 20-50 cm. These two phenomena, coupled with tectonic subsidence, resulted in movement of the shoreline inward by 30-50 meters. People fleeing the hotel after the earthquake reported water and soil "boiling out of the ground" (EERI, 2000).

Four SASW centerlines were used at this location in order to investigate the full extent of the on-shore portion of the lateral spread. The centerlines were spaced at 22.5 meters along a line oriented approximately 15 degrees west-of-north that ran from the northeast corner of the hotel to the entrance. A site map showing the locations of the SASW test arrays is shown in Figure 2.33.

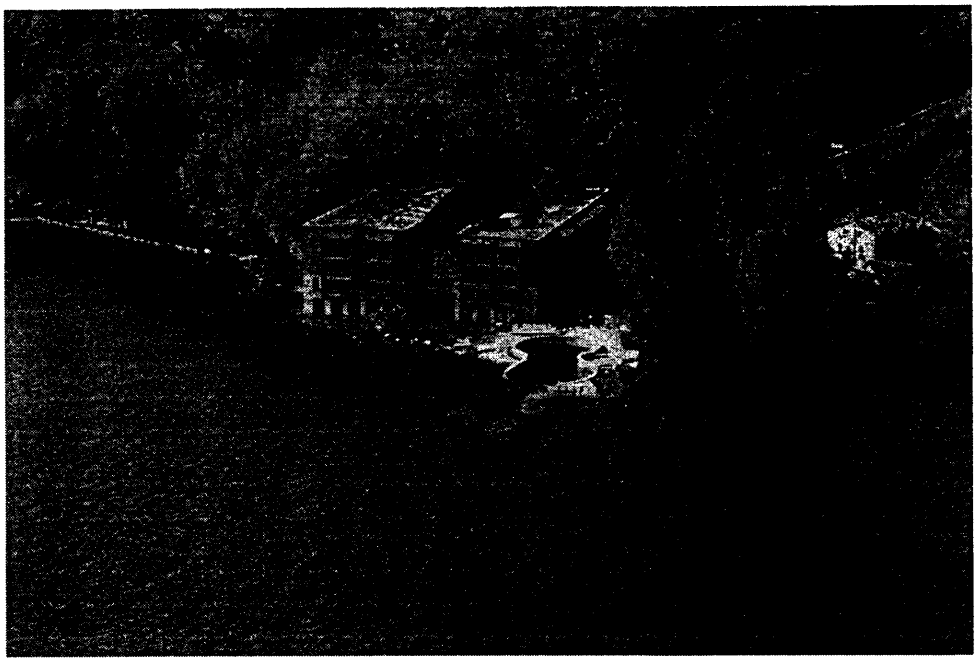

Figure 2.32 Hotel Sapanca carried partially into the lake as a result of several earthquake phenomena (from http://peer.berkeley.edu/turkey/adapazari).

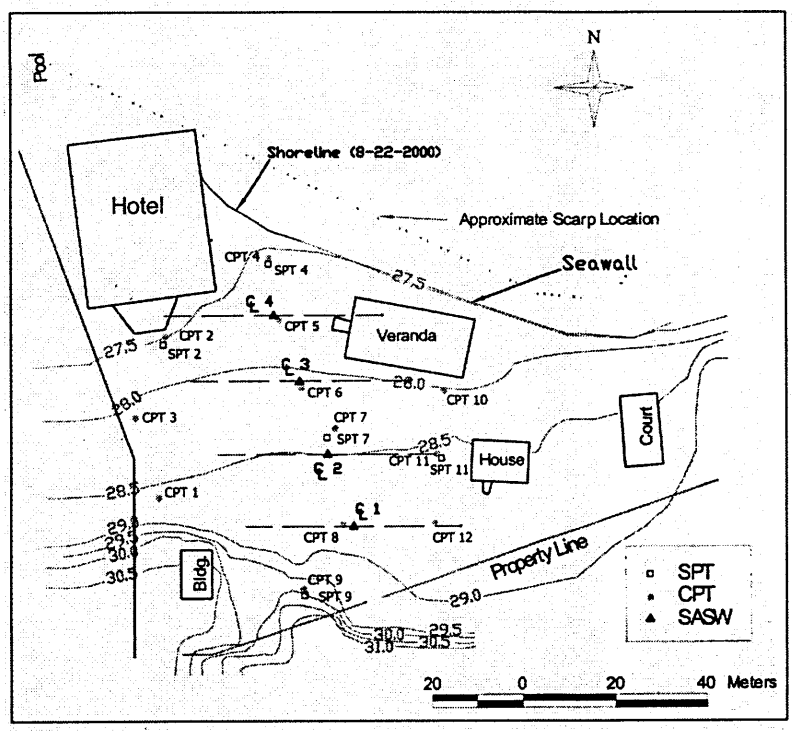

Figure 2.33 Plan view of Hotel Sapanca showing the location of four SASW centerlines (modified from http://peer.berkeley.edu/turkey/adapazari).

Figure 2.34 shows the shear wave velocity profile at Centerline 1 determined from forward modeling, and Table 2.12 presents the tabulated values of layer properties that were used to generate the theoretical dispersion curve and shear wave velocity profile.

Figure 2.35 shows the shear wave velocity profile at Centerline 2 determined from forward modeling, and Table 2.13 presents the tabulated values of layer properties that were used to generate the theoretical dispersion curve and shear wave velocity profile.

Figure 2.36 shows the shear wave velocity profile at Centerline 3 determined from forward modeling, and Table 2.14 presents the tabulated values of layer properties that were used to generate the theoretical dispersion curve and shear wave velocity profile.

Figure 2.37 shows the shear wave velocity profile at Centerline 4 determined from forward modeling, and Table 2.15 presents the tabulated values of layer properties that were used to generate the theoretical dispersion curve and shear wave velocity profile.

The water table at Hotel Sapanca ranges from a depth of approximately 0.5 meters beneath Centerline 4, to a depth of 1.25 meters beneath Centerlines 3, 2, and 1. Sufficient wavelengths were generated at this site to extend the shear wave velocity profiles to a depth of 15 meters. Each of the four shear wave velocity profiles shows soils that are very soft, with most depth intervals having velocities less than 200 m/s.

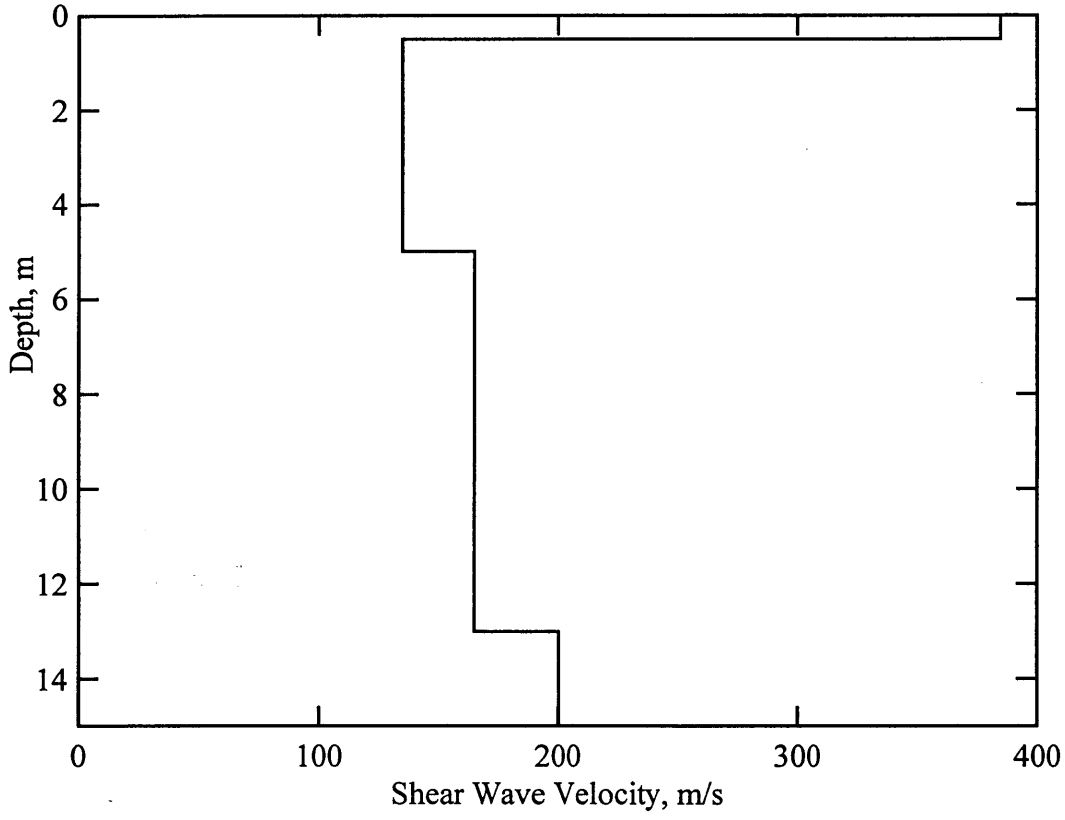

Figure 2.34 Shear wave velocity profile determined from forward modeling of Hotel Sapanca Centerline 1.

Table 2.12 Tabulated values of layer properties determined from forward modeling of Hotel Sapanca Centerline 1

			Assumed Values		
Depth to Top of Layer, m	Layer Thickness, m	Shear Wave Velocity, m/s	P-Wave Velocity, m/s	Poisson's Ratio	Mass Density, g/cc
0	0.5	385	720.3	0.3	1.92
0.5	0.75	135	330.7	0.4	1.92
1.25	3.75	135	1500	0.4959	2.0
5.0	8.0	165	1500	0.4939	2.0
13.0	2.0	200	1500	0.491	2.0

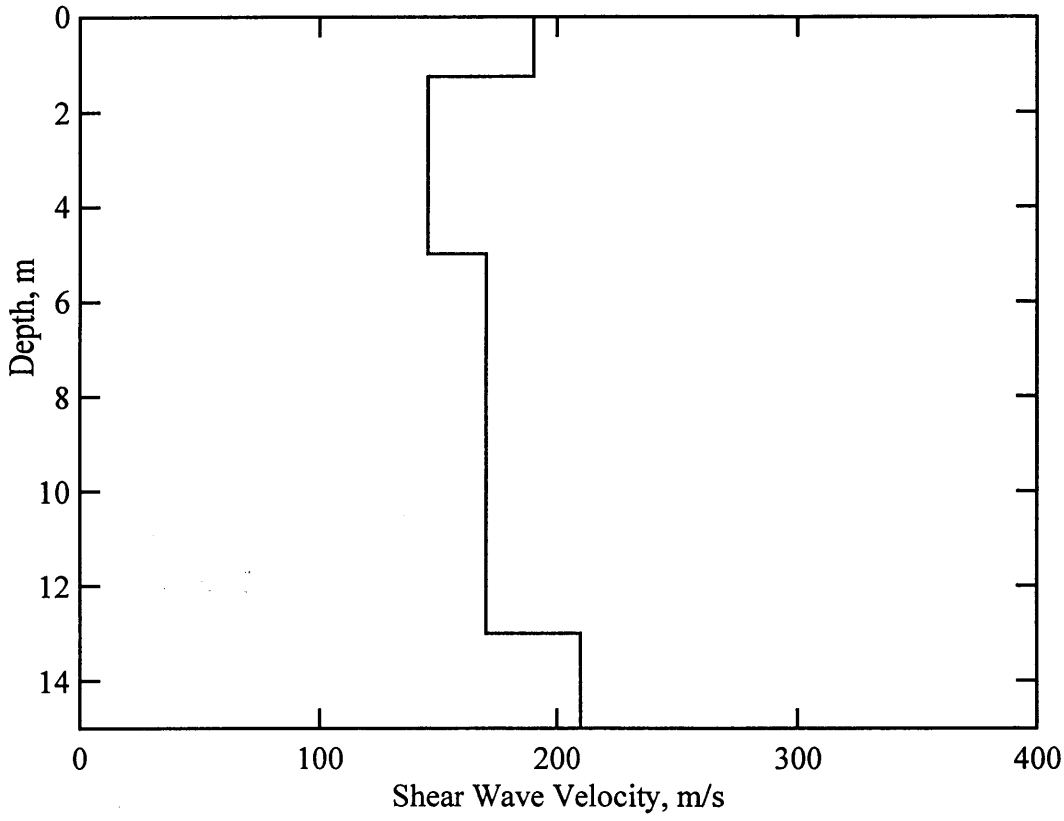

Figure 2.35 Shear wave velocity profile determined from forward modeling of Hotel Sapanca Centerline 2.

Table 2.13 Tabulated values of layer properties determined from forward modeling of Hotel Sapanca Centerline 2

			Assumed Values		
Depth to Top of Layer, m	Layer Thickness, m	Shear Wave Velocity, m/s	P-Wave Velocity, m/s	Poisson's Ratio	Mass Density, g/cc
0	1.25	190	355.5	0.3	1.92
1.25	3.75	145	1500	0.4953	2.0
5.0	8.0	170	1500	0.4935	2.0
13.0	2.0	210	1500	0.49	2.0

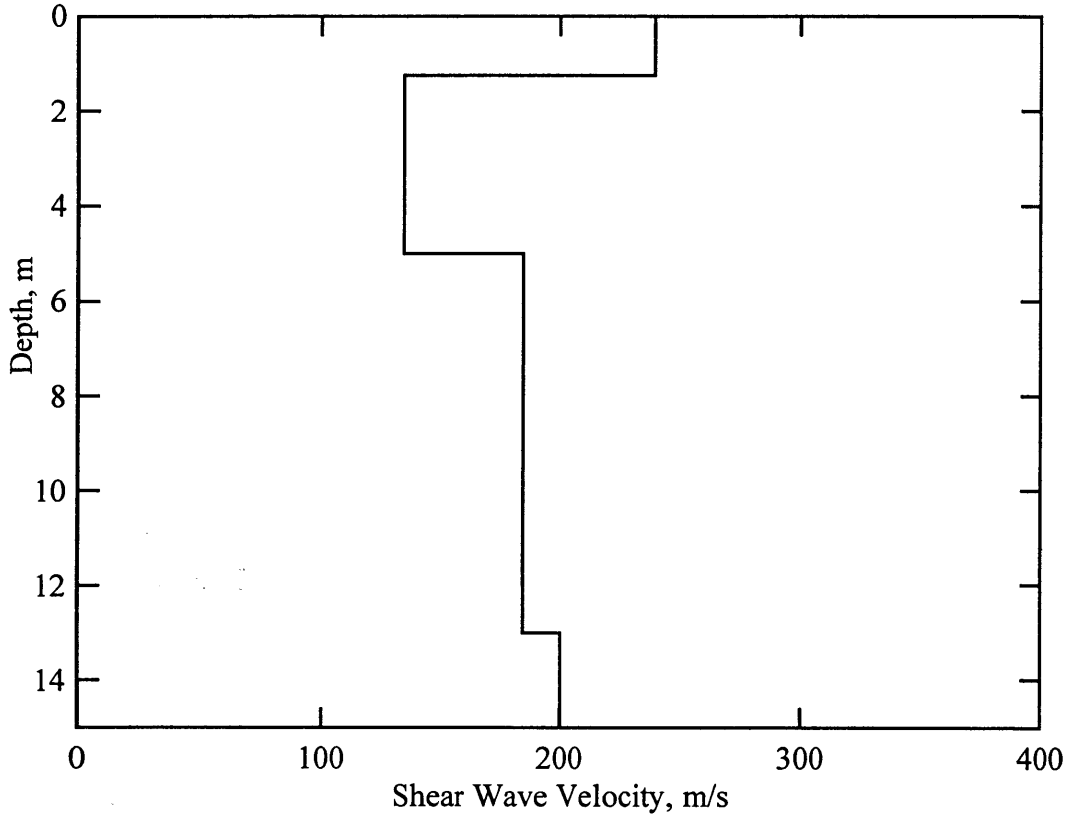

Figure 2.36 Shear wave velocity profile determined from forward modeling of Hotel Sapanca Centerline 3.

Table 2.14 Tabulated values of layer properties determined from forward modeling of Hotel Sapanca Centerline 3

			Assumed Values		
Depth to Top of Layer, m	Layer Thickness, m	Shear Wave Velocity, m/s	P-Wave Velocity, m/s	Poisson's Ratio	Mass Density, g/cc
0	1.25	240	499.6	0.35	1.92
1.25	3.75	135	1500	0.4959	2.0
5.0	8.0	185	1500	0.4923	2.0
13.0	2.0	200	1500	0.491	2.0

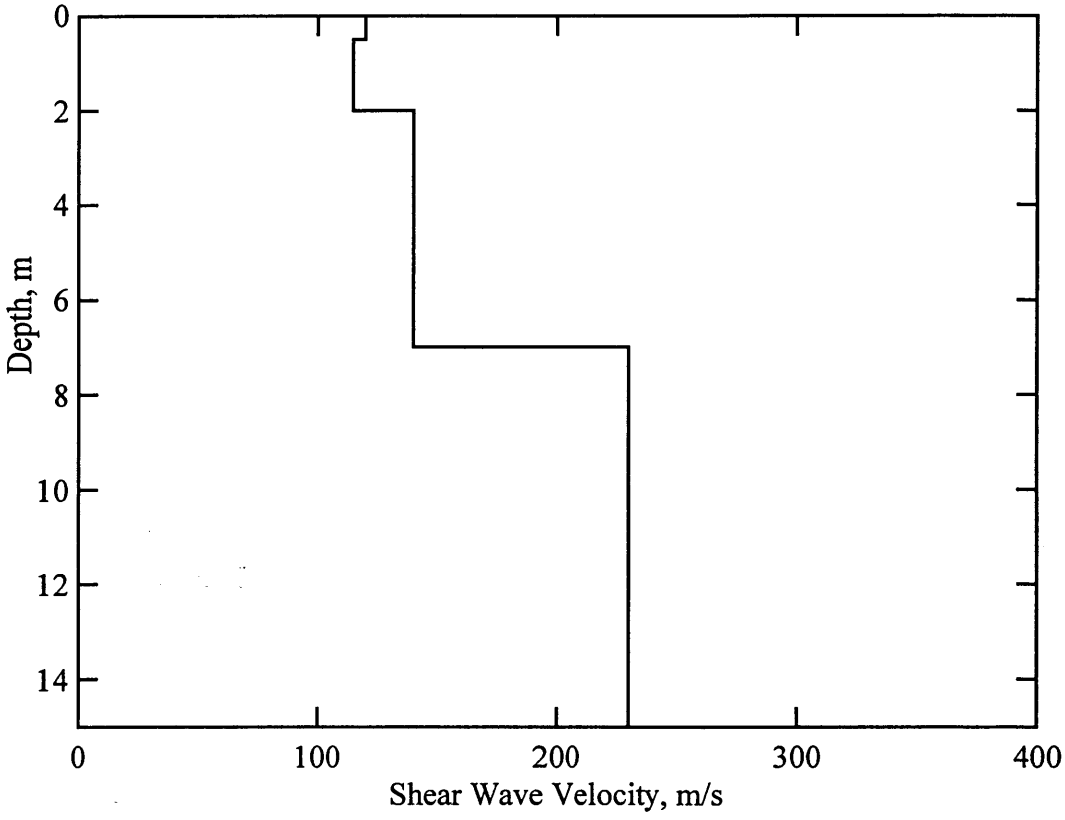

Figure 2.37 Shear wave velocity profile determined from forward modeling of Hotel Sapanca Centerline 4.

Table 2.15 Tabulated values of layer properties determined from forward modeling of Hotel Sapanca Centerline 4

			Assumed Values		
Depth to Top of Layer, m	Layer Thickness, m	Shear Wave Velocity, m/s	P-Wave Velocity, m/s	Poisson's Ratio	Mass Density, g/cc
0	0.5	120	224.5	0.3	1.92
0.5	1.5	115	1500	0.497	2.0
2.0	5.0	140	1500	0.4956	2.0
7.0	8.0	230	1500	0.488	2.0

2.2.3 Izmit Bay

Numerous coastal failures occurred along the Marmara coast on the north, east, and south shores of Izmit Bay. These failures ranged from minor lateral spreading in the free field to catastrophic stability failures that carried buildings and people into the bay. In addition to liquefaction-related failures, major coastal subsidence also occurred in the Golcuk area (EERI, 2000). Four liquefaction-induced lateral spread sites located in this region will be discussed below. Refer back to Figure 3.4 for site locations.

2.2.3.1 Degirmendere Nose Degirmendere Nose is located on the south shore of Izmit Bay in Degirmendere. Its latitude and longitude coordinates are 40.7219° north and 29.7820° east, respectively. A plan view of Degirmendere Nose is shown in Figure 2.38. This map also shows the SASW centerline location with respect to the SPT and CPT test locations. The largest and most devastating coastal stability failure occurred here. A large section of fill, along with a hotel and two restaurants, was carried into the bay. Notice the former shoreline and new shoreline designations in Figure 2.38. Figure 2.39 is an aerial view of the site that shows a barge-mounted crane searching for the remains of those who died in the hotel. The cause of this enormous failure is not fully understood. Small lateral spread cracks were observed along the on-shore part of the failure behind a large head scarp. Figure 2.40 shows the shear wave velocity profile at the site determined from forward modeling, and Table 2.16 presents the tabulated values of layer properties that were used to generate the theoretical dispersion curve and shear wave velocity profile.

The water table at Degirmendere Nose is located at a depth of approximately 1.5 meters. Sufficient wavelengths were generated at this site to extend the shear wave velocity profile to a depth of 15 meters. The majority of the soil profile here consists of soils that have a shear wave velocity of 200 m/s.

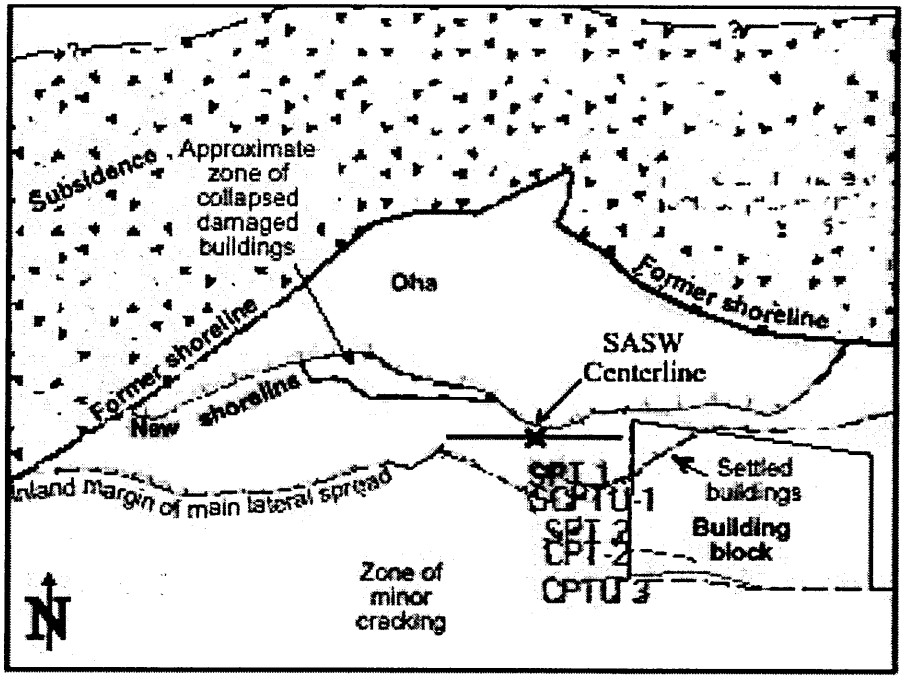

Figure 2.38 Plan view of Degirmendere Nose showing the location of one SASW centerline (modified from http://peer.berkeley.edu/turkey/adapazari).

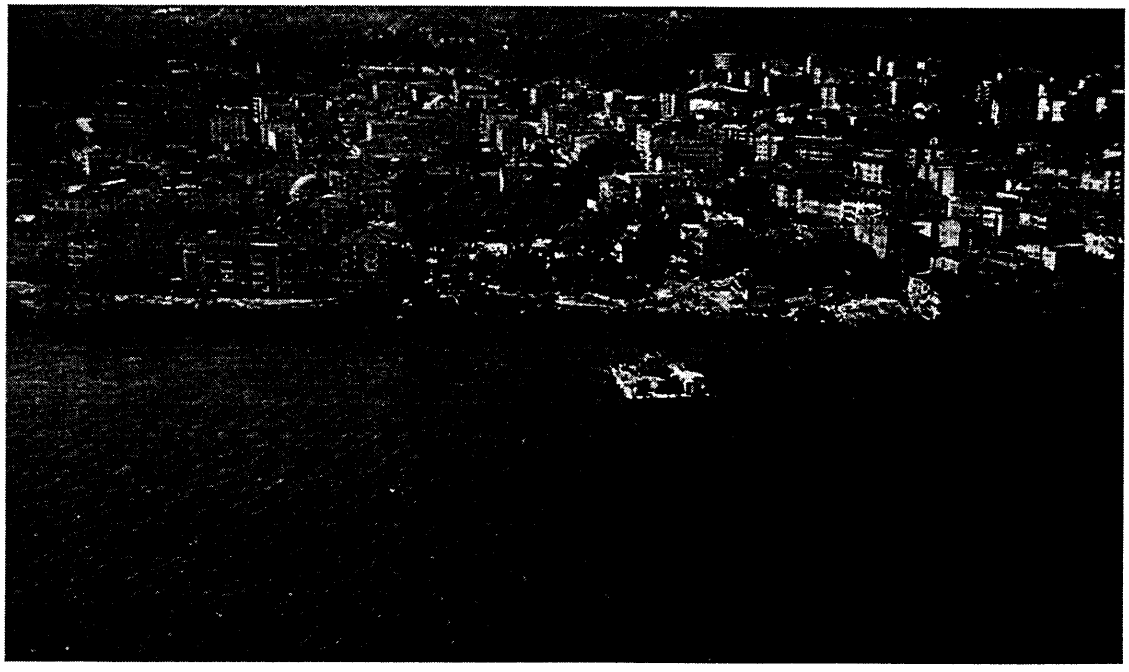

Figure 2.39 Photograph showing the barge-mounted crane that was used to search for the remains of people carried into the bay at Degirmendere Nose (from http://peer.berkeley.edu/turkey/adapazari).

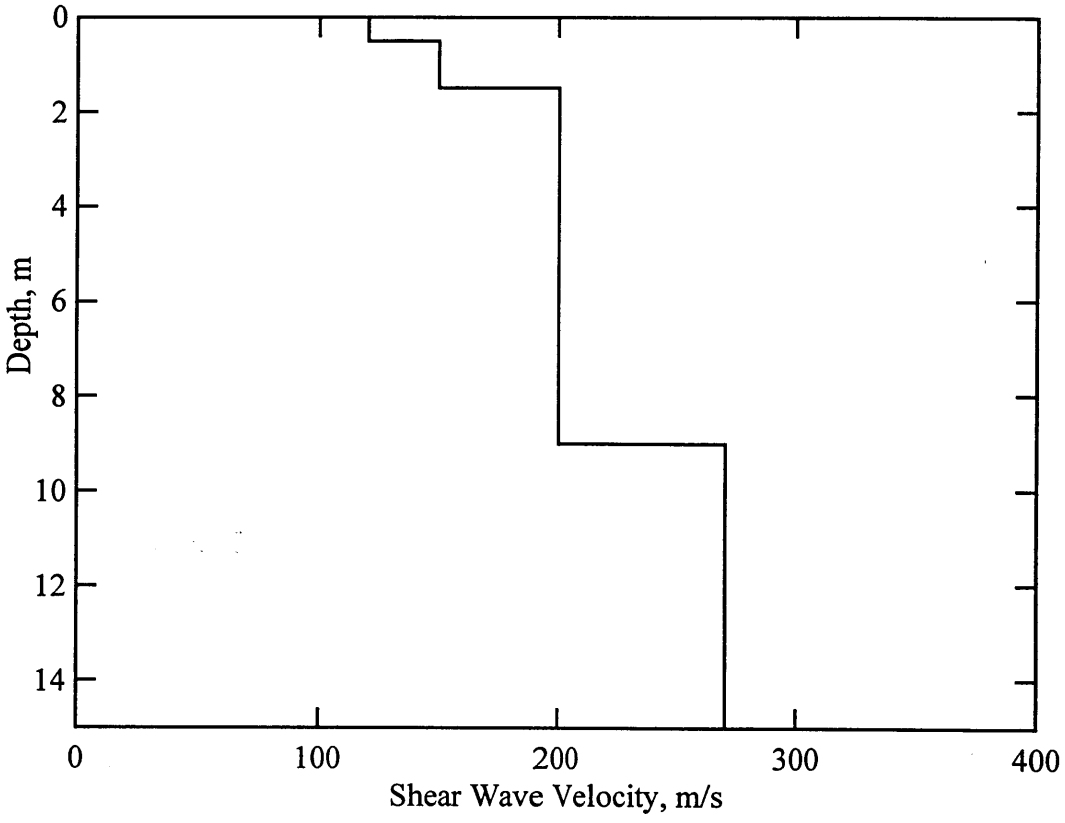

Figure 2.40 Shear wave velocity profile determined from forward modeling of Degirmendere Nose.

Table 2.16 Tabulated values of layer properties determined from forward modeling of Degirmendere Nose

			Assumed Values		
Depth to Top of Layer, m	Layer Thickness, m	Shear Wave Velocity, m/s	P-Wave Velocity, m/s	Poisson's Ratio	Mass Density, g/cc
0	0.5	120	224.5	0.3	1.92
0.5	1.0	150	280.6	0.3	1.92
1.5	7.5	200	1500	0.491	2.0
9	6.0	270	1500	0.4833	2.0

2.2.3.2 Police Station Police Station is a lateral spread site at the eastern end of Izmit Bay. The reason this site is designated as Police Station is obscure, as there are no nearby police stations. Its latitude and longitude coordinates are 40.7215° north and 29.9373° east, respectively. A plan view of Police Station is shown in Figure 2.41. This map also shows the SASW centerline location with respect to the SPT and CPT test locations. This site is directly adjacent to where the fault surface rupture exits the eastern end of Izmit Bay. No structures are located nearby. Figure 2.42 shows a picture of the large ground cracking that occurred here. Some evidence of liquefaction ejecta was also observed. Figure 2.43 shows the shear wave velocity profile at the site determined from forward modeling, and Table 2.17 presents the tabulated values of layer properties that were used to generate the theoretical dispersion curve and shear wave velocity profile.

The water table at Police Station is located at a depth of approximately 1.0 meter. Sufficient wavelengths were generated at this site to extend the shear wave velocity profile to a depth of 20 meters. Two extremely soft soil layers were identified here between the depths of 1.5 – 16 meters.

2.2.3.3 Soccer Field Soccer Field is another lateral spread site located along the south shore of Izmit Bay. Its latitude and longitude coordinates are 40.7177° north and 29.9273° east respectively. A plan view of Soccer Field showing the approximate location of the SASW centerline is shown in Figure 2.44. The site is a small soccer field where large ground cracks occurred due to lateral spreading into the Bay. A photograph of the site is shown in Figure 2.45. Figure 2.46 shows the shear wave velocity profile at the site determined from forward modeling, and Table 2.18 presents the tabulated values of layer properties that were used to generate the theoretical dispersion curve and shear wave velocity profile.

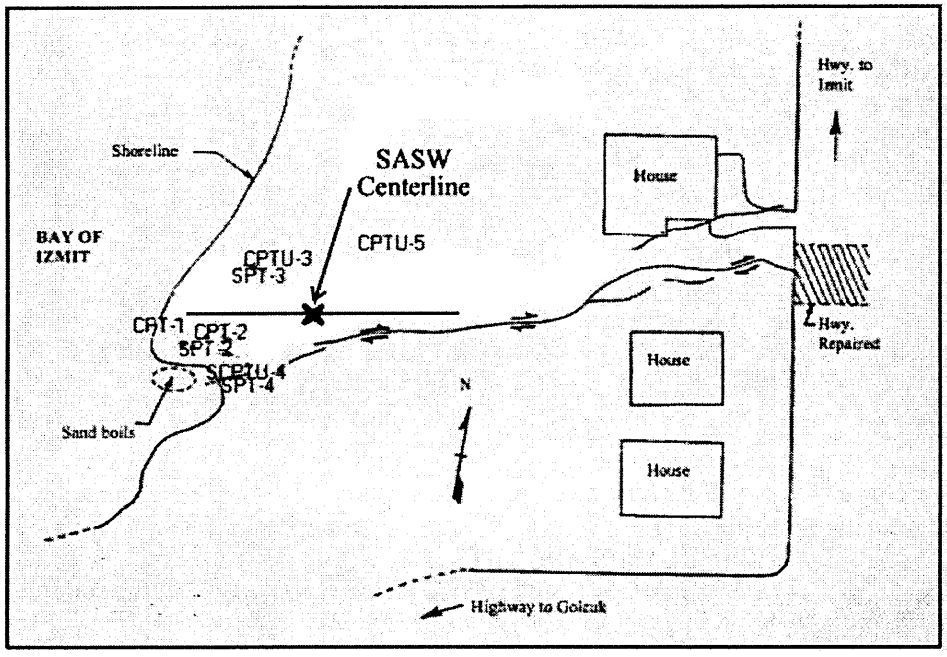

Figure 2.41 Plan view of Police Station showing the location of one SASW centerline (modified from http://peer.berkeley.edu/turkey/adapazari).

Figure 2.42 Photograph showing the large ground cracking that occurred at Police Station during the earthquake. The surface fault rupture exits the bay near here.

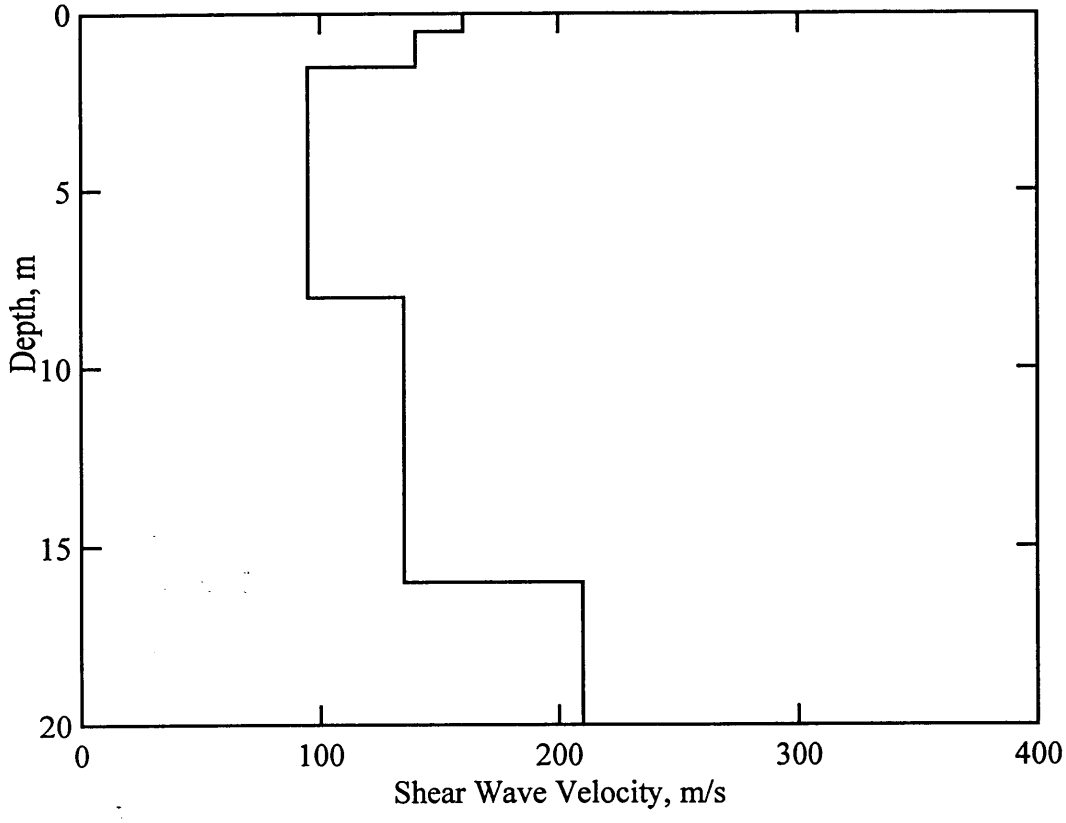

Figure 2.43 Shear wave velocity profile determined from forward modeling of Police Station.

Table 2.17 Tabulated values of layer properties determined from forward modeling of Police Station

			Assumed Values		
Depth to Top of Layer, m	Layer Thickness, m	Shear Wave Velocity, m/s	P-Wave Velocity, m/s	Poisson's Ratio	Mass Density, g/cc
0.0	0.5	160	299.3	0.3	1.92
0.5	0.5	140	216.9	0.3	1.92
1.0	0.5	140	820.3	0.485	2.0
1.5	6.5	95	1500	0.498	2.0
8.0	8.0	135	1500	0.4959	2.0
16.0	4.0	210	1500	0.49	2.0

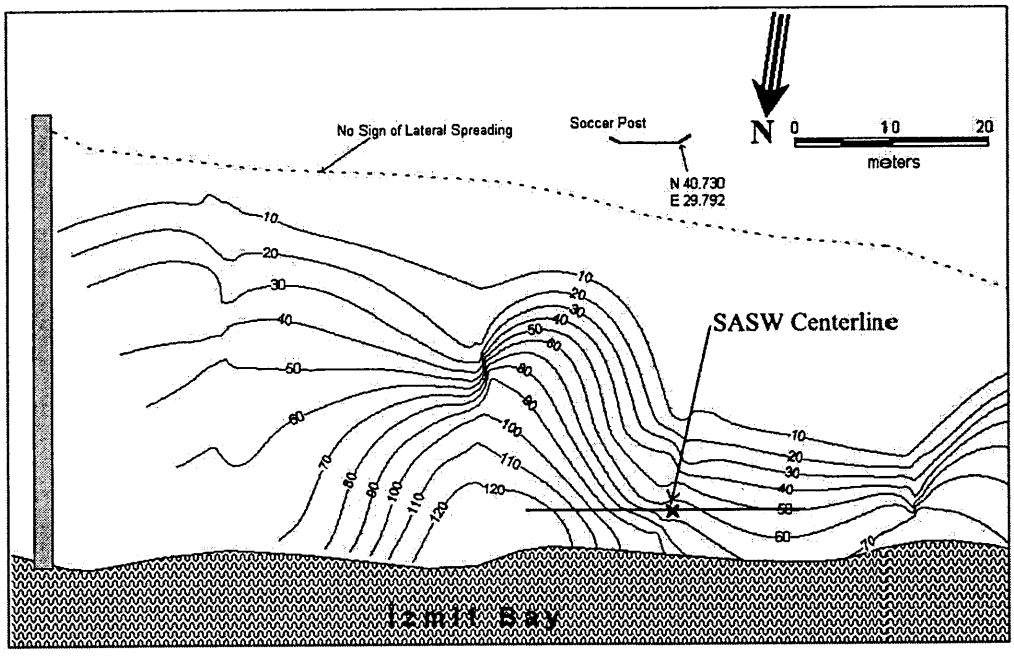

Figure 2.44 Plan view of Soccer Field showing the location of one SASW centerline (modified from http://peer.berkeley.edu/turkey/adapazari).

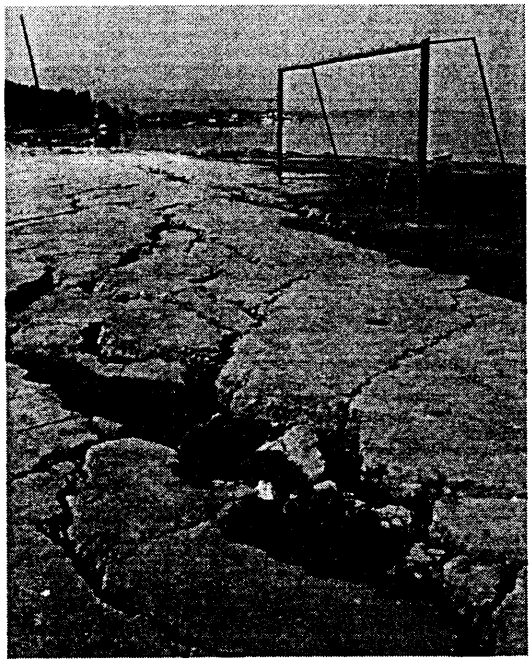

Figure 2.45 Photograph showing the ground cracks caused by lateral spreading into Izmit Bay at Soccer Field (from http://peer.berkeley.edu/turkey/adapazari).

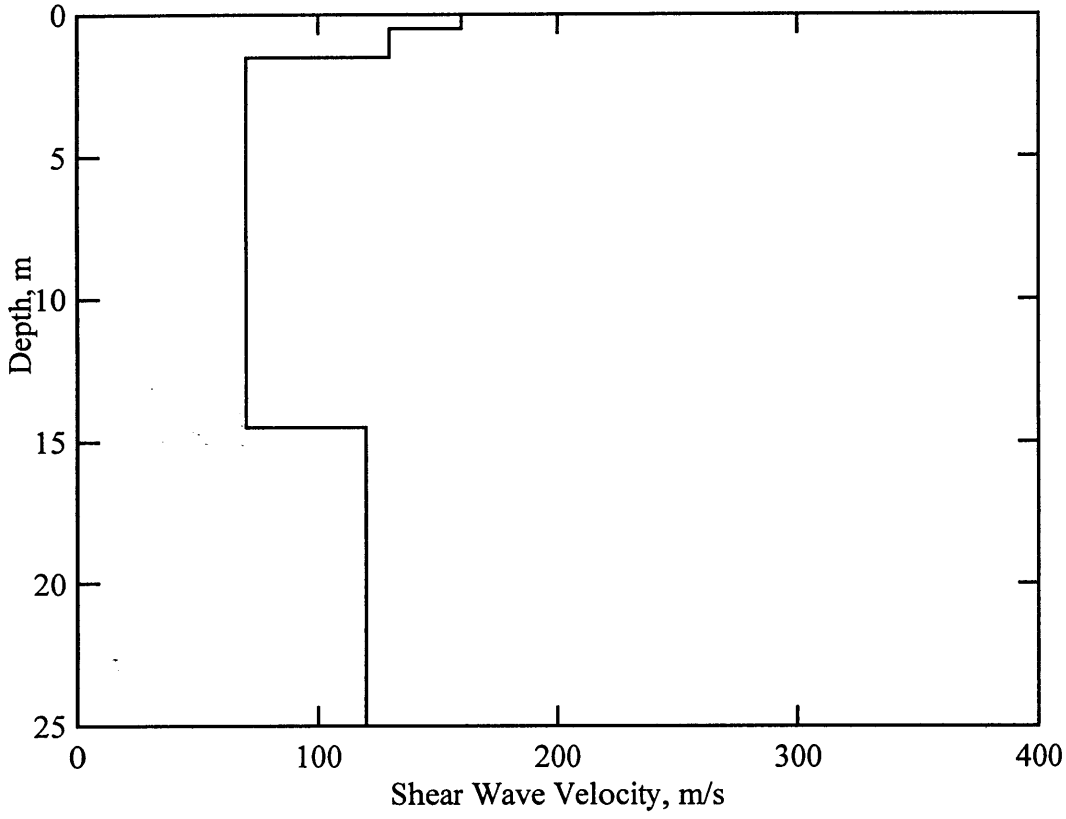

Figure 2.46 Shear wave velocity profile determined from forward modeling of Soccer Field.

Table 2.18 Tabulated values of layer properties determined from forward modeling of Soccer Field

			Assumed Values		
Depth to Top of Layer, m	Layer Thickness, m	Shear Wave Velocity, m/s	P-Wave Velocity, m/s	Poisson's Ratio	Mass Density, g/cc
0	0.5	160	299.3	0.3	1.92
0.5	0.5	130	318.4	0.4	1.92
1.0	0.5	130	477.7	0.46	2.0
1.5	13.0	70	1500	0.4978	2.0
14.5	10.5	120	1500	0.4968	2.0

The water table at Soccer Field is located at a depth of approximately 1.0 meter. Sufficient wavelengths were generated at this site to extend the shear wave velocity profile to a depth of 25 meters. This site contains the softest soil encountered during SASW testing in Turkey. A 13-meter thick layer of soil having a shear wave velocity of 70 m/s is located between the depths of 1.5 – 14.5 meters

2.2.3.4 Yalova Harbor Yalova Harbor is located on the southern shore of Izmit Bay in the town of Yalova. Its latitude and longitude coordinates are 40.6597° north and 29.2689° east, respectively. A plan view of Yalova Harbor is shown in Figure 2.47. This map also shows the SASW centerline location with respect to the SPT and CPT test locations. This site is the westernmost area where liquefaction evidence was observed. Lateral spread cracking was observed in both the cobblestone and paved parking areas at the Harbor. The photograph in Figure 2.48 shows one of the large cracks that occurred in the paved parking area. Figure 2.49 shows the shear wave velocity profile at the site determined from forward modeling, and Table 2.19 presents the tabulated values of layer properties that were used to generate the theoretical dispersion curve and shear wave velocity profile.

The water table at Yalova Harbor is located at a depth of approximately 0.75 meters. Sufficient wavelengths were generated at this site to extend the shear wave velocity profile to a depth of 10 meters. The top layer shows the stiff cobblestone crust. The remainder of the soil profile is extremely soft.

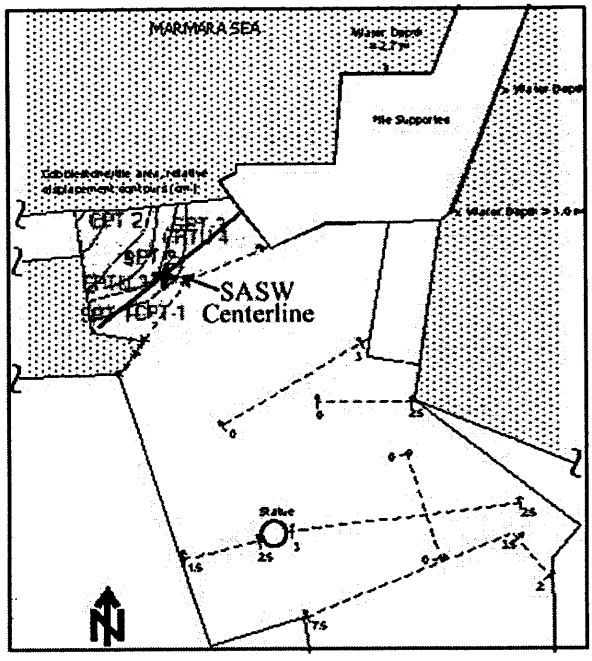

Figure 2.47 Plan view of Yalova Harbor showing the location of one SASW centerline (modified from http://peer.berkeley.edu/turkey/adapazari).

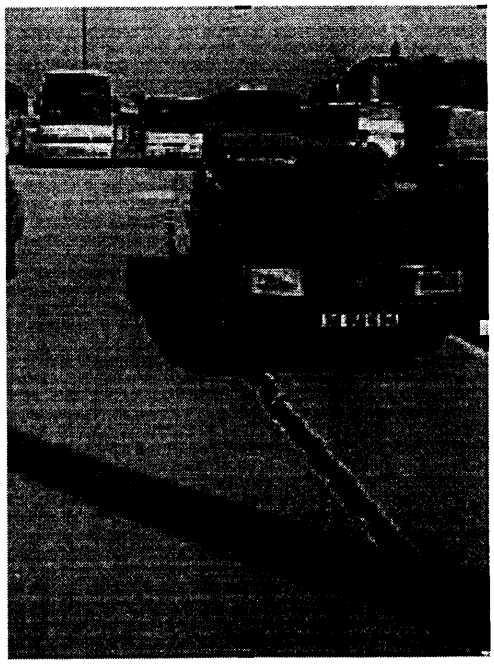

Figure 2.48 Photograph showing a lateral spread crack that developed in the paved parking area at Yalova Harbor. The cobblestone parking area was also damaged (from http://peer.berkeley.edu/turkey/adapazari).

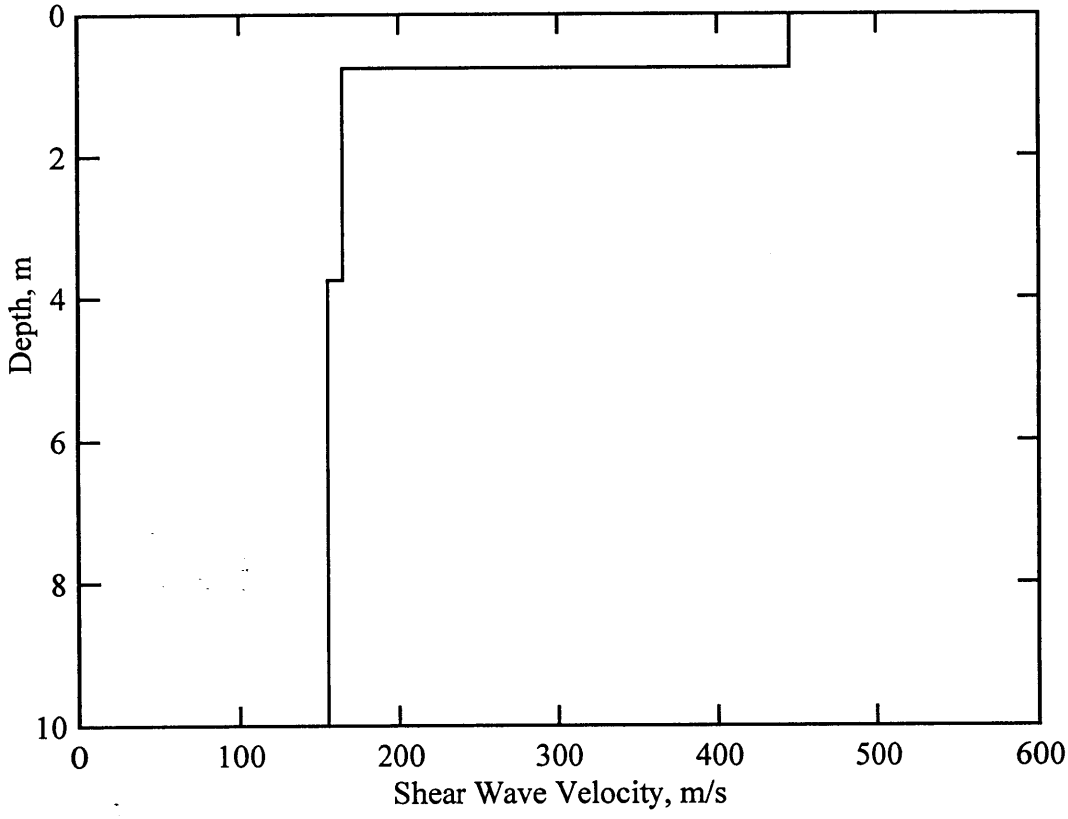

Figure 2.49 Shear wave velocity profile determined from forward modeling of Yalova Harbor.

Table 2.19 Tabulated values of layer properties determined from forward modeling of Yalova Harbor

			Assumed Values		
Depth to Top of Layer, m	Layer Thickness, m	Shear Wave Velocity, m/s	P-Wave Velocity, m/s	Poisson's Ratio	Mass Density, g/cc
0.0	0.75	445	832.5	0.3	1.92
0.75	3.0	165	1500	0.4939	2.0
3.75	6.25	155	1500	0.4946	2.0

CHAPTER 3

LIQUEFACTION ANALYSIS PROCEDURES

3.1 INTRODUCTION

Chapter 2 presented site descriptions and shear wave velocity profiles for the liquefaction sites that were tested after the 1999 Kocaeli, Turkey earthquake. This chapter focuses on the procedures used to determine which soil layers most likely participated in liquefaction at each site. The first step in this process was to delineate a potentially liquefiable region at each site. This was accomplished through use of the simplified shear wave velocity method (Andrus et al., 2001). All depths within the soil profile where the cyclic stress ratio (CSR) is greater that the soil cyclic resistance ratio (CRR) were considered potentially liquefiable, meaning that the soil was soft enough to liquefy. However, soil stiffness alone does not control liquefaction. Therefore, the second step in determining which soil layers most likely liquefied was to separate liquefiable soils from nonliquefiable soils. At sites where actual soil samples were available, this was accomplished by using the Chinese Criteria (Seed and Idriss, 1982) and the Andrews and Martin Criteria (Andrews and Martin, 2000). At sites where only CPT data were available, this was accomplished by determining the soil behavior type index (I_C) (Robertson and Wride, 1998).

3.2 THE V_S-BASED SIMPLIFIED PROCEDURE

The simplified shear wave velocity (V_s) procedure requires the calculation of two parameters in order evaluate liquefaction susceptibility (Andrus and Stokoe, 2000). These are, 1, the level of cyclic loading caused by the earthquake expressed as a CSR, and 2, the resistance of the soil to liquefaction expressed as a CRR. This section addresses the calculation of these parameters.

3.2.1The Cyclic Stress Ratio (CSR)

CSR represents the ratio of shear stress induced by earthquake shaking to vertical effective stress in the soil. In the V_s simplified procedure, CSR is calculated using the same approach as the original simplified liquefaction analysis procedure developed by Seed and Idriss (1971). This approach has been updated the 1996 NCEER workshop on liquefaction assessment (Youd and Idriss 2001). The equation to calculate CSR is:

$$CSR = \frac{\tau_{av}}{\sigma'_{vo}} = 0.65\left(\frac{a_{max}}{g}\right)\left(\frac{\sigma_{vo}}{\sigma'_{vo}}\right)r_d, \qquad \text{(Eq. 3.1)}$$

where: CSR = cyclic stress ratio,
τ_{av} = average shear stress in the soil profile,
a_{max} = peak horizontal ground surface acceleration,
g = acceleration of gravity,
σ_{vo} = initial total vertical overburden stress,
σ'_{vo} = initial effective vertical overburden stress,
r_d = stress reduction coefficient which accounts for the flexibility of the soil profile.

3.2.2 The Cyclic Resistance Ratio (CRR)

CRR represents the CSR that is required to cause liquefaction in a given soil. CRR is a function of the soil properties, and the magnitude of earthquake. Higher magnitude earthquakes induce more cycles of shaking than lower magnitude earthquakes, hence, larger magnitude earthquakes will induce liquefaction at a lower CSR than a lower magnitude earthquake (Youd and Idriss 2001). CRR can be estimate using standard penetration testing, cone penetration testing, and shear wave velocity. The shear wave velocity is employed herein.

3.2.2.1 Corrected Shear Wave Velocities For a sand of constant void ratio, the shear wave velocity will increase with depth because of the effects of increased effective confining pressure. Hence, it is believed that a correlation between CRR and V_S should be based upon shear wave velocities that have been normalized with respect to effective overburden pressure (Robertson, Woeller, and Finn, 1992). This suggestion is in harmony with the tradition of normalizing penetration-based resistance parameters due to

overburden pressure. Robertson, Woeller, and Finn (1992) have suggested the following equation for calculating the normalized shear wave velocity (V_{S1}):

$$V_{S1} = (V_S)(C_V) = V_S\left(\frac{P_a}{\sigma'_{vo}}\right)^{0.25} \qquad \text{(Eq. 3.2)}$$

where: V_{S1} = normalized shear wave velocity, in meters per second,
V_S = shear wave velocity, in meters per second,
C_v = factor to correct measured shear wave velocity for overburden pressure,
P_a = reference stress of 100 kPa (approximately one atmosphere)
σ'_{vo} = initial effective vertical overburden stress, in kPa.

NCEER Workshop participants also recommend this equation for correcting V_S (Youd and Idriss, 2001). Andrus et al. (2001) suggests limiting C_v to a maximum value of 1.4 at shallow depths. In applying Eq. 3.2 it is implicitly assumed that the effective stress ratio, K'_o, is approximately equal to 0.5 (Andrus and Stokoe, 2000).

3.2.2.2 The V_S-Based Cyclic Resistance Ratio Both V_S and CRR are similarly influenced by soil density, overburden pressure, stress history, geologic age, and soil type and fabric (Robertson et al, 1992; Kayabali, 1996; Yamamoto et al., 2000). Several researchers have developed relationships between V_S and CRR (Dobry et al., 1982), (Tokimatsu and Uchida, 1990), (Robertson, et al, 1992), (Kayen et al., 1992), (Lodge 1994), (Andrus and Stokoe, 1997), and (Andrus, et al., 1999). The relationship developed by Andrus, et al. (1999) is the relationship recommended by the 1996 NCEER workshop (Youd and Idriss, 2001)

The relationships developed by Andrus, et al. (1999) are shown in Figure 3.1. These relationships can be described using the following equation:

$$CRR = MSF\left(0.022\left(\frac{V_{S1}}{100}\right)^2 + 2.8\left(\left(\frac{1}{V^*_{S1} - V_{S1}}\right) - \left(\frac{1}{V^*_{S1}}\right)\right)\right) \quad \text{(Eq. 3.3)}$$

where: CRR = cyclic resistance ratio,
MSF = magnitude scaling factor to account for the effect of earthquake magnitude (described below),
V_{S1} = normalized shear wave velocity,
V^*_{S1} = limiting upper value of V_{S1} for cyclic liquefaction occurrence (described below).

The magnitude scaling factor recommended by the 1996 NCEER is (Youd and Idriss, 2001):

$$MSF = \left(\frac{M_W}{7.5}\right)^{-2.56} \quad \text{(Eq. 3.4)}$$

where: MSF = magnitude scaling factor,
M_W = moment magnitude of earthquake.

The limiting upper value of V_{S1} for liquefaction occurrence, V^*_{S1} is dependent upon fines content. these values are (Andrus et al. 2001):

$V^*_{S1} = 215$ m/s for sands with FC < 5% (Eq. 3.5a)
$V^*_{S1} = 215 - 0.5(FC-5)$ m/s for sands with 5% < FC < 35% (Eq. 3.5b)
$V^*_{S1} = 200$ m/s for sands and silts with FC > 35% (Eq. 3.5c)

where: V^*_{S1} = limiting upper value of V_{S1} for cyclic liquefaction occurrence, in meters per second,
FC = average fines content of the soil, in percent by mass.

When the CSR generated earthquake shaking exceeds the CRR, then the soil will be likely to experience liquefaction.

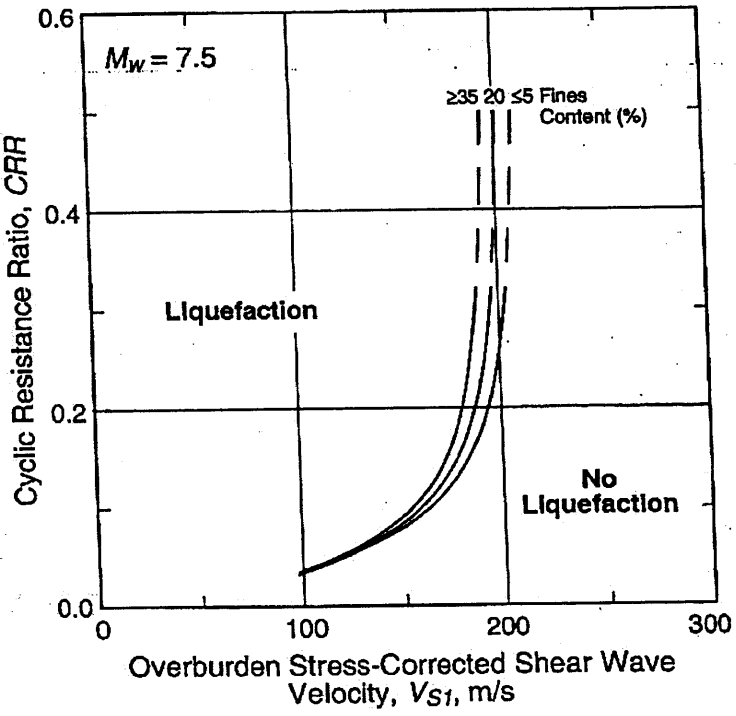

Figure 3.1 Curves with various fines contents recommended for calculation of CRR from V_{S1} (after Andrus, et al., 1999).

3.3 Methodology for Obtaining Site Accelerations

In order to calculate CSR's an estimate of peak ground surface acceleration must first be made. Traditionally ground accelerations at liquefaction sites have been predicted using attenuation relationships that were developed from large databases of recorded earthquake ground-motions. However, prior to the 1999 Kocaeli earthquake, there were fewer than 10 ground-motion records for moment magnitude (M_W) 7.0 or greater earthquakes recorded within 20 kilometers of the fault rupture throughout the world. Distances less than approximately 20 kilometers from the fault rupture have been termed the "near-field." Six near-field Strong Motion Stations (SMS's) recorded ground-motions during the Kocaeli earthquake (EERI, 2000). Five of these stations are located in close proximity to the liquefaction sites. These five SMS's are Sakarya (SKR), Izmit (IZT), Yarimca (YPT), Gebze (GBZ), and Arcelik (ARC). A map showing the locations

of test sites and SMS's is shown in Figure 3.2. Figure 3.3 compares the geometric mean of the recorded maximum horizontal acceleration at these stations with rock attenuation relationships as proposed by various researchers for $M_W = 7.4$ earthquakes. This figure has been modified from EERI (2000) to reflect the most recent distances from SMS's to the surface fault rupture as provided by Rathje (2001). It can be seen that current attenuation relationships over-predict the measured near-field ground accelerations from the Kocaeli earthquake.

All of the liquefaction sites discussed in Chapter 2, with the exception of Yalova Harbor, are located within 10 km of the surface fault rupture. Yalova Harbor is located within 25 km. Thus, all of the liquefaction case histories discussed in this paper are located within the near-field region. Therefore, ground accelerations at these liquefaction sites cannot simply be estimated from current attenuation relationships.

Clearly, the best method for obtaining ground accelerations at these sites is to use recorded ground-motions from the nearby stations. However, all of the liquefaction sites are located on soft soil and the near-field SMS's range from soft soil to rock site classifications. Additionally, distances from the fault to the liquefaction sites are not equal to the distances from the fault to the SMS's. These concerns necessitated correcting each recorded ground motion for both site classification and distance. To complicate matters further, rupture directivity also strongly influenced recorded near-field motions.

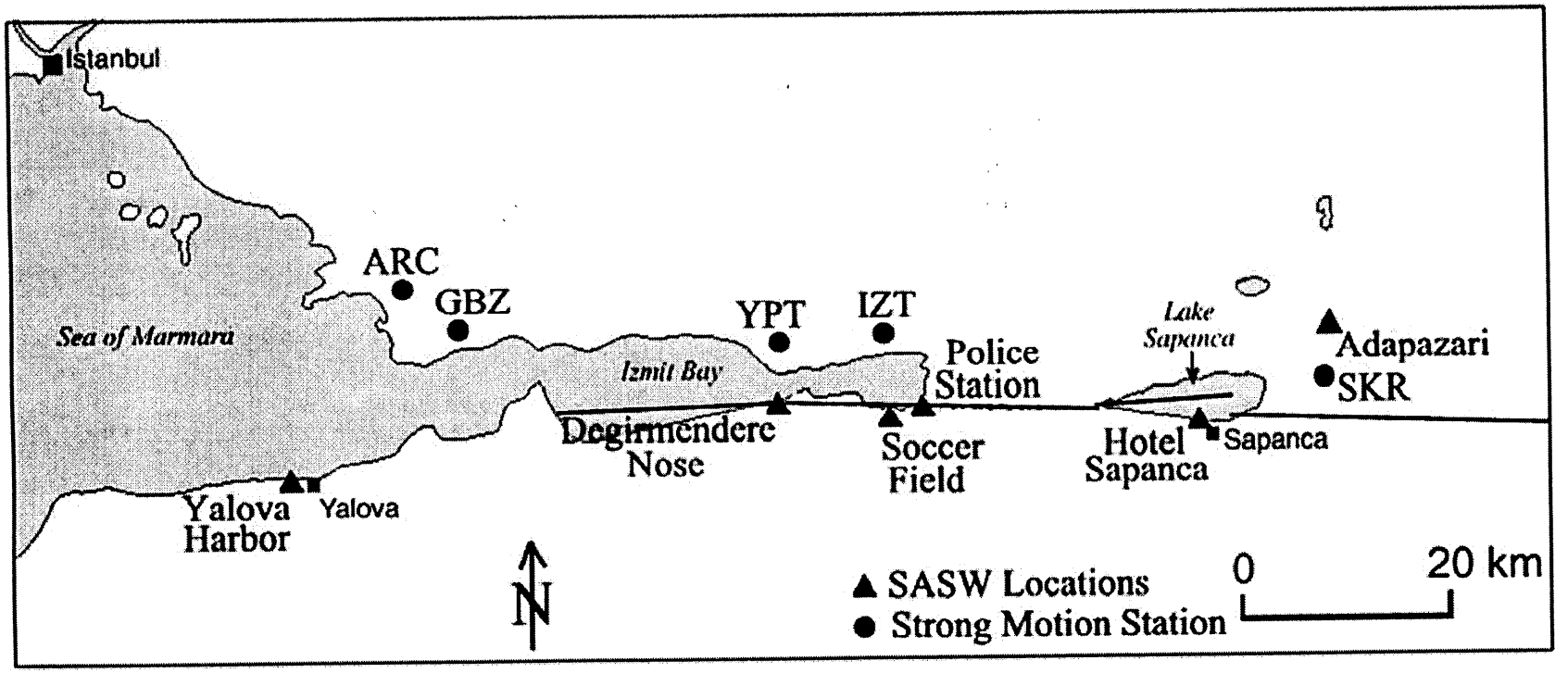

Figure 3.2 Locations of five near-field strong motion stations in relation to the SASW liquefaction test sites. Also shown is the approximate location of the surface fault rupture (modified from http://peer.berkeley.edu/turkey/adapazari).

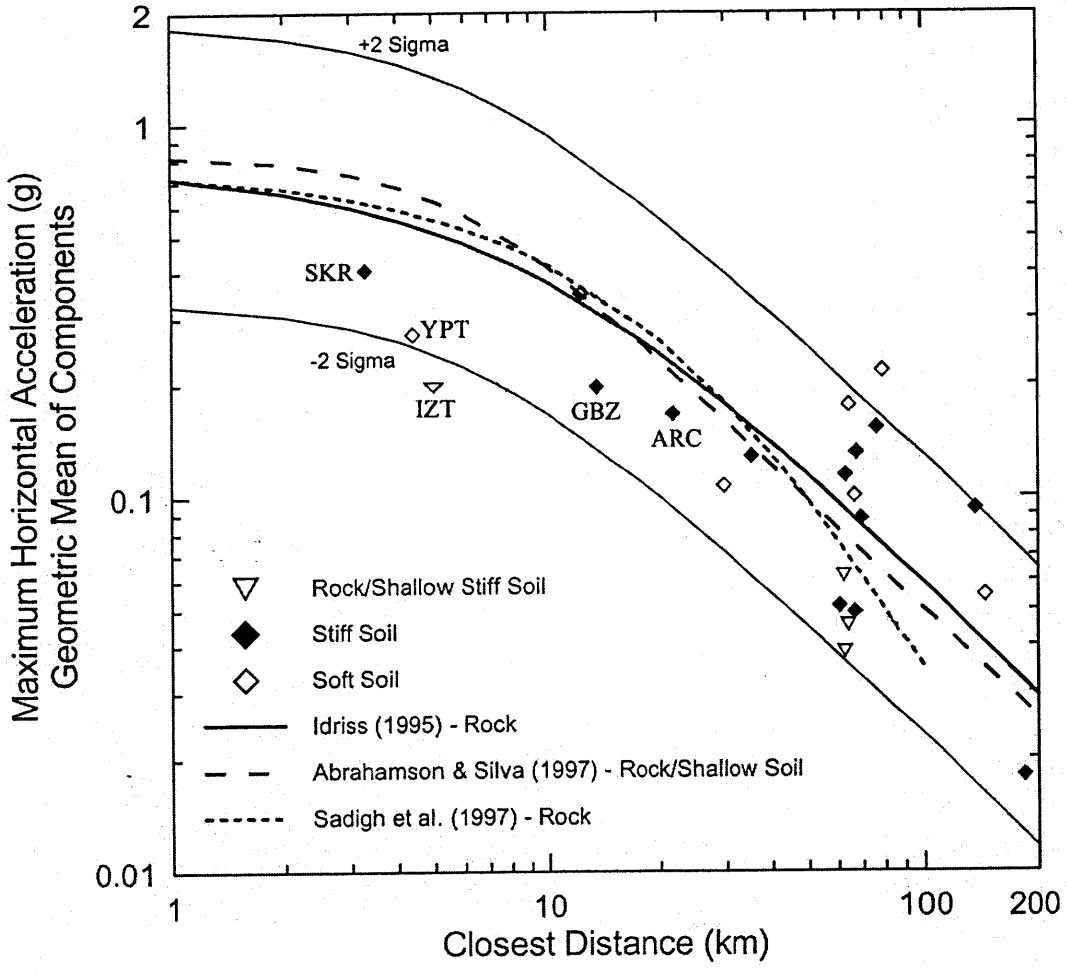

Figure 3.3 Comparison between the geometric mean of the recorded horizontal acceleration at the strong motion stations and rock attenuation relationships proposed by various researchers for M_W = 7.4 earthquakes (modified from EERI, 2000).

In order to account for this variation, each liquefaction site was paired with the nearest SMS, or SMS's, that recorded the Kocaeli earthquake. These parings are presented in Table 3.1. All of the distances shown in Table 3.1 were measured from the specified location to the closest vertical projection of the surface fault rupture. Fault rupture segment coordinates and the most recent distances to all SMS's were provided by Rathje (2001). Magnitudes of the recorded ground surface accelerations, and site classifications at each SMS, were obtained from EERI (2000). If the SMS was not located on a rock site, then the geometric mean of the recorded peak horizontal ground surface acceleration was converted to an estimated rock site acceleration by scaling off values from the graph proposed by Idriss as shown in Figure 3.4 (Kramer, 1996). This curve provides a rough relationship between rock accelerations and soft soil accelerations. Accelerations from SMS's located on stiff soil were converted to estimated rock accelerations by using values halfway between the 1-to-1 curve and the relationships from Figure 3.4 to account for the rate of acceleration attenuation (not the magnitude) over the distance separating the liquefaction site and the paired SMS. The curve by Sadigh et al. (EERI, 2000) was used to obtain predicted rock accelerations at the SMS distance and the liquefaction site distance. These values were then converted into a ratio by dividing the predicted liquefaction site rock acceleration by the predicted SMS rock acceleration. If the liquefaction site was closer to the fault than the SMS, then this ratio was greater than 1, if not, it was less than 1. An estimation of the rock acceleration at the liquefaction site was then obtained by multiplying the estimated rock acceleration at the SMS by the ratio of site-to-SMS predicted rock acceleration. Estimated rock accelerations at the liquefaction sites were then converted to estimated soft soil accelerations by using Figure 3.4.

Table 3.1 Methodology used to obtain estimated soft soil accelerations at each liquefaction site

Liquefaction Sites	Distance [1] from Fault to Site (km)	Nearest [2] Strong Motion Stations (SMS)	Distance [1] from Fault to SMS (km)	Recorded [3] Geometric Mean of PGA at SMS (g)	SMS [3] Site Class	Estimated [4] Rock Acceleration at SMS (g)	Predicted [5] Rock Acceleration at SMS (g)	Predicted [5] Rock Acceleration at Site (g)	Ratio of [6] Site-to-SMS Predicted Rock Accelerations	Estimated [7] Rock Acceleration at Site (g)	Estimated [8] Soft Soil Acceleratoin at Site (g)
Adapazari Sites	8.0	SKR	3.4	0.41	Stiff Soil	0.42	0.61	0.47	0.77	0.32	**0.38**
Hotel Sapanca	3.0	SKR	3.4	0.41	Stiff Soil	0.42	0.61	0.63	1.03	0.43	**0.40**
Degirmendere Nose, Soccer Field, and Police Station	< 1	IZT	5.0	0.19	Rock	0.19	0.55	0.72	1.31	0.25	**0.34**
		YPT	4.4	0.28	Soft Soil	0.15	0.57	0.72	1.26	0.19	**0.30**
Yalova Harbor	24.0	GBZ	13.5	0.20	Stiff Soil	0.13	0.34	0.22	0.65	0.08	**0.22**
		ARC	21.6	0.17	Stiff Soil	0.11	0.25	0.22	0.88	0.10	**0.24**

1. All distances are from the specified location to the closest vertical projection of the surface fault rupture. Fault rupture segment coordinates and most recent distances to all SMS were provided by Rathje (2001). Distances from the fault to each site were obtained from the latitude and longitude coordinates given in Chapter 3.
2. Figure 4.3 shows the location of the SMS with respect to the liquefaction sites and the surface fault rupture.
3. All SMS accelerations and preliminary site classifications were obtained from EERI (2000).
4. Accelerations from stiff and soft soil sites were converted to rock accelerations by scaling values from the graph developed by Idriss (Kramer, 1996) as shown in Figure 4.5.
5. Predicted rock accelerations were obtained by scaling values at the given distances from the attenuation curve by Sadigh et al. (EERI, 2000) as shown in Figure 4.4.
6. This ratio reflects the rate of attenuation (not magnitude) over the distance between the liquefaction site and the given SMS. If the liquefaction site is closer to the fault than the SMS then this value is greater than 1.
7. Estimated rock accelerations at liquefaction sites were obtained by multiplying the estimated rock accelerations for the SMS by the ratio of site-to-SMS predicted rock accelerations.
8. Estimated rock accelerations at liquefaction sites were converted to estimated soft soil accelerations by scaling values from the graph developed by Idriss (Kramer, 1996) as shown in Figure 4.5.

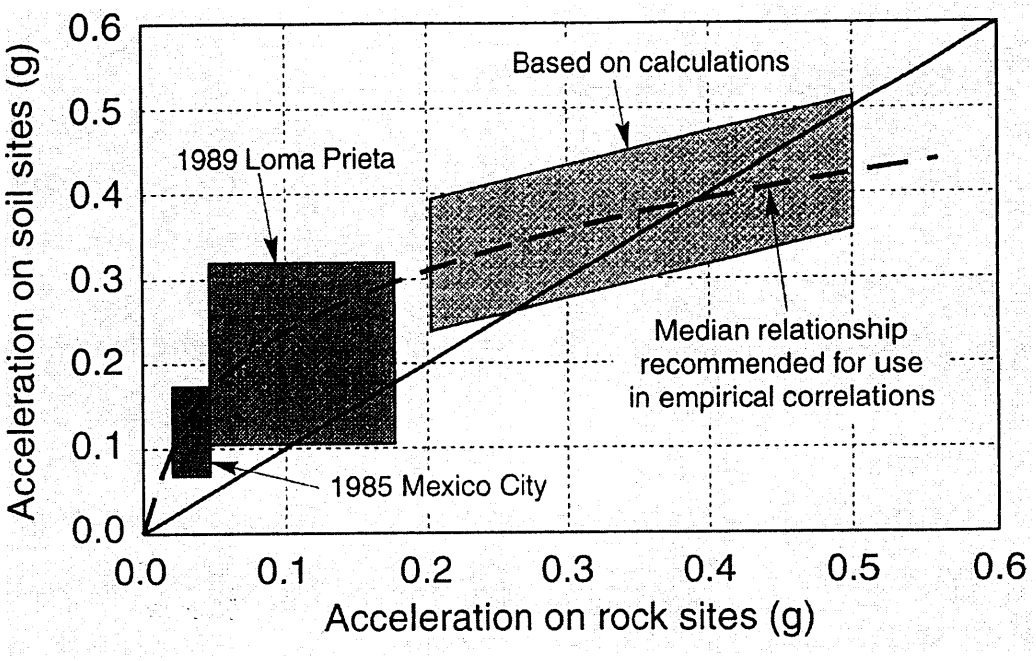

Figure 3.4 Curve developed by Idriss to approximate the relationship between peak accelerations on rock and soft soil sites (from Kramer, 1996).

Table 3.1 shows values obtained for each step described above. The 10 liquefaction sites in the city of Adapazari ranged from 7 to 9 km from the fault. These sites were all assigned a ground surface acceleration of 0.38 g by using the SKR station. It should be noted that the north-south component of the SKR station malfunctioned and did not make a recording. Therefore, the peak acceleration in the east-west direction was used instead of the geometric mean. Hotel Sapanca was assigned a ground surface acceleration of 0.4 g by using the SKR station. Degirmendere Nose, Soccer Field, and Police Station were all assigned a ground surface acceleration of 0.32 g. This value is the average of 0.34 g, determined by using the IZT station, and 0.30 g, determined by using the YPT station. Yalova Harbor was assigned a ground surface acceleration of 0.23 g. This value is the average of 0.22 g, determined by using the GBZ station, and 0.24 g, determined by using the ARC station.

These ground surface accelerations were used to calculate the CSR, at each liquefaction site, every one-tenth of a meter over the depth of the shear wave velocity profile. In order to account for the uncertainty in the procedure that was used to estimate

maximum ground surface accelerations at each site, CSR's were also calculated for values of acceleration +/- 0.05 g from the estimated value.

3.4 Determination of Liquefiable and Nonliquefiable Soils

SPT and CPT investigations were performed by a cooperative of researchers at liquefaction sites throughout the region affected by the Kocaeli earthquake. Through coordination with these researchers, shear wave velocity measurements were made at many of these same locations. The soil sample data examined in this chapter were obtained through split-spoon sampling. These data were used to determine liquefiable and nonliquefiable soils according to the Chinese Criteria and the Andrews and Martin Criteria. At sites where soil sample data were not available, CPT data were used as a substitute method for determining liquefiable and nonliquefiable soils. The general procedures used to make these determinations are discussed below.

3.4.1. The Chinese Criteria

Chinese researchers observed liquefaction occurrence in silty sand to slightly sandy silts during the 1975 Haicheng, and the 1976 Tangshan, China earthquakes (Andrews and Martin, 2000). Seed and Idriss (1982) presented these findings as a way to determine some sort of criteria to base the prediction of liquefaction in fine-grained soils. These criteria have come to be known as the Chinese Criteria. The Chinese Criteria state that soils with the following characteristics may be vulnerable to severe strength loss during earthquakes:

Clay Content (% finer than 0.005 mm)	<15%
Liquid Limit (LL)	<35
Water Content (W_n)	>(0.9)LL

Clayey soils that fail any of these criteria are considered nonliquefiable.

3.4.2. Andrews and Martin Criteria

Andrews and Martin (2000) have "refined" the Chinese Criteria based primarily on the different definitions of liquid limit and clay content between China and the United States. The liquid limits from the original Chinese data were determined by the fall cone penetrometer, whereas liquid limits in the United States are most typically determined by the Casagrande-type percussion apparatus. Andrews and Martin maintain that a liquid limit of 35 with the fall cone penetrometer corresponds to a liquid limit of 32 with the Casagrande-type apparatus. In addition, in China the clay content is defined as particles finer than 0.005 mm while in the United States clay content is defined as particles finer than 0.002 mm. Because of this difference, Andrews and Martin base their criteria on a clay particle size of 0.002 mm. They also maintain that the liquid limit and clay content are "key" soil parameters while the water content is not. Therefore, water content is not a part of their criteria. Upon this basis, Andrews and Martin have developed the criteria shown in Table 3.2.

Table 3.2 Andrews and Martin Criteria for evaluation of fine-grained soil liquefaction (after Andrews and Martin, 2000)

	Liquid Limit < 32[1]	Liquid Limit ≥ 32
Clay Content < 10%[2]	Susceptible	Further Studies Required *(Considering plastic non-clay sized grains - such as Mica)*
Clay Content ≥ 10%	Further Studies Required *(Considering non-plastic clay sized grains - such as mine and quarry tailings)*	Not Susceptible

3.4.3. CPT Criteria

The CPT friction ratio (sleeve resistance divided by cone tip resistance) generally increases with increasing fines content and soil plasticity. This allows for rough estimates of soil type to be determined from CPT data. The chart shown in Figure 3.5 was developed by Robertson (1990) for estimating soil type. The boundaries between soil types 2 - 7 can be approximated by concentric circles (Robertson and Wride, 1998). The radius of these concentric circles, called the soil behavior type index (I_C), can be calculated from the following equation:

$$I_C = \left[(3.47 - Q)^2 + (\log F + 1.22)^2\right]^{0.5} \quad \text{(Eq. 3.6)}$$

where: I_C = soil behavior type index,
Q = normalized cone penetration resistance (dimensionless),
F = normalized friction ratio, in percent.

The normalized cone penetration resistance is given by the following equation:

$$Q = \left(\frac{q_c - \sigma_{vo}}{P_a}\right)\left(\frac{P_a}{\sigma'_{vo}}\right)^n \quad \text{(Eq. 3.7)}$$

where: Q = normalized cone penetration resistance (dimensionless),
q_c = measured cone tip penetration resistance, in kPa,
σ_{vo} = total vertical overburden stress, in kPa,
σ'_{vo} = effective vertical overburden stress, in kPa,
P_a = reference stress of 100 kPa,
n = linear stress exponent (varies between 1 - 0.5).

The normalized friction ratio is given by the following equation:

$$F = \left[\frac{f_S}{(q_c - \sigma_{vo})}\right](100) \quad \text{(Eq. 3.8)}$$

where: F = normalized friction ratio, in percent,
f_S = CPT sleeve friction stress, in kPa,
q_c = measured cone tip penetration resistance, in kPa,
σ_{vo} = total vertical overburden stress, in kPa.

Robertson (1990) developed the chart shown in Figure 3.5 with the normalized cone penetration resistance (Q) having a linear stress exponent (n) equal to one. More recently it has been suggested that n should be varied between 1 and 0.5 in order to get more accurate I_C values for use in the CPT-based simplified procedure (Robertson and Wride,

1998; Youd and Idriss, 2001). In this study, all I_C values were calculated with n = 1 since the original soil classification chart was developed this way. If the calculated I_C value is greater than 2.6, then the soil is considered too clay-rich to liquefy (Youd and Idriss, 2001).

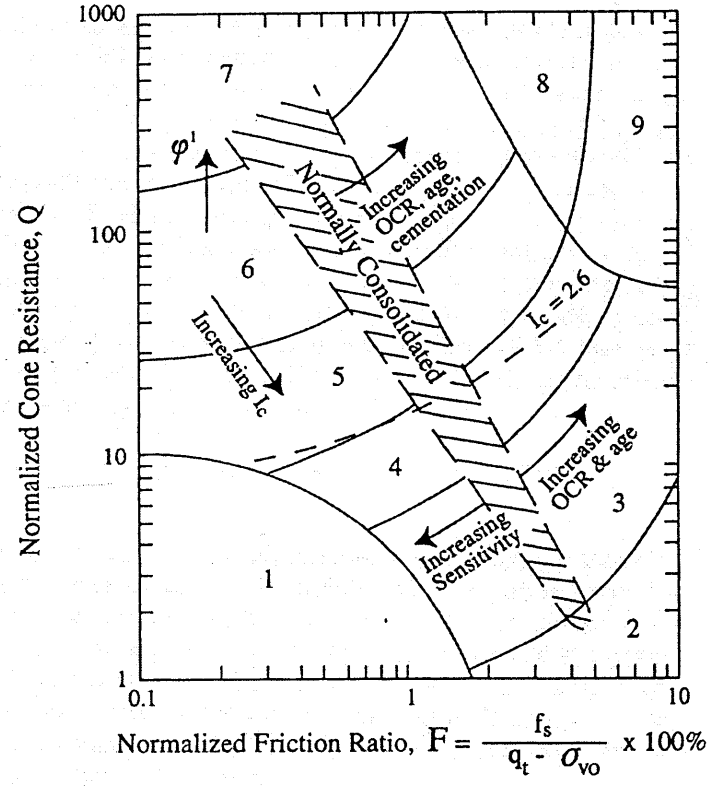

1. Sensitive, fine grained
2. Organic soils - peats
3. Clays - silty clay to clay
4. Silt mixtures - clayey silt to silty clay
5. Sand mixtures - silty sand to sandy silt
6. Sands - clean sand to silty sand
7. Gravelly sand to dense sand
8. Very stiff sand to clayey sand*
9. Very stiff, fine grained*

**Heavily overconsolidated or cemented*

Figure 3.5 CPT-based soil behavior type chart proposed by Robertson (1990). The boundaries separating soil types 2-7 are approximated by the soil behavior type index, I_C.

CPT data were also used to estimate the fines content (FC) for use in 3.5 using the following equations:

for $I_C < 1.26$	$FC = 0$	(Eq. 3.9a)
for $1.26 < I_C < 3.5$;	$FC = 1.75(I_C)^{3.25} - 3.7$	(Eq. 3.9b)
for $I_C > 3.5$;	$FC = 100$	(Eq. 3.9c)

where: IC = soil behavior type index,
FC = apparent fines content, in %.

3.5 CONCLUSIONS

Shear wave velocities provide an alternative to SPT and CPT based simplified liquefaction assessments. Empirical correlations between corrected shear wave velocity and CRR and analysis procedures have been developed by Andrus and Stokoe, (2000). These procedures were followed for shear wave velocity profiles measured at Turkey liquefaction sites.

Liquefaction analysis also requires a determination of peak ground acceleration induced by earthquake shaking at each site. This assessment was complicated for this data by the fact that fourteen of the fifteen liquefaction sites were within 20 km (in the near-field) of the Kocaeli, earthquake fault rupture. There are very few measured near-field strong motion records, therefore, most empirically developed attenuation records do poorly at predicting near-field shaking, and did not predict the near-field Kocaeli earthquake shaking. This analysis relied primarily upon measured strong motion recordings with slight modifications.

Fine-grained soils pose an additional challenge for liquefaction analysis. The Chinese criteria reported by Seed and Idriss (1982) is the primary method that is currently used to differentiate liquefaction susceptible and nonsusceptible soils. This criteria has been modified slightly by Andrews and Martin (2000) largely to account for differences between soil index measurements in the US and China. Both criteria are applied to the fine-grained soils encountered at the Turkey liquefaction sites.

At liquefaction sites where soil index-testing results were not available, fines content and liquefaction susceptibility were inferred from CPT results.

CHAPTER 4

LIQUEFACTION ANALYSIS RESULTS

4.1 INTRODUCTION

This chapter contains the results of the liquefaction evaluations at the fifteen liquefaction sites tested. Ground failure was observed at all of these sites except site 1-24 on the Cark Canal where lateral spreading was expected but not observed. All fifteen sites had soil layers that were sufficiently soft to liquefy based upon shear wave velocity. However four sites in the city of Adapazari (site A, C, G, and J) only had soil that would be characterized as nonsusceptible to liquefaction based upon their clay size particle content and their plasticity. It is possible that soils that would be classified as nonsusceptible to liquefaction at other sites also participated in ground failure.

These results cast some doubt on the reliability of the Chinese criteria, and the Andrews and Martin criteria for identifying soils that are susceptible to liquefaction. Clay size particle criteria appear especially poorly suited to differentiating liquefaction susceptible and nonsusceptible soils at these sites.

One other site of interest is Degirmendere Nose. This site experienced massive lateral spreading, however, only a relatively thin layer of soil between 8 to 9 meters of depth had a corrected shear wave velocity that was barely low enough to be classified as liquefiable. It would be surprising if this relatively deep, stiff layer could be responsible for the level of failure observed.

4.2 LIQUEFACTION SITE EVALUATIONS

The following section uses the procedures outlined in chapter 3 to evaluate the liquefaction susceptibility each site where SASW testing was performed. The layer, or layers, most susceptible to liquefaction have been determined through combining shear wave velocity data, soil sample data, and CPT data. Site descriptions for each liquefaction site are found in Chapter 2. Soil sample data, obtained from split-spoon

sampling, were available at all liquefaction sites in the city of Adapazari. Therefore, the potentially liquefiable region at each of these sites was evaluated for liquefaction susceptibility by using the Chinese Criteria and the Andrews and Martin Criteria. Soil sample data were not available for any of the other liquefaction sites. Therefore, the potentially liquefiable region at each of these sites was evaluated for liquefaction susceptibility by using I_C values calculated from CPT data.

4.2.1 Adapazari

4.2.1.1 Site A The graphs developed for Site A to delineate potentially liquefiable soil using the shear wave velocity simplified procedure are shown in Figure 4.1. Figure 4.1a shows the shear wave velocity profile (V_S) and the corrected shear wave velocity profile (V_{S1}) for the site. Figure 4.1b shows the average fines content from all samples within each layer. Figure 4.1c shows the CRR of the soil along with three CSR profiles. The central profile represents the CSR generated using the most probable ground acceleration predicted for this site. The other two profiles result from bracketing this acceleration by +/- 0.05 g. From this graph, it can be seen that the potentially liquefiable region is between the depths of 0.75 - 6 meters. The graphs developed for Site A to delineate soils susceptible to liquefaction using the Chinese Criteria and the Andrews and Martin Criteria are shown in Figure 4.2. The soil data for this site was obtained from four separate boreholes. Figure 4.2a shows the assumed USCS profile along with the total number of samples, and the number of non-plastic samples, included in each layer. Figure 4.2b shows average values for plastic limit, water content, and liquid limit in each layer. The 2 and 5 μm clay contents are plotted in Figure 4.2c.

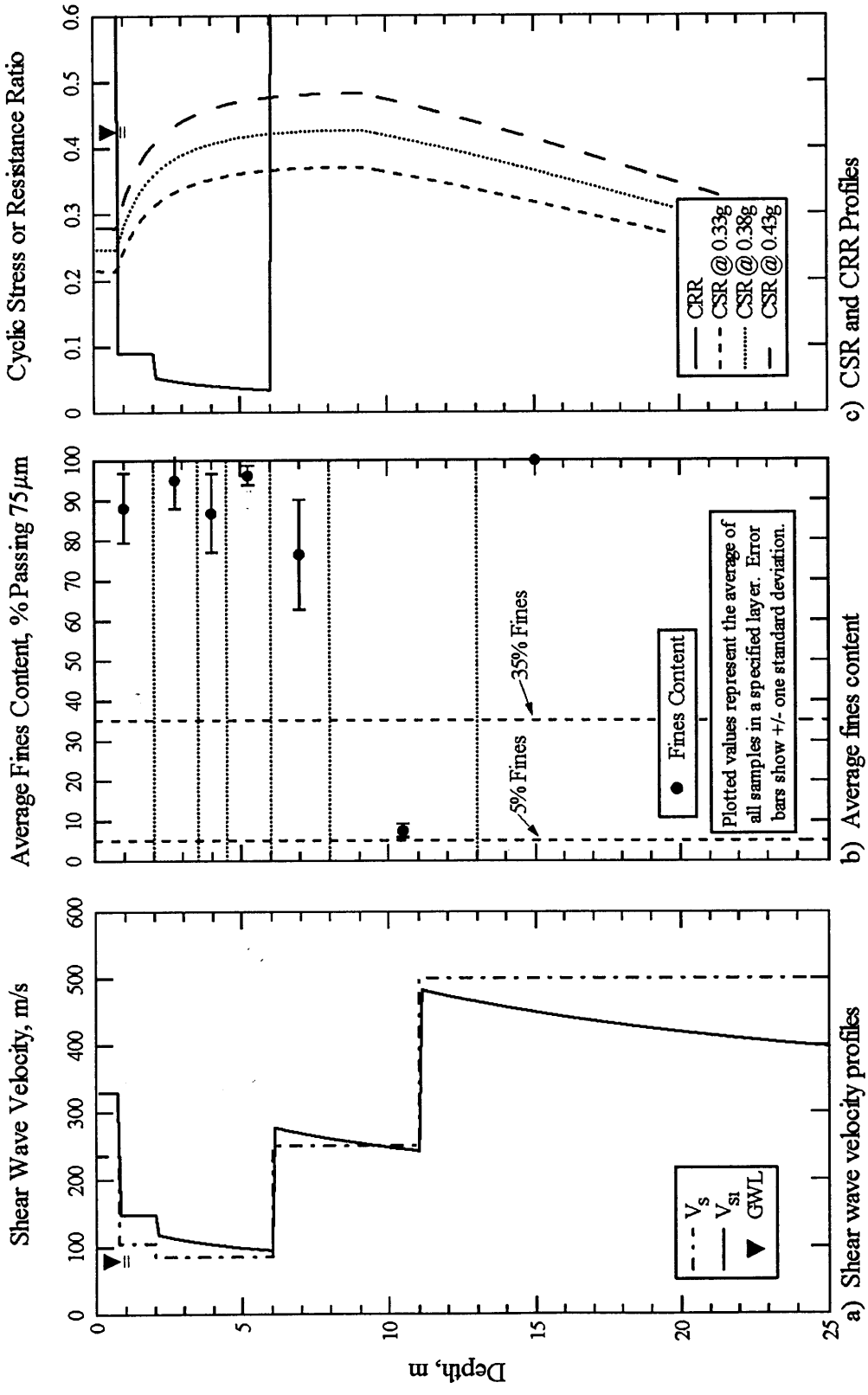

Figure 4.1 Graphs developed to delineate liquefiable soil using the simplified shear wave velocity procedure at Site A, Adapazari, Turkey (fines content obtained from http://peer.berkeley.edu/turkey/adapazari).

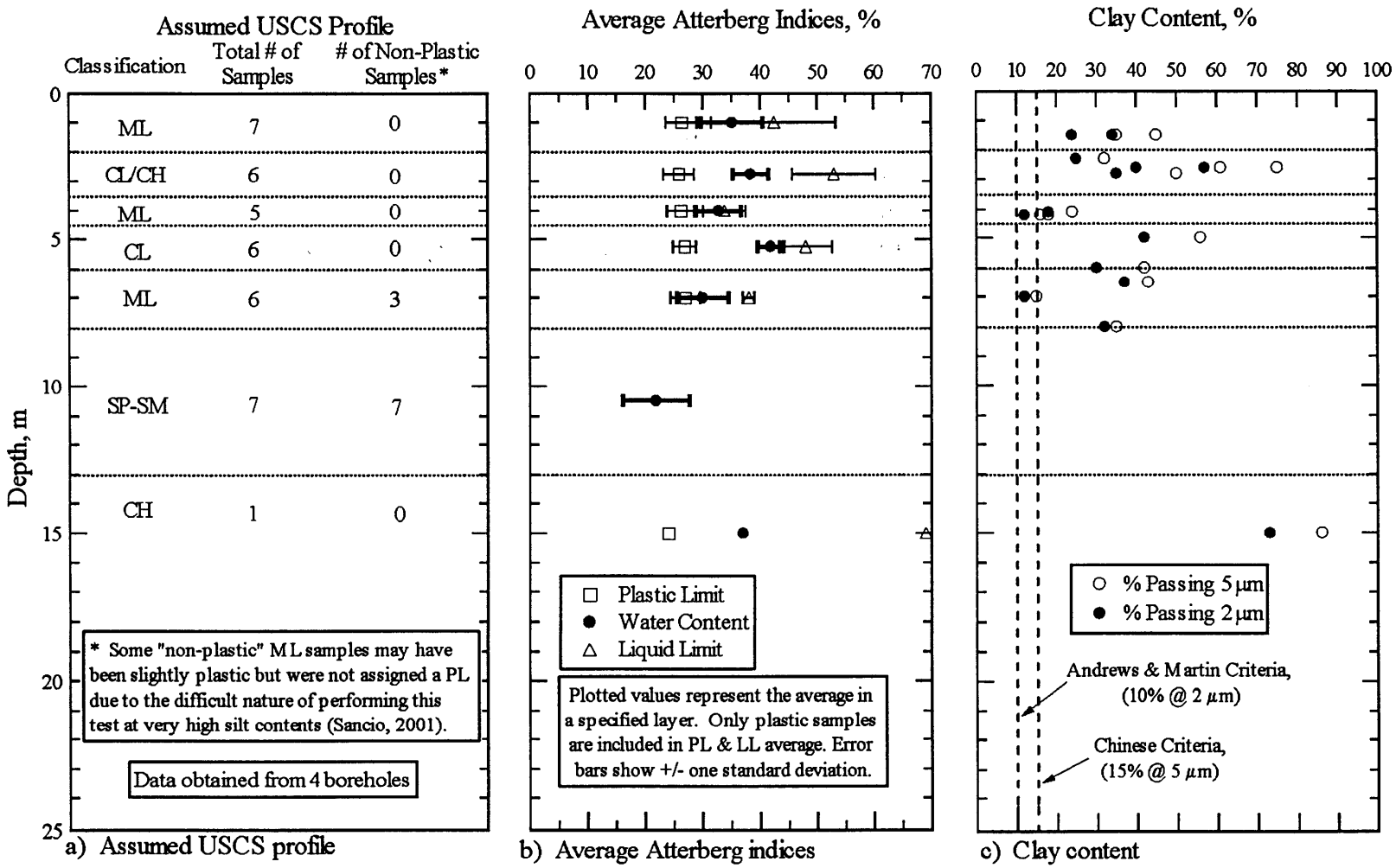

Figure 4.2 Graphs developed to delineate soils susceptible to liquefaction using the Chinese Criteria and the Andrews and Martin Criteria at Site A, Adapazari, Turkey (raw soil data from http://peer.berkeley.edu/turkey/adapazari)

Table 4.1 summarizes the data for all soil layers located within the potentially liquefiable region at Site A. None of these layers appear to be susceptible to liquefaction according the Chinese Criteria or the Andrews and Martin Criteria. However, the depth interval from 3.5 - 4.5 meters only fails the Chinese Criteria due to a slightly high clay content (i.e. 18% rather than 15%). This layer of silt is also extremely soft, with an average CRR/CSR equal to 0.1. Therefore, it is believed that this is the most likely layer to have liquefied. However, it is unlikely that this layer could have been the lone culprit behind the ground failure that occurred here. At Site A, a five-story apartment building settled differentially by 1.5 meters. It is unlikely that failure of a one-meter thick silt layer could have caused that amount of settlement. It is likely that other layers participated in this ground failure also, but none of them even come close to fulfilling either the Chinese Criteria or the Andrews and Martin Criteria.

Table 4.1 Average properties for soil layers located within the potentially liquefiable region at Site A

Depth Interval (m)	Average (CRR/CSR)	USCS	Average LL (%)	Average (W_n/LL)	Average 5 μm Clay Content (%)	Average 2 μm Clay Content (%)	Liquefiable by Chinese Criteria	Liquefiable by Andrews & Martin Criteria
0.75 - 2	0.29	ML	42.4 [1]	0.83	40	29	no	no
2 - 3.5	0.12	CL/CH	53.0 [2]	0.72	55	39	no	no
3.5 - 4.5	0.10	ML	33.8 [3]	0.97	18	14	no	no
4.5 - 6	0.08	CL/CH	48.0 [4]	0.87	43	36	no	no

1. 0/7 samples in this layer were non-plastic.
2. 0/6 samples in this layer were non-plastic.
3. 0/5 samples in this layer were non-plastic.
4. 0/6 samples in this layer were non-plastic.

4.2.1.2 Site B The graphs developed for Site B to delineate potentially liquefiable soil using the shear wave velocity simplified procedure are shown in Figure 4.3. Figure 4.3a shows the shear wave velocity profile (V_S) and the corrected shear wave velocity profile (V_{S1}) for the site. Figure 4.3b shows the average fines content from all samples within each layer. Figure 4.3c shows the CRR of the soil along with three CSR profiles. The central profile represents the CSR generated using the most probable ground

acceleration predicted for this site. The other two profiles result from bracketing this acceleration by +/- 0.05 g. From this graph, it can be seen that the potentially liquefiable region is broken into two portions. This is due to the corrected shear wave velocity having a value just over 215 m/s from approximately 3 - 4.5 meters. The liquefiable region is between the depths of 2 - 3 meters, and 5 - 7 meters. The graphs developed for Site B to delineate soils susceptible to liquefaction using the Chinese Criteria and the Andrews and Martin Criteria are shown in Figure 4.4. The soil data for this site were obtained from two separate boreholes. Figure 4.4a shows the assumed USCS profile along with the total number of samples, and the number of non-plastic samples, included in each layer. Figure 4.4b shows average values for plastic limit, water content, and liquid limit in each layer. The 2 and 5 μm clay contents are plotted in Figure 4.4c.

Table 4.2 summarizes the data for all soil layers located within the potentially liquefiable region at Site B. The softest layer is between the depths of 2 - 3 meters. However, this layer is predicted nonliquefiable by both the Chinese Criteria and the Andrews and Martin Criteria. The material most likely to have liquefied is the 2-meter layer of sand between the depths of 5 - 7 meters. This weakened soil induced a bearing capacity failure that toppled a five-story building.

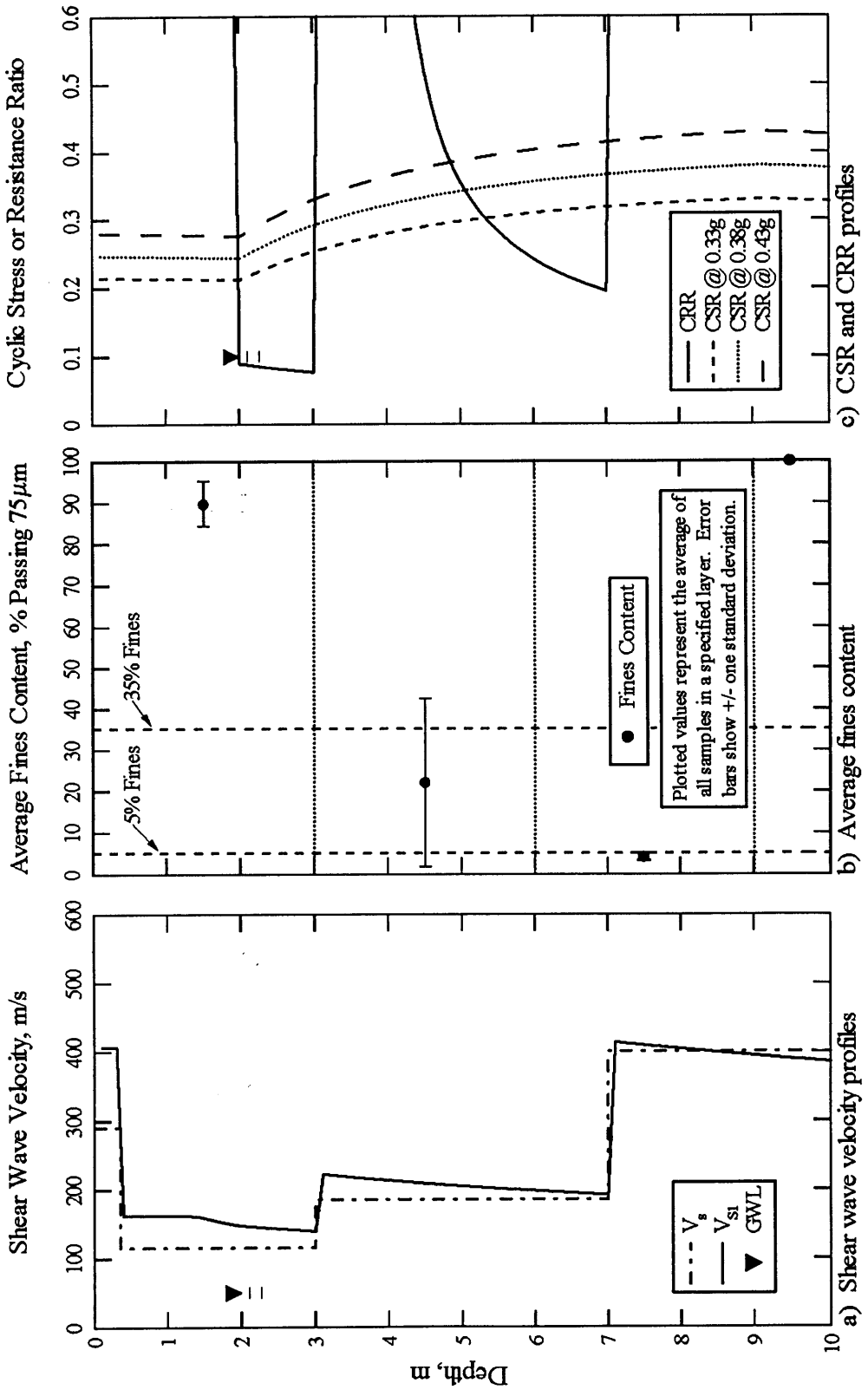

Figure 4.3 Graphs developed to delineate liquefiable soil using the simplified shear wave velocity procedure at Site B, Adapazari, Turkey (fines content obtained from http://peer.berkeley.edu/turkey/adapazari).

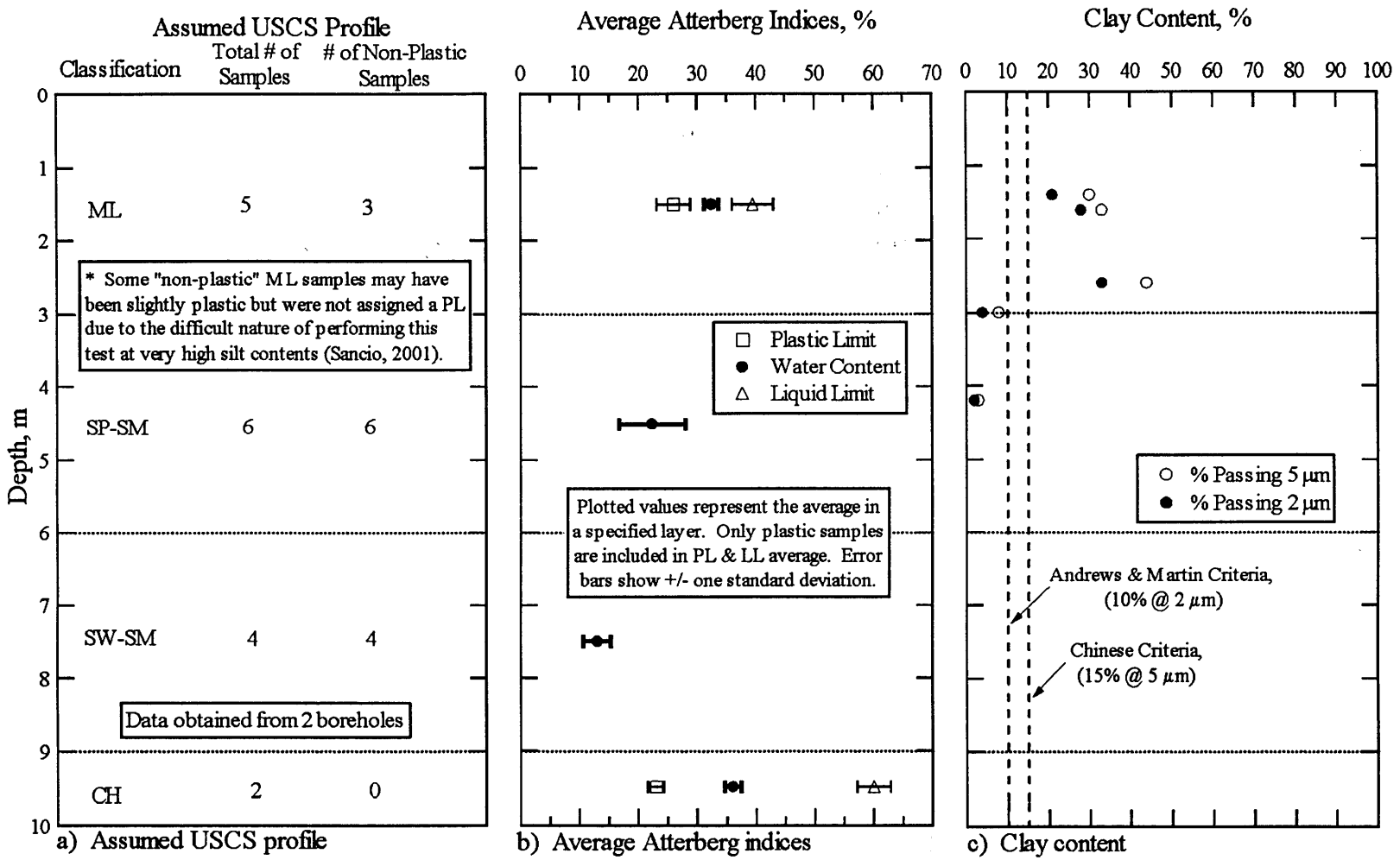

Figure 4.4 Graphs developed to delineate soils susceptible to liquefaction using the Chinese Criteria and the Andrews and Martin Criteria at Site B, Adapazari, Turkey (raw soil data from http://peer.berkeley.edu/turkey/adapazari).

Table 4.2 Average properties for soil layers located within the potentially liquefiable region at Site B

Depth Interval (m)	Average (CRR/CSR)	USCS	Average LL (%)	Average (W_n/LL)	Average 5 μm Clay Content (%)	Average 2 μm Clay Content (%)	Liquefiable by Chinese Criteria	Liquefiable by Andrews & Martin Criteria
2 - 3	0.31	ML	39.5 [1]	0.82	29	22	no	no
5 - 6	0.81	SP-SM	-	-	3	2	yes	yes
6 - 7	0.59	SW-SM	-	-	-	-	yes	yes

1. 3/7 samples in this layer were non-plastic.

4.2.1.3 Site C Two SASW centerlines were used at Site C in order to investigate the strange performance of three identical buildings during the Kocaeli earthquake (refer to section 2.2.1.3). The southernmost building experienced no visible distress while the other two buildings to the north settled considerably. Soil information from seven separate boreholes was provided for this site. An attempt was made to divide the site into two separate soil profiles (one the north and one to the south). However, based upon available subsurface data, differences in the subsurface material were not distinguishable. Therefore, all seven boreholes were used to develop one soil profile for Site C.

The graphs developed for Site C North Centerline to delineate potentially liquefiable soil using the shear wave velocity simplified procedure are shown in Figure 4.5. Figure 4.5a shows the shear wave velocity profile (V_S) and the corrected shear wave velocity profile (V_{S1}) for the north centerline. Figure 4.5b shows the average fines content from all samples within each layer. Figure 4.5c shows the CRR of the soil along with three CSR profiles. The central profile represents the CSR generated using the most probable ground acceleration predicted for this site. The other two profiles result from bracketing this acceleration by +/- 0.05 g. From this graph, it can be seen that the potentially liquefiable region is broken into two portions. This is due to the corrected shear wave velocity having a value just over 200 m/s from approximately 5 – 5.75 meters. With the exception of this small area, the entire depth of the shear wave velocity profile below the water table appears to be potentially liquefiable.

The graphs developed for Site C South Centerline to delineate potentially liquefiable soil using the shear wave velocity simplified procedure are shown in Figure 4.6. Figure 4.6a shows the shear wave velocity profile (V_S) and the corrected shear wave velocity profile (V_{S1}) for the south centerline. Figure 4.6b shows the average fines content from all samples within each layer. Figure 4.6c shows the CRR of the soil along with three CSR profiles. The central profile represents the CSR generated using the most probable ground acceleration predicted for this site. The other two profiles result from bracketing this acceleration by +/- 0.05 g. At this centerline, it can be seen that the potentially liquefiable region extends from the water table throughout the entire depth of the shear wave velocity profile.

The graphs developed for Site C to delineate soils susceptible to liquefaction using the Chinese Criteria and the Andrews and Martin Criteria are shown in Figure 4.7. As explained above, these soil data were used for both centerlines. Figure 4.7a shows the assumed USCS profile along with the total number of samples, and the number of non-plastic samples, included in each layer. Figure 4.7b shows average values for plastic limit, water content, and liquid limit in each layer. The 2 and 5 μm clay contents are plotted in Figure 4.7c.

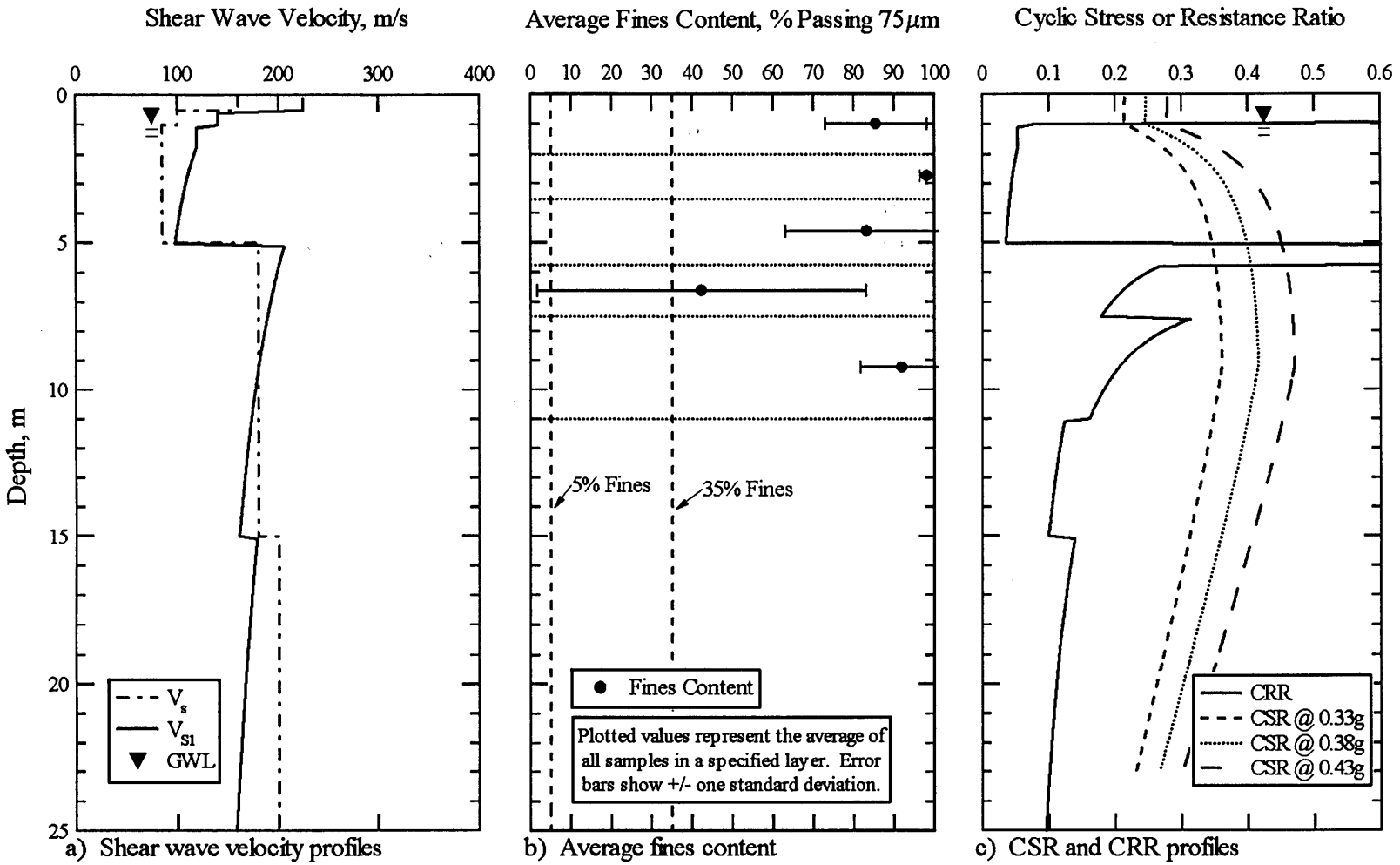

Figure 4.5 Graphs developed to delineate liquefiable soil using the simplified shear wave velocity procedure at Site C North Centerline, Adapazari, Turkey (fines content obtained from http://peer.berkeley.edu/turkey/adapazari).

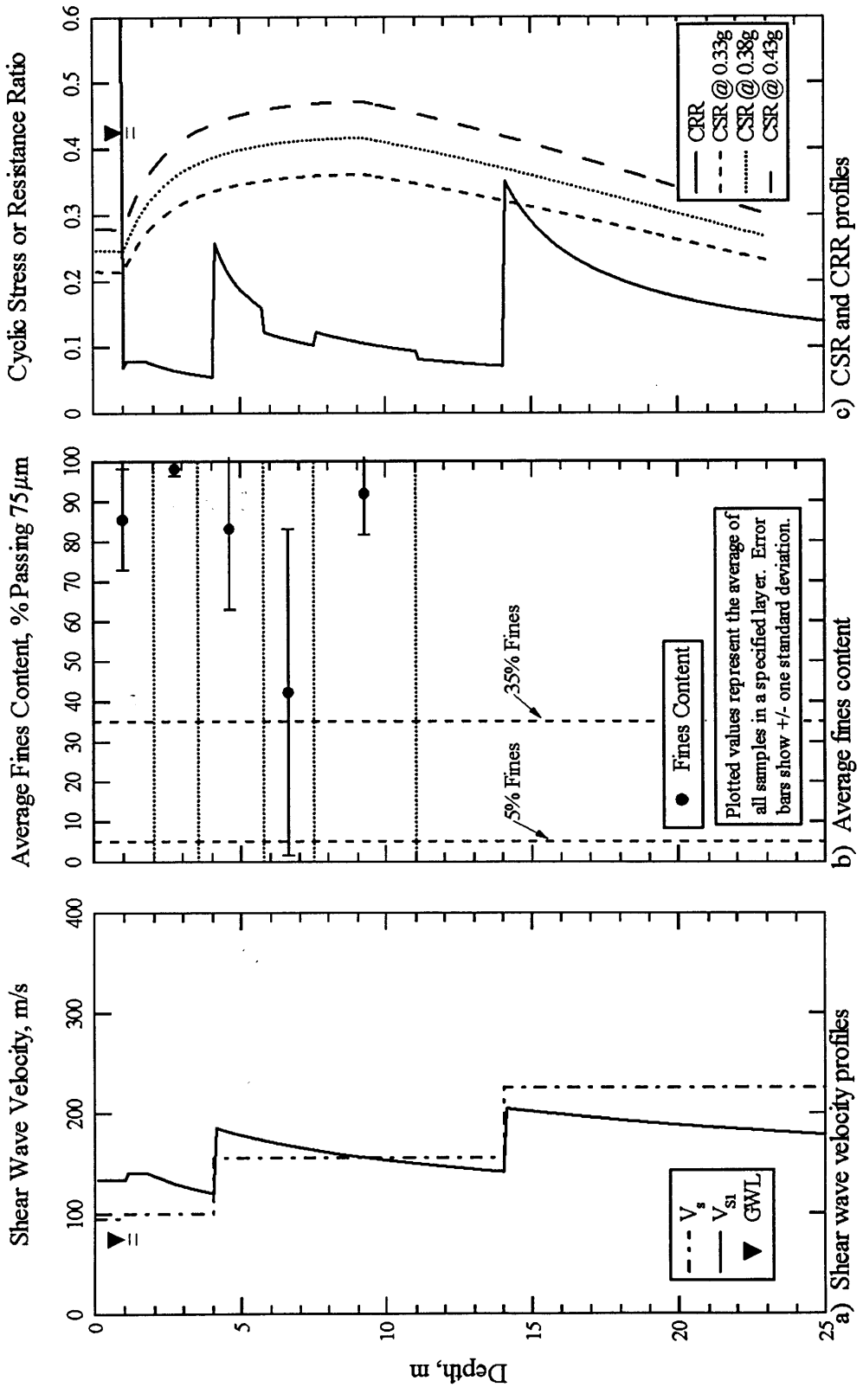

Figure 4.6 Graphs developed to delineate liquefiable soil using the simplified shear wave velocity procedure at Site C South Centerline, Adapazari, Turkey (fines content obtained from http://peer.berkeley.edu/turkey/adapazari).

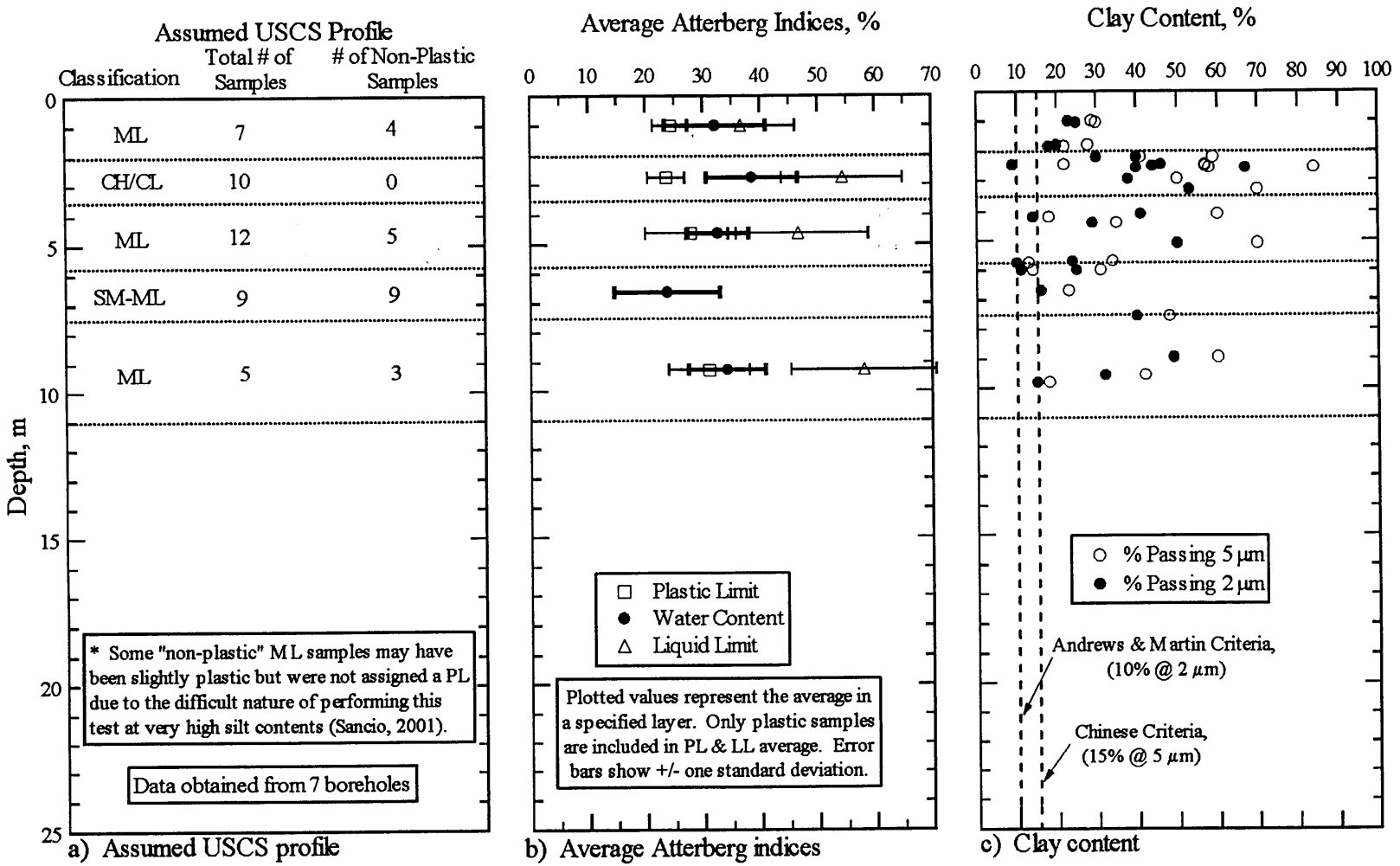

Figure 4.7 Graphs developed to delineate soils susceptible to liquefaction using the Chinese Criteria and the Andrews and Martin Criteria at Site C South Centerline, Adapazari, Turkey (raw soil data from http://peer.berkeley.edu/turkey/adapazari).

Table 4.3 summarizes the data for all soil layers located within the potentially liquefiable region at Site C North Centerline. Table 4.4 summarizes the data for all soil layers located within the potentially liquefiable region at Site C South Centerline. It is important to notice that soil property values do not change between these tables because only one soil profile was developed for the entire site. However, depth intervals and average values for CRR/CSR do vary. In general, the depth interval from 1 - 5.75 meters is stiffer beneath the south centerline, while the depth interval from 5.75 - 11 meters is stiffer beneath the north centerline. However, great differences in the two profiles are not expected since both profiles are in the vicinity of the two northernmost buildings (C1 and C2) that experienced similar degrees of liquefaction damage. None of the soil layers at Site C appear to be susceptible to liquefaction according the Chinese Criteria or the Andrews and Martin Criteria. However, the depth interval from 5.75 - 7.5 meters only fails the Chinese Criteria only due to a slightly high clay content (i.e. 20% rather than 15%). This layer was likely to have contributed to the ground failure at the site. However, it is questionable whether or not this 1.75-meter thick layer was the sole culprit that caused the 30 - 40 cm of settlement experienced at buildings C1 and C2. Other layers may have also participated in the ground failure.

Table 4.3 Average properties for soil layers located within the potentially liquefiable region at Site C North Centerline

Depth Interval (m)	Average (CRR/CSR)	USCS	Average LL (%)	Average (W_n/LL)	Average 5 μm Clay Content (%)	Average 2 μm Clay Content (%)	Liquefiable by Chinese Criteria	Liquefiable by Andrews & Martin Criteria
1 - 2	0.19	ML	36.7 [1]	0.88	27	22	no	no
2 - 3.5	0.13	CH/CL	54.3 [2]	0.71	55	45	no	no
3.5 - 5	0.10	ML	46.6 [3]	0.70	43	32	no	no
5.75 - 7.5	0.52	SM-ML	-	-	20	16	no	no
7.5 - 11	0.52	ML	58.0 [4]	0.59	42	34	no	no

1. 4/7 samples in this layer were non-plastic.
2. 0/10 samples in this layer were non-plastic.
3. 5/12 samples in this layer were non-plastic.
4. 3/5 samples in this layer were non-plastic.

Table 4.4 Average properties for soil layers located within the potentially liquefiable region at Site C South Centerline

Depth Interval (m)	Average (CRR/CSR)	USCS	Average LL (%)	Average (W_n/LL)	Average 5 μm Clay Content (%)	Average 2 μm Clay Content (%)	Liquefiable by Chinese Criteria	Liquefiable by Andrews & Martin Criteria
1 - 2	0.27	ML	36.7 [1]	0.88	27	22	no	no
2 - 3.5	0.18	CH/CL	54.3 [2]	0.71	55	45	no	no
3.5 - 5.75	0.42	ML	46.6 [3]	0.70	43	32	no	no
5.75 - 7.5	0.27	SM-ML	-	-	20	16	no	no
7.5 - 11	0.26	ML	58.0 [4]	0.59	42	34	no	no

1. 4/7 samples in this layer were non-plastic.
2. 0/10 samples in this layer were non-plastic.
3. 5/12 samples in this layer were non-plastic.
4. 3/5 samples in this layer were non-plastic.

4.2.1.4 Site D The graphs developed for Site D to delineate potentially liquefiable soil using the shear wave velocity simplified procedure are shown in Figure 4.8. Figure 4.8a shows the shear wave velocity profile (V_S) and the corrected shear wave velocity profile (V_{S1}) for the site. Figure 4.8b shows the average fines content from all samples within each layer. Figure 4.8c shows the CRR of the soil along with three CSR profiles. The central profile represents the CSR generated using the most probable ground acceleration predicted for this site. The other two profiles result from bracketing this acceleration by +/- 0.05 g. From this graph, it can be seen that the potentially liquefiable region extends from a depth of approximately 2.3 meters throughout the entire depth of the profile. The graphs developed for Site D to delineate soils susceptible to liquefaction using the Chinese Criteria and the Andrews and Martin Criteria are shown in Figure 4.9. The soil data for this site were obtained from three separate boreholes. Figure 4.9a shows the assumed USCS profile along with the total number of samples, and the number of non-plastic samples, included in each layer. Figure 4.9b shows average values for plastic limit, water content, and liquid limit in each layer. The 2 and 5 μm clay contents are plotted in Figure 4.9c.

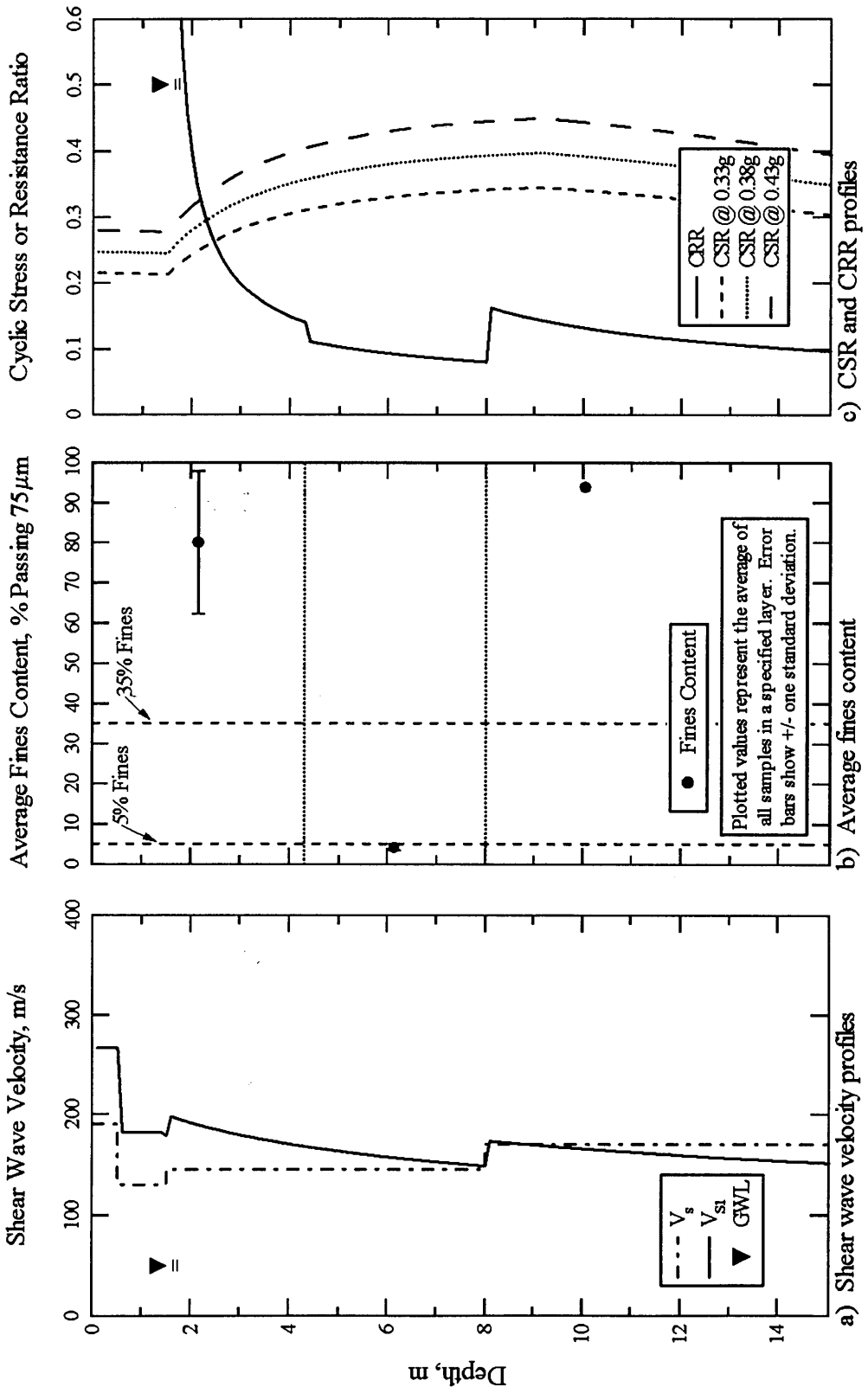

Figure 4.8 Graphs developed to delineate liquefiable soil using the simplified shear wave velocity procedure at Site D, Adapazari, Turkey (fines content obtained from http://peer.berkeley.edu/turkey/adapazari).

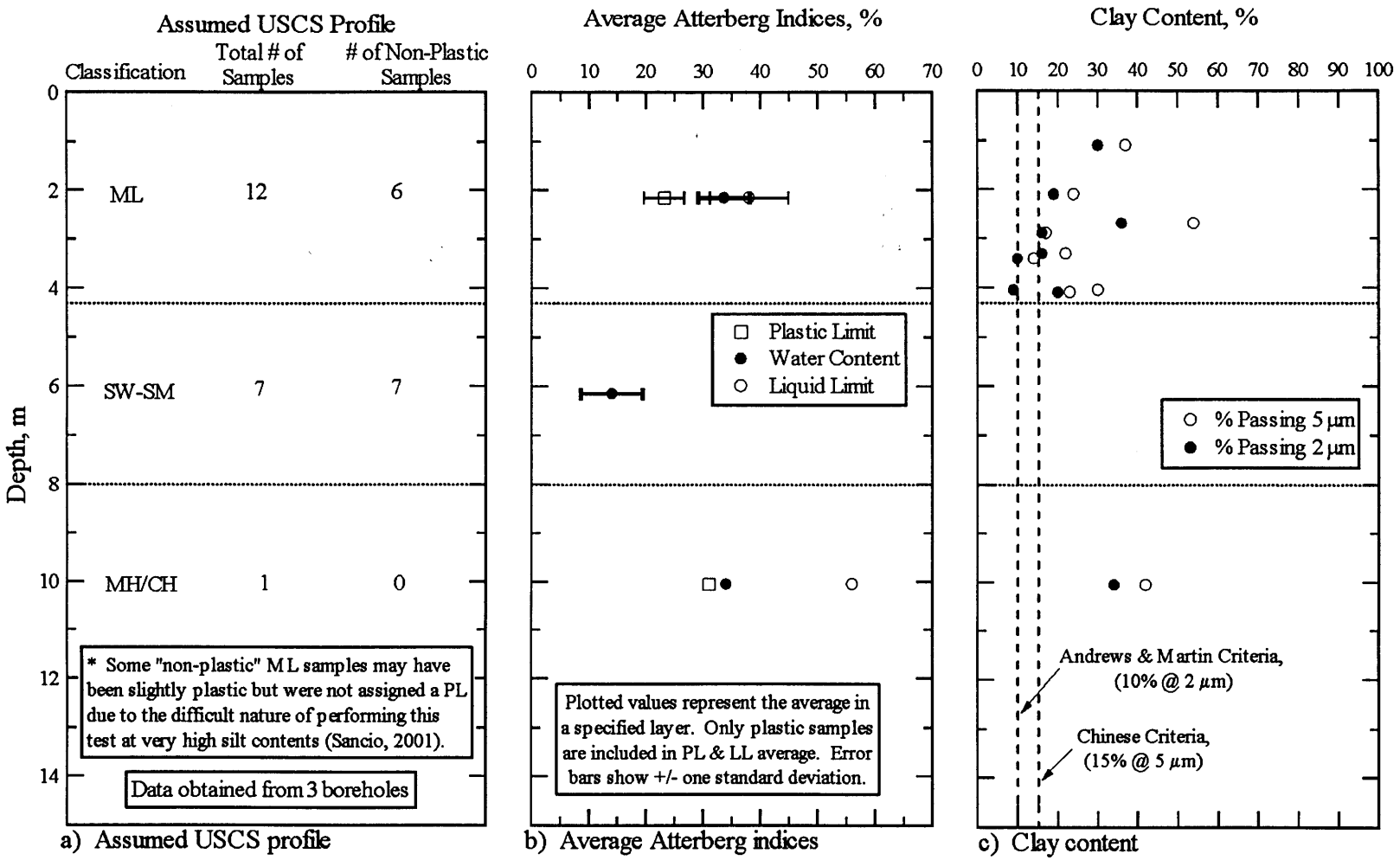

Figure 4.9 Graphs developed to delineate soils susceptible to liquefaction using the Chinese Criteria and the Andrews and Martin Criteria at Site D, Adapazari, Turkey (raw soil data from http://peer.berkeley.edu/turkey/adapazari).

Table 4.5 summarizes the data for all soil layers located within the potentially liquefiable region at Site D. The softest layer is between the depths of 4.3 - 8 meters. This layer is granular and would be expected to liquefy. The other layers in the liquefiable region are predicted as nonliquefiable by both the Chinese Criteria and the Andrews and Martin Criteria. Hence, the nearly 4-meter thick layer of sand most likely caused this five-story building to settle 44 cm.

Table 4.5 Average properties for soil layers located within the potentially liquefiable region at Site D

Depth Interval (m)	Average (CRR/CSR)	USCS	Average LL (%)	Average (W_n/LL)	Average 5 μm Clay Content (%)	Average 2 μm Clay Content (%)	Liquefiable by Chinese Criteria	Liquefiable by Andrews & Martin Criteria
2.3 - 4.3	0.58	ML	38.0 [1]	0.89	28	20	no	no
4.3 - 8	0.24	SW-SM	-	-	-	-	yes	yes
10	0.34	MH/CH	56.0 [2]	0.61	43	32	no	no

1. 6/12 samples in this layer were non-plastic.
2. 0/1 samples in this layer were non-plastic.

4.2.1.5 Site G The graphs developed for Site G to delineate potentially liquefiable soil using the shear wave velocity simplified procedure are shown in Figure 4.10. Figure 4.10a shows the shear wave velocity profile (V_S) and the corrected shear wave velocity profile (V_{S1}) for the site. Figure 4.10b shows the average fines content from all samples within each layer. Figure 4.10c shows the CRR of the soil along with three CSR profiles. The central profile represents the CSR generated using the most probable ground acceleration predicted for this site. The other two profiles result from bracketing this acceleration by +/- 0.05 g. From this graph, it can be seen that the potentially liquefiable region extends from a depth of 0.5 meters throughout the entire depth of the profile. The graphs developed for Site G to delineate soils susceptible to liquefaction using the Chinese Criteria and the Andrews and Martin Criteria are shown in Figure 4.11. The soil data for this site were obtained from three separate boreholes. Figure 4.11a shows the assumed USCS profile along with the total number of samples, and the number of non-

plastic samples, included in each layer. Figure 4.11b shows average values for plastic limit, water content, and liquid limit in each layer. The 2 and 5 μm clay contents are plotted in Figure 4.11c.

Table 4.6 summarizes the data for all soil layers located within the potentially liquefiable region at Site G. Neither of these layers are predicted as liquefiable by the Chinese Criteria or the Andrews and Martin Criteria. The layer most likely to have liquefied is located between 0.5 - 7 meters. It is important to notice that this layer is largely non-plastic (10/12 samples were non-plastic) and that the LL reported is only based upon two plastic samples. Therefore, this silt layer only fails the Chinese Criteria due to high clay content. Failure of this layer would have been more than adequate to cause the two buildings located at this site to tip over.

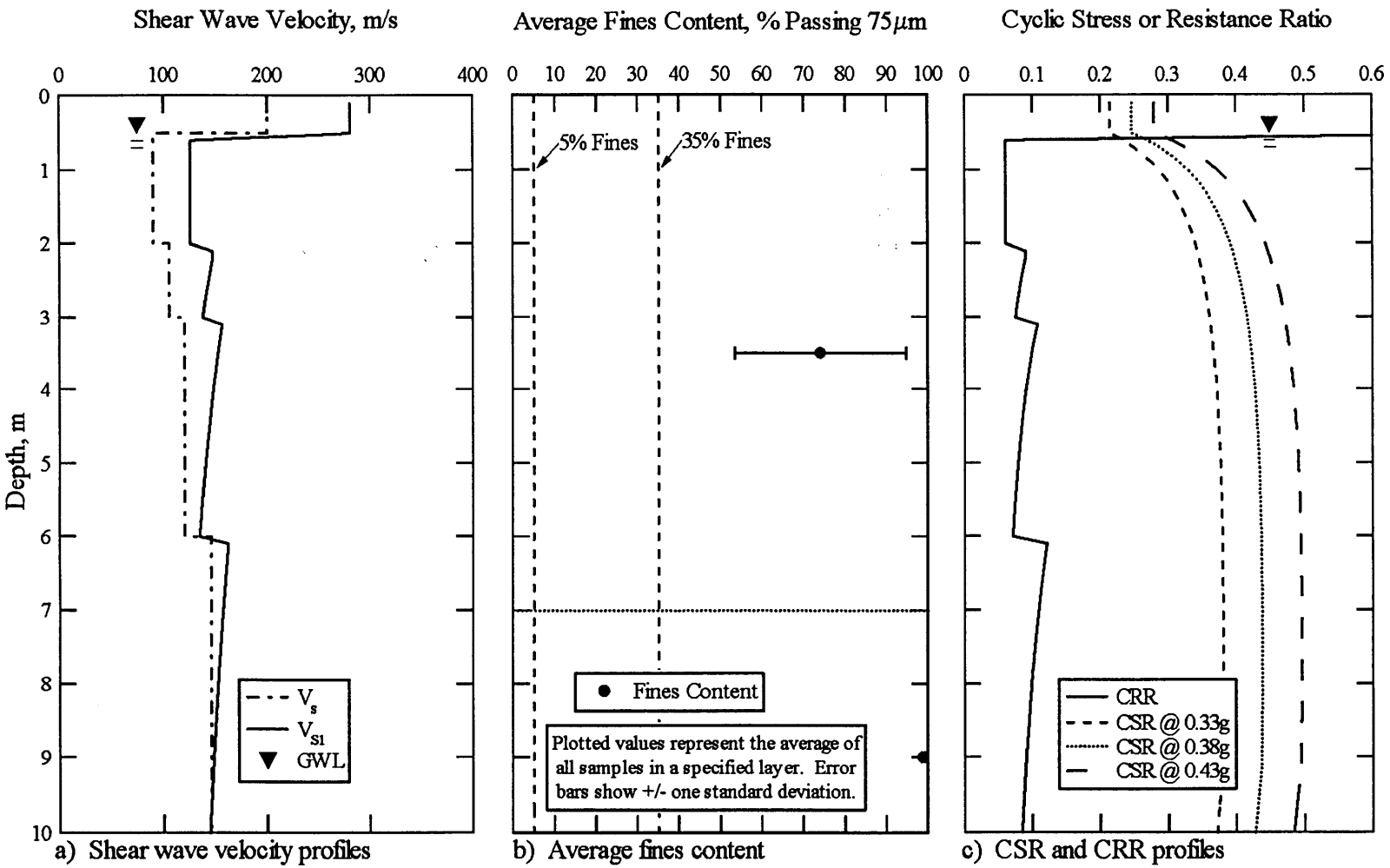

Figure 4.10 Graphs developed to delineate liquefiable soil using the simplified shear wave velocity procedure at Site G, Adapazari, Turkey (fines content obtained from http://peer.berkeley.edu/turkey/adapazari).

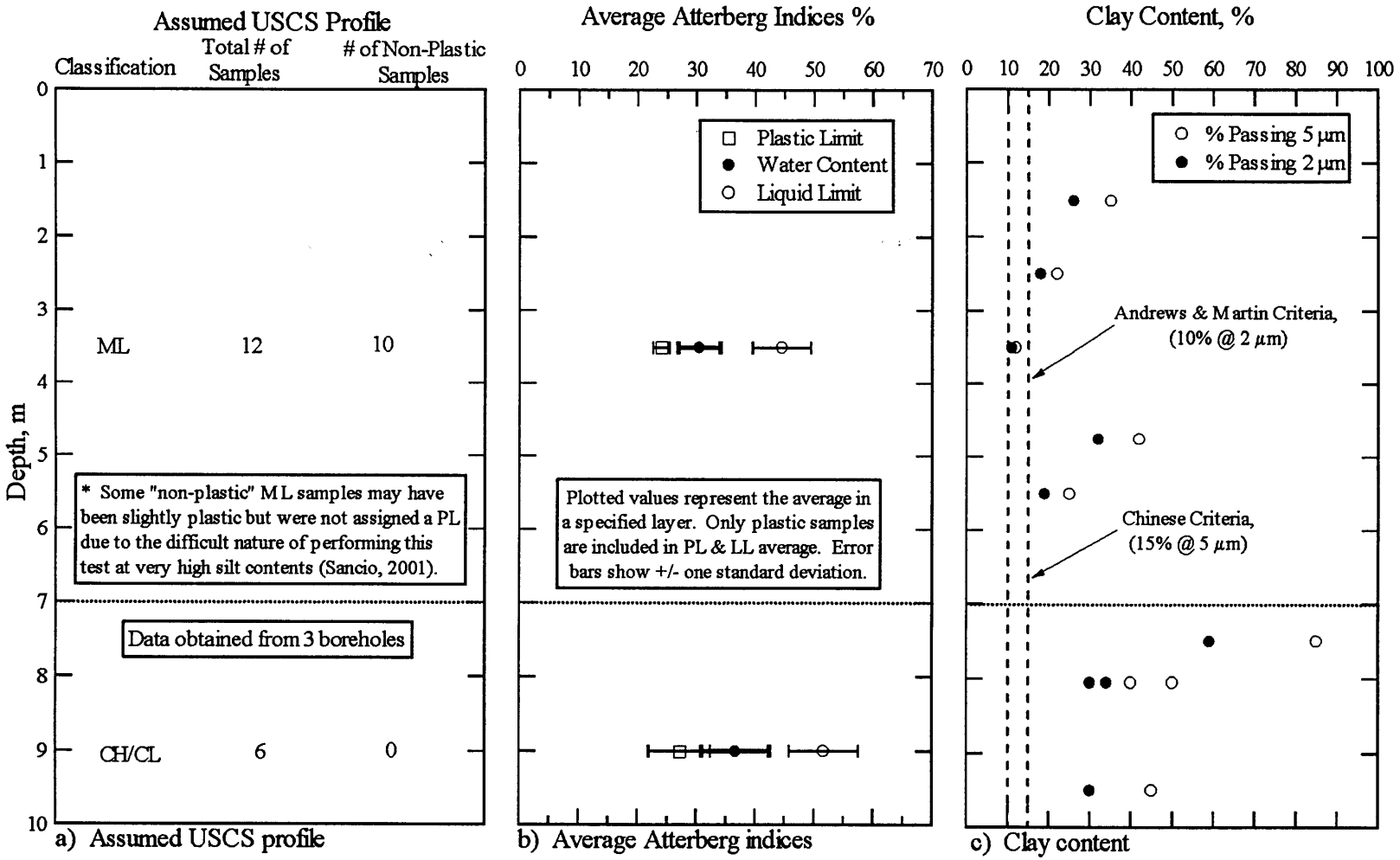

Figure 4.11 Graphs developed to delineate soils susceptible to liquefaction using the Chinese Criteria and the Andrews and Martin Criteria at Site G, Adapazari, Turkey (raw soil data from http://peer.berkeley.edu/turkey/adapazari).

Table 4.6 Average properties for soil layers located within the potentially liquefiable region at Site G.

Depth Interval (m)	Average (CRR/CSR)	USCS	Average LL (%)	Average (W_n/LL)	Average 5 μm Clay Content (%)	Average 2 μm Clay Content (%)	Liquefiable by Chinese Criteria	Liquefiable by Andrews & Martin Criteria
0.5 - 7	0.20	ML	44.5 [1]	0.68	27	24	no	no
7 - 10	0.22	CH/CL	51.7 [2]	0.71	56	41	no	no

1. 10/12 samples in this layer were non-plastic.
2. 0/6 samples in this layer were non-plastic.

4.2.1.6 Site J The graphs developed for Site J to delineate potentially liquefiable soil using the shear wave velocity simplified procedure are shown in Figure 4.12. Figure 4.12a shows the shear wave velocity profile (V_S) and the corrected shear wave velocity profile (V_{S1}) for the site. Figure 4.12b shows the average fines content from all samples within each layer. Figure 4.12c shows the CRR of the soil along with three CSR profiles. The central profile represents the CSR generated using the most probable ground acceleration predicted for this site. The other two profiles result from bracketing this acceleration by +/- 0.05 g. From this graph, it can be seen that the potentially liquefiable region extends from a depth of 0.5 meters through at least 23 meters. CSR values are not extended deeper than this because simplified procedures are not verified at greater depths. However, the soil profile is extremely soft down to 36 meters. The graphs developed for Site , to delineate soils susceptible to liquefaction using the Chinese Criteria and the Andrews and Martin Criteria are shown in Figure 4.13. The soil data for this site were obtained from four separate boreholes. Figure 4.13a shows the assumed USCS profile along with the total number of samples, and the number of non-plastic samples, included in each layer. Figure 4.13b shows average values for plastic limit, water content, and liquid limit in each layer. The 2 and 5 μm clay contents are plotted in Figure 4.13c.

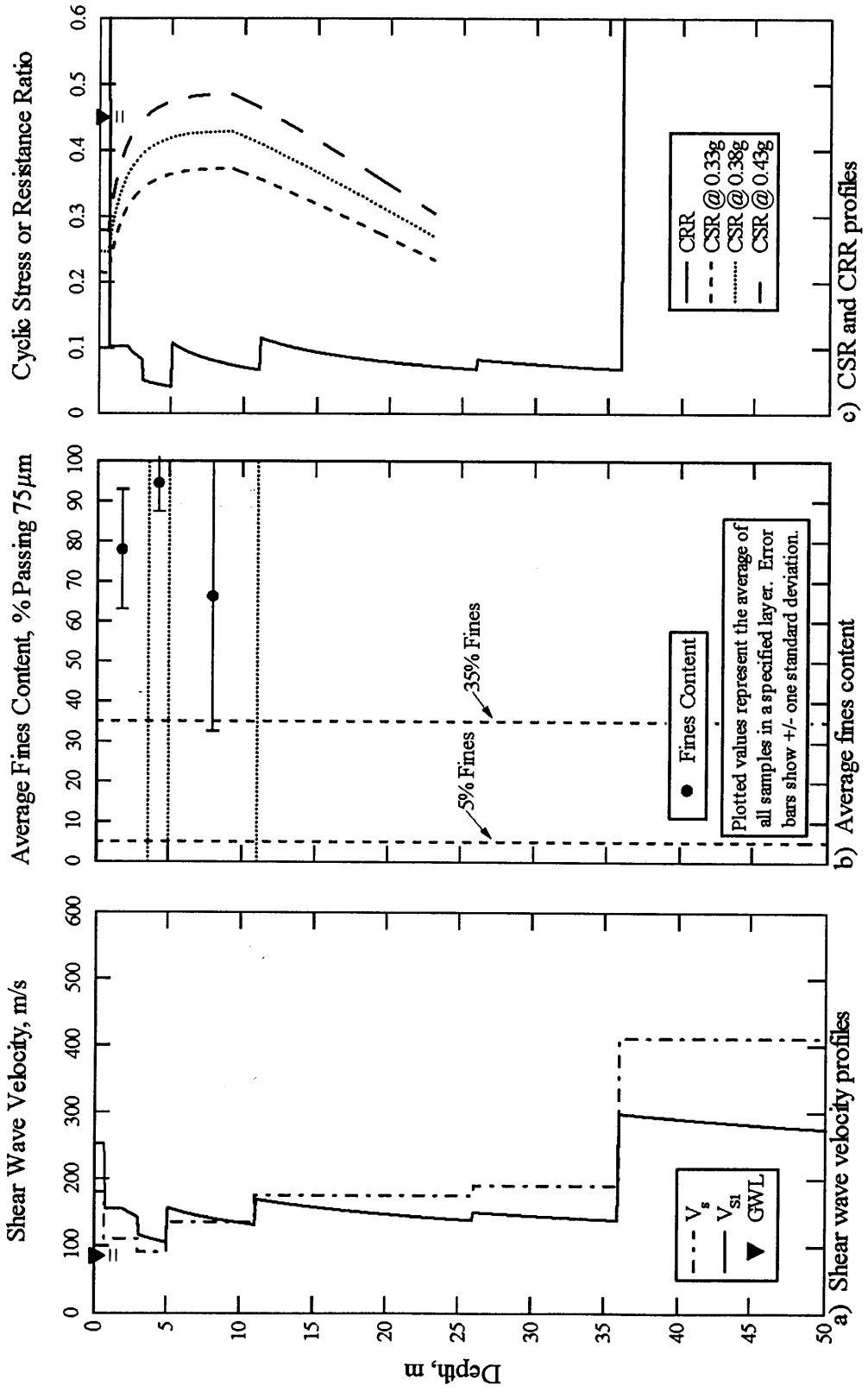

Figure 4.12 Graphs developed to delineate liquefiable soil using the simplified shear wave velocity procedure at Site J, Adapazari, Turkey (fines content obtained from http://peer.berkeley.edu/turkey/adapazari).

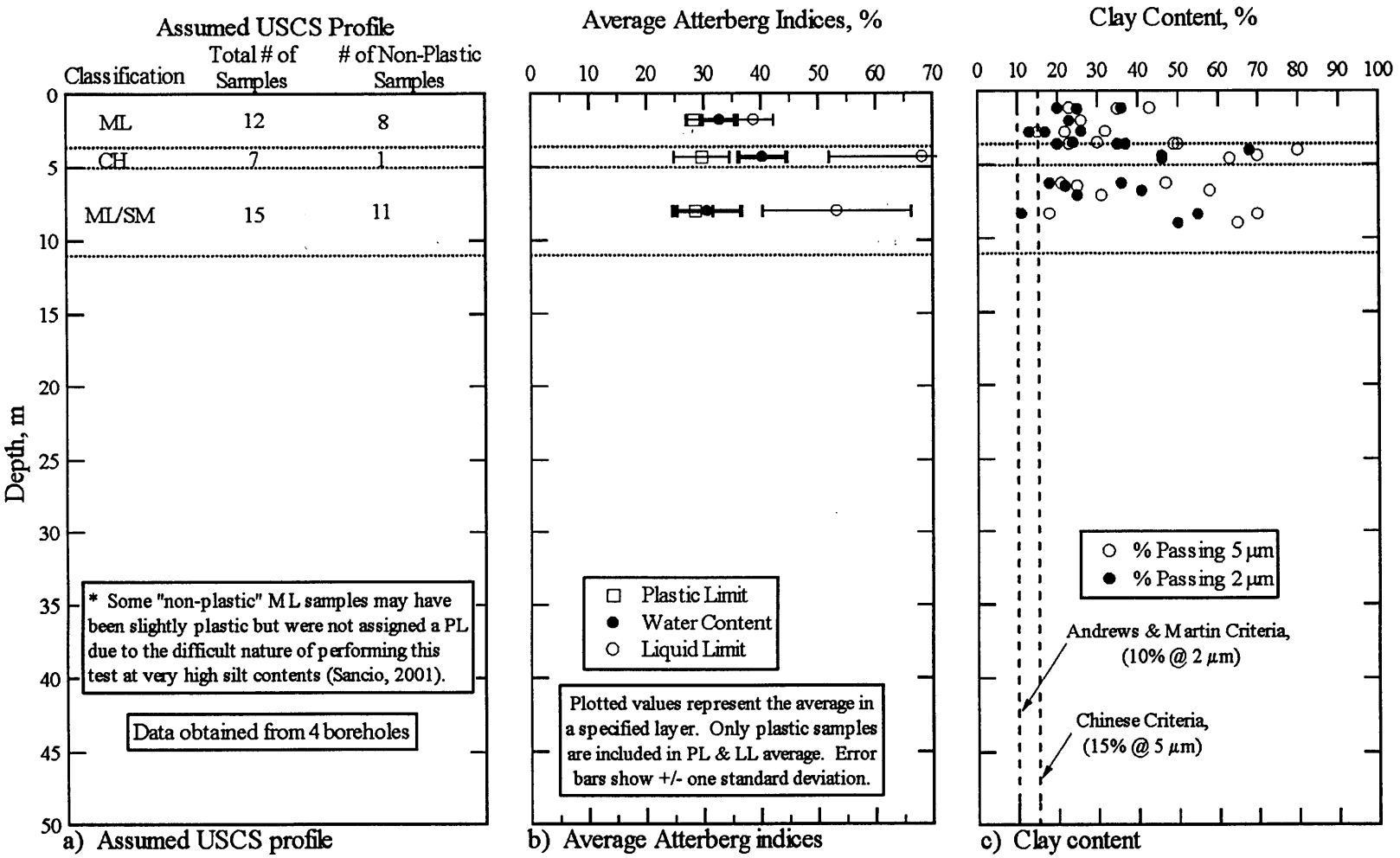

Figure 4.13 Graphs developed to delineate soils susceptible to liquefaction using the Chinese Criteria and the Andrews and Martin Criteria at Site J, Adapazari, Turkey (raw soil data from http://peer.berkeley.edu/turkey/adapazari).

Table 4.7 summarizes the data for all soil layers located within the potentially liquefiable region at Site J. All depth intervals are predicted as nonliquefiable by the Chinese Criteria and the Andrews and Martin Criteria. However, the depth interval from 0.7 - 3.6 meters comes closest to satisfying these criteria. The average reported LL for the plastic samples in the layer is 38.8, however, the majority (8 out of 12) of the samples are non-plastic. Therefore, this layer only fails the Chinese Criteria due to a high clay content. It is assumed that this nearly 3-meter thick layer of silt could have caused the two buildings at Site J to settle 25 cm.

Table 4.7 Average properties for soil layers located within the potentially liquefiable region at Site J

Depth Interval (m)	Average (CRR/CSR)	USCS	Average LL (%)	Average (W_n/LL)	Average 5 μm Clay Content (%)	Average 2 μm Clay Content (%)	Liquefiable by Chinese Criteria	Liquefiable by Andrews & Martin Criteria
0.7 - 3.6	0.25	ML	38.8 [1]	0.85	28	23	no	no
3.6 - 5	0.11	CH	68.2 [2]	0.59	56	42	no	no
5 - 11	0.19	ML/SM	53.3 [3]	0.57	42	32	no	no

1. 8/12 samples in this layer were non-plastic.
2. 1/7 samples in this layer were non-plastic.
3. 11/15 samples in this layer were non-plastic.

4.2.1.7 Site 1-11 The graphs developed for Site 1-11 to delineate potentially liquefiable soil using the shear wave velocity simplified procedure are shown in Figure 4.14. Figure 4.14a shows the shear wave velocity profile (V_S) and the corrected shear wave velocity profile (V_{S1}) for the site. Figure 4.14b shows the average fines content from all samples within each layer. Figure 4.14c shows the CRR of the soil along with three CSR profiles. The central profile represents the CSR generated using the most probable ground acceleration predicted for this site. The other two profiles result from bracketing this acceleration by +/- 0.05 g. From this graph, it can be seen that the potentially liquefiable region extends from a depth of 0.5 meters throughout the entire depth of the profile. The graphs developed for Site 1-11 to delineate soils susceptible to liquefaction using the Chinese Criteria and the Andrews and Martin Criteria are shown in Figure 4.15. The soil data for this site were obtained from one borehole. Figure 4.15a

shows the assumed USCS profile along with the total number of samples, and the number of non-plastic samples, included in each layer. Figure 4.15b shows average values for plastic limit, water content, and liquid limit in each layer. The 2 and 5 μm clay contents are plotted in Figure 4.15c.

Table 4.8 summarizes the data for all soil layers located within the potentially liquefiable region at Site 1-11. All depth intervals, except for one, are predicted as nonliquefiable by the Chinese Criteria and the Andrews and Martin Criteria. The layer predicted as susceptible is a silty-sand between the depths of 6 - 7 meters. However, it is questionable if a one-meter thick layer could have been the lone culprit that caused building N-1 to settle approximately 30 cm.

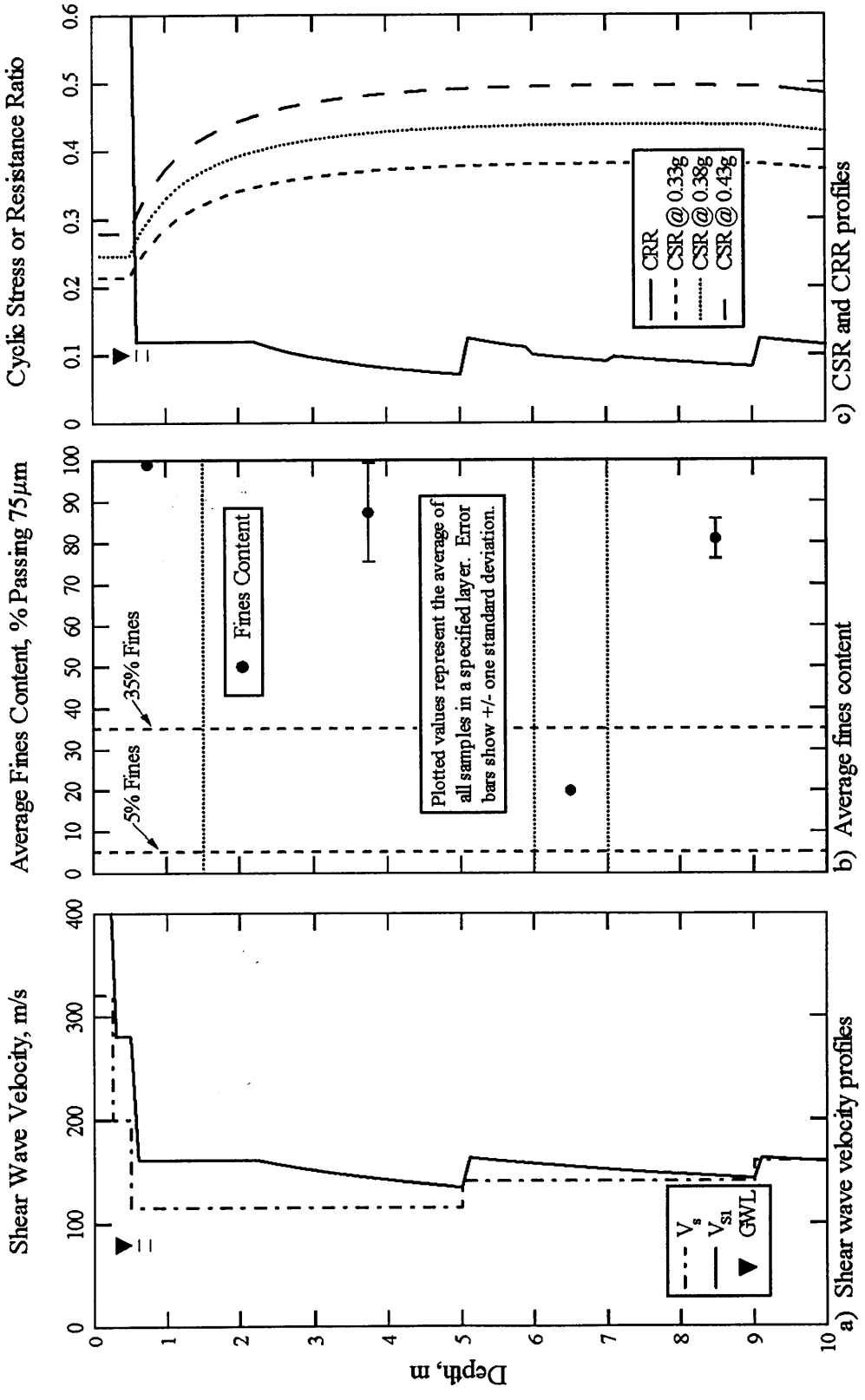

Figure 4.14 Graphs developed to delineate liquefiable soil using the simplified shear wave velocity procedure at Site 1-11, Adapazari, Turkey (fines content obtained from http://peer.berkeley.edu/turkey/adapazari).

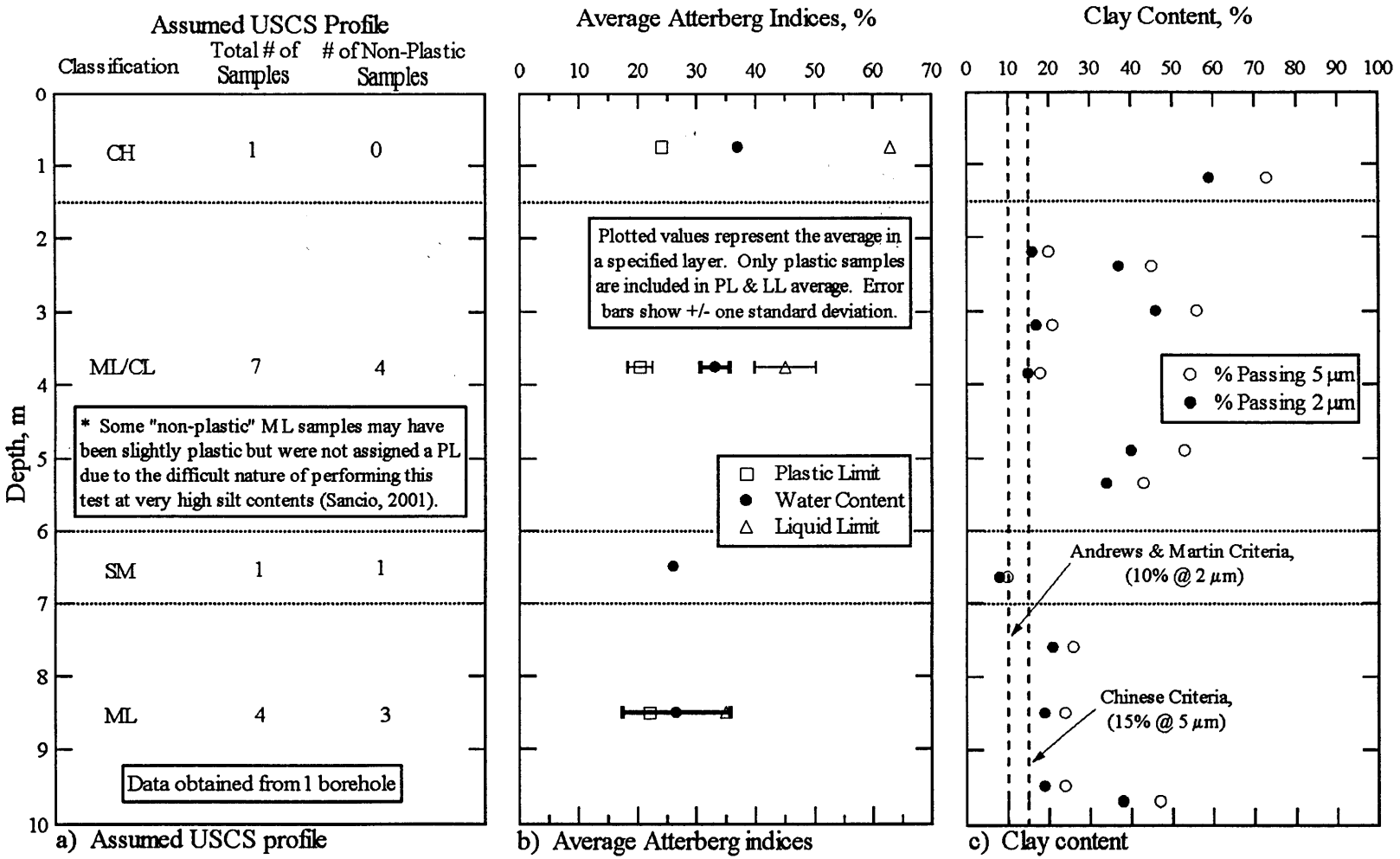

Figure 4.15 Graphs developed to delineate soils susceptible to liquefaction using the Chinese Criteria and the Andrews and Martin Criteria at Site 1-11, Adapazari, Turkey (raw soil data from http://peer.berkeley.edu/turkey/adapazari).

Table 4.8 Average properties for soil layers located within the potentially liquefiable region at Site 1-11

Depth Interval (m)	Average (CRR/CSR)	USCS	Average LL (%)	Average (Wn/LL)	Average 5_m Clay Content (%)	Average 2_m Clay Content (%)	Liquefiable by Chinese Criteria	Liquefiable by Andrews & Martin Criteria
0.5 - 1.5	0.37	CH	63.0 1	0.59	73	59	no	no
1.5 - 6	0.24	ML/CL	45.0 2	0.74	37	29	no	no
6 - 7	0.21	SM	-	-	10	8	yes	yes
7 - 10	0.23	ML	35.0 3	0.76	30	24	no	no

1. 0/1 samples in this layer were non-plastic.
2. 4/7 samples in this layer were non-plastic.
3. 3/4 samples in this layer were non-plastic.

4.2.1.8 Site 1-24 The graphs developed for Site 1-24 to delineate potentially liquefiable soil using the shear wave velocity simplified procedure are shown in Figure 4.16. Figure 4.16a shows the shear wave velocity profile (VS) and the corrected shear wave velocity profile (VS1) for the site. Figure 4.16b shows the average fines content from all samples within each layer. Figure 4.16c shows the CRR of the soil along with three CSR profiles. The central profile represents the CSR generated using the most probable ground acceleration predicted for this site. The other two profiles result from bracketing this acceleration by +/- 0.05 g. From this graph, it can be seen that the potentially liquefiable region extends from a depth of 2.5 meters throughout the entire depth of the profile. The graphs developed for Site 1-24 to delineate soils susceptible to liquefaction using the Chinese Criteria and the Andrews and Martin Criteria are shown in Figure 4.17. The soil data for this site were obtained from one borehole. Figure 4.17a shows the assumed USCS profile along with the total number of samples, and the number of non-plastic samples, included in each layer. Figure 4.17b shows average values for

plastic limit, water content, and liquid limit in each layer. The 2 and 5 μm clay contents are plotted in Figure 4.17c.

Table 4.9 summarizes the data for all soil layers located within the potentially liquefiable region at Site 1-24. The depth interval from 2.5 - 6.25 meters is predicted as nonliquefiable by the Chinese Criteria and the Andrews and Martin Criteria. The depth interval from 6.25 - 9 meters is a sandy layer that would have been expected to liquefy. This layer also has the lowest CRR/CSR value at 0.24. However, Site 1-24 is located along the banks of the Cark Canal, where no signs of liquefaction-induced lateral spreading were observed. Either this sand layer did not liquefy during the earthquake, or it did liquefy without surface expression.

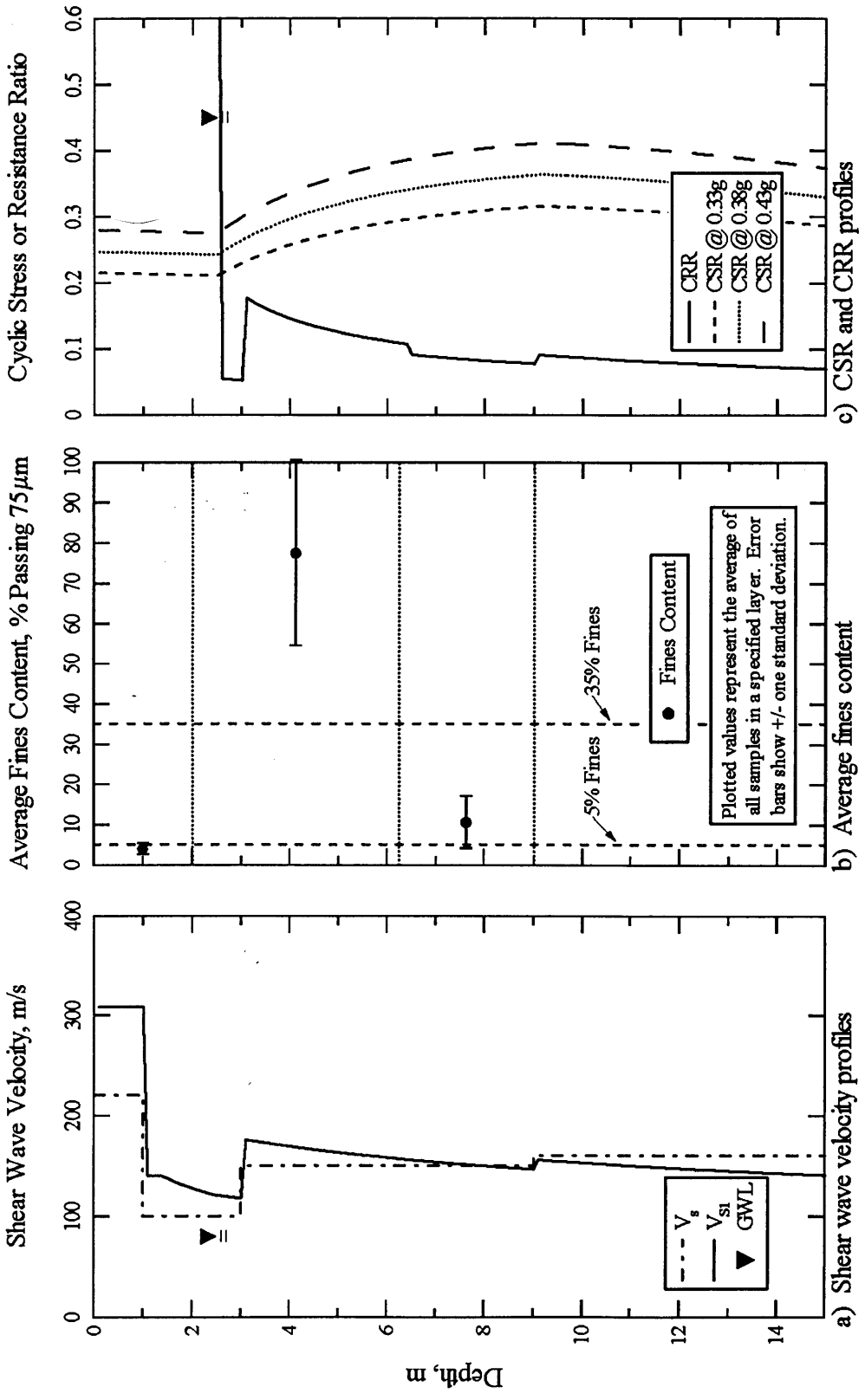

Figure 4.16 Graphs developed to delineate liquefiable soil using the simplified shear wave velocity procedure at Site 1-24, Adapazari, Turkey (fines content obtained from http://peer.berkeley.edu/turkey/adapazari).

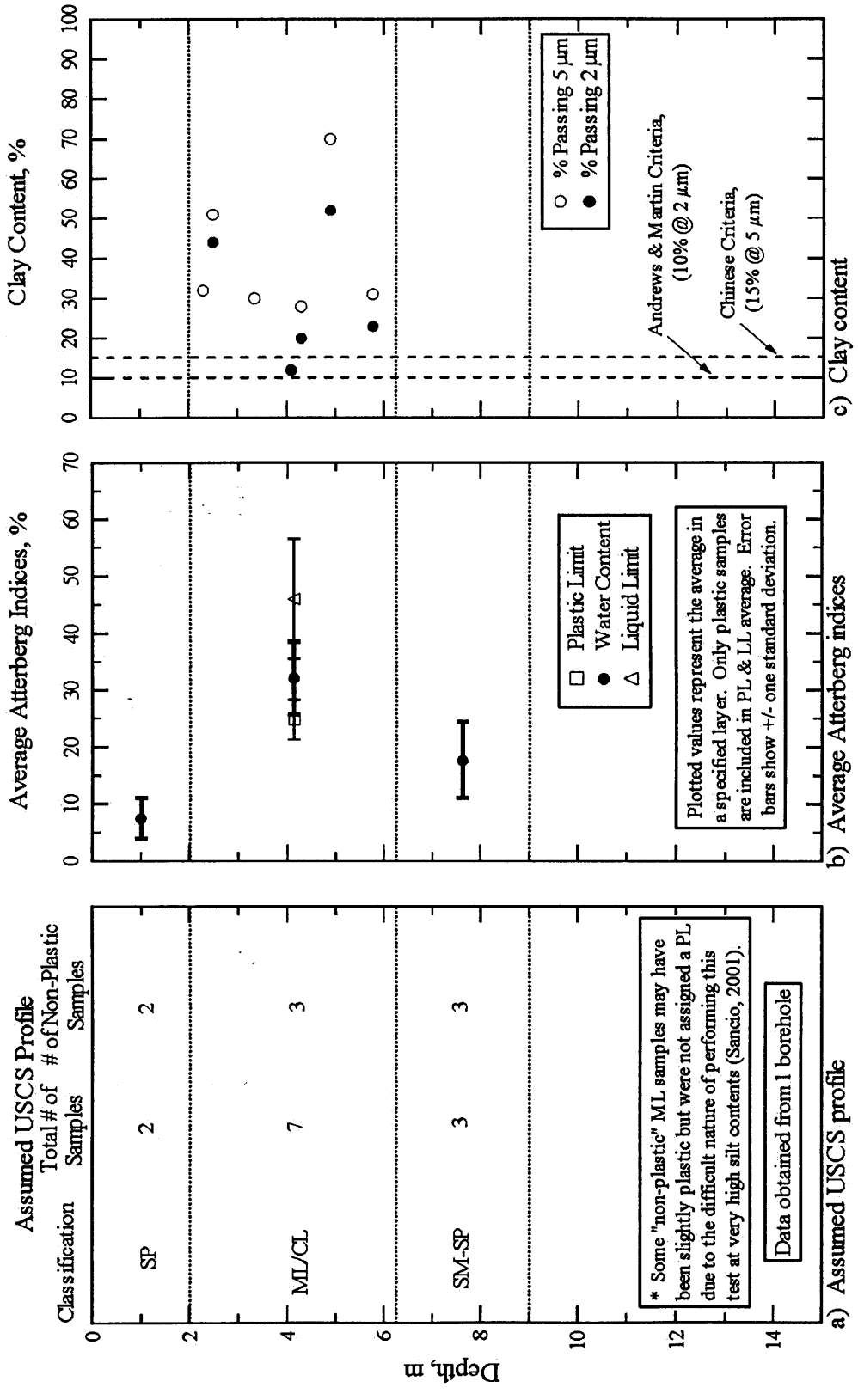

Figure 4.17 Graphs developed to delineate soils susceptible to liquefaction using the Chinese Criteria and the Andrews and Martin Criteria at Site 1-24, Adapazari, Turkey (raw soil data from http://peer.berkeley.edu/turkey/adapazari).

Table 4.9 Average properties for soil layers located within the potentially liquefiable region at Site 1.24

Depth Interval (m)	Average (CRR/CSR)	USCS	Average LL (%)	Average (Wn/LL)	Average 5_m Clay Content (%)	Average 2_m Clay Content (%)	Liquefiable by Chinese Criteria	Liquefiable by Andrews & Martin Criteria
2.5 - 6.25	0.41	ML/CL	46.0 1	0.70	36	30	no	no
6.25 - 9	0.24	SM-SP	-	-	-	-	yes	yes

1. 3/7 samples in this layer were non-plastic.

4.2.1.9 Site 1-41 The graphs developed for Site 1-41 to delineate potentially liquefiable soil using the shear wave velocity simplified procedure are shown in Figure 4.18. Figure 4.18a shows the shear wave velocity profile (VS) and the corrected shear wave velocity profile (VS1) for the site. Figure 4.18b shows the average fines content from all samples within each layer. Figure 4.18c shows the CRR of the soil along with three CSR profiles. The central profile represents the CSR generated using the most probable ground acceleration predicted for this site. The other two profiles result from bracketing this acceleration by +/- 0.05 g. From this graph, it can be seen that the potentially liquefiable region is broken into several portions. This is due to the corrected shear wave velocity being very close to the maximum liquefiable velocity of 200 m/s. The liquefiable region is between the depths of 0.5 - 3 meters, and 5.25 - 8 meters. It appears that there might be another portion of the liquefiable region below 9.5 meters but no soil data are available at this site below 10 meters. The graphs developed for Site 1-41 to delineate soils susceptible to liquefaction using the Chinese Criteria and the Andrews and Martin Criteria are shown in Figure 4.19. The soil data for this site were obtained from one borehole. Figure 4.19a shows the assumed USCS profile along with the total number of samples, and the number of non-plastic samples, included in each layer.

Figure 4.19b shows average values for plastic limit, water content, and liquid limit in each layer. The 2 and 5 μm clay contents are plotted in Figure 4.19c.

Table 4.10 summarizes the data for all soil layers located within the potentially liquefiable region at Site 1-41. The depth interval from 0.5 - 3 meters is predicted as nonliquefiable by the Chinese Criteria and the Andrews and Martin Criteria. The depth interval from 5.25 - 8 meters is a sandy layer that would be expected to liquefy. This layer also has the lowest CRR/CSR value at 0.39. This layer most likely caused the 10 - 20 cm of building settlement that occurred here.

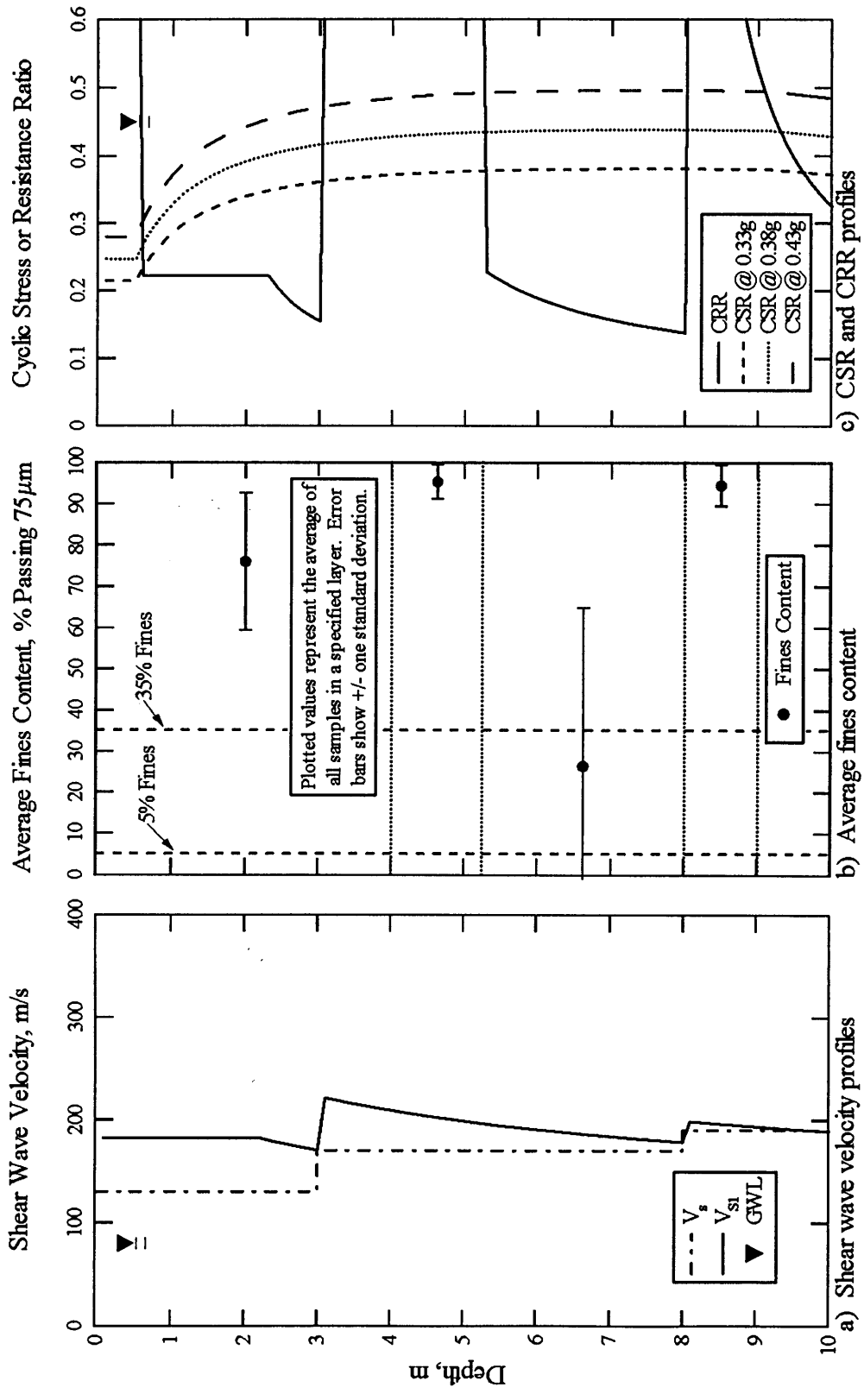

Figure 4.18 Graphs developed to delineate liquefiable soil using the simplified shear wave velocity procedure at Site 1-41, Adapazari, Turkey (fines content obtained from http://peer.berkeley.edu/turkey/adapazari).

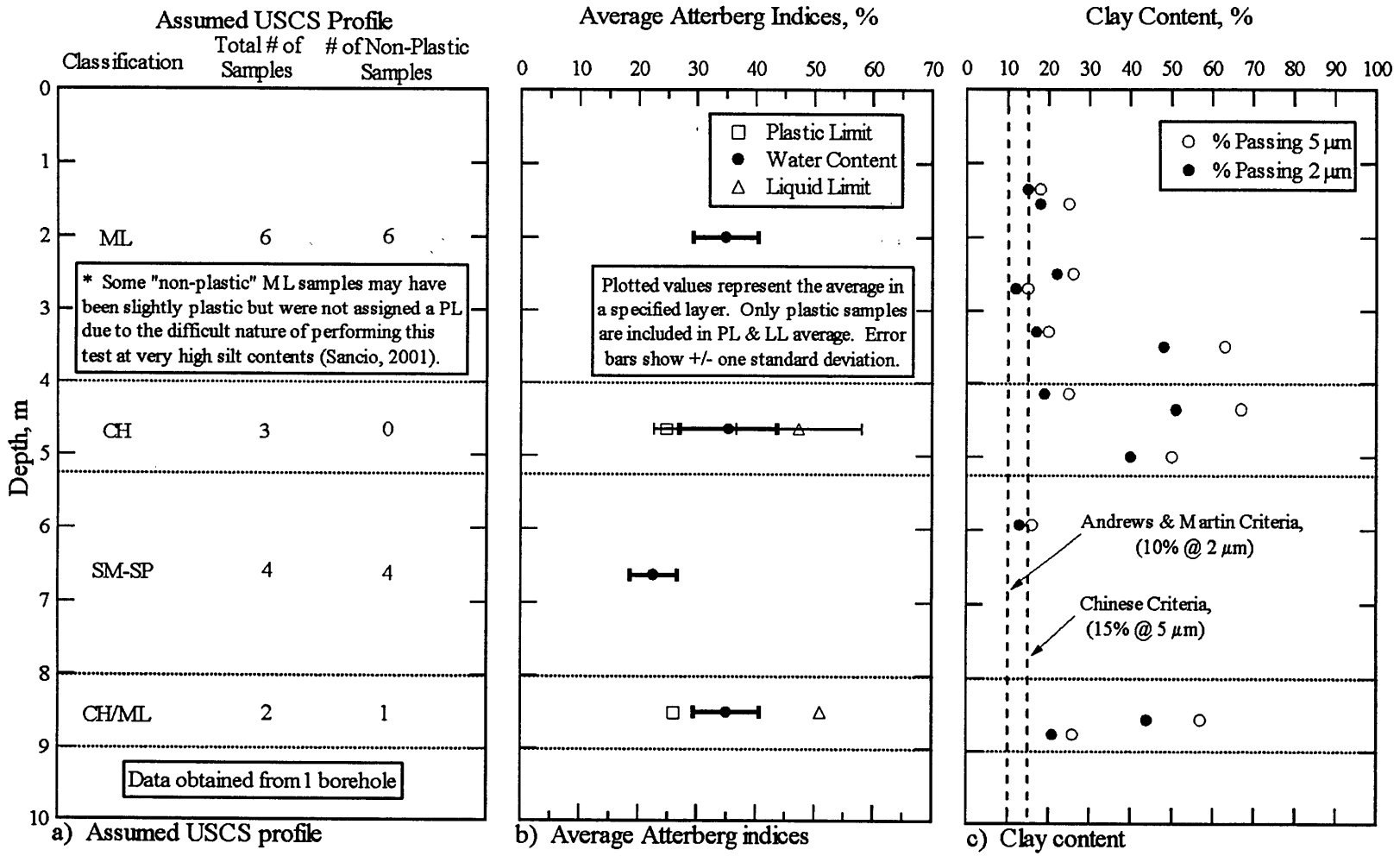

Figure 4.19 Graphs developed to delineate soils susceptible to liquefaction using the Chinese Criteria and the Andrews and Martin Criteria at Site 1-41, Adapazari, Turkey (raw soil data from http://peer.berkeley.edu/turkey/adapazari).

Table 4.10 Average properties for soil layers located within the potentially liquefiable region at Site 1-41

Depth Interval (m)	Average (CRR/CSR)	USCS	Average LL (%)	Average (W_n/LL)	Average 5 μm Clay Content (%)	Average 2 μm Clay Content (%)	Liquefiable by Chinese Criteria	Liquefiable by Andrews & Martin Criteria
0.5 - 3	0.58	ML	-	-	28	22	no	no
5.25 - 8	0.39	SM-SP	-	-	-	-	yes	yes

4.2.1.10 Site 1-42 The graphs developed for Site 1-42 to delineate potentially liquefiable soil using the shear wave velocity simplified procedure are shown in Figure 4.20. Figure 4.20a shows the shear wave velocity profile (V_S) and the corrected shear wave velocity profile (V_{S1}) for the site. Figure 4.20b shows the average fines content from all samples within each layer. Figure 4.20c shows the CRR of the soil along with three CSR profiles. The central profile represents the CSR generated using the most probable ground acceleration predicted for this site. The other two profiles result from bracketing this acceleration by +/- 0.05 g. From this graph, it can be seen that the potentially liquefiable region extends from a depth of 0.5 meters throughout the entire depth of the profile. The graphs developed for Site 1-42 to delineate soils susceptible to liquefaction using the Chinese Criteria and the Andrews and Martin Criteria are shown in Figure 4.21. The soil data for this site were obtained from one borehole. Figure 4.21a shows the assumed USCS profile along with the total number of samples, and the number of non-plastic samples, included in each layer. Figure 4.21b shows average values for plastic limit, water content, and liquid limit in each layer. The 2 and 5 μm clay contents are plotted in Figure 4.21c.

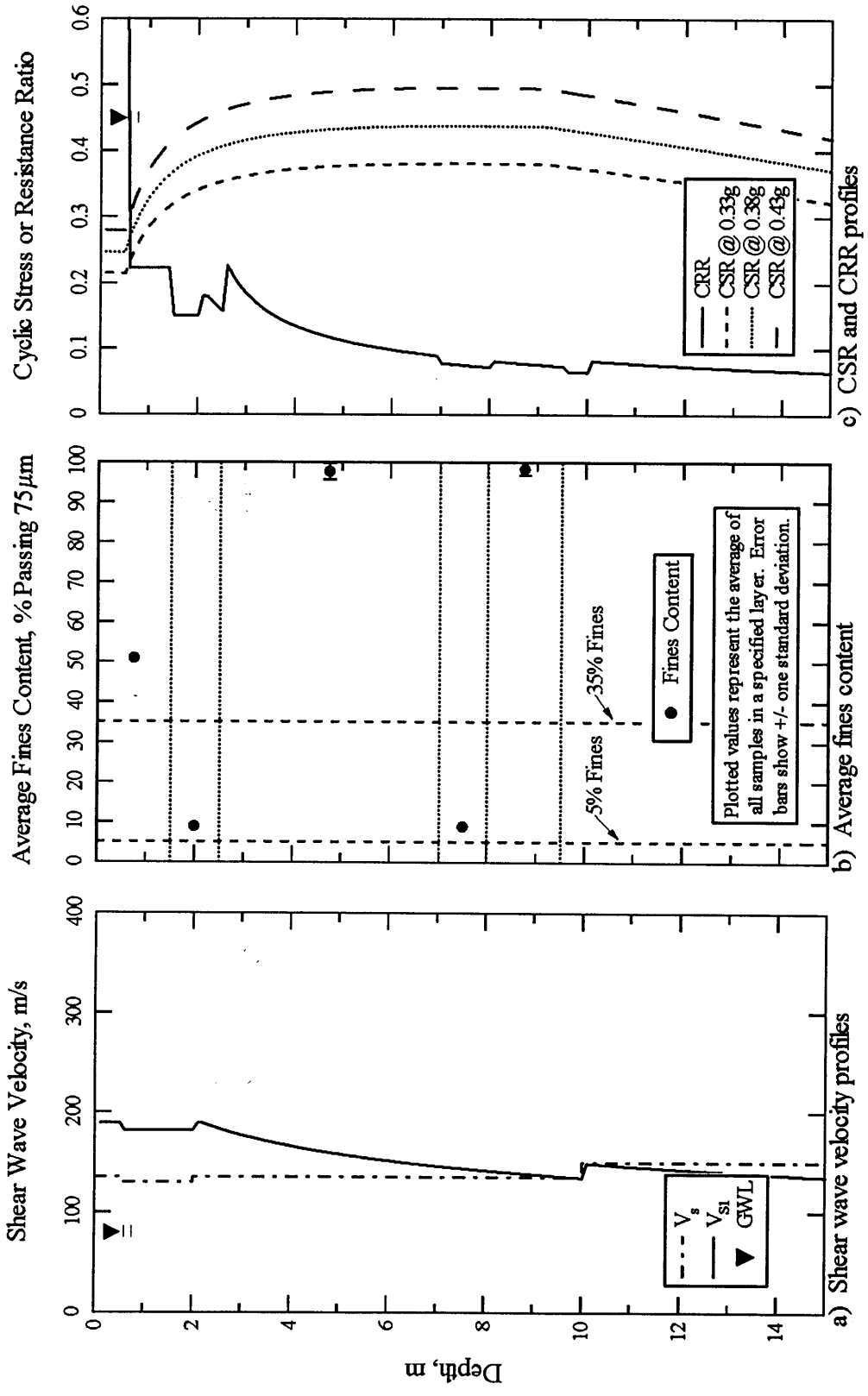

Figure 4.20 Graphs developed to delineate liquefiable soil using the simplified shear wave velocity procedure at Site 1-42, Adapazari, Turkey (fines content obtained from http://peer.berkeley.edu/turkey/adapazari).

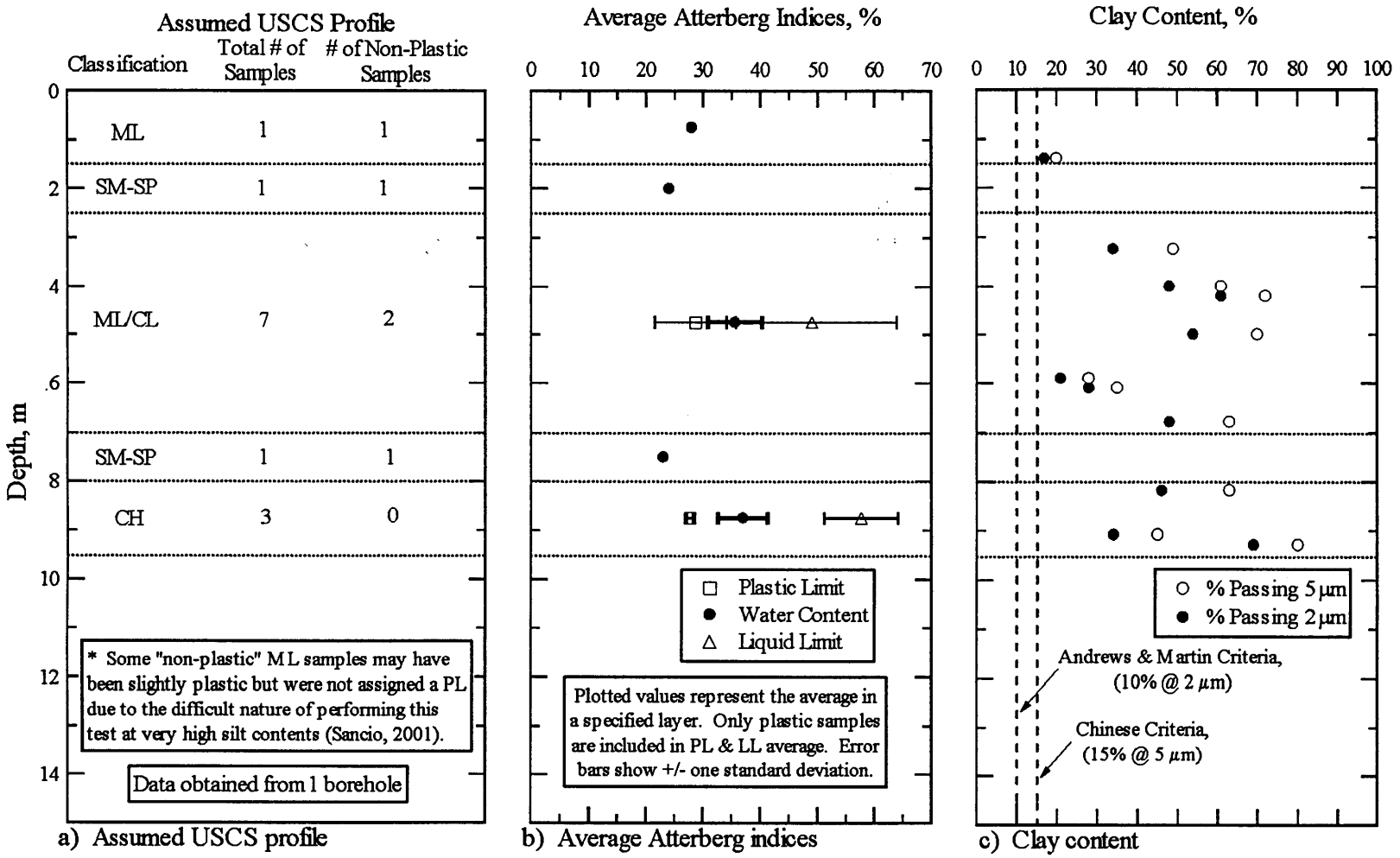

Figure 4.21 Graphs developed to delineate soils susceptible to liquefaction using the Chinese Criteria and the Andrews and Martin Criteria at Site 1-42, Adapazari, Turkey (raw soil data from http://peer.berkeley.edu/turkey/adapazari).

Table 4.11 summarizes the data for all soil layers located within the potentially liquefiable region at Site 1-42. Two of the depth intervals would be predicted as susceptible to liquefaction. One is a sand layer between the depths of 1.5 - 2.5 meters. The other is also a sand layer between the depths of 7 - 8 meters. Either one or both could have liquefied during the earthquake. However, the lower layer has a smaller value of CRR/CSR and would therefore be predicted as the most critical layer. These layers most likely caused the two buildings at Site 1-42 to settle 4 cm.

Table 4.11 Average properties for soil layers located within the potentially liquefiable region at Site 1-42

Depth Interval (m)	Average (CRR/CSR)	USCS	Average LL (%)	Average (W_n/LL)	Average 5 μm Clay Content (%)	Average 2 μm Clay Content (%)	Liquefiable by Chinese Criteria	Liquefiable by Andrews & Martin Criteria
0.5 - 1.5	0.66	ML	-	-	20	17	no	no
1.5 - 2.5	0.41	SM-SP	-	-	-	-	yes	yes
2.5 - 7	0.29	ML/CL	49.0 [1]	0.73	54	42	no	no
7 - 8	0.17	SM-SP	-	-	-	-	yes	yes
8 - 9.5	0.17	CH	57.7 [2]	0.64	63	50	no	no

1. 2/7 samples in this layer were non-plastic.
2. 0/3 samples in this layer were non-plastic.

4.2.2 Hotel Sapanca

Four SASW centerlines were used at Hotel Sapanca in order to investigate the full extent of the on-shore portion of the lateral spread that occurred here. More than 10 CPT soundings were available at this site. However, only the five soundings closest to the SASW centerlines were used for developing a soil profile at the site. Upon investigation of these soundings, it was clear that the soil over the entire area was uniform, consisting of sand/sand mixtures throughout. Therefore, only one soil profile was developed for the site.

The graphs developed for Centerline 1 at Hotel Sapanca to delineate potentially liquefiable soil using the shear wave velocity simplified procedure, are shown in Figure 4.22. Figure 4.22a shows the shear wave velocity profile (V_S) and the corrected shear wave velocity profile (V_{S1}) for the site. Figure 4.22b shows the fines content used for the calculation of CRR's. Figure 4.22c shows the CRR of the soil along with three CSR profiles. The central profile represents the CSR generated using the most probable ground acceleration predicted for this site. The other two profiles result from bracketing this acceleration by +/- 0.05 g. From this graph, it can be seen that the potentially liquefiable region extends from a depth of 1.25 meters throughout the entire depth of the profile.

The graphs developed for Centerline 2 at Hotel Sapanca to delineate potentially liquefiable soil using the shear wave velocity simplified procedure are shown in Figure 4.23. Figure 4.23a shows the shear wave velocity profile (V_S) and the corrected shear wave velocity profile (V_{S1}) for the site. Figure 4.23b shows the fines content used for the calculation of CRR's. Figure 4.23c shows the CRR of the soil along with three CSR profiles. The central profile represents the CSR generated using the most probable ground acceleration predicted for this site. The other two profiles result from bracketing this acceleration by +/- 0.05 g. From this graph, it can be seen that the potentially liquefiable region extends from a depth of 1.6 meters throughout the entire depth of the profile.

The graphs developed for Centerline 3 at Hotel Sapanca to delineate potentially liquefiable soil using the shear wave velocity simplified procedure are shown in Figure 4.24. Figure 4.24a shows the shear wave velocity profile (V_S) and the corrected shear wave velocity profile (V_{S1}) for the site. Figure 4.24b shows the fines content used for the calculation of CRR's. Figure 4.24c shows the CRR of the soil along with three CSR profiles. The central profile represents the CSR generated using the most probable ground acceleration predicted for this site. The other two profiles result from bracketing this acceleration by +/- 0.05 g. From this graph, it can be seen that the potentially liquefiable region is broken into two portions. This is due to the corrected shear wave

velocity having a value just over 215 m/s from approximately 5 - 5.5 meters. The liquefiable region is between the depths of 1.25 - 5 meters, and 5.5 - 15 meters.

The graphs developed for Centerline 4 at Hotel Sapanca to delineate potentially liquefiable soil using the shear wave velocity simplified procedure are shown in Figure 4.25. Figure 4.25a shows the shear wave velocity profile (V_S) and the corrected shear wave velocity profile (V_{S1}) for the site. Figure 4.25b shows the fines content used for the calculation of CRR's. Figure 4.25c shows the CRR of the soil along with three CSR profiles. The central profile represents the CSR generated using the most probable ground acceleration predicted for this site. The other two profiles result from bracketing this acceleration by +/- 0.05 g. From this graph, it can be seen that the potentially liquefiable region extends from a depth of 0.5 - 7 meters.

As mentioned above, five CPT soundings were analyzed at Hotel Sapanca. The graphs developed from CPT-SH4, to characterize the subsurface, are shown in Figure 4.26. The graphs developed from CPT-SH5, to characterize the subsurface, are shown in Figure 4.27. The graphs developed from CPT-SH6, to characterize the subsurface, are shown in Figure 4.28. The graphs developed from CPT-SH7 are shown in Figure 4.29. The graphs developed from CPT-SH8 are shown in Figure 4.30. Figure 4.31 shows the idealized soil profile and layer properties at Hotel Sapanca as determined from combining the data from these five cone soundings.

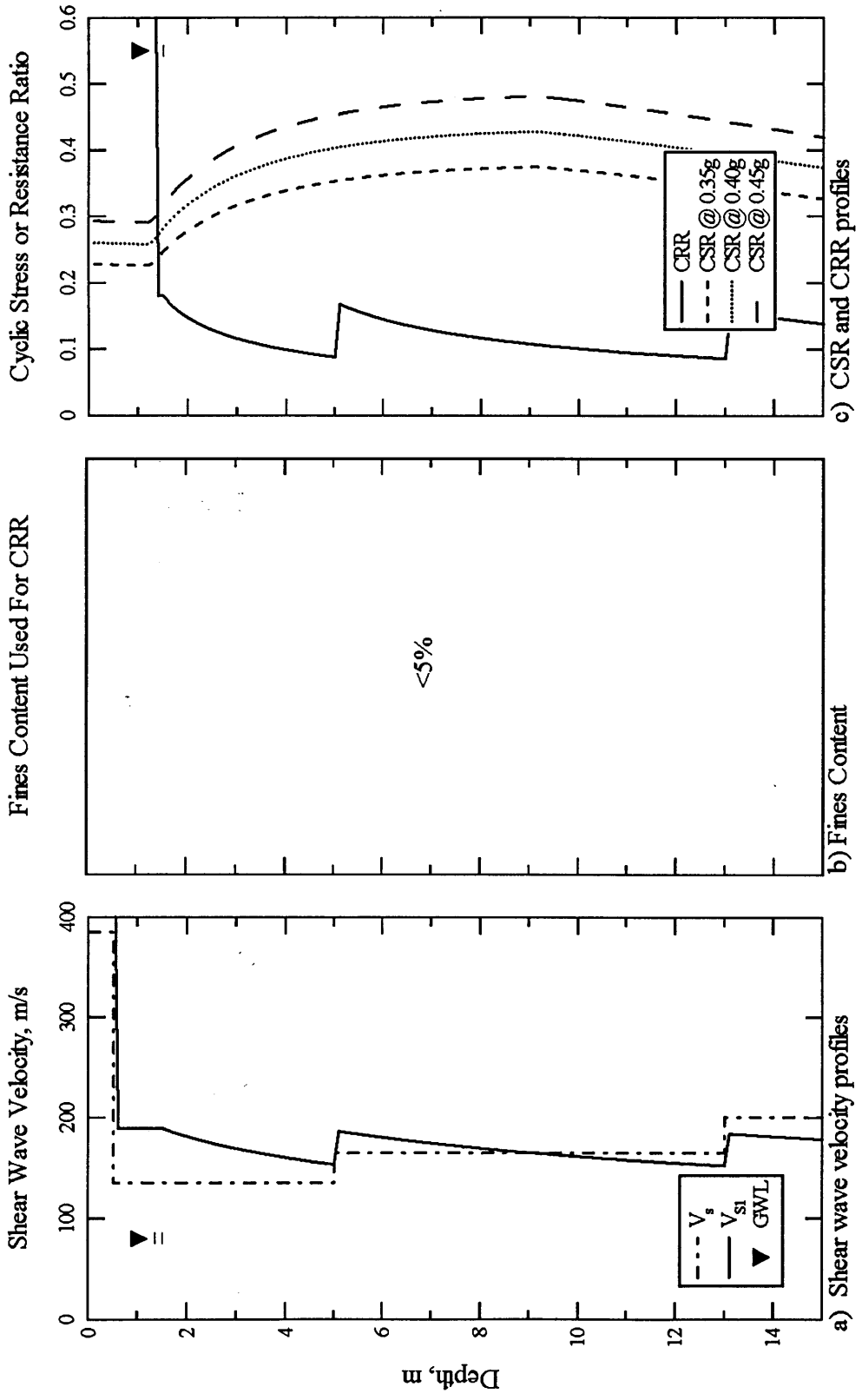

Figure 4.22 Graphs developed to delineate liquefiable soil using the simplified shear wave velocity procedure at Centerline 1, Hotel Sapanca, Sapanca, Turkey.

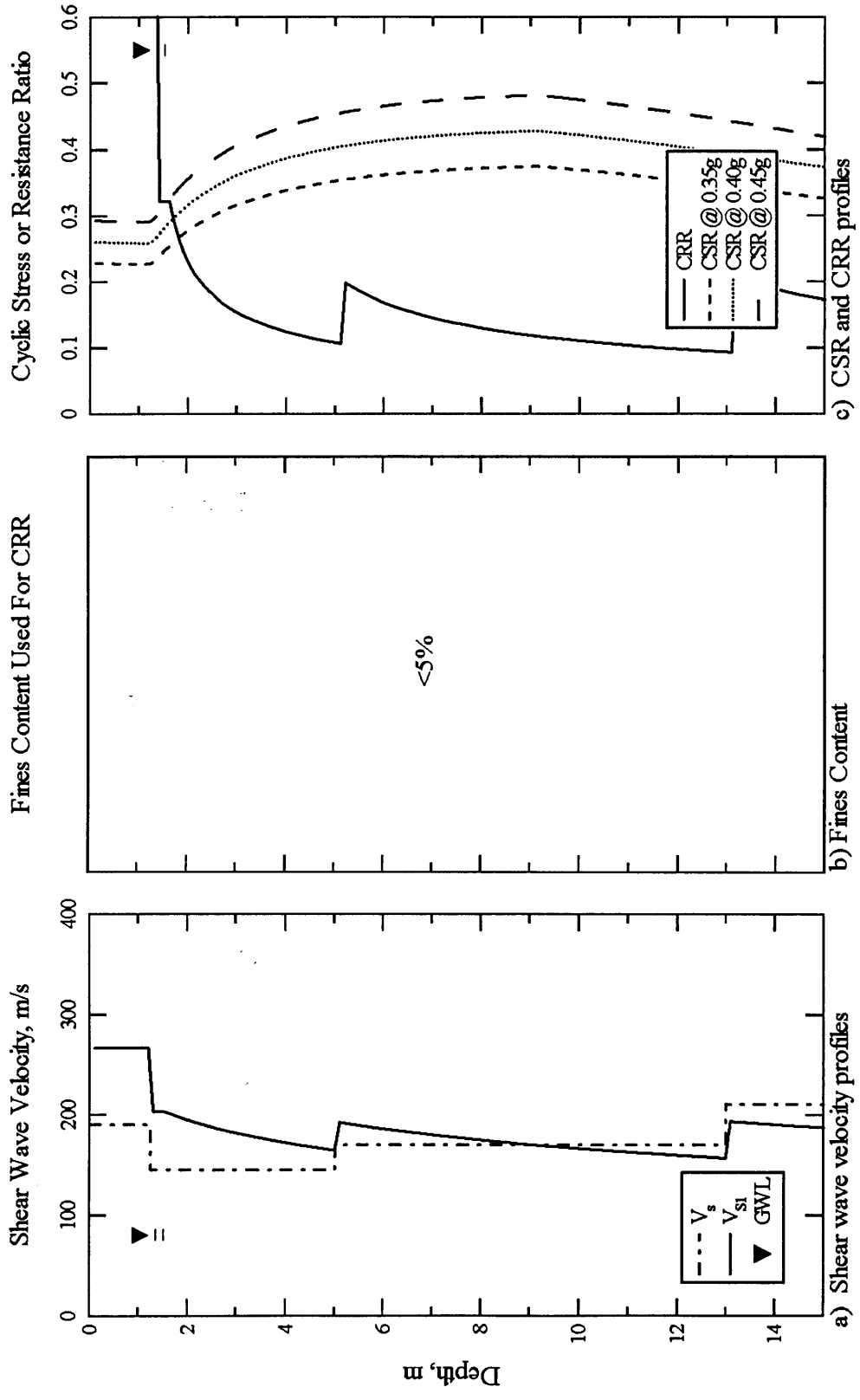

Figure 4.23 Graphs developed to delineate liquefiable soil using the simplified shear wave velocity procedure at Centerline 2, Hotel Sapanca, Sapanca, Turkey.

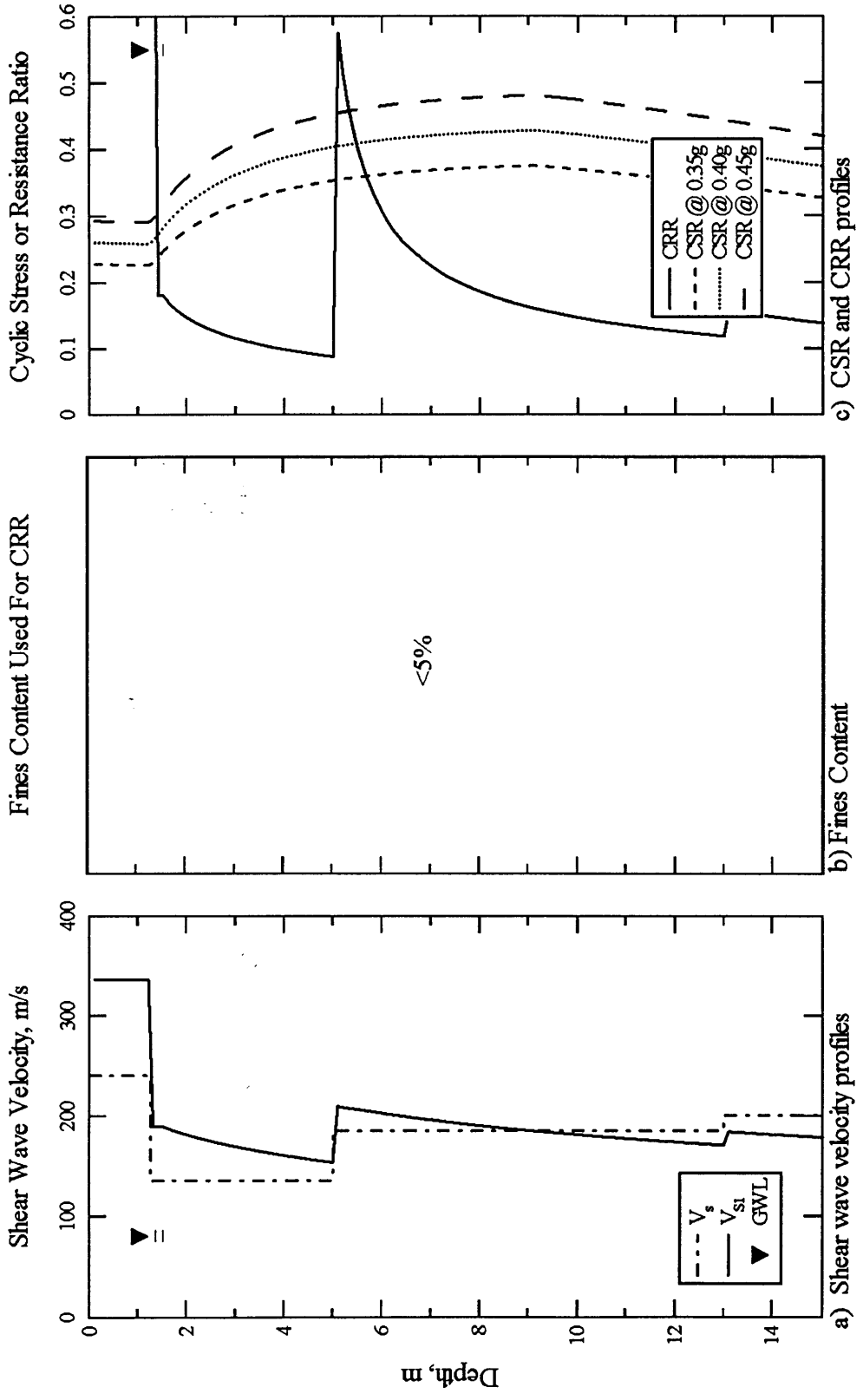

Figure 4.24 Graphs developed to delineate liquefiable soil using the simplified shear wave velocity procedure at Centerline 3, Hotel Sapanca, Sapanca, Turkey.

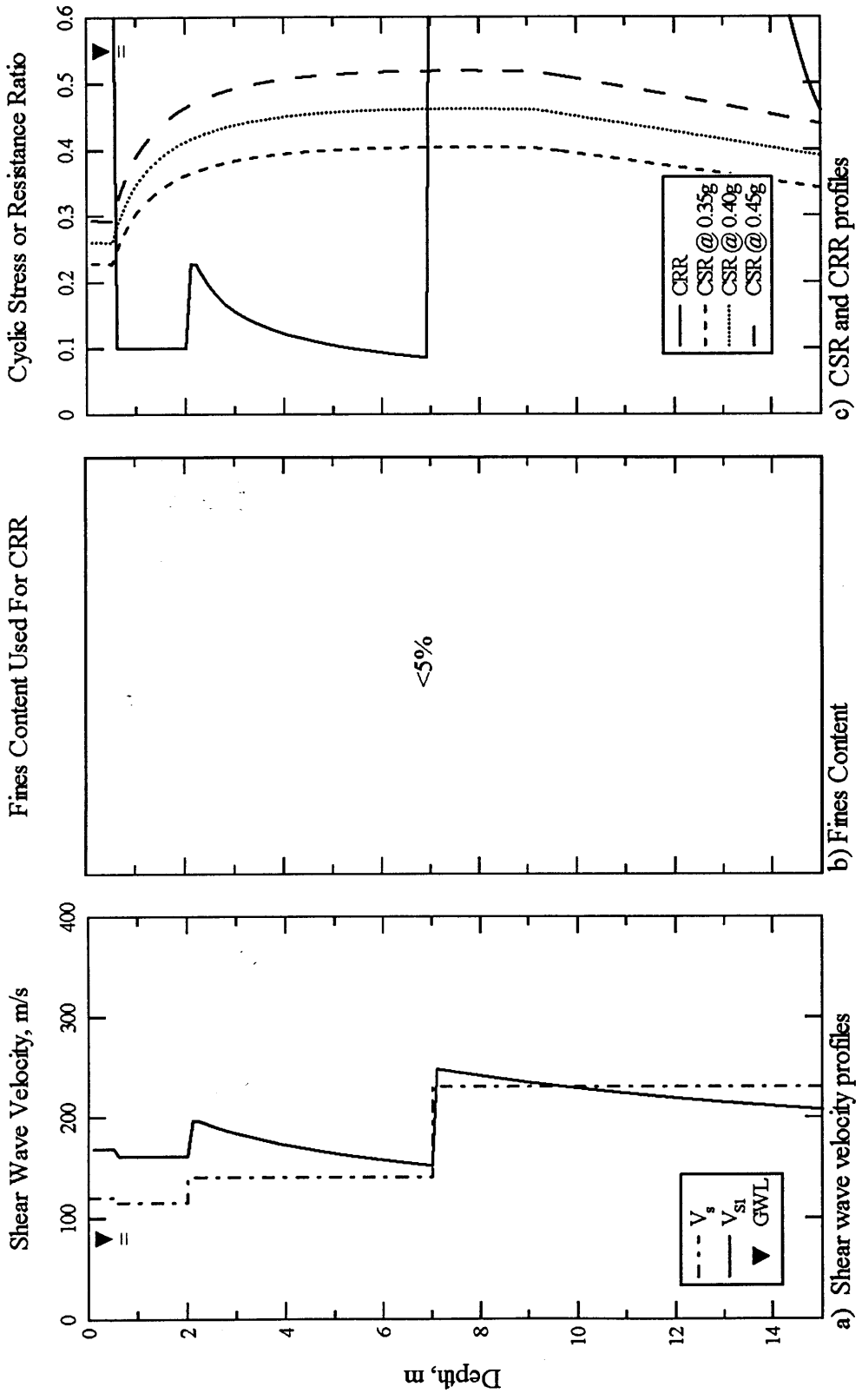

Figure 4.25 Graphs developed to delineate liquefiable soil using the simplified shear wave velocity procedure at Centerline 4, Hotel Sapanca, Sapanca, Turkey.

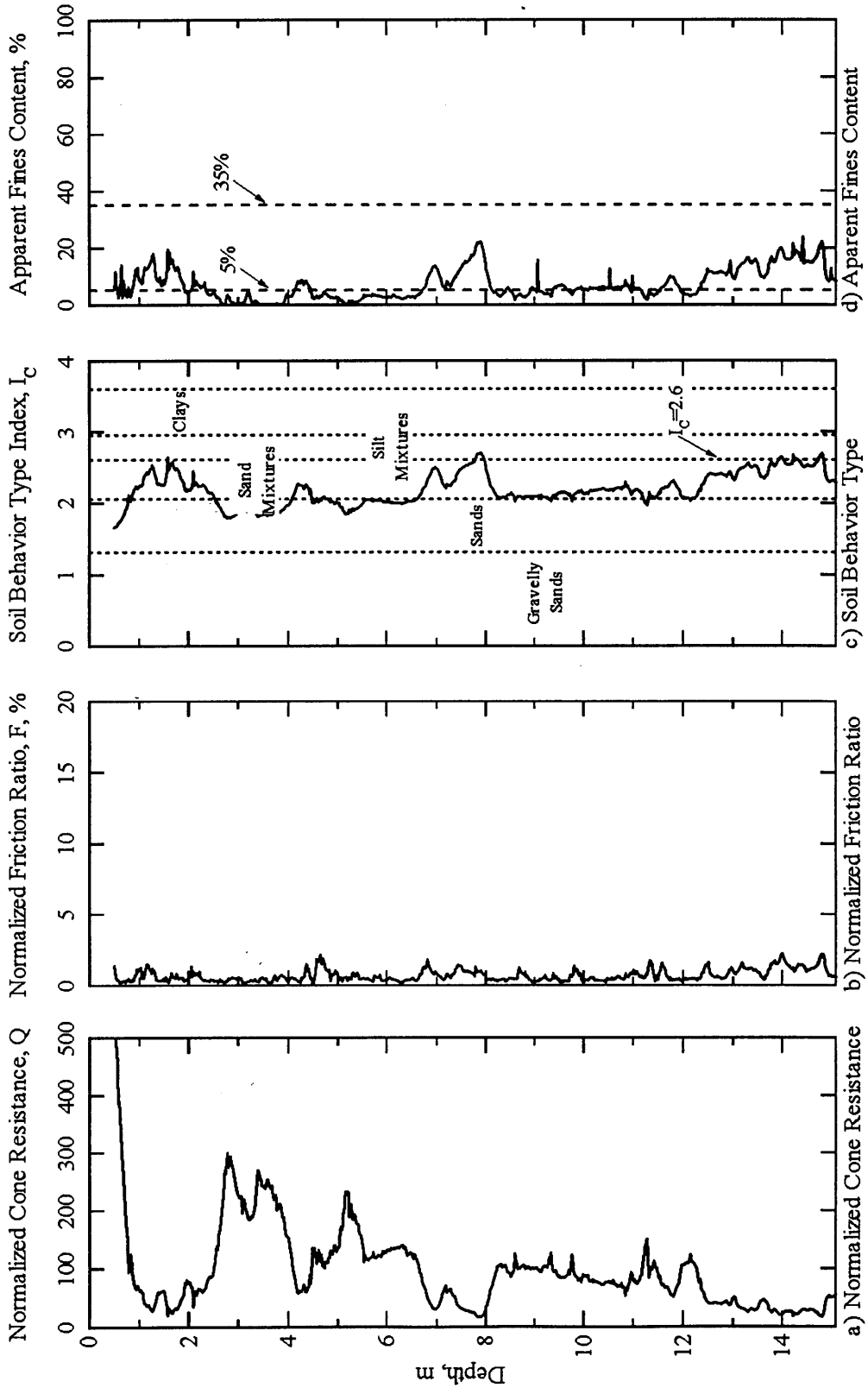

Figure 4.26 Graphs developed from CPT-SH4 to characterize the subsurface at Hotel Sapanca, Sapanca, Turkey (raw cone data from http://peer.berkeley.edu/turkey/adapazari).

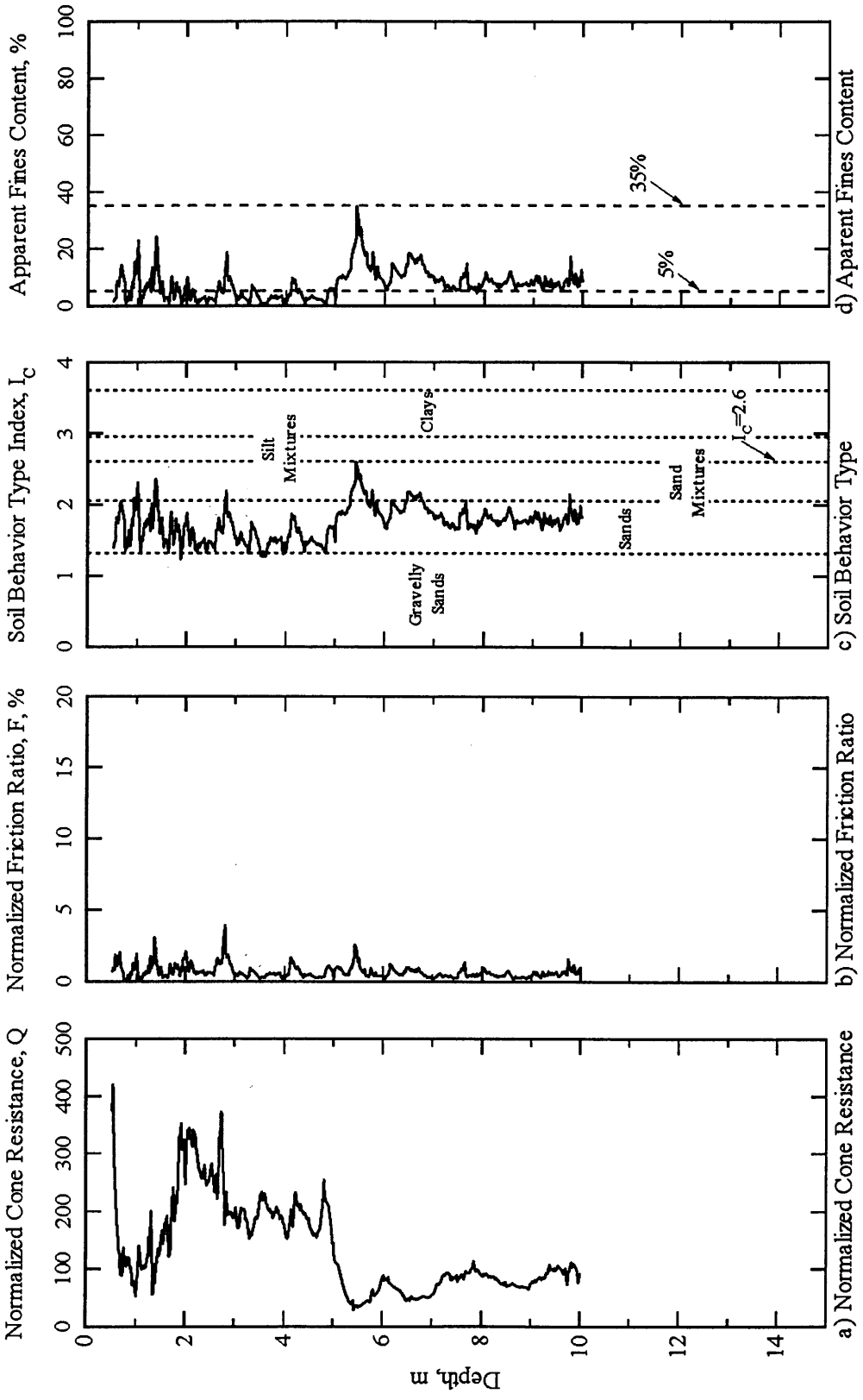

Figure 4.27 Graphs developed from CPT-SH5 to characterize the subsurface at Hotel Sapanca, Sapanca, Turkey (raw cone data from http://peer.berkeley.edu/turkey/adapazari).

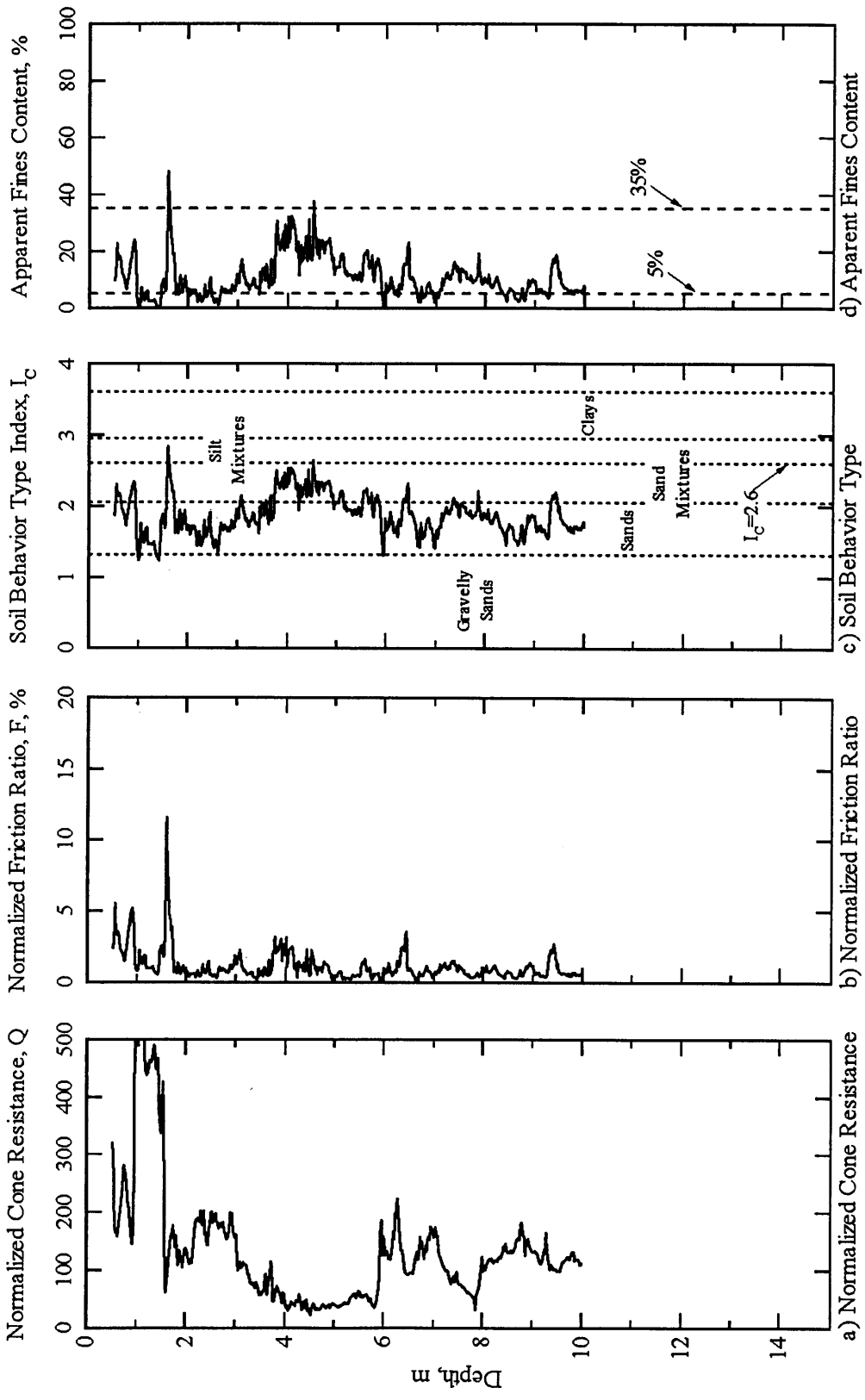

Figure 4.28 Graphs developed from CPT-SH6 to characterize the subsurface at Hotel Sapanca, Sapanca, Turkey (raw cone data from http://peer.berkeley.edu/turkey/adapazari).

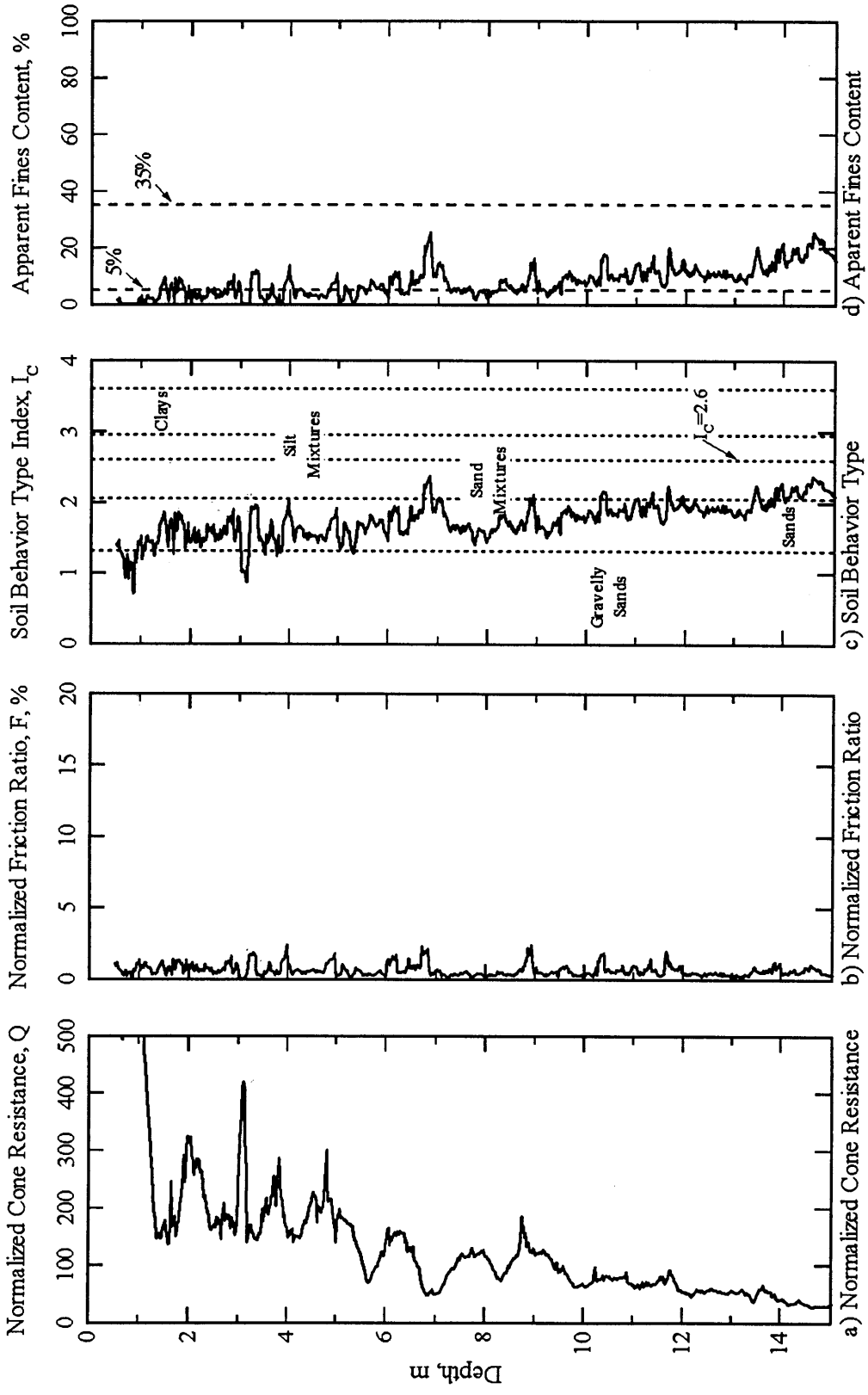

Figure 4.29 Graphs developed from CPT-SH7 to characterize the subsurface at Hotel Sapanca, Sapanca, Turkey (raw cone data from http://peer.berkeley.edu/turkey/adapazari).

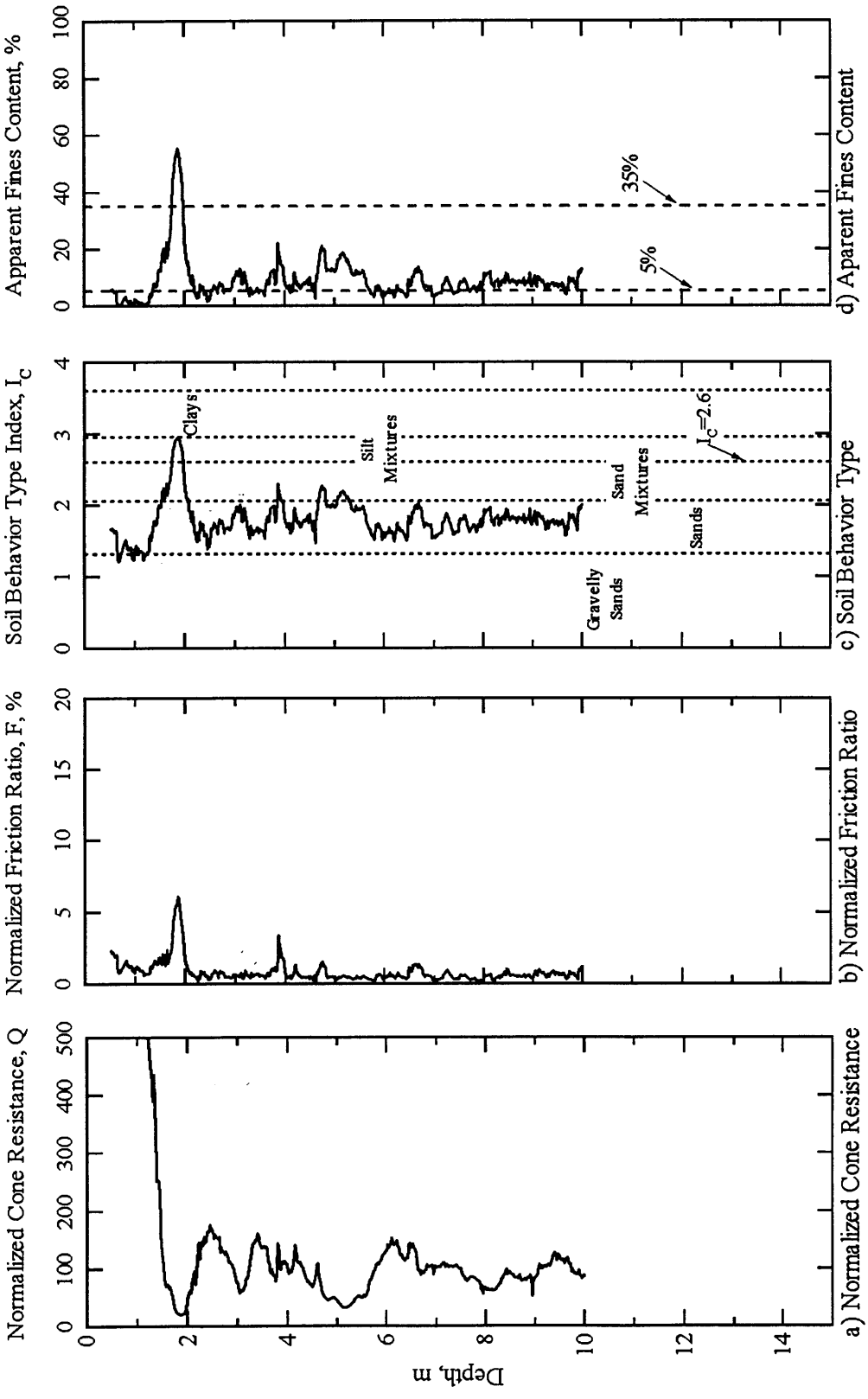

Figure 4.30 Graphs developed from CPT-SH8 to characterize the subsurface at Hotel Sapanca, Sapanca, Turkey (raw cone data from http://peer.berkeley.edu/turkey/adapazari).

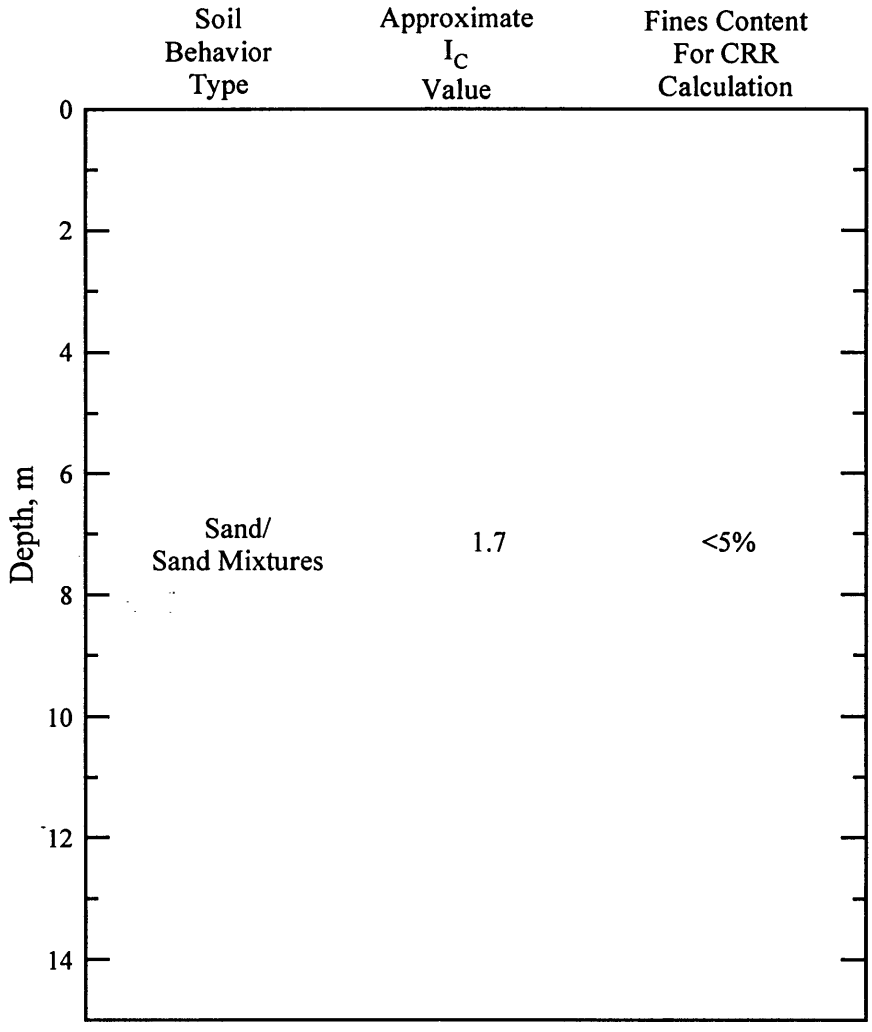

Figure 4.31 Idealized soil profile and layer properties as determined from five CPT soundings at Hotel Sapanca, Sapanca, Turkey.

Table 4.12 summarizes the data for the depth intervals located within the potentially liquefiable region at Centerline 1. Table 4.13 summarizes the data for the depth intervals located within the potentially liquefiable region at Centerline 2. Table 4.14 summarizes the data for the depth intervals located within the potentially liquefiable region at Centerline 3. Table 4.15 summarizes the data for the depth intervals located within the potentially liquefiable region at Centerline 4. The soil properties in each of these tables are the same and show a sand/sand mixture soil profile with an approximate I_C value of 1.7. Each centerline varies slightly in values for CRR/CSR. However, there

is plenty of sandy soil predicted as liquefiable underneath all four centerlines. These types of conditions would explain the dramatic subsidence and lateral spreading that caused the Hotel to be carried partially into the lake.

Table 4.12 Properties for soil layers located within the potentially liquefiable region at Hotel Sapanca, Centerline 1

Depth Interval (m)	Average (CRR/CSR)	Soil Behavior Type	Approximate I_C Value	Predicted as Liquefiable by CPT
1.25 - 15	0.31	Sand/Sand Mixtures	1.7	yes

Table 4.13 Properties for soil layers located within the potentially liquefiable region at Hotel Sapanca, Centerline 2

Depth Interval (m)	Average (CRR/CSR)	Soil Behavior Type	Approximate I_C Value	Predicted as Liquefiable by CPT
1.6 - 15	0.36	Sand/Sand Mixtures	1.7	yes

Table 4.14 Properties for soil layers located within the potentially liquefiable region at Hotel Sapanca, Centerline 3

Depth Interval (m)	Average (CRR/CSR)	Soil Behavior Type	Approximate I_C Value	Predicted as Liquefiable by CPT
1.25 - 5	0.35	Sand/Sand Mixtures	1.7	yes
5.5 - 15	0.42	Sand/Sand Mixtures	1.7	yes

Table 4.15 Properties for soil layers located within the potentially liquefiable region at Hotel Sapanca, Centerline 4

Depth Interval (m)	Average (CRR/CSR)	Soil Behavior Type	Approximate I_C Value	Predicted as Liquefiable by CPT
.5 - 7	0.28	Sand/Sand Mixtures	1.7	yes

4.2.3 Izmit Bay

4.2.3.1 Degirmendere Nose The graphs developed for Degirmendere Nose to delineate potentially liquefiable soil using the shear wave velocity simplified procedure, are shown in Figure 4.32. Figure 4.32a shows the shear wave velocity profile (V_S) and the corrected shear wave velocity profile (V_{S1}) for the site. Figure 4.32b shows the fines content used for the calculation of CRR's. Figure 4.32c shows the CRR of the soil along with three CSR profiles. The central profile represents the CSR generated using the most probable ground acceleration predicted for this site. The other two profiles result from bracketing this acceleration by +/- 0.05 g. From this graph, it can be seen that the potentially liquefiable region only extends between the depths of 8 - 9 meters. Three CPT soundings were available at Degirmendere Nose. The graphs developed from CPT-DN1 are shown in Figure 4.33. The graphs developed from CPT-DN2 are shown in Figure 4.34. The graphs developed from CPT-DN3 are shown in Figure 4.35. Figure 4.36 shows the idealized soil profile and layer properties at Degirmendere Nose as determined from combining the data from these three cone soundings.

Table 4.16 summarizes the data for the depth interval located within the potentially liquefiable region at Degirmendere Nose. The soil at the site is composed of sand/sand mixtures and would have been predicted to liquefy. All of the soil at this site, except for the 8 - 9 meter interval, is considered as too stiff to liquefy according to the simplified shear wave velocity evaluation. The largest and most devastating coastal stability failure from the Kocaeli earthquake occurred at this location. Given the relatively stiff soil profile at this site and the depth at a liquefiable layer it is doubtful the all these deformations could have been caused by soil liquefaction. Tectonic deformation and settlement probably also played a role in this failure.

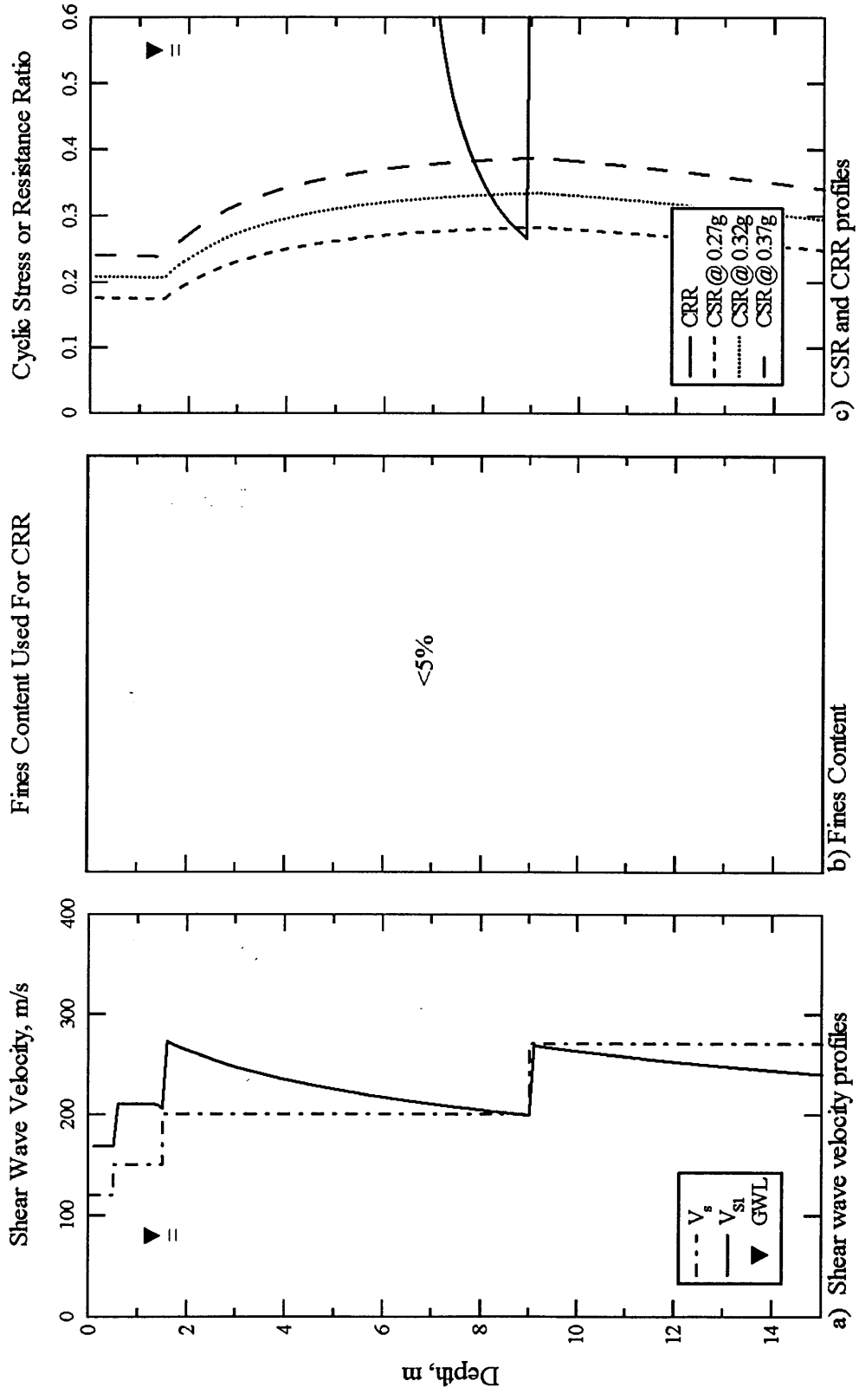

Figure 4.32 Graphs developed to delineate liquefiable soil using the simplified shear wave velocity procedure at Degirmendere Nose, Degirmendere, Turkey.

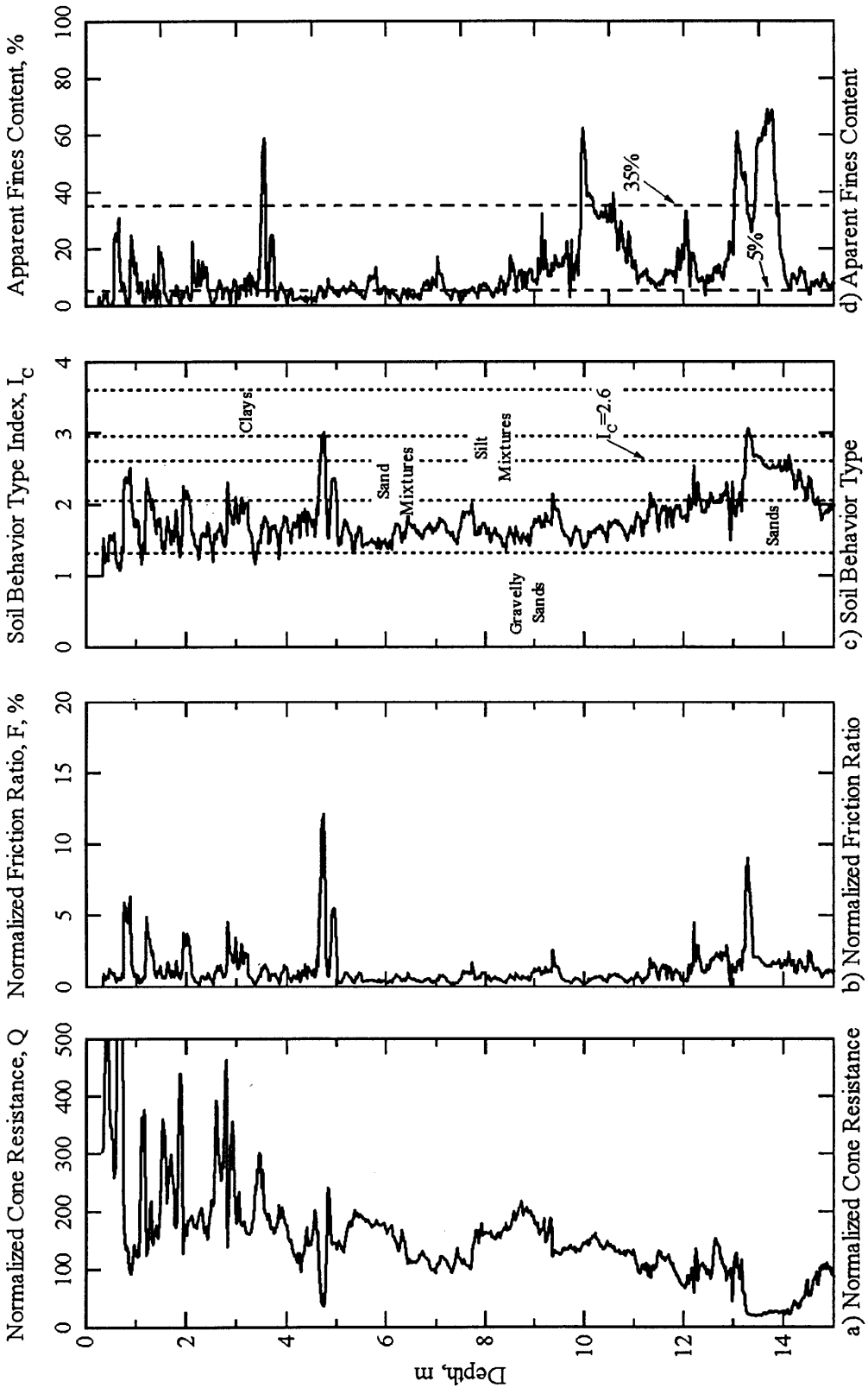

Figure 4.33 Graphs developed from CPT-DN1 to characterize the subsurface at Degirmendere Nose, Degirmendere, Turkey (raw cone data from http://peer.berkeley.edu/turkey/adapazari).

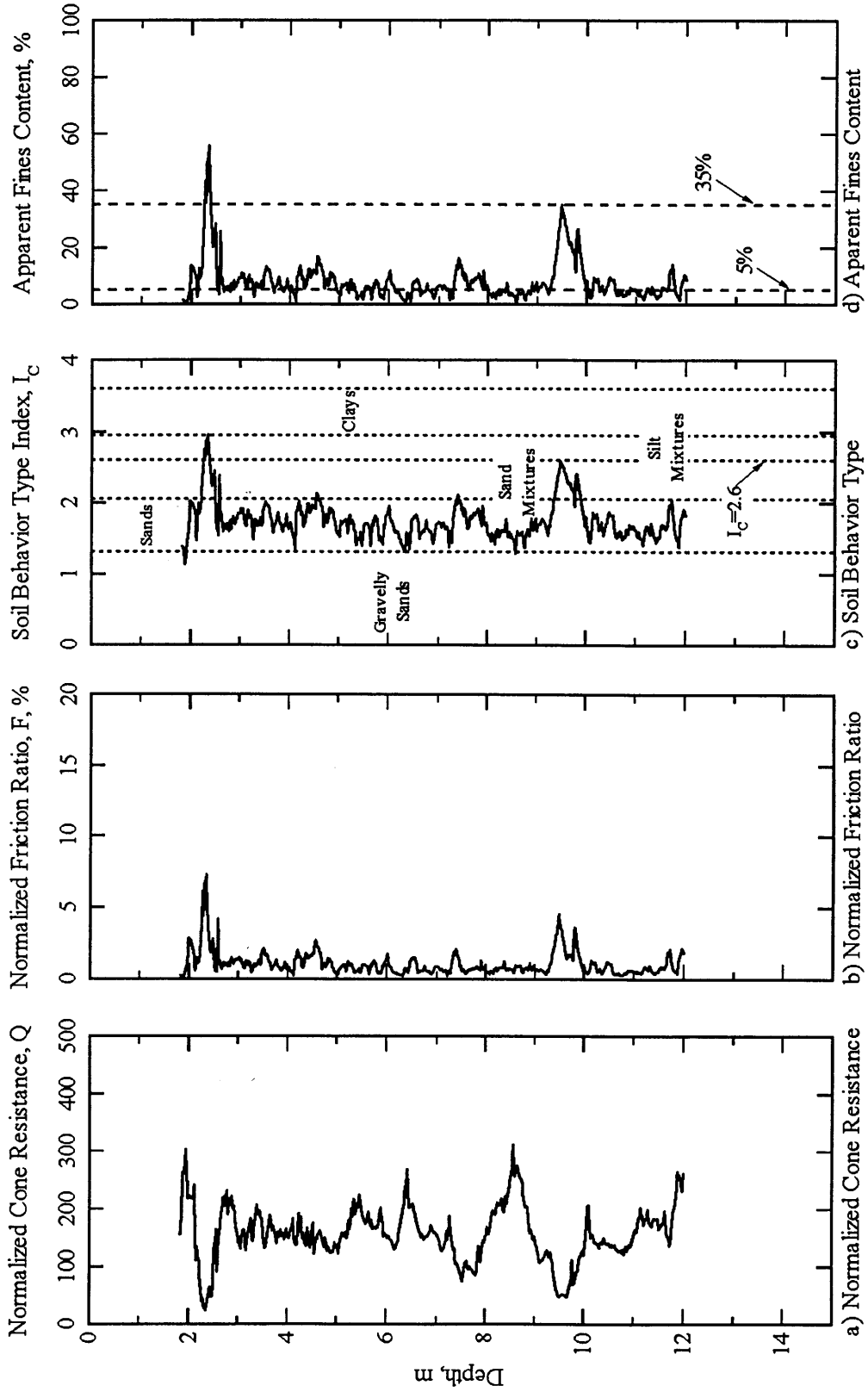

Figure 4.34 Graphs developed from CPT-DN2 to characterize the subsurface at Degirmendere Nose, Degirmendere, Turkey (raw cone data from http://peer.berkeley.edu/turkey/adapazari).

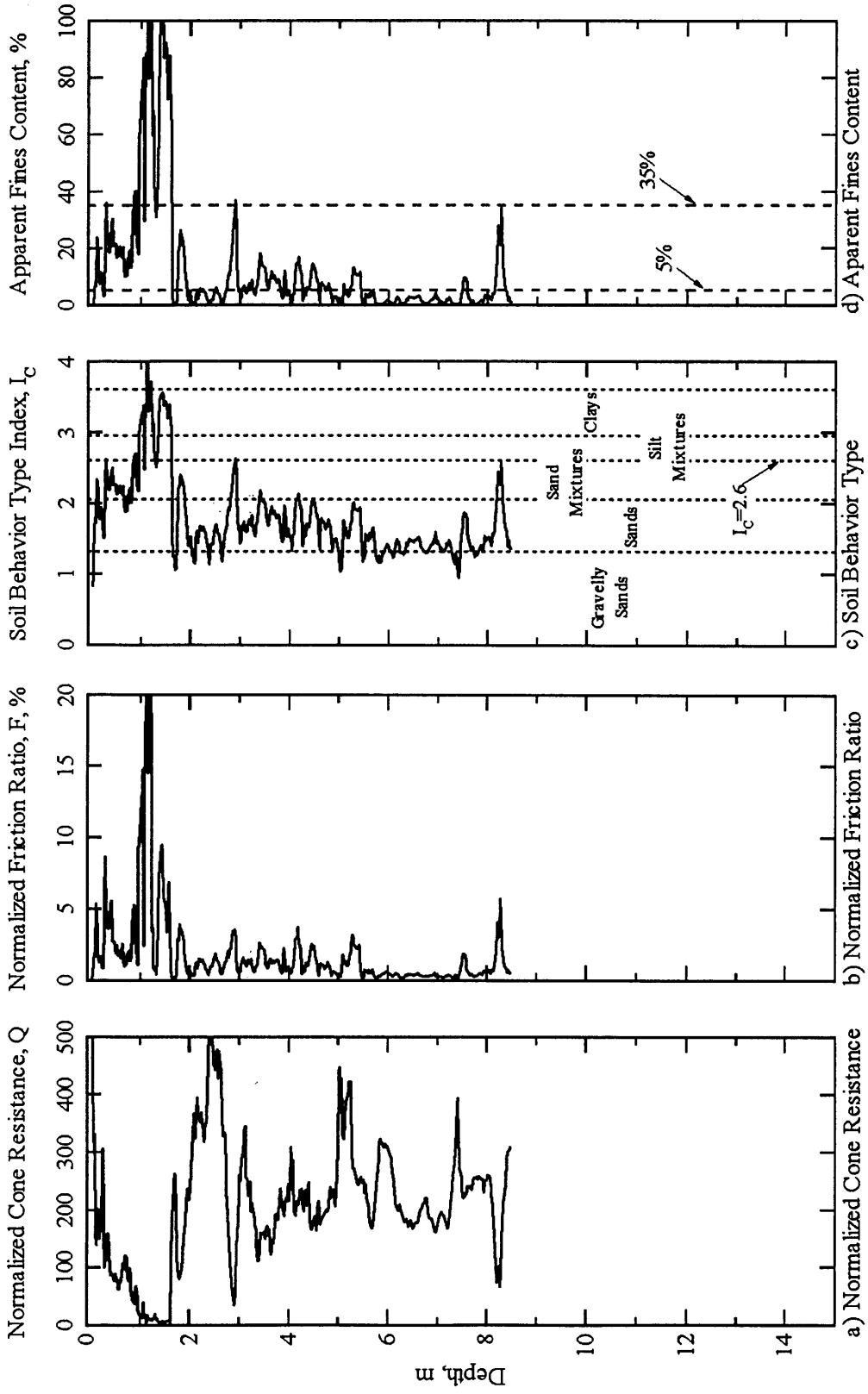

Figure 4.35 Graphs developed from CPT-DN3 to characterize the subsurface at Degirmendere Nose, Degirmendere, Turkey (raw cone data from http://peer.berkeley.edu/turkey/adapazari).

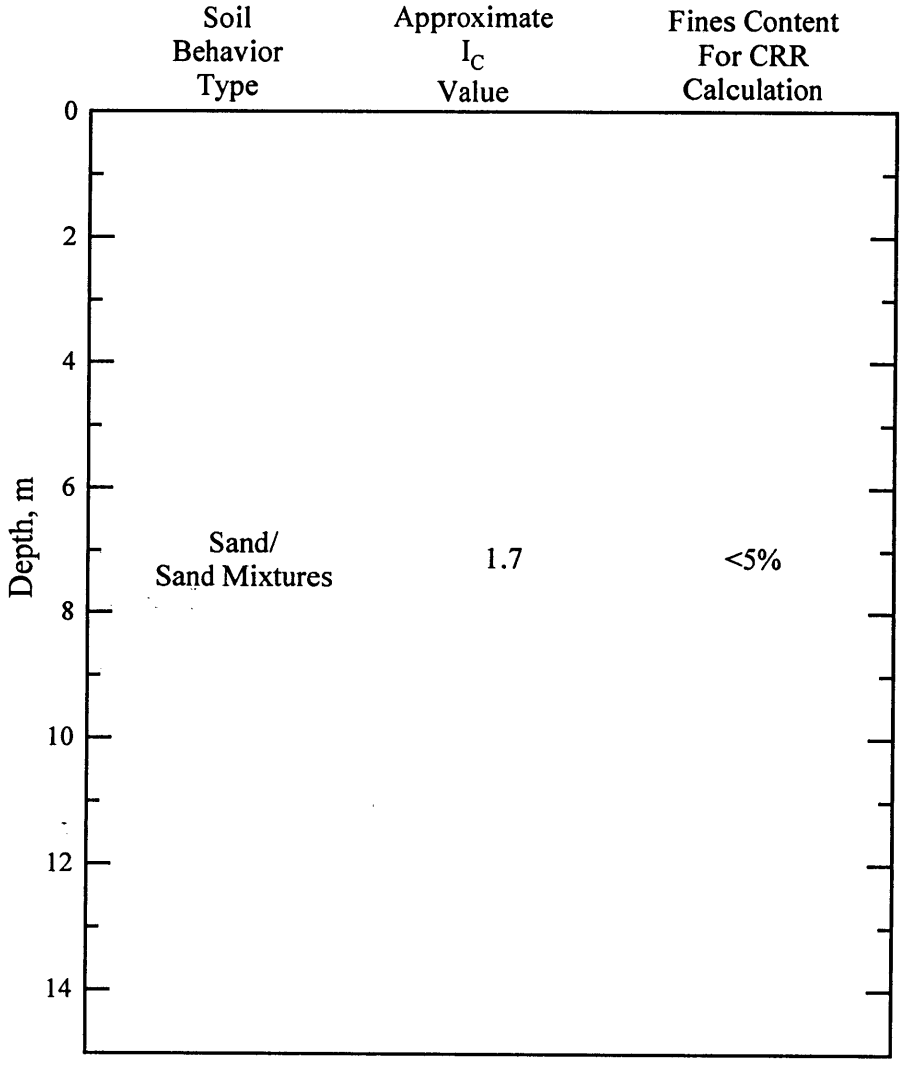

Figure 4.36 Idealized soil profile and layer properties as determined from three CPT soundings at Degirmendere Nose, Degirmendere, Turkey.

Table 4.16 Properties for soil layers located within the potentially liquefiable region at Degirmendere Nose

Depth Interval (m)	Average (CRR/CSR)	Soil Behavior Type	Approximate I_C Value	Predicted as Liquefiable by CPT
8 - 9	0.90	Sand/Sand Mixtures	1.7	yes

4.2.3.2 Police Station The graphs developed for Police Station to delineate potentially liquefiable soil using the shear wave velocity simplified procedure are shown in Figure 4.37. Figure 4.37a shows the shear wave velocity profile (V_S) and the corrected shear wave velocity profile (V_{S1}) for the site. Figure 4.37b shows the fines content used for the calculation of CRR's in each layer. Figure 4.37c shows the CRR of the soil along with three CSR profiles. The central profile represents the CSR generated using the most probable ground acceleration predicted for this site. The other two profiles result from bracketing this acceleration by +/- 0.05 g. From this graph, it can be seen that the potentially liquefiable region extends from a depth of 1.5 meters throughout the entire depth of the profile. Five CPT soundings were available at Police Station. The graphs developed from CPT-PS1 are shown in Figure 4.38. The graphs developed from CPT-PS2 are shown in Figure 4.39. The graphs developed from CPT-PS3 are shown in Figure 4.40. The graphs developed from CPT-PS4 are shown in Figure 4.41. The graphs developed from CPT-PS5 are shown in Figure 4.42. Figure 4.43 shows the idealized soil profile and layer properties at Police Station as determined from combining the data from these five cone soundings.

Table 4.17 summarizes the data for the depth intervals located within the potentially liquefiable region at Police Station. The soil located between the depths of 1.5 - 3 meters is sand/sand mixtures with an approximate I_C value of 2.1. This layer would be predicted as liquefiable. The soil located between the depths of 6.5 - 8 meters is also sand with a lower approximate I_C value of 1.4. This layer is also the softest layer with an average CRR/CSR of 0.1. It is very likely that both of these layers liquefied during the earthquake, inducing the lateral spreading that occurred here. All of the other depth intervals at this site have I_C values greater than 2.6 and are considered nonliquefiable.

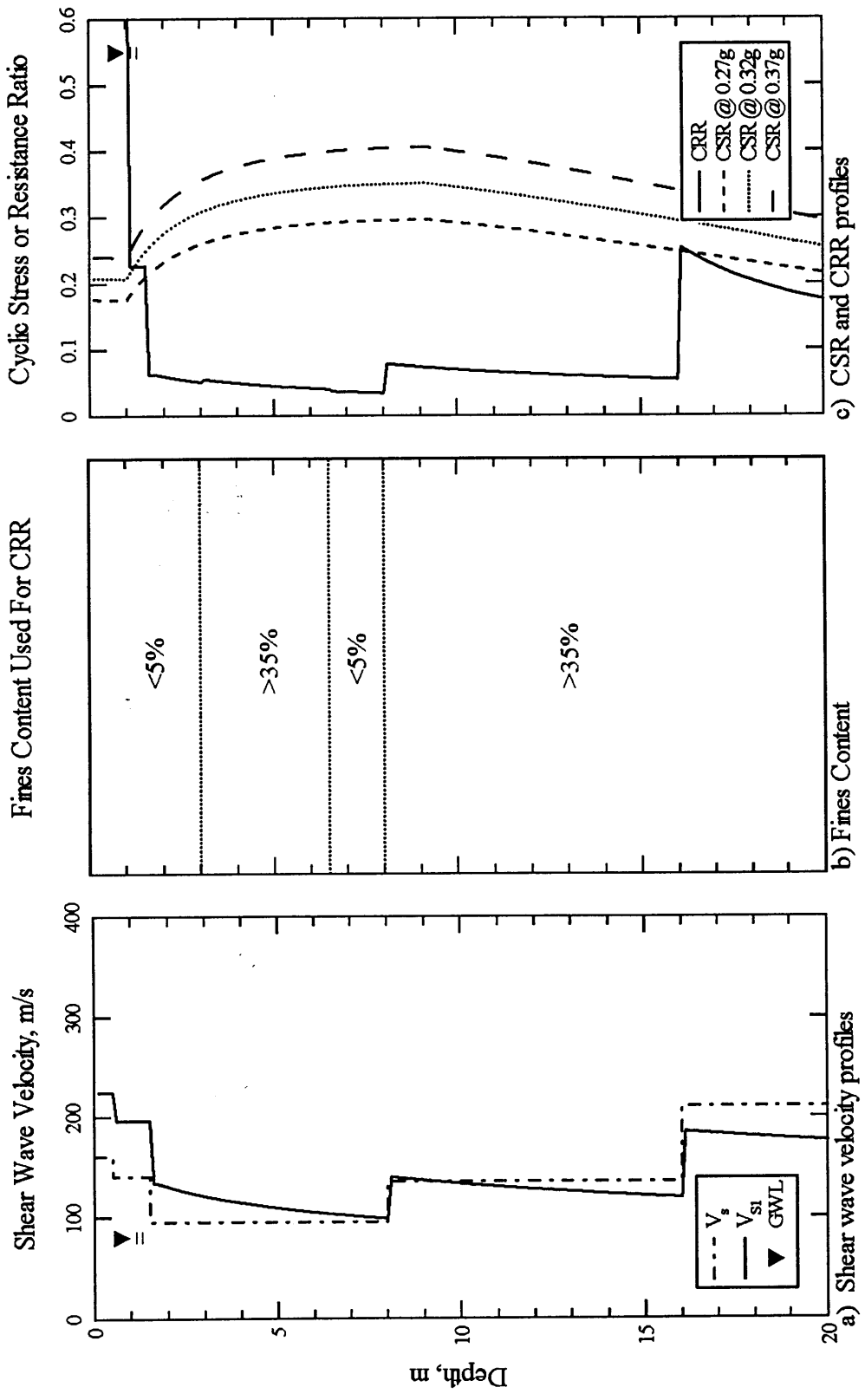

Figure 4.37 Graphs developed to delineate liquefiable soil using the simplified shear wave velocity procedure at Police Station, Golcuk, Turkey.

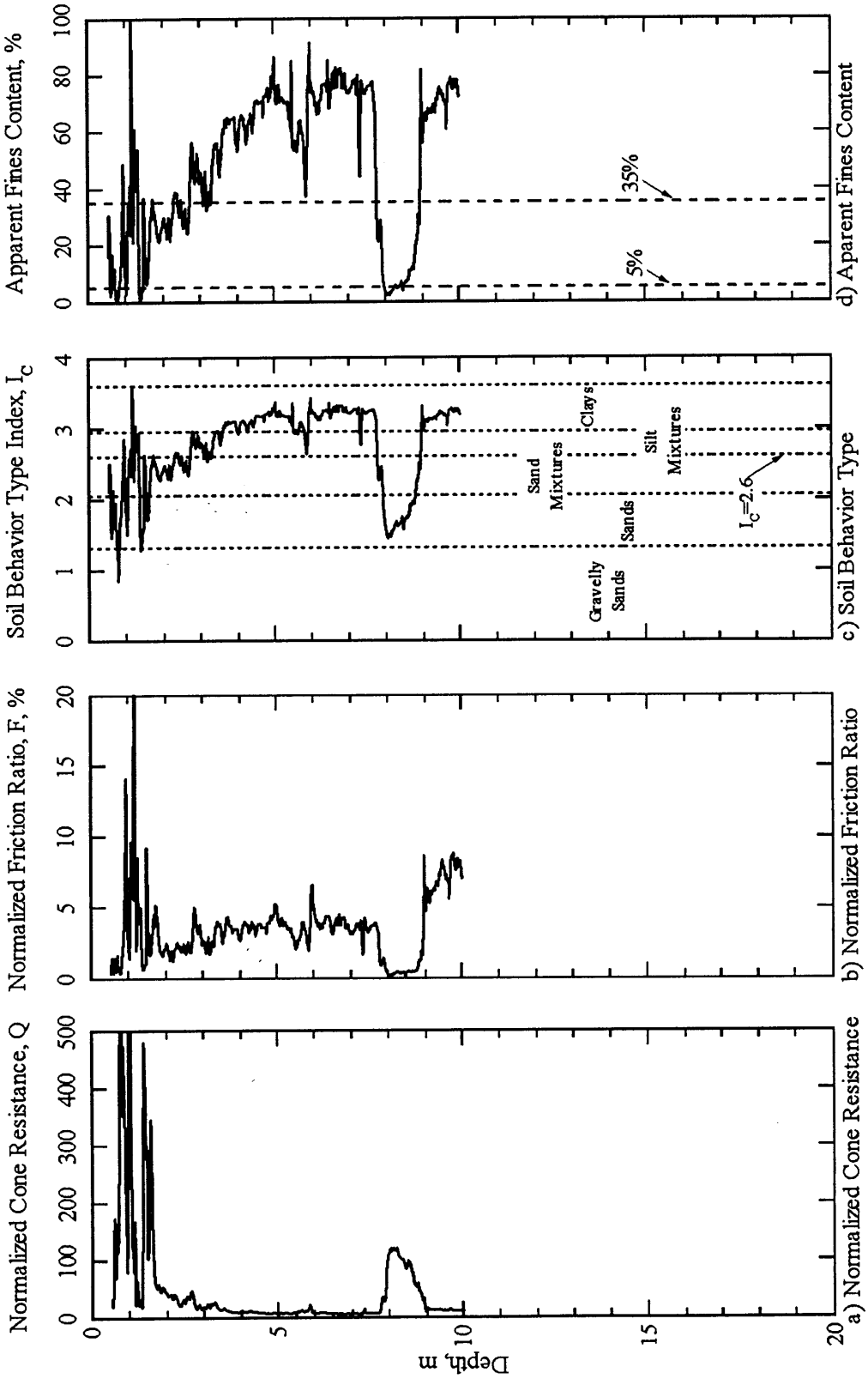

Figure 4.38 Graphs developed from CPT-PS1 to characterize the subsurface at Police Station, Golcuk, Turkey (raw cone data from http://peer.berkeley.edu/turkey/adapazari).

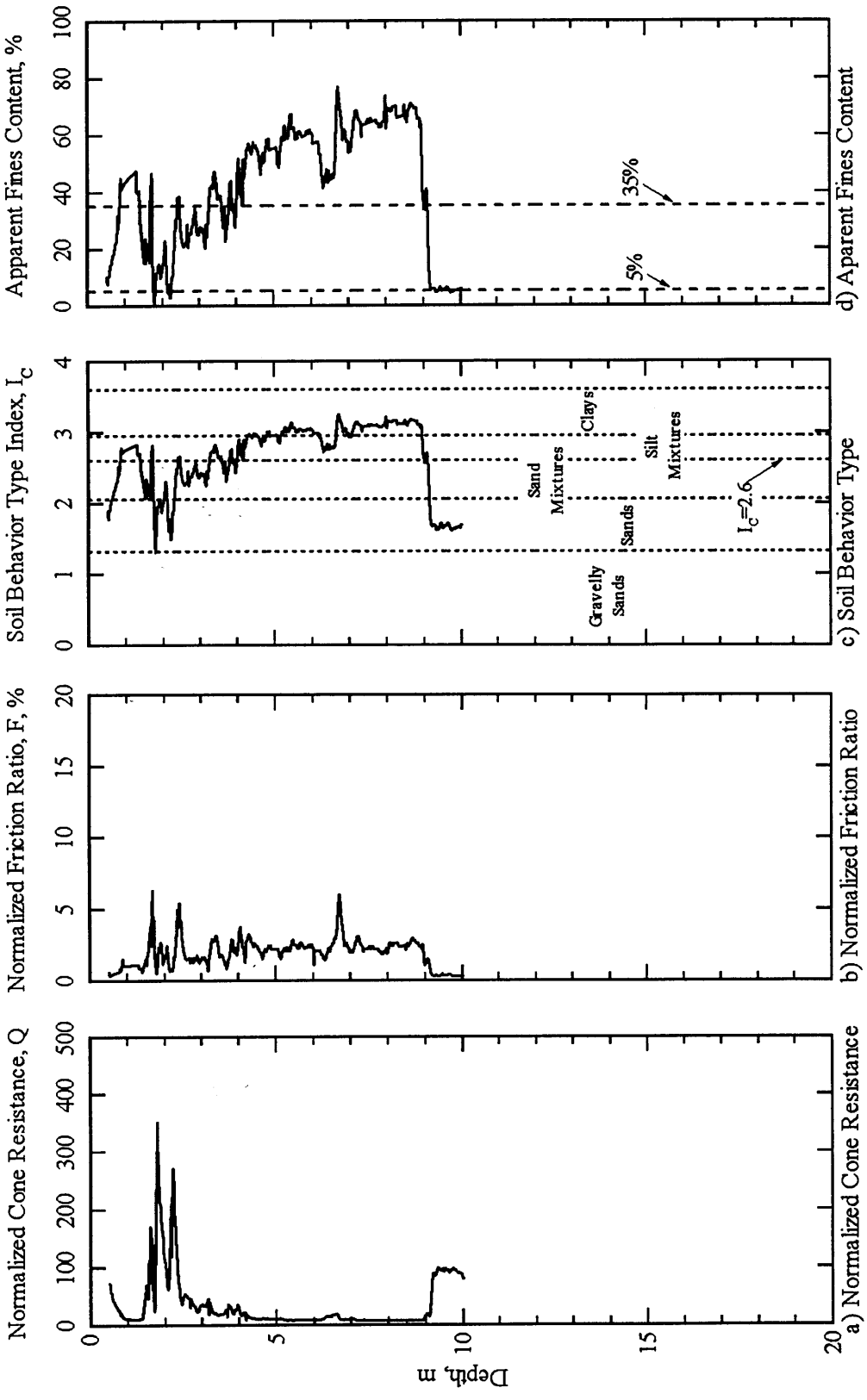

Figure 4.39 Graphs developed from CPT-PS2 to characterize the subsurface at Police Station, Golcuk, Turkey (raw cone data from **http://peer.berkeley.edu/turkey/adapazari**).

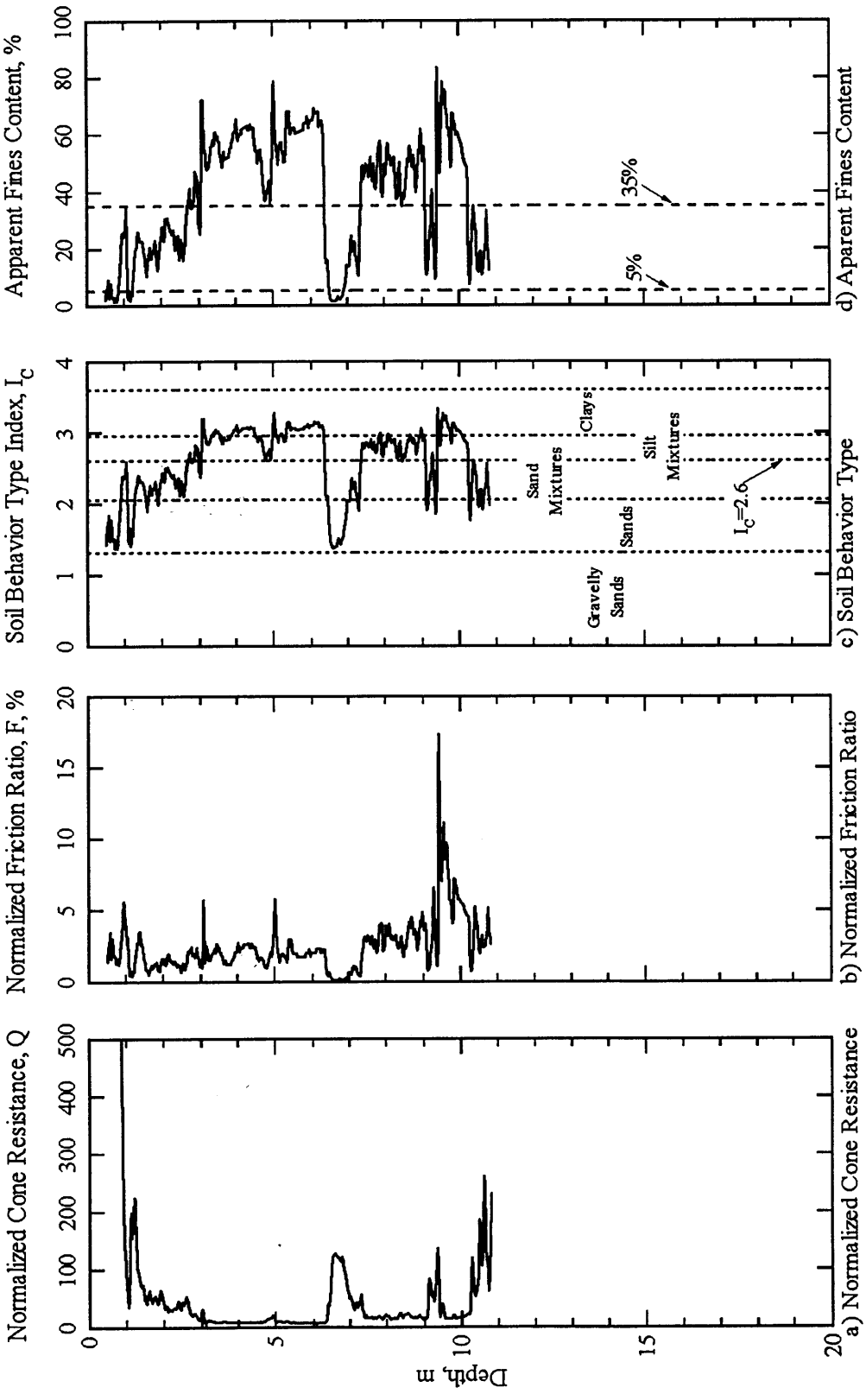

Figure 4.40 Graphs developed from CPT-PS3 to characterize the subsurface at Police Station, Golcuk, Turkey (raw cone data from http://peer.berkeley.edu/turkey/adapazari).

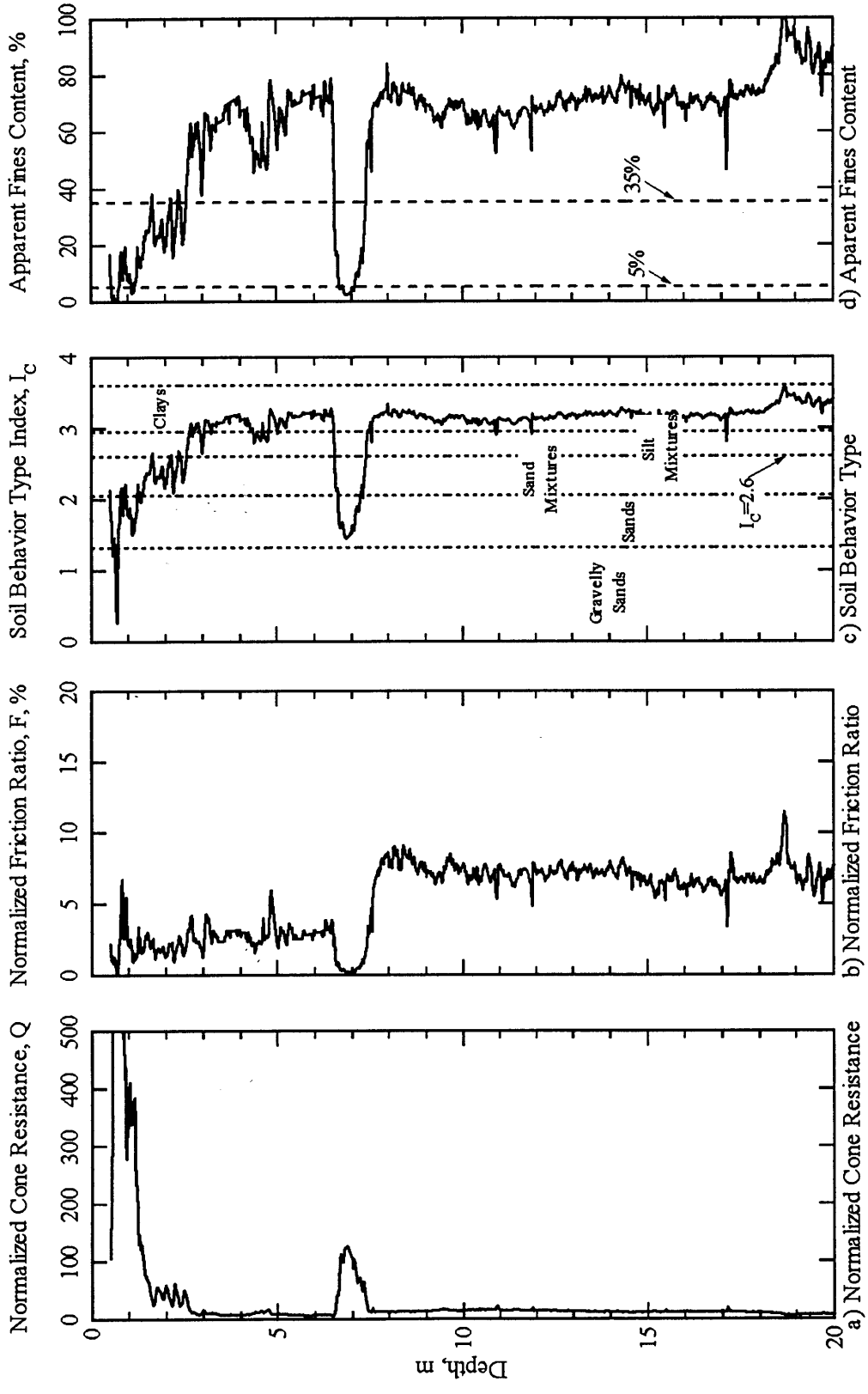

Figure 4.41 Graphs developed from CPT-PS4 to characterize the subsurface at Police Station, Golcuk, Turkey (raw cone data from http://peer.berkeley.edu/turkey/adapazari).

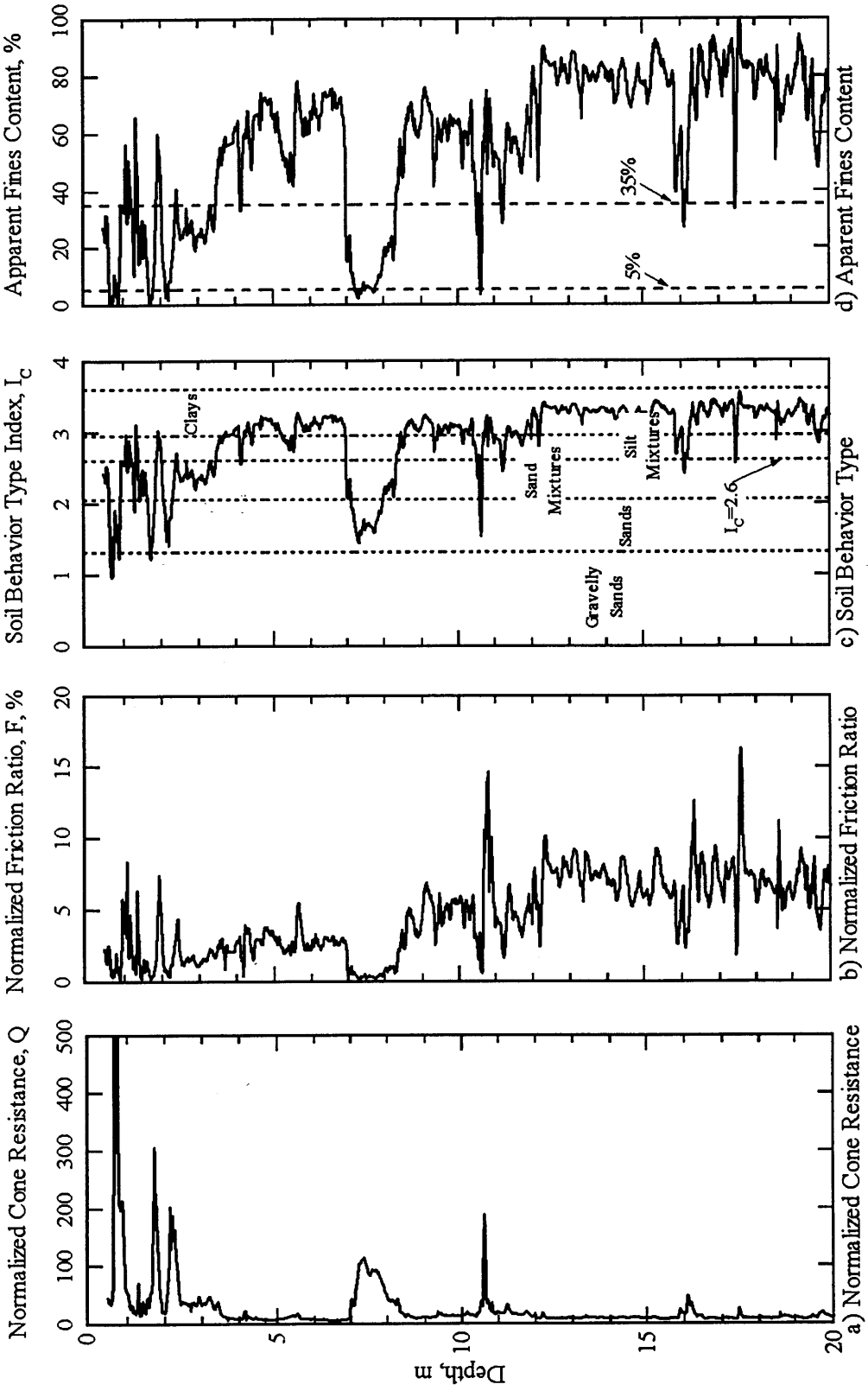

Figure 4.42 Graphs developed from CPT-PS5 to characterize the subsurface at Police Station, Golcuk, Turkey (raw cone data from http://peer.berkeley.edu/turkey/adapazari).

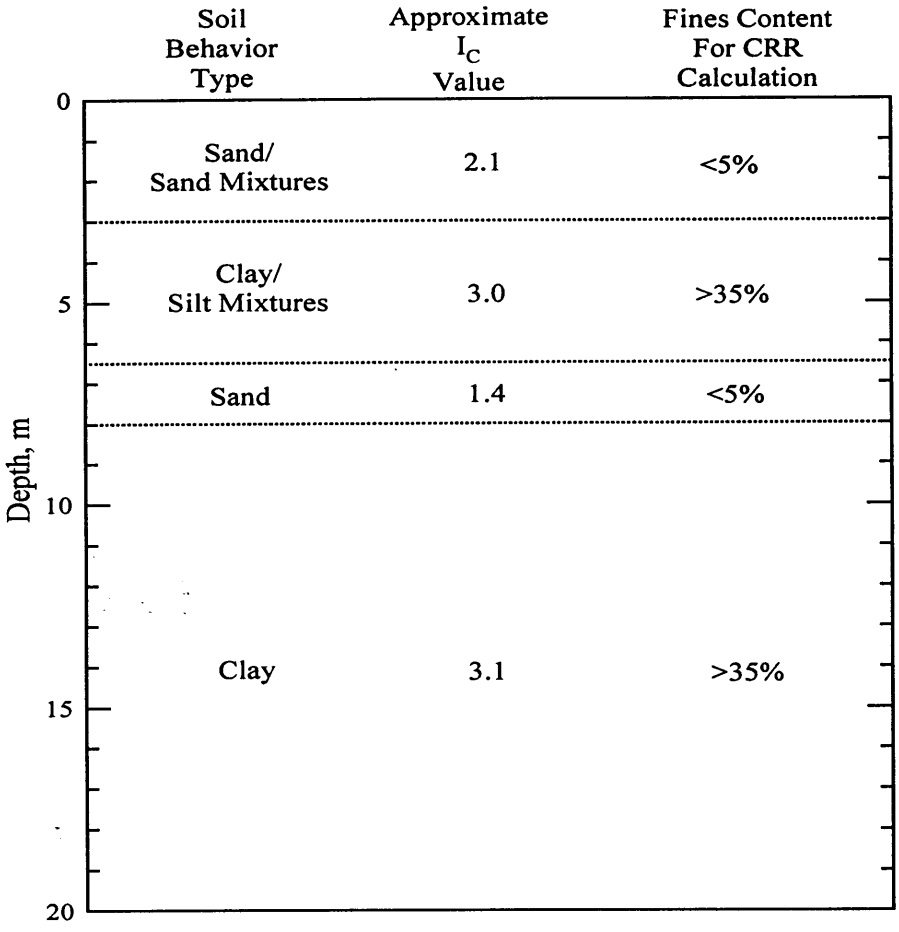

Figure 4.43 Idealized soil profile and layer properties as determined from five CPT soundings at Police Station, Golcuk, Turkey.

Table 4.17 Properties for soil layers located within the potentially liquefiable region at Police Station

Depth Interval (m)	Average (CRR/CSR)	Soil Behavior Type	Approximate I_C Value	Predicted as Liquefiable by CPT
1.5 - 3	0.20	Sand/Sand Mixtures	2.1	yes
3 - 6.5	0.13	Clay/Silt Mixtures	3.0	no
6.5 - 8	0.10	Sand	1.4	yes
8 -20	0.29	Clay	3.1	no

4.2.3.3 Soccer Field The graphs developed for Soccer Field to delineate potentially liquefiable soil using the shear wave velocity simplified procedure are shown in Figure 4.44. Figure 4.44a shows the shear wave velocity profile (V_S) and the corrected shear wave velocity profile (V_{S1}) for the site. Figure 4.44b shows the fines content used for the calculation of CRR's in each layer. Figure 4.44c shows the CRR of the soil along with three CSR profiles. The central profile represents the CSR generated using the most probable ground acceleration predicted for this site. The other two profiles result from bracketing this acceleration by +/- 0.05 g. From this graph, it can be seen that the potentially liquefiable region extends from a depth of 1 meter throughout the entire depth of the profile. Five CPT soundings were available at Soccer Field. The graphs developed from CPT-SF1 are shown in Figure 4.45. The graphs developed from CPT-SF2 are shown in Figure 4.46. The graphs developed from CPT-SF3 are shown in Figure 4.47. The graphs developed from CPT-SF4 are shown in Figure 4.48. The graphs developed from CPT-SF5 are shown in Figure 4.49. Figure 4.50 shows the idealized soil profile and layer properties at Soccer Field as determined from combining the data from these five cone soundings.

Table 4.18 summarizes the data for the depth intervals located within the potentially liquefiable region at Soccer Field. The soil located between the depths of 1 - 3 meters is sand/sand mixtures with an approximate I_C value of 2.3. This layer would be predicted as liquefiable and is the one most likely to have liquefied and induced the lateral spreading at this site. The remainder of the profile is extremely soft with an average CRR/CSR of 0.09 and an approximate I_C value of 3.4. However, it is unlikely that this clayey material would have liquefied.

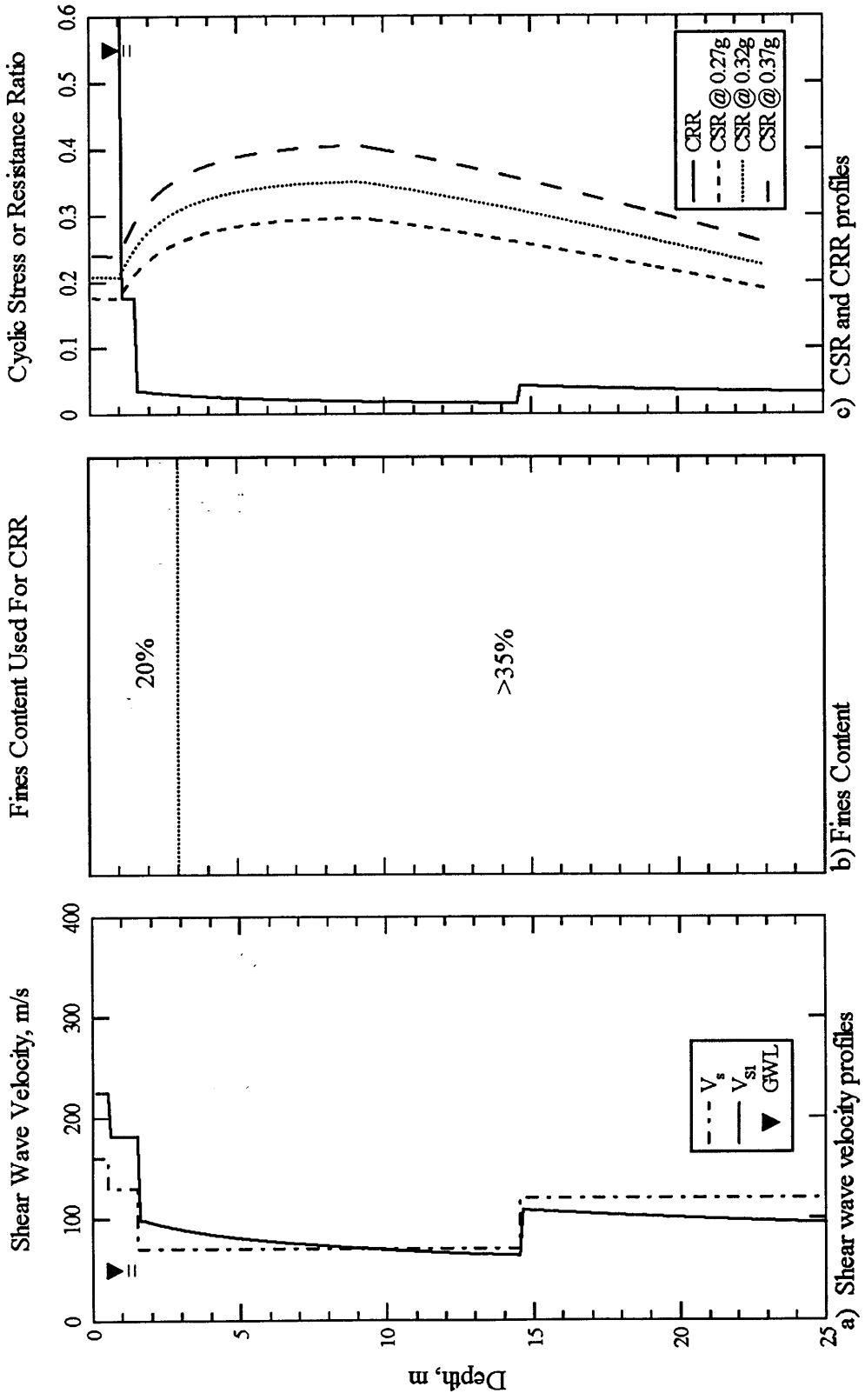

Figure 4.44 Graphs developed to delineate liquefiable soil using the simplified shear wave velocity procedure at Soccer Field, Golcuk, Turkey.

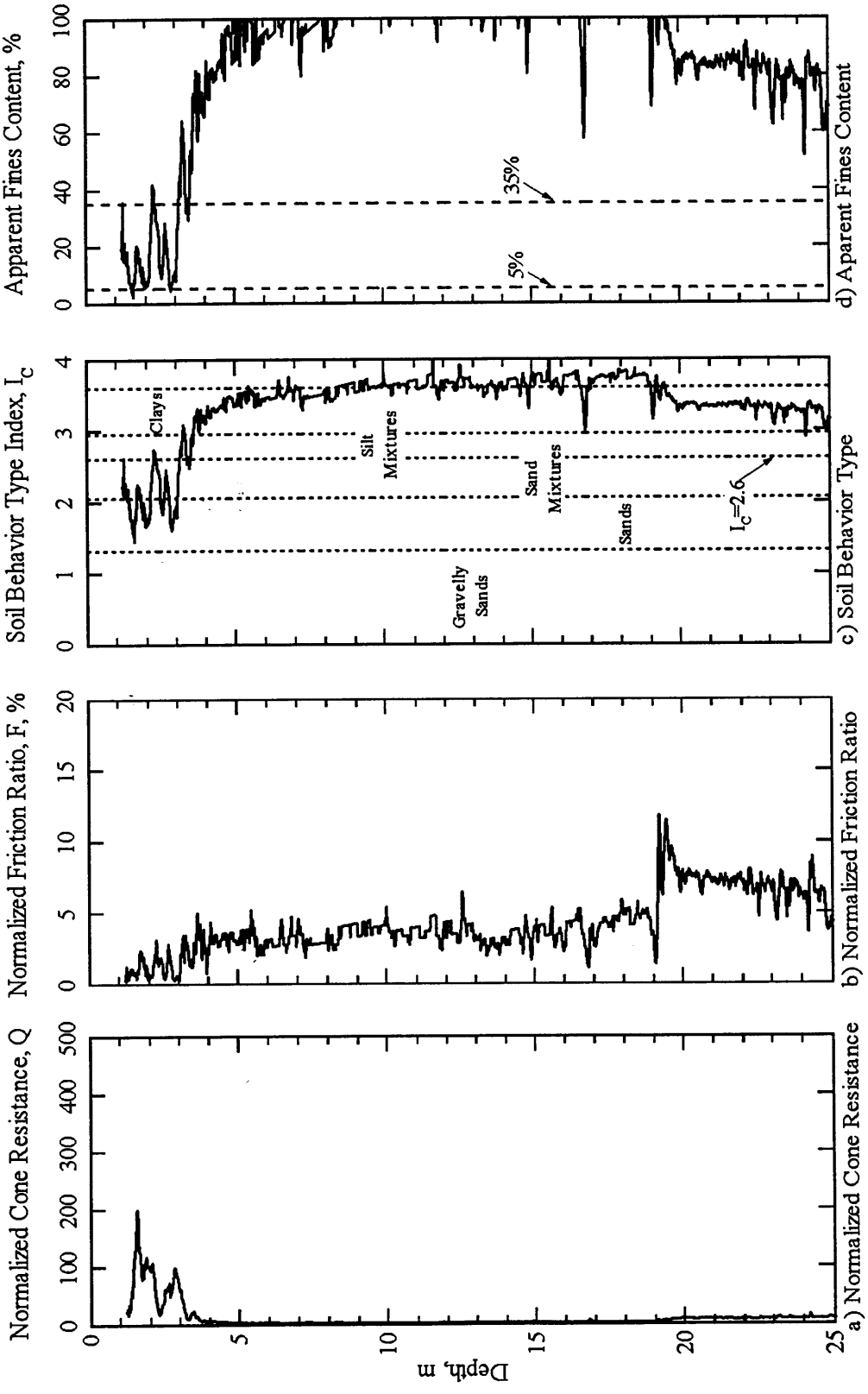

Figure 4.45 Graphs developed from CPT-SF1 to characterize the subsurface at Soccer Field, Golcuk, Turkey (raw cone data from http://peer.berkeley.edu/turkey/adapazari).

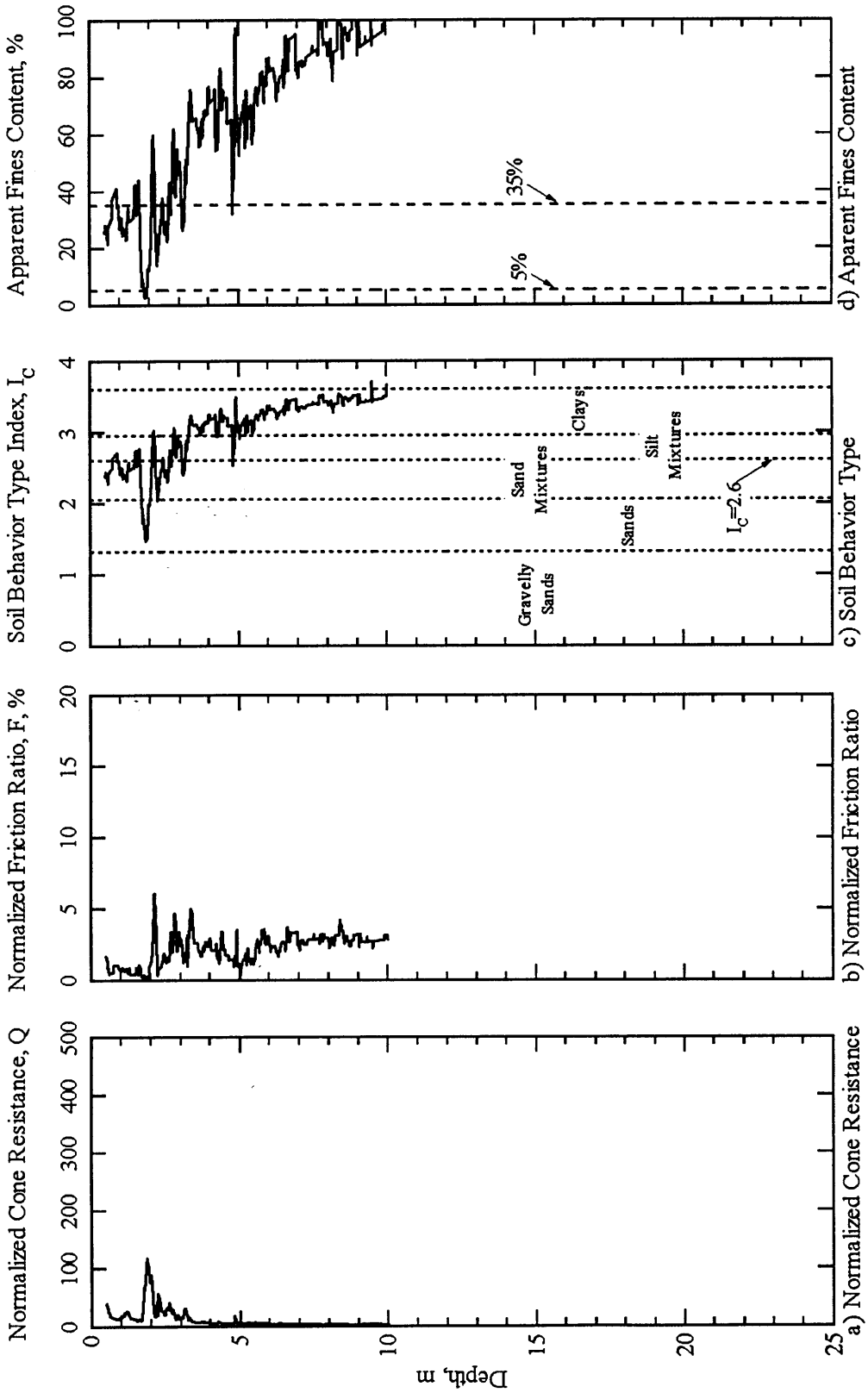

Figure 4.46 Graphs developed from CPT-SF2 to characterize the subsurface at Soccer Field, Golcuk, Turkey (raw cone data from http://peer.berkeley.edu/turkey/adapazari).

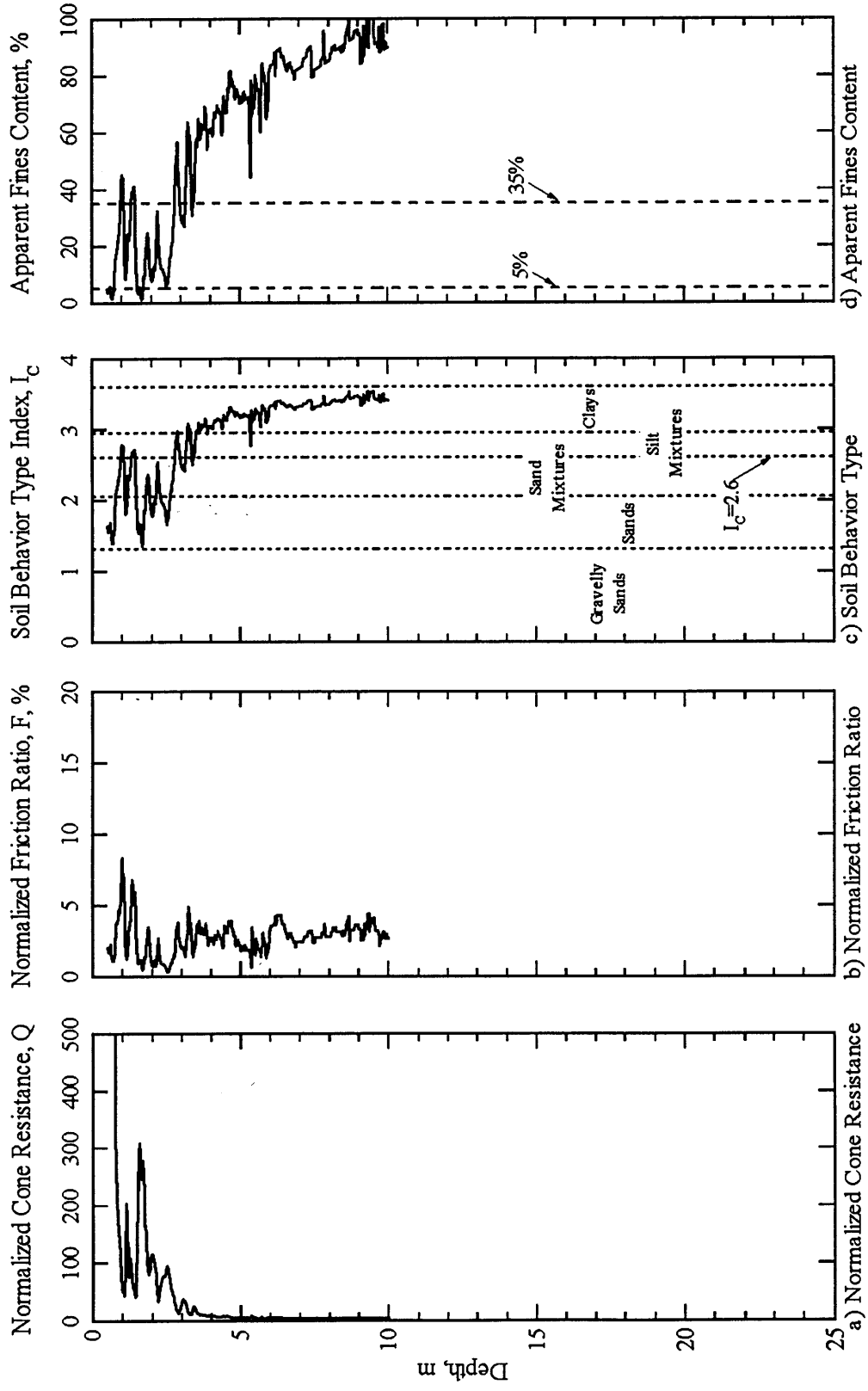

Figure 4.47 Graphs developed from CPT-SF3 to characterize the subsurface at Soccer Field, Golcuk, Turkey (raw cone data from http://peer.berkeley.edu/turkey/adapazari).

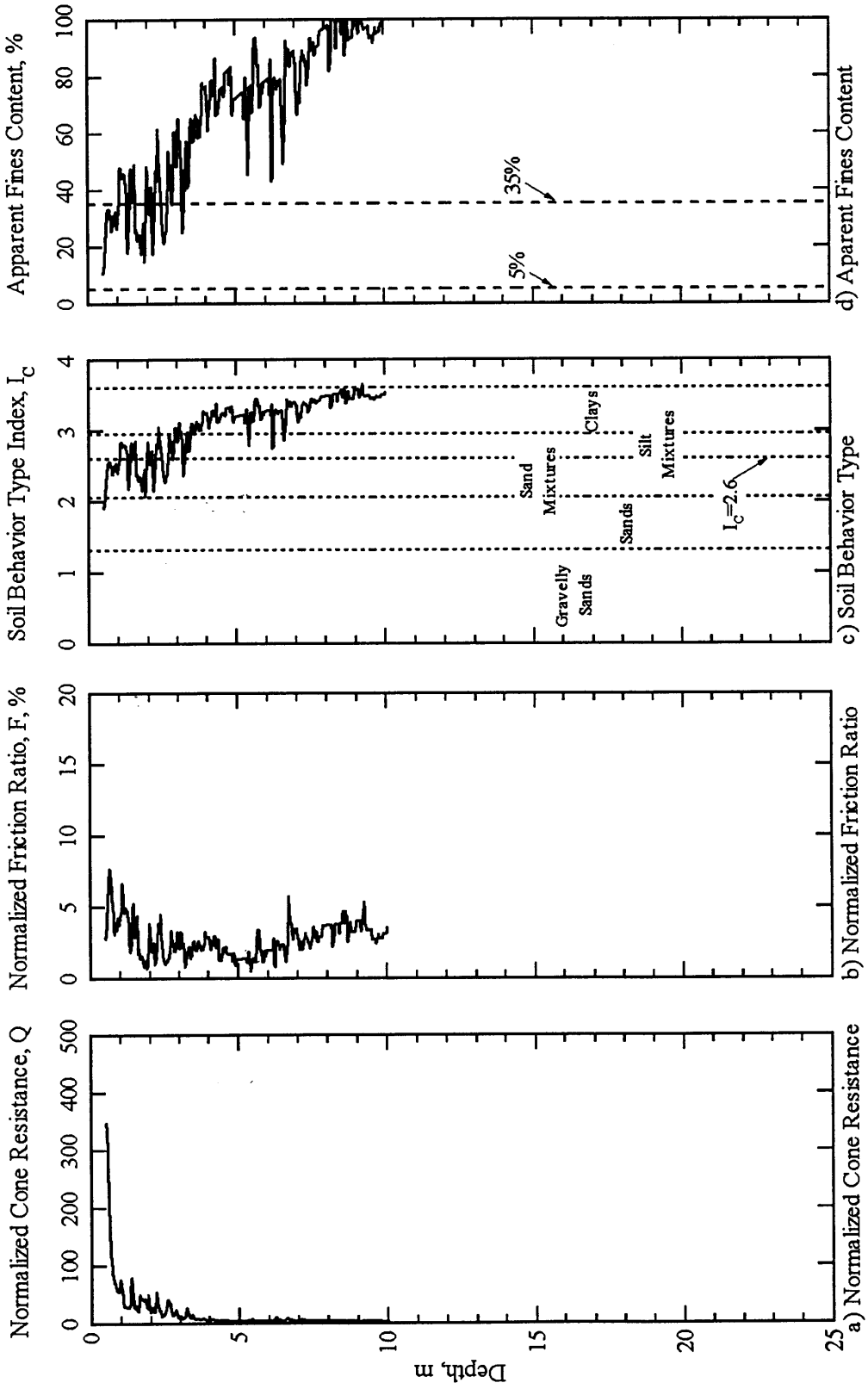

Figure 4.48 Graphs developed from CPT-SF4 to characterize the subsurface at Soccer Field, Golcuk, Turkey (raw cone data from http://peer.berkeley.edu/turkey/adapazari).

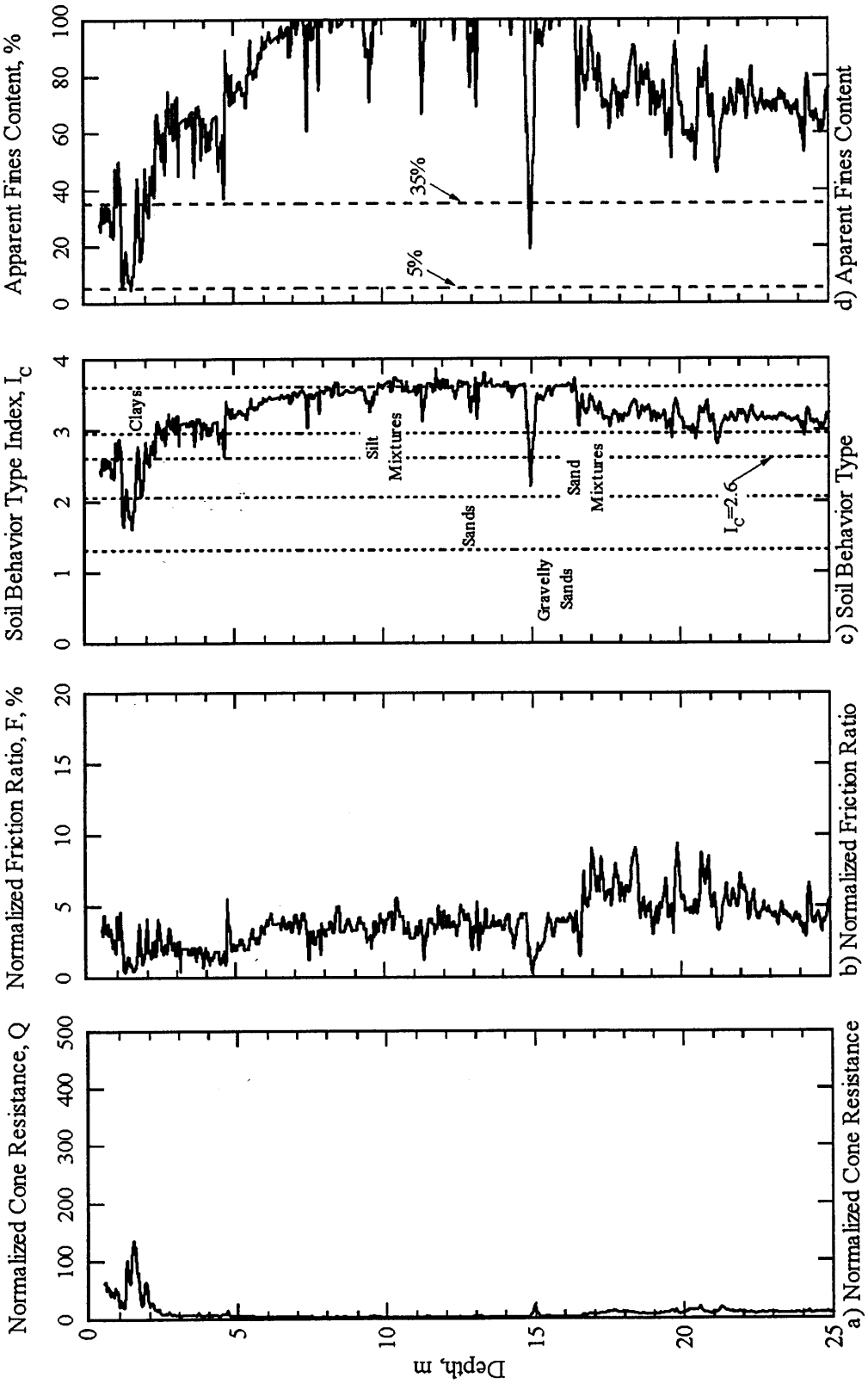

Figure 4.49 Graphs developed from CPT-SF5 to characterize the subsurface at Soccer Field, Golcuk, Turkey (raw cone data from http://peer.berkeley.edu/turkey/adapazari).

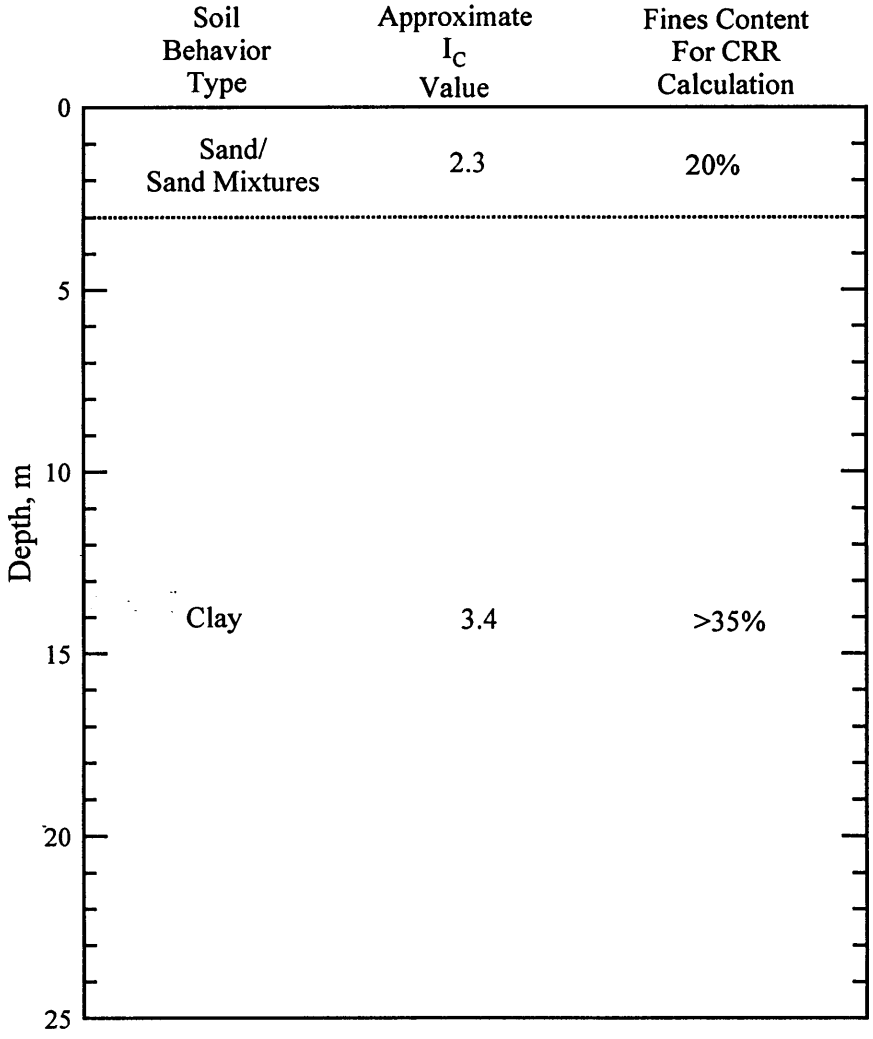

Figure 4.50 Idealized soil profile and layer properties as determined from five CPT soundings at Soccer Field, Golcuk, Turkey.

Table 4.18 Properties for soil layers located within the potentially liquefiable region at Soccer Field

Depth Interval (m)	Average (CRR/CSR)	Soil Behavior Type	Approximate I_C Value	Predicted as Liquefiable by CPT
1 - 3	0.30	Sand/Sand Mixtures	2.3	yes
3 - 23	0.09	Clay	3.4	no

4.2.3.4 Yalova Harbor The graphs developed for Yalova Harbor to delineate potentially liquefiable soil using the shear wave velocity simplified procedure, are shown in Figure 4.51. Figure 4.51a shows the shear wave velocity profile (V_S) and the corrected shear wave velocity profile (V_{S1}) for the site. Figure 4.51b shows the fines content used for the calculation of CRR's in each layer. Figure 4.51c shows the CRR of the soil along with three CSR profiles. The central profile represents the CSR generated using the most probable ground acceleration predicted for this site. The other two profiles result from bracketing this acceleration by +/- 0.05 g. From this graph, it can be seen that the potentially liquefiable region extends from a depth of 3.75 meters throughout the rest of the profile. Four CPT soundings were available at Yalova Harbor. The graphs developed from CPT-YH1 are shown in Figure 4.52. The graphs developed from CPT-YH2, are shown in Figure 4.53. The graphs developed from CPT-YH3 are shown in Figure 4.54. The graphs developed from CPT-YH4 are shown in Figure 4.55. Figure 4.56 shows the idealized soil profile and layer properties at Yalova Harbor as determined from combining the data from these four cone soundings.

Table 4.19 summarizes the data for the depth intervals located within the potentially liquefiable region at Yalova Harbor. The soil located between the depths of 3 - 8 meters is sand/sand mixtures with an approximate I_C value of 1.8. This layer would be predicted as liquefiable and is the one most likely to have liquefied and induced the lateral spreading at this site. The remainder of the profile is clay/silt mixtures that would be predicted as unlikely to have liquefied based upon the high clay content.

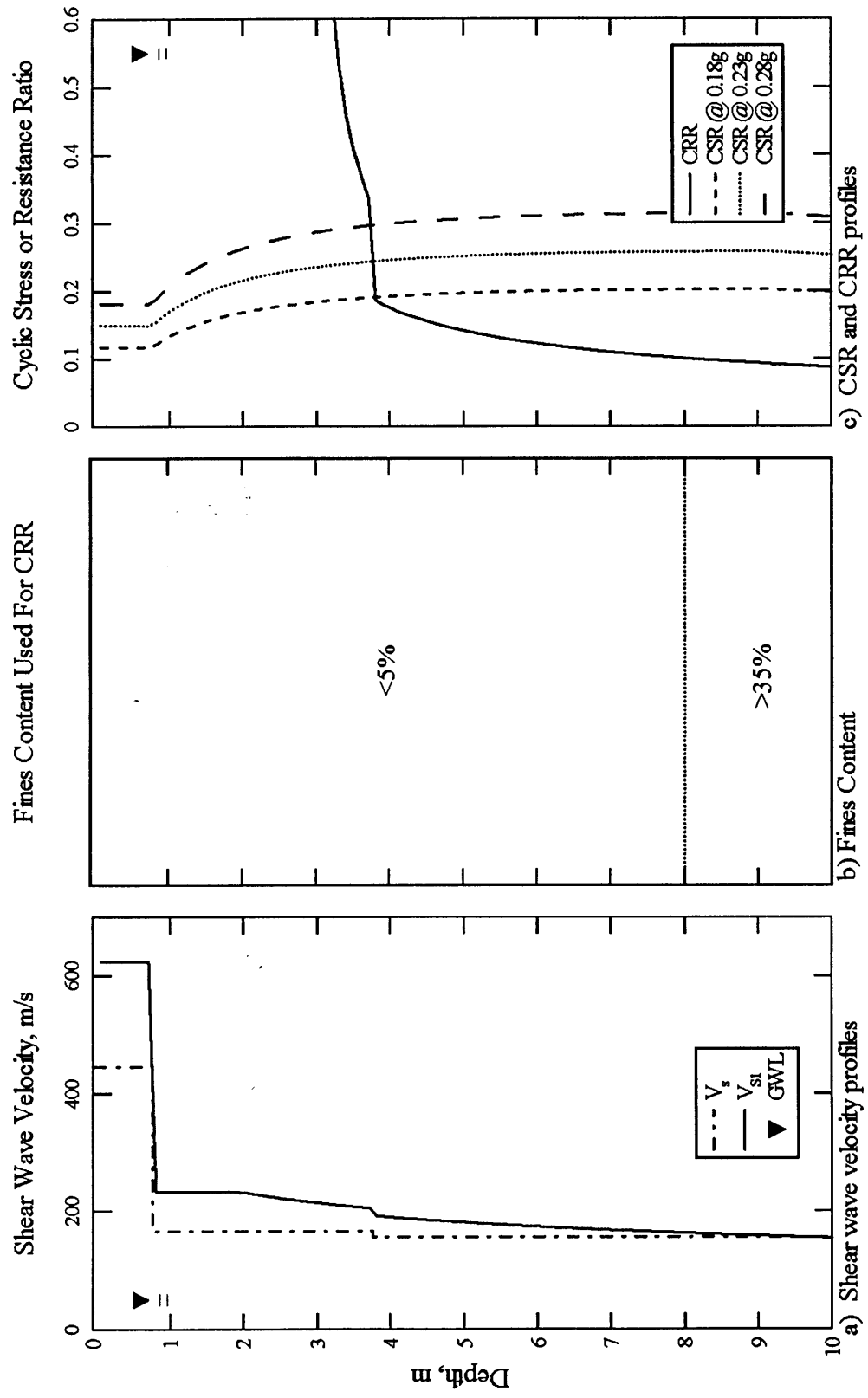

Figure 4.51 Graphs developed to delineate liquefiable soil using the simplified shear wave velocity procedure at Yalova Harbor, Yalova, Turkey.

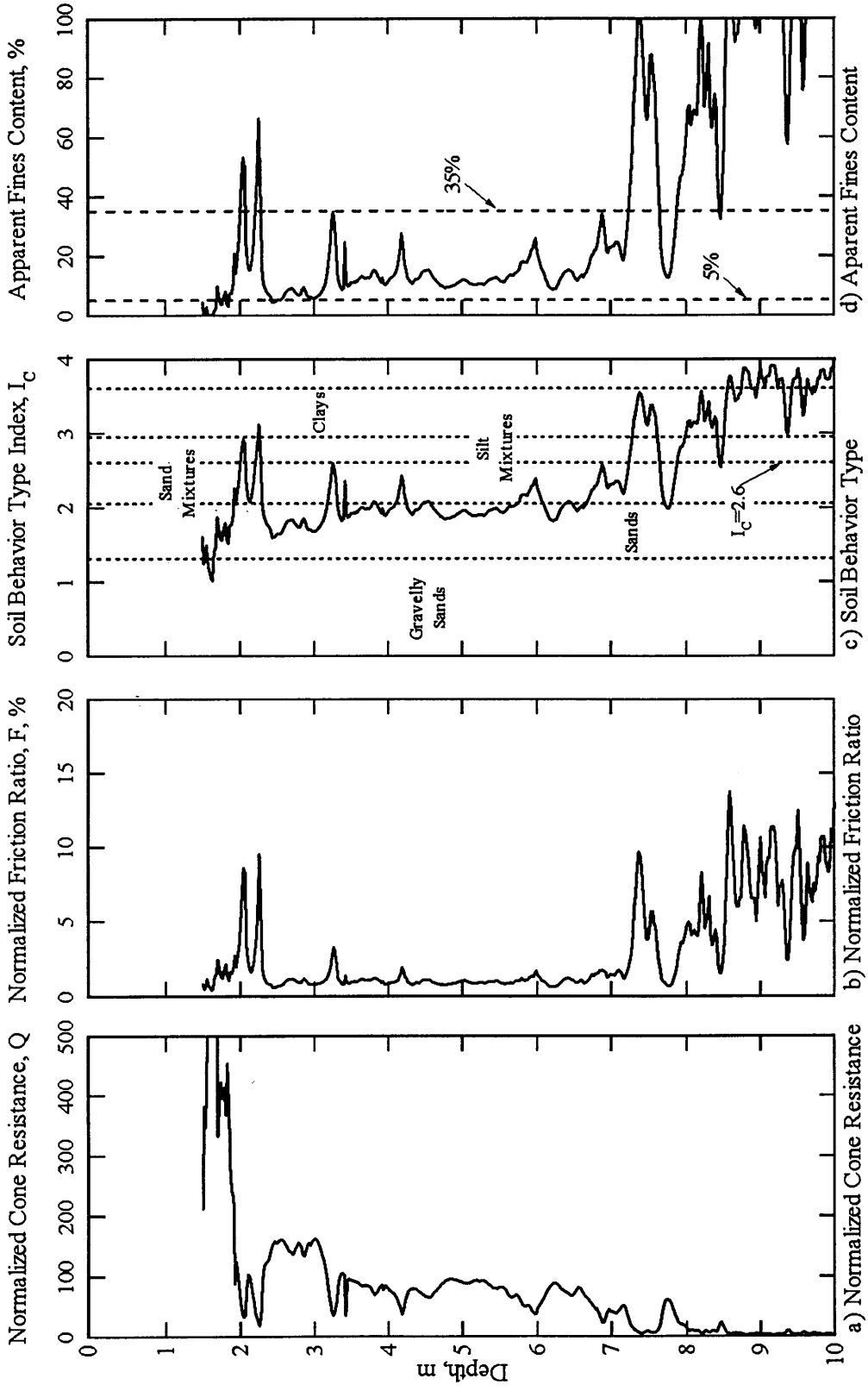

Figure 4.52 Graphs developed from CPT-YH1 to characterize the subsurface at Yalova Harbor, Yalova, Turkey (raw cone data from http://peer.berkeley.edu/turkey/adapazari).

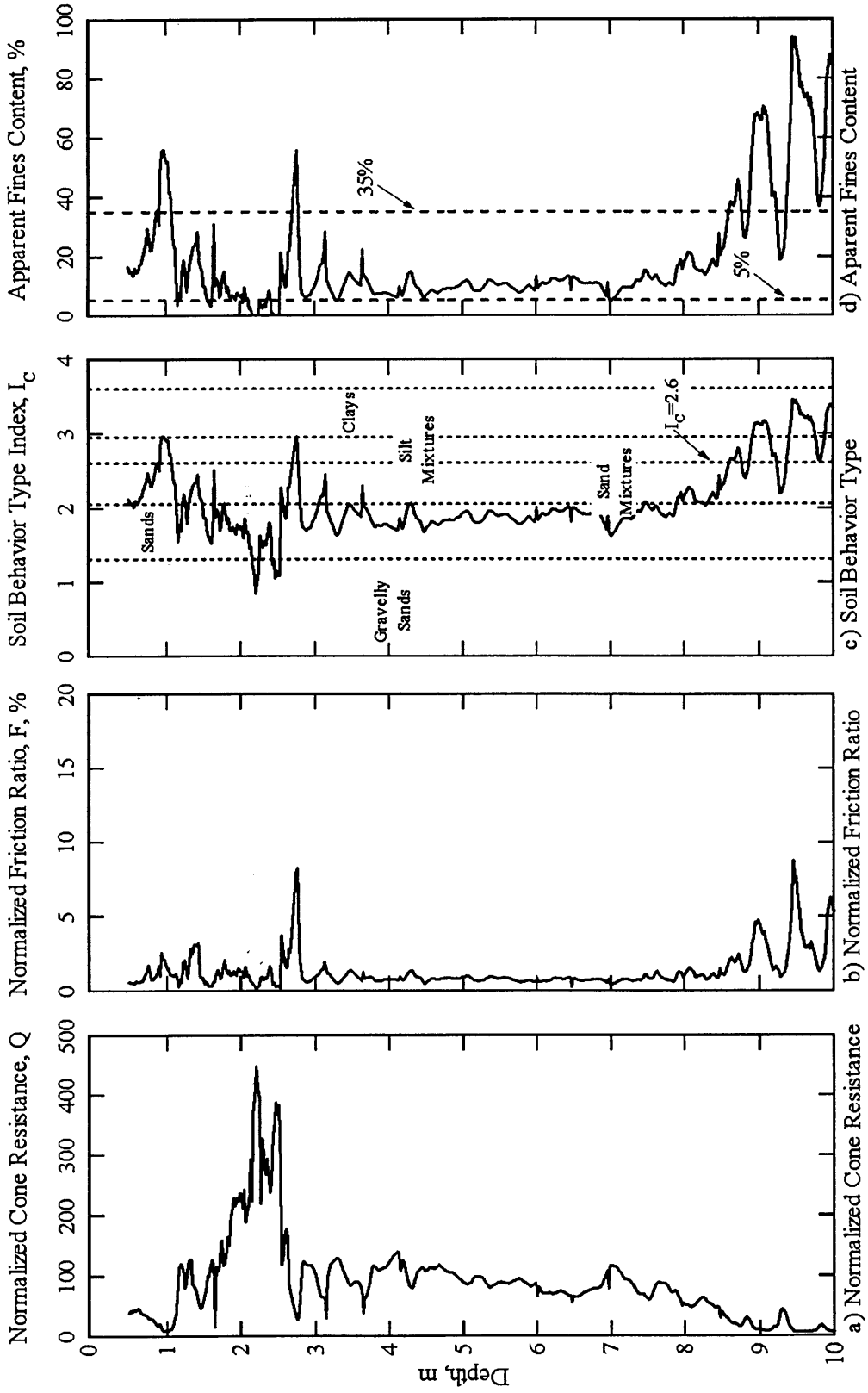

Figure 4.53 Graphs developed from CPT-YH2 to characterize the subsurface at Yalova Harbor, Yalova, Turkey (raw cone data from http://peer.berkeley.edu/turkey/adapazari).

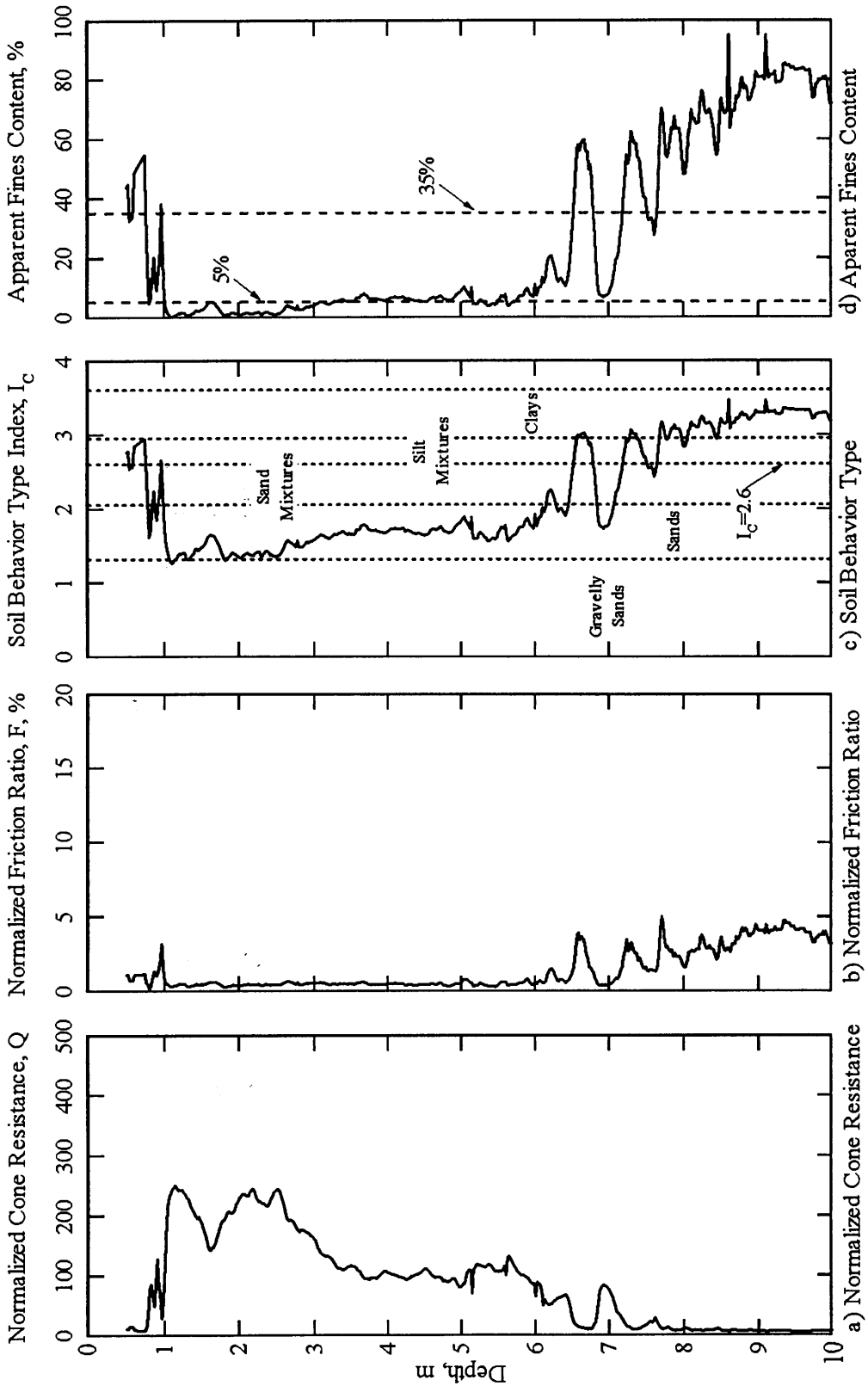

Figure 4.54 Graphs developed from CPT-YH3 to characterize the subsurface at Yalova Harbor, Yalova, Turkey (raw cone data from http://peer.berkeley.edu/turkey/adapazari).

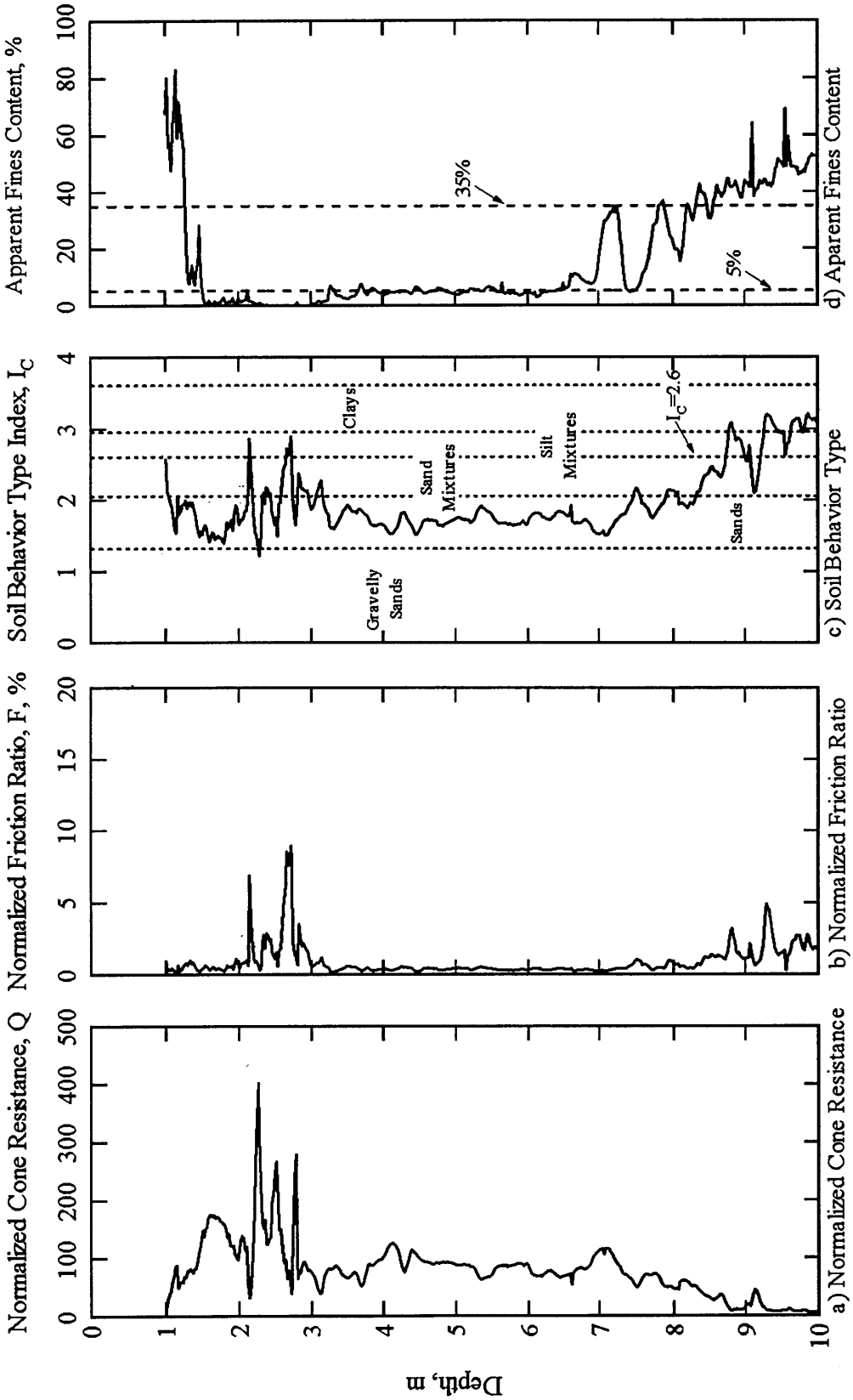

Figure 4.55 Graphs developed from CPT-YH4 to characterize the subsurface at Yalova Harbor, Yalova, Turkey (raw cone data from http://peer.berkeley.edu/turkey/adapazari).

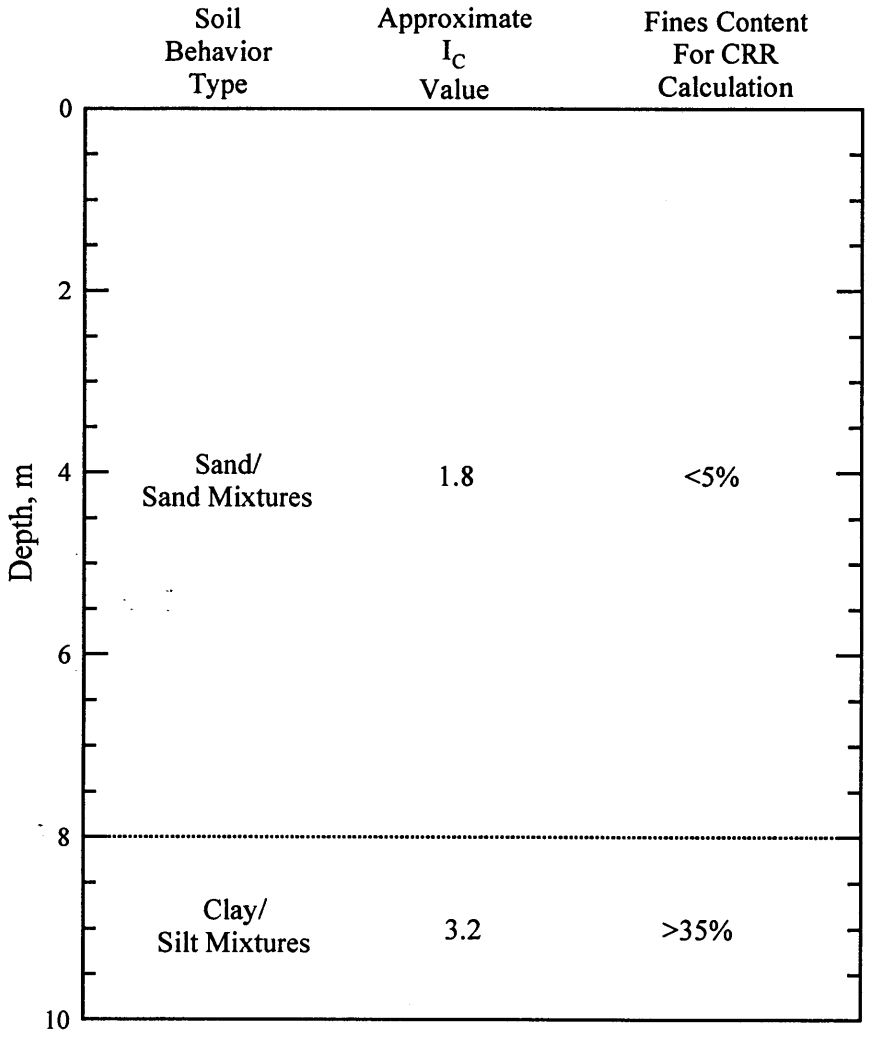

Figure 4.56 Idealized soil profile and layer properties as determined from four CPT soundings at Yalova Harbor, Yalova, Turkey.

Table 4.19 Properties for soil layers located within the potentially liquefiable region at Yalova Harbor

Depth Interval (m)	Average (CRR/CSR)	Soil Behavior Type	Approximate I_C Value	Predicted as Liquefiable by CPT
3.75 - 8	0.51	Sand/Sand Mixtures	1.8	yes
8 - 10	0.36	Clay/Silt Mixtures	3.2	no

4.3 SUMMARY

The results of liquefaction analysis of 15 sites that experienced ground shaking during the 1999 Kocaeli, Turkey earthquake are presented in this chapter. Fourteen of these sites experienced ground failure, and one site, site 1-24 along the Cark Canal in Adapazari, had no evidence of ground failure. The liquefaction analysis was a two step procedure, first potentially liquefiable layers were identified using simplified shear wave velocity procedure, then an evaluation was made regarding the susceptibility of potentially liquefiable layers based upon soil type.

The simplified shear wave velocity procedure was used to delineate potentially liquefiable layers at each of these sites. A plot of CSR versus overburden stress corrected shear wave velocity for each critical layer is shown in Figure 4.57 along with the liquefaction curves developed by Andrus, et al (1999). This plot shows that each site had soil layers that would be identified as liquefiable, including the site with no observed ground failure. One other site of interest is Degirmendere Nose on Izmit Bay. This site experienced massive lateral spreading, however, only a thin layer between 8 and 9 m barely classifies as liquefiable according to the simplified procedure. This point is identified in Figure 4.57. The level of ground failure at such a stiff site is somewhat surprising.

Then, each potentially liquefiable soil layer was then evaluated to determine if the soil was of the type that would classify as susceptible to liquefaction. In general, plastic soils and soils with high clay contents are not considered susceptible to liquefaction. This classification was accomplished in one of two ways. First, results of index testing on soil samples recovered from each site were compiled, and the Chinese Criteria and the Andrews and Martin Criteria were applied to differentiate susceptible and nonsusceptible soils based upon the soil plasticity and clay content. Second, at sites where only CPT data were available the soil behavior type index (I_C) was used to identify liquefaction susceptible soil.

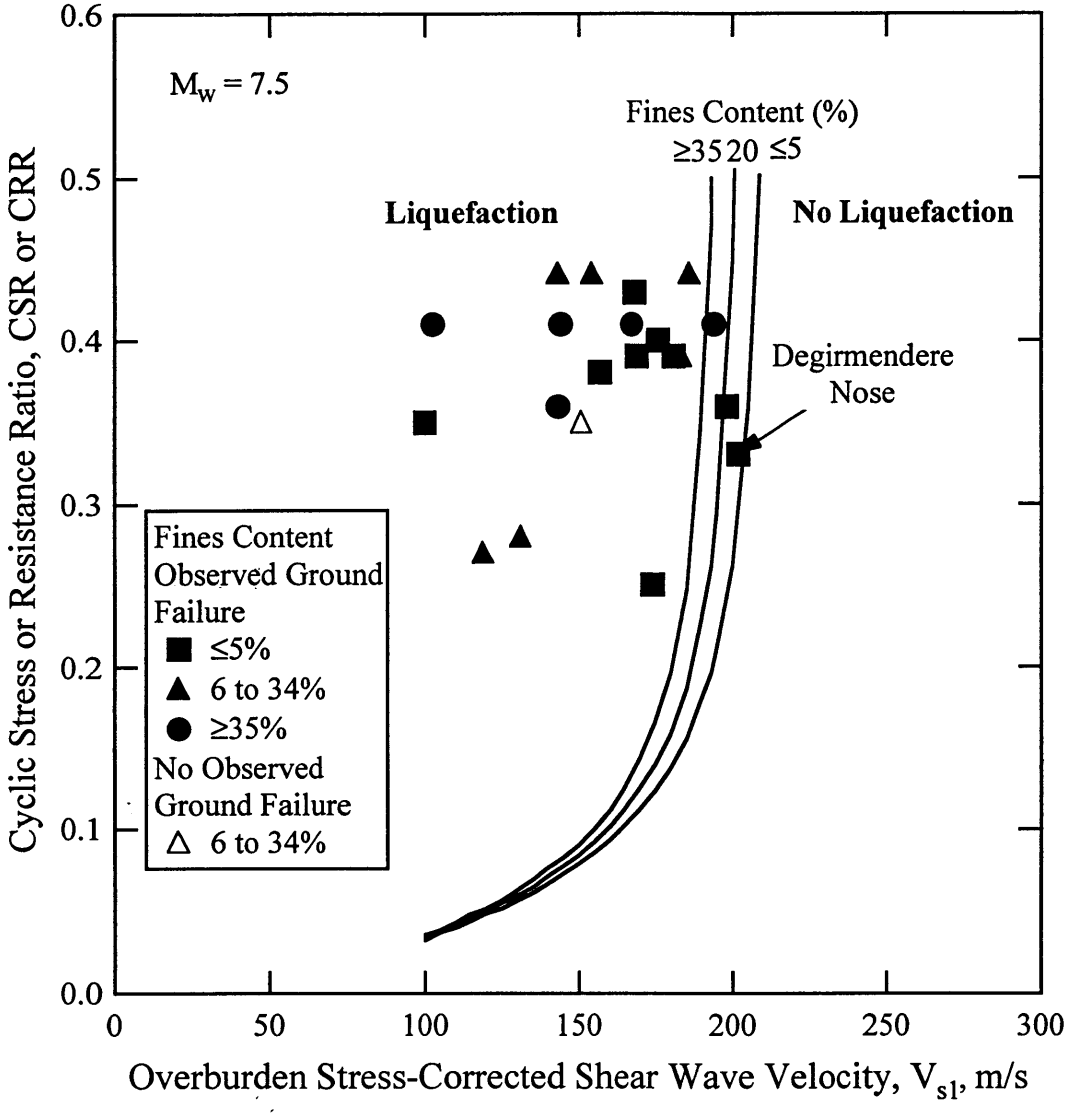

Figure 4.57 CSR and overburden stress corrected shear wave velocity of critical layers at each Turkey liquefaction site along with liquefaction curves developed by Andrus, et al. (1999)

At four sites in Adapazari where ground failure was observed, all of the soils in the potentially liquefiable layers were classified as nonliquefable according to both the Chinese criteria and the Andrews and Martin criteria. These sites are Sites A, C, G, and J. At three sites, Sites C, G, and J, the soils failed to classify as liquefiable only based upon the clay contents being too high. At site A, the soils failed to classify as liquefiable based upon both clay content and plasticity (liquid limit), however, the liquid limits were

only slightly above the criteria. At other sites in Adapazari, it is quite likely that soils with high clay contests also contributed to the observed ground failures.

These results suggest that criteria based on percentage of clay size particles are not always useful in differentiating liquefiable and nonliquefiable soils. It is possible to have soils with silt particles smaller than 2μm. These small silt particles would elevate the clay size particle percentage without decreasing the soils liquefaction susceptibility.

CHAPTER 5

CONCLUSIONS

5.1 INTRODUCTION

The 1999 Kocaeli, Turkey earthquake was one of the most damaging earthquakes in history, both in terms of life lost and property damaged. Soil liquefaction played a major role in this destruction. The purpose of this work was to develop shear wave velocity profiles at 15 sites where liquefaction induced ground failure was an issue, and evaluate how well the shear wave velocity based liquefaction analysis method predicts ground failure.

5.2 SUMMARY OF METHODOLOGY

Shear wave velocity profiles were measured at each of the 15 sites using the Spectral-Analysis-of-Surface-Waves (SASW) method. Profiles where measured to a depth of at least 10 m at each site. Descriptions of each site and measured shear wave velocity profiles are found in Chapter 2.

Potentially liquefiable layers were identified in each of the shear wave velocity profiles using the shear wave simplified method developed by Andrus et al. (1999). Chapter 3 contains a detailed discussion of the methods employed and the analyses results are in Chapter 4.

Soil stiffness alone does not control earthquake-induced soil liquefaction. The type of soil also effects the soils liquefaction susceptibility. In general, plastic soils and soils with high clay contents are thought to be nonsusceptible to liquefaction. Two general approaches are available to distinguish susceptible and nonsusceptible soils. Seed and Idriss (1982) outline criteria developed in China based upon liquid limit, water content and clay content. This criteria has been updated by Andrews and Martin (2000) to account for differences in soil index testing in the United States and in China. The

other approach, developed by Robertson and Wride (1998), uses the results of CPT sounds to differentiate susceptible and nonsusceptible soils based upon soil behavior index (I_C).

Boring, sampling, and CPT testing were performed at each of the liquefaction sites by researchers from the University of California and Brigham Young University (http://peer.berkeley.edu/turkey/adapazari/). Soil properties and indices were measured on recovered soil samples by researchers from the University of California. These results were used to differentiate susceptible and nonsusceptible soils. When results of testing on soil samples were available, those data were employed in the Chinese criteria and Andrews and Martin criteria. Where no soil testing results where available, the CPT approach was utilized. Results of these analyses are reported in Chapter 4.

5.3 Conclusions from Liquefaction Analyses

Brief synopses of the most interesting liquefaction analyses are presented below. The sites are divided into Adapazari Sites, Hotel Sapanca, and Izmit Bay sites.

5.3.1 Adapazari Sites

The city of Adapazari, located approximately 7 km north of the fault rupture, suffered the highest degree of property damage and life loss of any city affected by the Kocaeli earthquake. The city experienced spectacular and extensive occurrences of soil liquefaction as hundreds of buildings settled, tilted, or translated excessively (EERI, 2000). Ten liquefaction sites from Adapazari were analyzed in this study. Ground failure was observed at 9 of the 10 sites. Conditions at the other site, site 1-24, on the Cark Canal, appeared to be ideal for lateral spreading, however, no lateral spreading or other ground failures was observed.

5.3.1.1 Site A At Site A, very soft layers were encountered, however, no layers satisfy all criteria to be classified as liquefiable. The soil layer coming closest to satisfying all criteria is a 1-meter thick layer of silt at 3.5-m depth. It is extremely soft with an average CRR/CSR of 0.10. All of the soil samples within this layer were

somewhat plastic; the average LL was approximately 34 and the average W_n/LL was 0.97. The average 5 μm clay content was 18% and the average 2 μm clay content was 14%. While predicted as not susceptible to liquefaction by both the Chinese Criteria and the Andrews and Martin Criteria, this layer only fails the Chinese Criteria due to a slightly high amount of clay-sized particles. However, it fails the Andrews and Martin Criteria due to both a high clay content and a high LL. At this site, a 5-story building settled 1.5 m. It is doubtful that a ground failure limited to a 1-m thick soil layer could have caused that magnitude of failure, therefore, it is likely that other layers were also involved.

5.3.1.2 Site C At Site C, very soft layers were encountered, however, no layers satisfy all criteria to be classified as liquefiable. The soil layer coming closest to satisfying all criteria is an approximately 2-meter thick layer of silty-sand and silts at a depth of 3.5 m. It has a CRR/CSR of approximately 0.4. None of the soil samples within this layer were considered as plastic. The average 5 μm clay content was 20% and the average 2 μm clay content was 16%. Therefore, this layer is considered as not susceptible to liquefaction, according to the Chinese Criteria, only due to a high amount of clay-sized particles. Technically, since the layer is totally non-plastic, the Andrews and Martin Criteria would classify this soil as "further studies required." However, since no guidance is given as to what those studies might be, the site would not be considered susceptible to liquefaction due to high clay-sized particle content.

5.3.1.3 Site G At Site G, very soft layers were encountered, however, no layers satisfy all criteria to be classified as liquefiable. The soil layer coming closest to satisfying all criteria is a 6-meter thick layer of silt at a depth of 0.5 m. It has an average CRR/CSR of 0.20. While this layer was assigned a LL of 44.5, however, 10 of the 12 samples within it were classified as non-plastic. The average 5 μm clay content was 27% and the average 2 μm clay content was 24%. Therefore, this layer would not be considered susceptible to liquefaction only due to a high amount of clay-sized particles.

5.3.1.4 Site J At Site J, very soft layers were encountered, however, no layers satisfy all criteria to be classified as liquefiable. The soil layer coming closest to satisfying all criteria is an approximately 3-meter thick layer of silt at a depth of 0.7 m. It has an average CRR/CSR of 0.25. While this layer was assigned a LL of approximately 39, 8 of the 12 samples within it were classified as non-plastic. The average 5 μm clay content was 28% and the average 2 μm clay content was 23%. Therefore, theis layer would not be considered susceptible to liquefaction due to a high amount of clay-sized particles.

5.3.1.4 Site 1-24 Another site of interest in Adapazari is Site 1-24. This site is located along the banks of the Cark Canal, a likely site for liquefaction-induced lateral spreading. A nearly 3-meter thick layer of soft sand was identified here at a depth of approximately 6 meters. This sand layer was soft enough to liquefy with an average CRR/CSR of 0.24. However, no surface evidence of liquefaction was observed.

5.3.2 Hotel Sapanca

Hotel Sapanca is located on the southern shore of Lake Sapanca. Tectonic subsidence, liquefaction-induced settlement, and lateral spreading were all observed on hotel grounds during the Kocaeli earthquake. As a result of these events, the four-story hotel was carried partially into the lake. Lateral movements toward the lake were on the order of 2 meters and the hotel settled between 20 - 50 cm. These two phenomena, coupled with tectonic subsidence, resulted in movement of the shoreline inward by 30 - 50 meters (EERI, 2000).

Four SASW centerlines were used at this location in order to investigate the full extent of the on-shore portion of the lateral spread. These centerlines were spaced evenly along a line approximately 75 meters in length. Nearly all of the soil down to a depth of 15 meters is soft enough to liquefy. Values for CRR/CSR vary slightly with depth and centerline; however, most lie between 0.3 - 0.4. Cone data were used at this site to classify the subsurface material. The soil is sand/sand mixtures with an approximate I_C value of 1.7. These types of conditions indicate liquefaction susceptibility, and help to

explain the dramatic subsidence and lateral spreading that caused the hotel to be carried partially into the lake.

5.3.3 Izmit Bay

Numerous coastal failures occurred along the Marmara coast on the north, east, and south shores of Izmit Bay. These failures ranged from minor lateral spreading in the free field to catastrophic stability failures that carried buildings and people into the Bay. In addition to liquefaction-related failures, major coastal subsidence also occurred in the Golcuk area (EERI, 2000). Four liquefaction-induced lateral spread sites located in this region will be discussed below.

5.3.3.1 Degirmendere Nose The largest and most devastating coastal stability failure occurred at Degirmendere Nose. Here, a large section of fill, along with a hotel and two restaurants, was carried into the bay. The cause of this enormous failure is not fully understood. Small lateral spread cracks were observed along the on-shore part of the failure behind a large head scarp. This study only identified a 1-meter thick layer, located between 8 - 9 meters in depth that was soft enough to liquefy. This layer has an average CRR/CSR of 0.9. Cone data were used at this site to classify the subsurface material. The soil is sand/sand mixtures with an approximate I_C value of 1.7. It is probable that this layer did liquefy; however, it is unlikely that soil liquefaction was the only mechanism responsible for the ground failure. Tectonic deformation may have also played a large role in the catastrophic failure at this site

5.3.3.2 Other Izmit Bay Sites At each of the other three liquefaction sites along Izmit Bay (Police Station, Soccer Field, and Yalova Harbor), layers of sand/sand mixtures were identified within the potentially liquefiable region. It was assumed that these layers were the ones responsible for the liquefaction observed at these sites.

5.4 Current State of Practice

It is well understood that granular soils, under the right conditions, can and do liquefy during earthquakes. However, the liquefaction behavior of finer grained soils,

such as silts and silt-clay mixtures, is more poorly understood. Under the current state of practice, the Chinese Criteria (Seed and Idriss, 1982) is generally used to identify fine grained soils susceptible to liquefaction. More recently the Andrews and Martin Criteria (Andrews and Martin, 2000) have been developed as a refinement of the Chinese Criteria. Both of these criteria are based on Atterberg limits and grain size. Whether the authors intended it or not, the grain size part of these criteria has become a simple test used to separate "liquefiable" from "nonliquefiable" soils.

This study has shown that these criteria do not work for every case. Four of the 10 sites studied in the city of Adapazari, where liquefaction was observed, have been predicted as not susceptible to liquefaction. In each case, the layer identified as the one most likely to have liquefied is classified as a low-plasticity silt. At three of these sites, the soil layers were either largely non-plastic, or slightly plastic silts. The other site had a layer of plastic silt with a LL of slightly less than 35. Therefore, the primary basis for labeling them nonliquefiable is the fact that they all contained high amounts clay-sized particles (i.e. 15 - 25% finer than 2 μm). Soils at other sites in the city of Adapazari also had soil layers very similar to those at these four sites.

This study has shown that soils should not be labeled as nonliquefiable just because of a large fraction of clay-sized particles. Particle size criteria do not account for the possibility of small silt particles being misidentified as clay. Liquid limit appears to provide a better liquefaction criteria. If only the liquid limit criteria had been used at the Adapazari sites, then liquefaction would have been predicted at all of the sites except one, and that site would have been on the borderline

REFERENCES

Andrews, D.C.A., and G.R. Martin. 2000. Criteria for liquefaction of silty soils. Twelfth World Conference on Earthquake Engineering, January 29-February 5, Auckland, New Zealand.

Andrus, R.D., and K.H. II Stokoe. 1997. Liquefaction resistance based on shear wave velocity. NCEER Workshop on Evaluation of Liquefaction Resistance of Soils, January 4-5 1996, Salt Lake City, UT, p. 89-128.

Andrus, R.D., and K.H. II Stokoe. 2000. Liquefaction resistance of soils from shear wave velocity. Journal of Geotechnical and Geoenvironmental Engineering, ASCE 126(11):1015-1025.

Andrus, R.D., K.H. II Stokoe, J.A. Bay, and R.M. Chung. 1998. Delineation of densified sand at Treasure Island by SASW testing, p. 459-464. In P.K. Robertson and P.W. Mayne (Eds.). Geotechnical site characterization. A.A. Balkema, Rotterdam, Netherlands.

Andrus, R.D., K.H. II Stokoe, and R.M. Chung. 1999. Draft guidelines for evaluating liquefaction resistance using shear wave velocity measurements and simplified procedures. NISTIR 6277, National Institute of Standards and Technology, Gaithersburg, Maryland, 121 p.

Andrus, R.D., K.H. II Stokoe, R.M. Chung, and C.H. Juang. 2001. Guidelines for evaluating liquefaction resistance using shear wave velocity measurements and simplified procedures. National Institute of Standards and Technology, Gaithersburg, Maryland. In press.

Atukorala, U., D. Wijewickreme, and N. McCammon. 2000. Some observations related to liquefaction susceptibility of silty soils. Twelfth World Conference on Earthquake Engineering, January 29-February 5, Auckland, New Zealand.

Brown, L.T, D.M. Boore, and K.H.II Stokoe. 2000. Comparison of shear wave velocity profiles from SASW and downhole seismic tests at a strong-motion site. Twelfth World Conference on Earthquake Engineering, January 29-February 5, Auckland, New Zealand.

Dobry, R., R.D. Ladd, F.Y. Yokel, R.M. Chung, and D. Powell. 1982. Prediction of pore water pressure buildup and liquefaction of sands during earthquakes by the cyclic strain method. NBS Building Science Series 138, National Bureau of Standards, Gaithersburg, Maryland, 152 p.

Earthquake Engineering Research Institute (EERI). 2000. 1999 Kocaeli, Turkey, Earthquake Reconnaissance Report, Earthquake Spectra: The Professional Journal

of the Earthquake Engineering Research Institute, Supplement A to Volume 16, December 2000, 461 p.

Guo, T., and S. Prakash. 2000. Liquefaction of silt-clay mixtures. Twelfth World Conference on Earthquake Engineering, January 29-February 5, Auckland, New Zealand.

Joh, S.-H. 1992. User's Guide to WinSASW, a Program for Data Reduction and Analysis of SASW Measurements, The University of Texas at Austin. 287 p.

Kayabali, K. 1996. Soil liquefaction evaluation using shear wave velocity. Engineering Geology 44(4):121-127.

Kayen, R.E., J.K. Mitchell, R.B. Seed, A. Lodge, S. Nishio, and R. Coutinho. 1992. Evaluation of SPT-, CPT-, and shear wave-based methods for liquefaction potential assessment using loma prieta data. Fourth Japan-U.S. Workshop on Earthquake Resistant Design of Lifeline Facilities and Countermeasures for Soil Liquefaction, May 27-29,1992, Honolulu, Hawaii, p. 177-204.

Kramer, S.L. 1996. Geotechnical earthquake engineering. Prentice Hall, Upper Saddle River, New Jersey, 595 p.

Liao, S.S.C., and R.V. Whitman. 1986. Overburden correction factors for SPT in sands. Journal of Geotechnical Engineering, ASCE 112(3):373-377.

Lodge, A.L. 1994. Shear wave velocity measurements for subsurface characterization. Ph.D. dissertation. University of California, Berkeley, California. 243 p.

Nazarian, S., and K.H. II Stokoe. 1984. In situ shear wave velocities from spectral analysis of surface wave tests. Eighth World Conference on Earthquake Engineering, San Francisco, California, p. 31-38.

Rathjie, E. 2001. Professor at the University of Texas at Austin. Personal interview, May.

Robertson, P.K. 1990. Soil classification using CPT. Canadian Geotechnical Journal 27(1):151-158.

Robertson, P.K., and C.E. Wride. 1998. Evaluating cyclic liquefaction potential using the cone penetration test. Canadian Geotechnical Journal 35(3):442-459.

Robertson, P.K., D.J. Woeller, and W.D.L. Finn. 1992. Seismic cone penetration test for evaluation liquefaction potential under cyclic loading. Canadian Geotechnical Journal, Vol. 29, p. 686-695.

Sancio, R. 2001. Graduate student at the University of California. Personal interview, May.

Seed, H.B., and I.M. Idriss. 1971. Simplified procedure for evaluating soil liquefaction potential. Journal of the Soil Mechanics and Foundations Division, ASCE 97(SM9):1249-1273.

Seed, H.B., and I.M. Idriss. 1982. Ground motion and soil liquefaction during earthquakes. Earthquake Engineering Research Institute, Berkeley, California, 134 p.

Stokoe, K.H., II, S. Nazarian, G.J. Rix, I. Sanchez-Salinero, J.C. Sheu, and Y.J. Mok. 1988. In situ seismic testing of hard-to-sample soils by surface wave method, p. 264-289. In J.L. Von Thun (Ed.). Earthquake engineering and soil dynamics II—recent advances in ground-motion evaluation, Geotechnical Special Publications No. 20, ASCE.

Stokoe K.H., II, S.G. Wright, J.A. Bay, and J.M. Roesset. 1994. Characterization of geotechnical sites by SASW method, p. 1-24. In R.D. Woods (Ed.). Geophysical characterization of sites, IBH Oxford Press, New Delhi.

Tokimatsu, K., S. Kuwayama, and S. Tamura. 1991. Liquefaction potential evaluation based on Rayleigh wave investigation and its comparison with field behavior. Second International Conference on Recent Advances in Geotechnical Earthquake Engineering and Soil Dynamics, March 11-15, 1991, St. Louis, Missouri, University of Missouri at Rolla, p. 357-364.

Tokimatsu, K., and A. Uchida. 1990. Correlation between liquefaction resistance and shear wave velocity. Soils and Foundations, Japanese Society of Soil Mechanics and Foundation Engineering 30(2):33-42.

Yamamoto, A., H. Shinohara, and I. Furuta. 2000. Liquefaction potential using s-wave crosshole tomography. Twelfth World Conference on Earthquake Engineering, January 29-February 5, Auckland, New Zealand.

Yamamuro, J.A., and K.M. Covert. 2001. Monotonic and cyclic liquefaction of very loose sands with high silt content. Journal of Geotechnical and Geoenvironmental Engineering 127(4):314-324.

Youd, T.L., and I.M. Idriss. 1997. NCEER workshop on evaluation of liquefaction resistance of soils. National Center for Earthquake Engineering Research, Buffalo, New York, Technical Report no. NCEER-97-0022. 267 p.

Youd, T.L., and I.M. Idriss. 2001. Liquefaction resistance of soils: summary report from the 1996 NCEER and 1998 NCEER/NSF workshops on evaluation of liquefaction resistance of soils. Journal of Geotechnical and Geoenvironmental Engineering 127:297-313.